AD-A096 387 NAVAL POSTGRADUATE SCHOOL MONTEREY CA F/G 8/3
HEAT BUDGETS OF THE SOUTHEAST BEAUFORT SEA FOR THE YEARS 1974 A--ETC(U)
SEP 80 E L TUMMERS

UNCLASSIFIED NL

1 OF 3
AD A096387

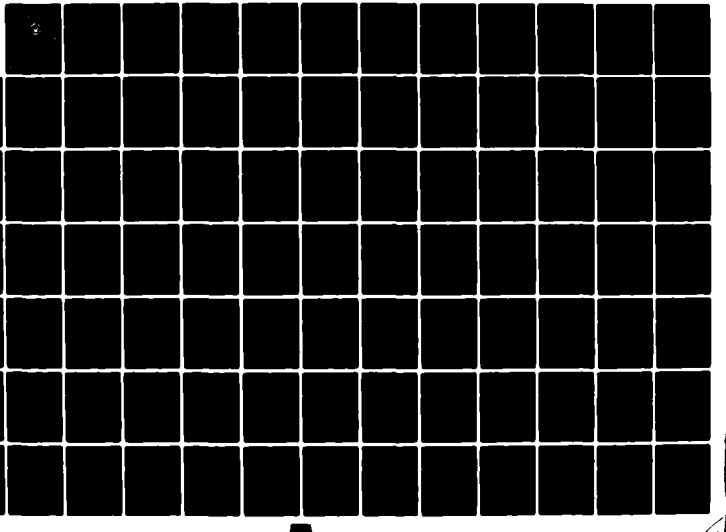

NAVAL POSTGRADUATE SCHOOL
Monterey, California

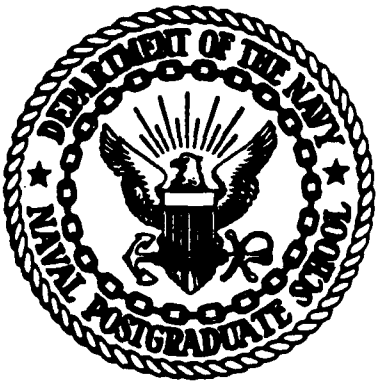

THESIS

HEAT BUDGETS OF THE SOUTHEAST BEAUFORT SEA FOR THE YEARS 1974 AND 1975,

by

Edward Leo/Tummers

September 1980

Thesis Advisor: A. R. Milne

Approved for public release; distribution unlimited.

UNCLASSIFIED

SECURITY CLASSIFICATION OF THIS PAGE (When Data Entered)

REPORT DOCUMENTATION PAGE		READ INSTRUCTIONS BEFORE COMPLETING FORM
1. REPORT NUMBER	2. GOVT ACCESSION NO. AD-A096 387	3. RECIPIENT'S CATALOG NUMBER
4. TITLE (and Subtitle) Heat Budgets of the Southeast Beaufort Sea for the Years 1974 and 1975		5. TYPE OF REPORT & PERIOD COVERED Master's Thesis; September 1980
		6. PERFORMING ORG. REPORT NUMBER
7. AUTHOR(s) Edward Leo Tummers		8. CONTRACT OR GRANT NUMBER(s)
9. PERFORMING ORGANIZATION NAME AND ADDRESS Naval Postgraduate School Monterey, California 93940		10. PROGRAM ELEMENT, PROJECT, TASK AREA & WORK UNIT NUMBERS
11. CONTROLLING OFFICE NAME AND ADDRESS Naval Postgraduate School Monterey, California 93940		12. REPORT DATE September 1980
		13. NUMBER OF PAGES 204
14. MONITORING AGENCY NAME & ADDRESS(if different from Controlling Office)		15. SECURITY CLASS. (of this report) Unclassified
		15a. DECLASSIFICATION/DOWNGRADING SCHEDULE

16. DISTRIBUTION STATEMENT (of this Report)

Approved for public release; distribution unlimited.

17. DISTRIBUTION STATEMENT (of the abstract entered in Block 20, if different from Report)

18. SUPPLEMENTARY NOTES

19. KEY WORDS (Continue on reverse side if necessary and identify by block number)

Arctic Ocean	Beaufort Sea	Latent Heat
Southeast Beaufort Sea	Heat Fluxes	Storage Heat
Heat Budgets	Ice Cover	Wind
Mackenzie Bay	Radiation	Thermal Structure
Mackenzie River	Sensible Heat	

20. ABSTRACT (Continue on reverse side if necessary and identify by block number)

Comparisons were made of the heat budgets of the Southeast Beaufort Sea for the summer of 1974 (a severe ice year) and the summer of 1975 (a good ice year). Local meteorological data and oceanographic measurements obtained during the Beaufort Sea Project during August of both years were used to obtain estimates of the various heat terms.

DD FORM 1 JAN 73 1473 (Page 1)

EDITION OF 1 NOV 65 IS OBSOLETE

S/N 0102-014-6601

UNCLASSIFIED

SECURITY CLASSIFICATION OF THIS PAGE (When Data Entered)

#20 - ABSTRACT - (CONTINUED)

Results indicate that:
(1) The major heat input to the sea is from absorbed solar radiation; (2) the overall heat contribution from the Mackenzie River is small in comparison to that from solar radiation; (3) the wind patterns in early spring are the major factor in determining the heat content of the water by summer; and (4) the wind patterns later in the spring and summer are the major factor in determining the ice coverage.

From the distribution of heat in the study area, three consistent features were found: (a) a warm water core in the vicinity of 70°N, 138°W; (b) a core of warmer water north of Atkinson Point associated with the early open-water area; and (c) a core of cold water north of Richard's Island.

Approved for public release, distribution unlimited.

Heat Budgets of the Southeast Beaufort Sea
for the years 1974 and 1975

by

Edward Leo Tummers
Captain, Canadian Armed Forces
BSc., Royal Military College of Canada, 1971

Submitted in partial fulfillment of the
requirements for the degree of

MASTER OF SCIENCE IN OCEANOGRAPHY

from the

NAVAL POSTGRADUATE SCHOOL
September, 1980

Author: E. Tummers

Approved by: Allen R. McIntyre
Thesis Advisor

Robert G. Paquette
Second Reader

Robert H. Bourke for
Chairman, Department of Oceanography

William M. Tolles
Dean of Science and Engineering

ABSTRACT

Comparisons were made of the heat budgets of the Southeast Beaufort Sea for the summer of 1974 (a severe ice year) and the summer of 1975 (a good ice year). Local meteorological data and oceanographic measurements obtained during the Beaufort Sea Project during August of both years were used to obtain estimates of the various heat terms.

Results indicate that:
(1) The major heat input to the sea is from absorbed solar radiation; (2) the overall heat contribution from the Mackenzie River is small in comparison to that from solar radiation; (3) the wind patterns in early spring are the major factor in determining the heat content of the water by summer; and (4) the wind patterns later in the spring and summer are the major factor in determining the ice coverage.

From the distribution of heat in the study area, three consistent features were found: (a) a warm water core in the vicinity of 70°N, 138°W; (b) a core of warmer water north of Atkinson Point associated with the early open-water area; and (c) a core of cold water north of Richard's Island.

TABLE OF CONTENTS

LIST OF FIGURES

Figure

Figure

Figure

Figure

Figure

LIST OF TABLES

SYMBOLS AND ABBREVIATIONS

Conversion Factors, Constants, and Notation

The following list of conversion factors, constants, and notation represents those most frequently used during the preparation of this paper and may be helpful in comparing results found elsewhere expressed in different units or using different notations.

Stefan-Boltzman constant	-	5.735×10^{-5} erg $sec^{-1} cm^{-2} {}^{\circ}K^{-4}$
		$= 1.18 \times 10^{-7}$ ly $day^{-1} {}^{\circ}K^{-4}$
1 watt m^{-2}	-	753 ly $year^{-1}$ = 2.063 ly day^{-1}
1 gm cal	-	4.183 joules
1 m^3 sec	-	35.31 cfs
1 m^2	-	10.76 ft^2
1 km^2	-	0.3861 $(\text{statute miles})^2$
		$= 0.2913 (\text{naut. miles})^2$
1 km	-	.5397 nm
1 knot	-	.514 m sec^{-1}
At 70°N, 1 degree latitude	-	~ 111.6 km
1 degree longitude	-	~ 38.75 km
1 degree square	-	~ 4326 km^2
A	-	Albedo
C	-	Cloud amount (tenths)
CONC	-	Concentration of ice (tenths)
E	-	Evaporation rate (cm day^{-1})

e - vapor pressure (mb)

e_a - vapor pressure of the air (mb)

e_w - vapor pressure of the surface (mb)

K - coefficient indicating surface roughness

K' - coefficient indicating atmospheric stability

$K\downarrow$ - incident short wave radiation at the surface of the earth (ly day^{-1})

$K\uparrow$ - reflected short wave radiation (ly day^{-1})

L - Latent heat (cal gm^{-1})

L_s - Latent heat of sublimation (taken as 677.0 cal gm^{-1})

L_v - Latent heat of vaporization (taken as 597.3 cal gm^{-1})

$L\downarrow$ - the incident long wave radiation at the earth's surface (ly day^{-1})

$L\uparrow$ - the reflected long wave radiation (ly day^{-1})

M_v - the molecular weight of water vapor = 0.622 Molecular weight of dry air

p - the density (gm cm^{-3})

Q_A - Resultant atmospheric flux (ly day^{-1})

$\overline{Q}_A$ - Accumulated atmospheric heat (ly)

Q_E - Latent heat flux at the surface (ly day^{-1})

$\overline{Q}_E$ - Accumulated latent heat at the surface (ly)

Q_F - Heat flux due to the cooling or warming of the ice and subsequent freezing or melting (ly day^{-1})

$\overline{Q}_F$ - Accumulated heat used in warming and melting the ice in place (ly)

Q_H - Sensible heat flux at the surface (ly day^{-1})

$\overline{Q}_H$ - Accumulated sensible heat (ly)

Q_I - Heat flux due to advection of ice (ly day^{-1})

$\overline{Q}_I$ - Accumulated heat due to ice advection (ly)

Q_S - The storage change in the water column (ly day^{-1})

$\bar{Q}_S$ - Accumulated storage heat due to oceanic fluxes (ly)

Q_T - The heat transported by Mackenzie River water (ly day^{-1})

$\bar{Q}_T$ - Accumulated Mackenzie River heat (ly)

Q_W - The heat due to the cooling or warming of water in the upper layer of the ocean (ly day^{-1})

$\bar{Q}_W$ - Accumulated heat used in warming the upper layers of the ocean (ly)

Q^* - The net radiation flux of downward and upward solar, terrestrial, and atmospheric radiation (ly day^{-1})

$\bar{Q}^*$ - Accumulated heat due to net radiation

R^* - The universal gas constant ($M_v/R^* = 9.08$ gm cal^{-1} °K) for dry air

T - Temperature (°C or °K as specified)

T_a - Air temperature

T_d - Dew point temperature

T_i - Ice surface temperature

T_s - Water surface temperature or ice surface temperature as applicable

T_w - Water surface temperature

V - Wind speed (m sec^{-1})

ε - Stefan-Boltzman constant

σ - Emissivity of the surface

Summary of Equations*

1. $Q^* + Q_E + Q_H + Q_T + Q_W + Q_F + Q_I = 0$ ---------- 32

2. $Q_A = Q^* + Q_E + Q_H$ ---------- 34

3. $Q_S = Q_T + Q_W + Q_F + Q_I$ ---------- 34

4. $Q_A + Q_S = 0$ ---------- 34

5. $\overline{Q}^* + \overline{Q}_E + \overline{Q}_H + \overline{Q}_T + \overline{Q}_W + \overline{Q}_F + \overline{Q}_I = 0$ ---------- 34

6. $\overline{Q}_A + \overline{Q}_S = 0$ ---------- 35

7. $Q^* = K\downarrow + K\uparrow + L\downarrow + L\uparrow$ ---------- 43

8. $K\downarrow + K\uparrow = K\downarrow(1 - A)$ ---------- 43

9. $L\downarrow + L\uparrow = \varepsilon\sigma T^4(1 - 0.44 - 0.08\sqrt{e})(1 - 0.083C)$ --------- 46

10. $E = KV(e_w - e_a)$ ---------- 50

11. $e = 6.11\ EXP[\frac{M_v L}{R^*}(\frac{1}{273} - \frac{1}{T})]$ ---------- 51

12. $Q_E = p\ LE$ ---------- 53

13. $Q_E + Q_E(ice)(CONC) + Q_E(water)(1 - CONC)$ ---------- 54

14. $Q_H = 30.24(T_s - T_a)$ ---------- 55

15. $Q_H = 0.42\ V\ (T_s - T_a)$ ---------- 56

* page numbers refer to first reference to equation

16. $\bar{Q}_S = \bar{Q}_T + \bar{Q}_W + \bar{Q}_F + \bar{Q}_I$ ---------- 58

17. $Q = Q(ice)(CONC) + Q(water)(1 - CONC)$ ---------- 72

ACKNOWLEDGMENT

The topic for this thesis was suggested by Adjunct Research Professor of Oceanography Allen R. Milne, Chair in Arctic Marine Sciences of the Naval Postgraduate School, Monterey, California. His invaluable experience in the Arctic and especially the Southeast Beaufort Sea, and his interest and guidance in directing the research efforts were an inspiration and contributed immensely to the successful completion of this research. Professor Robert G. Paquette, also of the Naval Postgraduate School provided helpful background ideas based on his own extensive experiences in the Arctic. The support and cooperation of the faculty and staff of the Naval Postgraduate School helped make the research enjoyable. The patient understanding of my wife, Sandra, and my son, Patrick, during the long hours of research was greatly appreciated. To these people, the author expresses his sincere thanks.

"If you want to know what men look for in that land (the Arctic) or why men go where there is such danger to their lives, it is the threefold nature of man that lures him on. One part of man wants fame, for man goes where there is great danger to make himself famous. Another part of man wants knowledge, wants to see those places he has heard of and find out if they are as he has been told. The third part is the desire for riches, for man pursues wealth wherever he thinks he can find it, even though he must pass through great dangers."

Unknown bard
from The Mirror of the King
(a thirteenth century
Viking ballad)

From The Northwest Passage, by Bern Keating, Rand McNally & Co., Chicago, New York, San Francisco, 1970, p. 9.

I. INTRODUCTION

The primary aim of this study was to compare the heat budgets during the summer open-water season of 1974 (a severe ice year) and of 1975 (a good ice year) in the Southeast Beaufort Sea study area (Figure 1). The heat fluxes during each period were estimated in order to obtain values for accumulated heat due to these fluxes for the period May 1 to August 15. Mid-August was chosen for the heat budget calculation because simultaneous meteorological and oceanographic observations in the study area were available for each year with which to calculate the individual terms of the heat budget equation (Section III).

The atmospheric flux Q_A was estimated for the early part of the season and calculated for August of each year when marine meteorological observations were available (Section III.C.). Walmsley (1966) conducted a similar study in Baffin Bay for the period 1919-1942 and Huyer and Barber (1970) calculated a heat budget for Barrow Strait in 1962. Both authors reported a maximum Q_A flux downward in July with a rapid decrease in August which was also evident in the study area (Section III.C.).

It was desired to take some steps to develop a basic understanding of the heat budget and the associated oceanography in the Southeastern Beaufort Sea, an area of increasing commercial importance. The problem differs from those of Walmsley

(1966) and Huyer and Barber (1970) in two ways in particular. In their cases, the advection of ice was reasonably predictable because the areas were relatively well-bounded. Also the present area of study includes the drainage from a major river, the Mackenzie, which tends to cause ice to melt earlier and thus increases the absorption of heat due to solar radiation.

The techniques of the present study are somewhat similar to those of the previous authors except that now a considerable number of oceanographic observations were available. These made it possible to calculate the storage heat and permit a comparison of the atmospheric terms and the oceanic terms with a resultant estimation of the advection of ice. The details of the calculations are described in Section III.

It was found that:

(1) the major heat input to the Southeast Beaufort Sea was from absorbed net radiation $\overline{Q}^*$, regardless of the severity of the ice cover;

(2) the overall heat contribution from the Mackenzie River $\overline{Q}_T$, varied little inter-annually and was small in comparison to the contribution from net radiation $\overline{Q}^*$;

(3) wind patterns in early spring were the major factor in determining the heat content of the water in summer and the severity of the ice early in the navigation season; and

(4) wind patterns later in the summer were the major factor in determining ice coverage. Onshore winds produced

severe ice conditions, whereas, offshore winds produced good ice conditions.

A summary of marine meteorological observations for air temperature, sea surface temperature, dew point temperature, cloud amount, wind speed and wind direction is presented in Appendix A. The results of the calculations of the individual atmospheric flux terms corresponding to the marine observations are presented in Appendix B. The extreme values of the atmospheric fluxes and the associated environmental conditions were examined in more detail in Appendix C. It was found that onshore winds (from 260° to 350°) produced maximum heat losses (upward fluxes). Conversely, offshore winds (from 090° to 190°) produced maximum heat gain (downward fluxes).

In addition, various data presentations having oceanographic interest have been made. The distribution of heat in the water column of the study area was determined from examination of the temperature profiles at each oceanographic station. The results are displayed and discussed in Appendix D. Based on the distribution of heat throughout the study area, selected temperature and density profiles and cross-sections were examined in more detail to highlight interesting features in the circulation pattern (Appendix E). It was found that

(1) the heat content of the water column $\overline{Q}_W$, was much higher in 1975, a good ice year, than in 1974, a severe ice year;

(2) a warm water core in the vicinity of 70°N, 138°W existed in both years and with a similar heat content;

(3) a core of warmer water north of Atkinson Point, apparently associated with the transient patch of open water which has come to be called the Bathurst Polynya, was evident in both years; and

(4) in August 1975, a core of cold water just north of Richard's Island indicated that upwelling occurred and that there was in-shore movement of cold Arctic surface water on the shelf from beyond the continental slope.

A detailed examination of the study area, the environmental conditions in each year of the study period, and the evaluation of each term of the heat budget equation follows.

II. DESCRIPTION OF THE STUDY AREA

A. GEOGRAPHY

The study area (Figure 2) extends in an east-west direction from Herschel Island at about 140°W to Cape Dalhousie at 128°W, and in a north-south direction from the shores of the Mackenzie Delta and Tuktoyaktuk Peninsula to as far north as oceanographic observations were available. Figure 3 shows the region's bathymetry and the northerly limits of pack ice in the study area for the summer of years 1974 and 1975. The Mackenzie Canyon (also known as Herschel Canyon) is seen to extend southward into Mackenzie Bay east of Herschel Island and toward the western outlet of the Mackenzie River in Shallow Bay. Along Richard's Island the Tuktoyaktuk Peninsula, the continental shelf extends seaward to a distance of 110-150 km. In the Mackenzie Bay region, the nearshore water is very shallow with the ten-meter isobath lying as far as 35 km offshore. Only ice scours and underwater pingoes mar the flatness of the continental shelf. There is a smaller canyon on the shelf just north of Richard's Island (noticeable in the 50-meter contour in Figure 3) extending southward towards Kugmallit Bay and the eastern outlet of the Mackenzie River. At the northern limit of the study area at the shelf break the slope drops quickly to depths over 1000 meters.

B. TYPICAL SEQUENCE OF ICE BREAKUP

Nearshore, ice breakup usually starts in the Delta region (Figure 4) one week after the mean air temperature exceeds 0°C on about June 18 and is caused by rising air temperatures, warm water input from the Mackenzie River, and the melting of the snow cover. These factors are in turn controlled by the solar radiation, air temperature, precipitation, wind, cloudiness, vapor pressure, and evaporation. The relatively warm water of the Mackenzie River at its peak freshet in mid-June hastens the breakup of ice in the vicinity of the Delta [Burns, 1973]. The breakup of ice begins in Shallow Bay, then Kugmallit Bay and then progresses along the coast in both directions. The ice may be expected to loosen and break up early in July and, except in a severe ice year, a wide expanse of open water exists along the coast throughout August and September. In severe ice years, like 1974, open water may not occur until well into August and ice may reform in September. The expanse of open water in summer depends largely on winds, which can vary considerably in their prevailing direction from year to year. Cold winds from the northwest sector blow onshore pressing the Beaufort Sea pack ice landward, and if they prevail throughout much of the summer, it will be a severe ice year. On the other hand, warm easterly and southerly winds blowing offshore in summer move the pack ice away from land and with melting open a passage from Point Barrow to Cape Bathurst.

Offshore, beyond the landfast ice, the development of flaw leads and polynyas occurs mostly in April and May when

the offshore wind patterns change to a southeasterly flow and refreezing is slower as air temperatures begin to rise [Markham, 1975]. The long-term mean surface pressure chart for May (Figure 5) illustrates the development of these offshore winds. The High over the Chukchi Sea in February moves eastward and combines with the trough developing in Central Alaska to give southeast winds in the Beaufort Sea. Polynya and lead formation seaward of the landfast ice follows quickly. The regions north of Cape Bathurst in the eastern part of the study area (Figure 4) become the centers for offshore disintegration of ice, allowing the penetration of solar energy into the water, furthering the breakup process by accelerating melting. The offshore breakup in the Southeast Beaufort Sea is highly dependent on a change in the wind regime, on increasing solar radiation, and to a lesser extent on the tides and oceanic circulation.

C. ACTUAL ENVIRONMENTAL CONDITIONS

1. Sequence of Ice Breakup

The sequence of ice breakup in the spring and summer of the study period is described below. In 1974, there was no open water until mid-May. Figure 6 shows a sequence of satellite photos taken in 1975 on March 21, April 2, and May 1 showing the development of the leads at the edge of the fast ice. The lead was almost entirely closed again by May 1 due to a shift in winds. The next series of figures (Figures 7, 8, 9) show the contrast in open water at the same time of year between 1974, a severe ice year, and 1975, a good ice year.

The summer of 1974 was characterized by the worst ice conditions for 20 years of records in the Southeast Beaufort Sea. In contrast, sea ice gave little trouble to shipping in the study area in 1975. Figure 7 shows satellite photos for mid-May of each year. The large expanse of open water north of Cape Bathurst has re-appeared in the 1975 imagery, whereas there is little open water in mid-May 1974. Figure 8 shows satellite imagery for the beginning of June of each year. The open-water area north of Cape Bathurst has continued to spread in 1975, whereas in 1974 there was virtually no open water. Figure 9 contrasts ice conditions at approximately 21 June, the summer solstice. In 1975, except for a fringe of landfast ice, the entire area is ice-free; whereas in 1974, there is still almost total ice cover. Visible satellite imagery for the remainder of each summer is poor due to cloud cover; infra-red satellite imagery is poor due to the small temperature differences between open water and the ice cover. Figure 10 plots the percentage of open-water area from May 1 to the end of September for each year.

From the middle to the end of July 1974, the limit of open water remained near the ten-meter depth contour. By mid-August, the limit had moved outward in an expanding arc from Herschel Island to 70°N and then eastward to Atkinson Point. By August 19, the ice had returned onshore at some places in between. North of the limit of open water there existed large areas of first-year ice in various states of decay. These ice conditions coincided with a lack of persistent

winds from the east and south which usually blow in summer forcing the ice offshore. The north-to-west winds held the ice onshore and made synoptic oceanographic observations of the study area impossible. Marine observations were limited to a narrow band of open water along the coast between Herschel Island and Atkinson Point. The resulting heat budget calculations were considered to be representative of a heavy-ice year.

2. Wind Conditions

The data collected during August of 1974 was sparse both in time and space. Because of rapidly changing conditions in the study area, it was not valid to assume that the oceanographic data was synoptic. As an alternative approach, the open-water study period in August was examined by considering three evident prevailing-wind conditions in the wind records included in the marine surface observations (Appendix A). By examining these three shorter time intervals, the assumption of synopticity is made more reasonable even though the number of observations in each wind period is reduced. The observation period from August 12 to September 1 was divided as follows (Figure 11);

August 12-20, 1974	Prevailing northwest winds
August 20-23, 1974	Light and variable winds (called the post-northwest winds)
August 24-31, 1974	Easterly winds (encompassing 010° to 180°)

In the summer of 1975, on the other hand, the main pack ice stayed north of 71°N throughout most of the study

area, and remained at about 70°N near Herschel Island. Thus the two research ships were able to work out to the edge of the continental shelf. Later in August 1975, westerly storms did bring ice further south, but in low concentrations which was less troublesome than the polar pack for navigation. The large expanse of open water resulted in deeper wind-mixing of the upper layer of the ocean in the summer of 1975. The long fetch and absence of ice allowed wind-waves to build and produced turbulent mixing of the upper layer. The dominant winds for August 1975 are shown in Figure 11.

August 5-12, 1975	prevailing northwest winds
August 12-16, 1975	southeast winds
August 16-20, 1975	northeast winds
August 21-24, 1975	northwest winds

In 1975 the large expanse of open water occupied by a relatively small number of oceanographic stations between August 5-24 did not permit the separation of data into shorter time intervals identified with the particular wind direction. Instead, a synoptic evaluation of the heat budget for the entire observation period August 5-24 was made, in contrast to the approach used in August 1974.

III. THE HEAT BUDGET EQUATION

Energy fluxes over Arctic Seas comprise a complicated interaction of a variety of energy mechanisms and feedback loops (Figure 12), which will be discussed in succeeding sections.

A. DEFINITION OF TERMS

Figure 13 shows the typical summer fluxes in the Southeastern Beaufort Sea. The energy gained by the system is denoted by negative fluxes. The energy lost by the system to its surroundings is denoted by positive fluxes. The resultant energy stored in the system is denoted by a positive sign if it is an increase in stored energy, or by a negative sign if it is a decrease in stored energy. All fluxes ('Q' terms) are expressed in units of "calories per square centimeter per day" (cal cm^{-2} day^{-1}) or equivalently as langleys per day (ly day^{-1}). The accumulated heat due to each flux, expressed as the time integral of the flux term, is written as a $\overline{Q}$ term, which includes all heat within the entire study area (46,794 km^2) attributable to the associated flux term. The units of the accumulated heat ($\overline{Q}$) terms are "gram-calories" (g cal). The fluxes shown in Figure 13 may be summed to give the heat flux equation:

$$Q^* + Q_E + Q_H + Q_T + Q_W + Q_F + Q_I = 0 \qquad (1)$$

where: $Q^*(-)$ is the net radiation flux of downward and upward solar, terrestrial, and atmospheric radiation (the negative sign indicates that the net radiation is directed downward and results in a net gain of heat by the system);

$Q_E(+)$ is the heat loss by the system due to the latent heat flux between the surface and the atmosphere (a positive sign indicates that a heat loss is due to evaporation; a negative sign would indicate that a heat gain was due to condensation);

$Q_H(+)$ is the upward transfer of sensible heat from the surface to the atmosphere and represents a heat loss by the system;

$Q_T(-)$ is the heat input due to the Mackenzie River freshet and represents a heat gain by the system;

$Q_W(+)$ is the heat used to warm the water in the upper layer of the ocean (a negative sign indicates that heat was released to the system from cooling of the water column);

$Q_F(+)$ is the heat used to warm the ice and subsequently melt it in place (a negative sign would indicate that freezing and cooling of the ice had occurred); and

$Q_I(+)$ is the heat used to melt imported ice (a negative sign would indicate that ice had been exported and that heat which would have been required to melt the ice is now available in the system as a gain of heat). Q_I is essentially the difference between the atmospheric heat Q_A and the sum of Q_T, Q_W and Q_F which in the absence of ice advection and errors in the other terms, would be zero.

Equation (1) may be simplified by grouping of the fluxes as atmospheric and oceanic. Thus

$$Q_A = Q^* + Q_E + Q_H \tag{2}$$

where Q_A (-) is the resultant atmospheric flux downward; and

$$Q_S = Q_T + Q_W + Q_F + Q_I \tag{3}$$

where Q_S (+) is the resultant oceanic flux or storage change in the water column and ice cover. The positive sign indicates that there has been an increase in stored energy in the water column and ice cover (as would be expected in the Arctic summer). A negative sign would indicate that there had been a decrease of stored energy (as would be expected in the Arctic winter).

The heat flux Equation (1) may now be written in simplified form by combining Equations (2) and (3) such that:

$$Q_A + Q_S = 0 \tag{4}$$

Each flux term ('Q') is associated with an accumulated heat term ('$\overline{Q}$'). Therefore by writing Equation (1) in terms of accumulated heat, the expression for the heat budget equation (Equation (5)) is derived:

$$\overline{Q}^* + \overline{Q}_E + \overline{Q}_H + \overline{Q}_T + \overline{Q}_W + \overline{Q}_F + \overline{Q}_I = 0 \tag{5}$$

where each term represents the accumulated heat or time integral of the related flux.

$\bar{Q}^*$ is the accumulated heat due to the net radiation;

$\bar{Q}_E$ is the accumulated latent heat;

$\bar{Q}_H$ is the accumulated sensible heat;

$\bar{Q}_T$ is the accumulated Mackenzie River heat;

$\bar{Q}_W$ is the accumulated heat used in warming the upper layers of the ocean;

$\bar{Q}_F$ is the accumulated heat used in warming and melting the ice in place (and is directly related to the ice coverage); and

$\bar{Q}_I$ is the accumulated heat due to ice advection.

Just as was done for the fluxes, Equation (5) may be simplified to

$$\bar{Q}_A + \bar{Q}_S = 0 \qquad (6)$$

where $\bar{Q}_A$ (-) is the accumulated heat due to the atmospheric fluxes representing a gain of heat by the system; and

$\bar{Q}_S$ (+) is the accumulated storage heat due to oceanic fluxes and represents the increase of stored energy in the water column and the ice cover. In words, Equation (6) says that the net heat gained by the system ($\bar{Q}_A$) is stored as energy in the system ($\bar{Q}_S$).

B. ASSUMPTIONS

The heat budget calculation is limited in its accuracy because it was not possible to obtain all the data required for a complete calculation of each term. The balance is also limited by uncertainties in each term which are discussed later in Section III. The following assumptions were made in the determination of the heat budget.

1. Start Time

It was assumed that the accumulation of heat began on May 1 of each study year, that being the approximate date that the ice breakup begins offshore of the landfast ice according to climatology [Markham, 1975]. The accumulated heat terms, $\overline{Q}$, are all zero on May 1. This amounts to assuming that all water columns are isothermal at -1.5°C, the reference temperature for the heat calculations. This is a reasonable assumption in view of Spring observations reported by Herlinveaux, de Lange Boom and Wilton (1976) which support the idea of an isothermal water column containing no heat relative to the reference temperature. The satellite photos for the early spring of 1975 (Figure 6) show that the open-water area in late March and early April was almost completely ice-covered again by May 1. Any heat that was absorbed by the open water during the period before May 1 can be safely assumed to have been extracted by the advection of ice into the region in the last week of April. The Mackenzie River input does not begin until mid-May after thawing begins [Davies, 1975].

2. Incident Shortwave Radiation

Incident shortwave radiation fluxes over the study area were assumed to be the same as those measured at Sachs Harbor [Department of the Environment (Canada) Radiation Summary, 1974 and 1975] until the time that the marine observations became available. Then values of incident solar radiation fluxes were used as discussed in Section III.C.1.a.

3. Albedo

The ice albedo was taken to be 80% until the end of May and then diminished stepwise linearly to 30% in July as puddling occurred at the height of the ice melt. Later for August the ice albedo was a slightly greater 40% corresponding to melting but drained ice. Over open water an albedo of 7% was used (see Table 1, Section III.C.1) [Orvig, 1970 and Sellers, 1965]. The effective albedo over the study area was calculated using the ice concentration, ice albedo, and open water albedo.

4. Cloud Amounts

The cloud amounts for the period from May 1 to the start of marine observations were the climatological averages reported by Burns (1974). During the period of marine observations in August, the cloud cover was assumed to be the same throughout the study area as that reported at the actual location.

5. Sensible and Latent Heat Fluxes

Sensible and latent heat fluxes over ice and water were based on climatology [Burns, 1973] for the period from

May 1 to the start of marine observations after which they were calculated based on actual observed parameters existing in the study area.

6. Mackenzie River Discharge

No discharge volumes were available for 1975. Because there is little inter-annual variation in discharge volumetric rates [Herlinveaux, 1976] it was assumed that the discharge rates for 1972 (a similarly good ice year) could be applied to 1975 (see Section III.D.1). This was assumed to be the only current advecting heat through the boundaries of the study area. The surface currents within the area vary considerably, but residual currents appear to be weak and would therefore cause little heat change by advection when compared to the river's heat input during the summer.

7. Heat Content of the Water

Temperature measurements were never taken right to the bottom so that the heat content below the deepest water temperature measurements was unknown. As such, it was assumed to be zero. When water temperatures were below -1.5°C (the reference temperature), there was little error, but in shallow water where temperatures often remained high right to the bottom, the calculated heat content will be less than the actual heat content of the water. This error will result in a consistent underestimate of $\overline{Q}_W$. The heat content below an ice surface was assumed to be zero.

8. Ice

a. Ice Temperature

It was assumed that the ice temperature was -7°C on May 1, that it warmed to 0°C throughout the entire thickness by May 15 and that it remained at 0°C for the duration of the summer, until freezing began again in September. Vapor pressures over ice were calculated based on a surface temperature of 0°C. There is some argument for assuming that ice surface temperatures can rise above 0°C due to warming of the melt water [Vowinckel and Orvig, 1964] which could result in small errors in the calculation of back radiation and smaller errors in the calculation of the latent and sensible heat fluxes over ice. It was further assumed that no heat was stored in the ice.

b. Ice Coverage

Ice coverage was determined from semi-monthly satellite photos for May and June and from weekly historical ice charts provided by the Atmospheric Environment Service of the Department of the Environment (Canada) for the period in which they were available. The ice coverage was assumed to be accurate to within 10%, and constant between successive records.

c. Ice Thickness

The ice was assumed to be a uniform layer two meters thick.

d. Ice Density

The density of sea ice was taken as 0.92 gm cm^{-3} with an initial salinity of 4‰.

e. Ice Melting and Advection

These terms, Q_F and Q_I, and the related accumulated heat terms $\bar{Q}_F$ and $\bar{Q}_I$, are discussed in greater detail in Section III.D. It should be pointed out here, though, that there is considerable overlap in the expression of the energy devoted to each of these terms in the equation. The following assumptions were made:

(1) Any decrease in ice coverage was due to the melting of ice in place and resulted in an increase in $\bar{Q}_F$, the heat used to melt the ice (Q_F is a positive flux since it represents heat lost by the system to melt ice in place);

(2) Any increase in ice coverage was due to the freezing of ice in place and resulted in a decrease of $\bar{Q}_F$, the heat released to the system by the freezing of the ice (Q_F is a negative flux since it represents a heat gain by the system). It will be seen that there is considerable artificiality in these two assumptions with regard to melting and almost complete artificiality with regard to freezing, since freezing during this period is actually slight. This arbitrary technique was followed as a convenience since it was impossible to know the real situation. Errors produced here are reflected reciprocally in the Q_I term.

(3) Ice advection $\bar{Q}_I$ is used to account for the balance of heat remaining in the equation. It is obtained as a direct

result of balancing the heat budget equation, not from any estimate of the physical processes. If Q_I is a positive flux, it represents a volume of ice being imported, since that represents a heat loss to the system in that the entire volume of imported ice must be melted so that the ice coverage does not change. If Q_I is a negative flux, it represents a volume of ice being exported, since that represents a heat gain to the system such that the volume of ice exported does not require heat from the system to melt the ice to obtain the ice coverage observed.

The values obtained for Q_I were then compared with the direction of ice advection expected from the observed winds. Offshore winds should result in ice export; onshore winds should result in ice import. Because the direction of the Q_I flux term corresponded to the prevailing winds, it was assumed to be representative of what had actually happened in the study area. The term $\bar{Q}_I$ represents the accumulated effects of advection during the entire period of the heat budget calculation.

C. ATMOSPHERIC HEAT FLUX Q_A

The calculation of atmospheric fluxes was based on meteorological data provided on magnetic tape from the historical files of the National Weather Records Center at Asheville, North Carolina. These records are filed by 10° Marsden Square, year, and month and comprise all known observations. Figure 14 shows the distribution of the 33 observations used

in the month of August 1974. The marine observations were confined to the narrow band of open water near the coast. Figure 15 shows the distribution of 159 observations used in the month of August 1975. These observations were more evenly distributed throughout the open-water area, but heavily weighted by the 39 observations in Marsden sub-square 982[1] east of Herschel Island. Each marine observation was taken to be representative of conditions over the entire study area at that time. In a few cases, simultaneous observations taken in different places were averaged and applied to the entire study area. About one-third of the observations in both years were either incomplete or inaccurately recorded and were therefore not suitable for use in the calculation of the atmospheric fluxes.

No marine observations existed before the beginning of August in each year. For these months, climatological data were used [Burns, 1973] to determine the atmospheric fluxes from May 1 to the beginning of the marine observations.

1. Net Radiation Q*

Q* is the net radiation flux of downward and upward solar, terrestrial, and atmospheric radiation. It has two components, shortwave radiation and longwave radiation, each of which has both an upward and a downward element [Walker, 1975]. Thus Q* may be expressed by Equation (7):

---

[1]See Appendix I for explanation of the Marsden Square grid system used.

$$Q^* = K\downarrow + K\uparrow + L\downarrow + L\uparrow \quad (7)$$

where

$K\downarrow$ is the incident shortwave radiation (a negative sign because it is directed downward and represents a heat gain to the system);

$K\uparrow$ is the reflected shortwave radiation (a positive sign because it is directed upward and represents a heat loss to the system);

$L\downarrow$ is the incident longwave radiation (also called downward infra-red, a negative sign because it is directed downward and represents a heat gain to the system); and

$L\uparrow$ is the back radiation or upward infra-red radiation (a positive sign because it represents a heat loss to the system).

These terms are discussed more fully in the following sections.

a. Shortwave Radiation ($K\downarrow + K\uparrow$)

The net shortwave radiation depends on the incident shortwave radiation and the surface albedo such that

$$K\downarrow + K\uparrow = K\downarrow(1 - A) \quad (8)$$

where A is the albedo of the surface and represents the fraction of the incident shortwave energy which is reflected.

The incident shortwave radiation $K\downarrow$ depends on several factors including the altitude of the sun, the duration

of daylight, the composition of the atmosphere, the cloud cover and the cloud type. Of these, the altitude of the sun and the duration of daylight are accurately known for any given position. The composition of the atmosphere varies according to the general circulation of the atmosphere and related synoptic systems combined with such local effects as the presence of open water and sources of local pollution. This factor was not considered directly. The cloud cover over the entire study area was assumed to be that recorded in the marine observations. The cloud type was generally unknown and was not considered.

Incident radiation values were available from monthly summaries of hourly radiation for Sachs Harbor and Inuvik, both near the rim of the study area. The daily totals of incident solar radiation $K\downarrow$ were plotted for each site and compared (Figure 16). The maximum downward values of radiation from both years were assumed to define a curve of maximum clear-sky radiation in the study area.

Laevastu (1960) predicts somewhat higher values in the early part of the period and lower values in the later part. The actual curve used was a compromise between the observed and the predicted values. This curve is shown in Figure 16. The daily values from this curve were then multiplied by a factor (1 - fraction of cloud cover) using a curve based on cloud amounts from ship observations in the study area (Figures 30 and 33 of Appendix A) to obtain the calculated

incident solar radiation (Figure 16). In each case, it was assumed that the ship observations were representative of the entire study area. When no ship observations were available (as in the period from May 1 to the beginning of August) the radiation values at Sachs Harbor were taken as representative of the study area (Figure 17A). The May and June 1975 $K\downarrow$ values are approximate because of equipment problems reported at Sachs Harbor. In July and August, 1975, the incident solar radiation at Sachs Harbor was less than during the same period in 1974. This was due to the fact that there was greater cloud cover in 1975 because of the larger expanse of open water in the Southeastern Beaufort Sea. The cloud cover was presumably even greater over open water, thus accounting for the reduction in calculated incident solar radiation compared to the observations at Sachs Harbor and Inuvik (Figure 16).

When the solar radiation reaches the earth, part of it is reflected and the remainder is absorbed. Solar radiation has some capability of penetrating ice and water [Maykut and Grenfell, 1975] and to a lesser extent snow [O'Neill and Gray, 1972]. The percentage absorbed is a function of the albedo, A, which is an important factor in the heat budget of the Arctic [Langleban, 1971], and is a function of the texture, wetness, and color of the surface, the angle of incidence of the solar beam and atmospheric scattering. Albedo usually increases with decreasing solar altitude and decreases

with increasing wetness. Snow and ice reflect most of the sun's rays and have a high albedo. Water has a low albedo, depending on the angle of incidence. The albedo is particularly important in the Spring when the change from ice and snow to water causes it to change suddenly. Table 1 shows representative values of albedo over various surfaces (after Sellers, 1965 and Orvig, 1970). Note the change from snow and ice (albedo 65%) to water in the summer (albedo 7%). Thus the net shortwave radiation is highly dependent on the effective albedo for the study area.

b. Longwave Radiation ($L\downarrow + L\uparrow$)

The net longwave radiation is the sum of the incident longwave radiation and the back radiation. The incident longwave radiation $L\downarrow$ is also referred to as the downward infra-red radiation and is the longwave radiation from the atmosphere, from moisture, and carbon dioxide in the air, and from clouds. The back radiation $L\uparrow$ is also known as the upward infrared radiation and depends on the emissivity of the surface and its temperature.

The expression used to calculate the net longwave radiation is based on Sverdrup (1942):

$$L\downarrow + L\uparrow = \varepsilon \sigma T^4 (1 - 0.44 - 0.08 \sqrt{e})(1 - 0.083C) \quad (9)$$

where

ε is the emissivity;

TABLE 1

Typical values of albedos over various surfaces
(after Orvig, 1970, Sellers)

Structure	Water Content and Colour	Albedo % Average
Freshly fallen snow	dry bright-white clean	88
Freshly fallen snow	wet bright-white	80
Freshly drifted snow	dry clean loosely packed	85
Freshly drifted snow	moist grey-white	77
Snow, fallen or drifted 2-5 days ago	dry clean	80
Snow, fallen or drifted 2-5 days ago	moist grey-white	75
Dense snow	dry clean	77
Dense snow	wet grey-white	70
Snow and ice	dry grey-white	65
Melting ice	wet grey	60
Melting ice	moist dirty grey	55
Snow, saturated with water (snow during intense thawing)	light green	35
Melt puddles in first period of thawing	light blue water	27
Melt puddles, 30 100 cm deep	green water	20
Melt puddles, 30 100 cm deep	blue water	22
Melt puddles covered with ice	smooth grey-green ice	25
Melt puddles covered with ice	smooth ice, covered with icy white hoar frost	33
Water surfaces	Winter 60°N	21
Water surfaces	Summer 60°N	7
Soil	dark	10
Soil	moist grey	15
Soil	dry sand	35

TABLE 1 (CONT.)

Structure	Water Content and Colour	Albedo % Average
Cloud	overcast cumuli-form	80
Cloud	stratus	70
Cloud	Altostratus	49
Cloud	Cirrostratus	47

σ is the Stefan-Boltzman constant

($\sigma = 1.18 \times 10^{-7}$ ly day^{-1} $°K^{-4}$);

T is the surface temperature (°K);

e is the vapor pressure of the atmosphere (mb); and

C is the cloud amount (tenths).

The surface temperatures are a minor source of possible error since they were bucket temperatures or temperatures measured at the sea-intake of the vessel. In any case, they were not the skin temperatures required in Equation (9). The error could be even larger in calculations over ice surfaces where the temperature was assumed to remain at 0°C, whereas considerable heating of melt water on the ice surface can occur (see Section III.B.8). The vapor pressure, e, was calculated using wet-and-dry bulb temperatures read from a vessel's bridge and subject to errors due to the presence of the vessel. Possible cloud amount errors arise due to errors in reporting and the assumption that the cloud amount was the same over the entire area.

c. Summary of Net Radiation Q*

Figure 17B compares the net radiation for 1974 and 1975. The net radiation Q* was significantly greater early in 1975 than during the corresponding period of 1974. This was presumably due to the greater expanse of open water in early 1975 which reduced the effective albedo allowing more radiation to penetrate the ocean. By mid-July, this effect was reduced by the more extensive cloud cover over the study

area in July and August of 1975. By reducing K↓, the net radiation was correspondingly reduced. In August, during the period of marine observations there was a correspondence between small Q* fluxes and onshore winds mainly due to the increased cloud cover during those periods. With offshore winds, clear skies usually persisted allowing larger amounts of incident solar radiation K↓ to penetrate.

The daily variation for radiation fluxes observed in August is shown in Appendix B.

2. Latent Heat Flux Q_E

a. Evaporation

The rate of evaporation depends on the deficiency of water vapor in the air immediately above the water surface and the rate at which the air is mixed. Mixing depends on the turbulence of the air, which is a function of wind speed and thermal convection. The amount of evaporation is often calculated from climatic data by the Sverdrup formula [Walmsley, 1966 and Huyer and Barber, 1970]. Thus,

$$E = K V (e_w - e_a) \qquad (10)$$

where E is the rate of evaporation of water (mm day^{-1});

K is an empirical coefficient;

V is the wind speed (m sec^{-1});

e_w is the water vapor pressure at the surface (mb);

e_a is the water vapor pressure in the air (mb).

There are other equally good formulae, but because Sverdrup's is so widely used it forms a basis for comparing heat budget calculations for different regions. Furthermore, in a summary of available evaporation formulae, Swinbank (1959) concludes that no fundamental improvement over the Sverdrup formula is available at present [Walmsley, 1966].

It has been found that the coefficient K varies with wind speed. The critical wind speed separating turbulent and smooth flow is generally taken as 12 knots. Lacking any information to the contrary, Walmsley's (1966) procedure was followed, where the evaporation coefficients for both water and ice surfaces are:

$$K = \begin{cases} 0.145 , & V > 6.2 \text{ m sec}^{-1} \\ 0.090 , & V \leq 6.2 \text{ m sec}^{-1} . \end{cases}$$

b. Vapor Pressure

Again, following Walmsley (1966) the Clausius-Clapeyron equation may be written in the form:

$$e = 6.11 \exp\left[\frac{M_v L}{R^*}\left(\frac{1}{273} - \frac{1}{T}\right)\right] \qquad (11)$$

where

M_v is the molecular weight of water vapor;

R^* is the universal gas constant; and

$M_v/R^* = 9.08 \text{ gm cal}^{-1} {}^\circ\text{K}$.

An explanation of the terms e, T, L in four different situations is given below.

(1) For the vapor pressure at eight meters above the surface:

$e = e_a$

$T = T_d$, the dew point temperature (°K); and

$L = L_v$, the latent heat of vaporization (cal gm^{-1}).

(2) For the saturated vapor pressure just above a water surface:

$e = e_w$

$T = T_w$, the sea surface temperature (°K); and

$L = L_v$.

(3) For the saturated vapor pressure just above an ice surface:

$e = e_i$

$T = T_i$, the ice surface temperature (°K); and

$L = L_s$, the latent heat of sublimation (cal gm^{-1}).

(4) For the saturated vapor pressure just above a melt-water surface:

$e = e_i$

$T = T_i$

$L = L_v$.

It was further assumed that if the temperature were greater than 0°C, the ice surface was a melt-water surface (Case 4 above), and if the temperature were less than or equal to 0°C, Case 3 above applied. The values for latent heat were taken from Hess (1959):

$L_v = 597.3$ cal gm^{-1} ; and

$L_s = 677.0$ cal gm^{-1} .

c. Latent Heat Flux

An expression for Q_E is

$$Q_E = p\ L\ E \qquad (12)$$

where

p is the density of water (gm cm^{-3});

L is the latent heat (cal gm^{-1}); and

E is the rate of evaporation (cm day^{-1}).

By combining Equations (10) and (11) and substituting into (12), the latent heat fluxes can be calculated using the observed meteorological data. Condensation is interpreted as negative evaporation and is a downward flux.

Sublimation is considered the same as melting followed by evaporation in the case of an upward flux, or condensation followed by freezing for a downward flux.

The terms Q_E and L in Equation (12) are further defined for two particular cases:

(1) Evaporation over an open-water surface:

$$Q_E = Q_E \text{ (water)}$$

$$L = L_v$$

(2) Evaporation over an ice surface or melt-water surface:

$$Q_E = Q_E \text{ (ice)}$$

$$L = L_s .$$

In this study, evaporation occurred from the surface of the Southeastern Beaufort Sea which was always at least partly ice-covered. The latent heat flux was calculated for each surface separately and then a weighted average of the fluxes over the ice surface and the open-water surface was taken:

$$Q_E = Q_E \text{ (ice)(CONC)} + Q_E \text{ (water)(1 - CONC)} \qquad (13)$$

where CONC is the ice coverage in tenths.

Figure 17C compares the latent heat fluxes for 1974 and 1975 in the study area. The fluxes were small in

both years but higher in 1975 due to the larger area of open water over which evaporation could take place. In August, the standard deviation of the calculated latent heat fluxes for each wind condition is also shown. It can be seen that there is great variability even under similar wind conditions. Generally, though, onshore winds cause evaporation due to the cold dry air blowing from the ice over the water. Offshore winds result in condensation as the warmer continental air is cooled and becomes saturated.

The daily variations in observed latent heat fluxes for August of each year are shown in Appendix B.

3. Sensible Heat Flux Q_H

The sensible heat flux at the surface depends mainly on the vertical temperature gradient. Again, following Walmsley (1966) and Huyer and Barber (1970), Shuleikin's (1953) formulae were used to calculate the sensible heat flux. If the surface temperature was warmer than the air temperature ($T_s > T_a$), Shuleikin (1953) used no wind factor in his formula for computing the exchange of sensible heat. The instability in the air caused by the temperature gradient created sufficient turbulence to maintain the mixing process. In this case:

$$Q_H = 30.24(T_s - T_a) \quad \text{for} \quad T_s > T_a \qquad (14)$$

where

T_s is the surface temperature (°C)

T_a is the air temperature (°C).

On the other hand, if the water were cooler than the air, Shuleikin (1953) used Equation (15) where wind speed was considered an important factor to maintain the mixing in spite of the stable temperature gradient. In this case:

$$Q_H = 0.42\ V(T_s - T_a) \quad \text{for} \quad T_s \leq T_a \qquad (15)$$

where V is the wind speed in (m sec^{-1}).

It is also important to note that the Shuleikin formulae (Equation (14) and (15)) were originally derived for use over partially ice-covered water surfaces [Matheson, 1967]. In this study, the sensible heat flux over the area is a weighted average of the fluxes over the ice surface and the open water. The weighting is determined using an equation similar to Equation (13).

Figure 17D compares the sensible heat fluxes for 1974 and 1975 in the study area. The fluxes were small in both years, but the losses were slightly greater in 1975 because of the higher water temperature and the greater expanse of open water through which sensible heat could be lost from the system. In August, the standard deviation of the calculated sensible heat fluxes for each wind condition are also shown. In 1974, the greatest heat loss corresponds to the post-northwest wind period. In 1975, the greatest heat loss corresponds to onshore winds blowing cold polar air from the ice over the study area. The daily variations in observed sensible heat fluxes for August of each year are shown in Appendix B.

4. Atmospheric Heat Flux Q_A

From Equation (2),

$$Q_A = Q^* + Q_E + Q_H \qquad (2)$$

Summing the individual fluxes discussed previously gives the resultant atmospheric flux shown in Figure 18. A comparison of the 1974 and 1975 fluxes shows that the heat gain early in the season in 1975 was much greater than in 1974 due to the large expanse of open water into which solar radiation could penetrate. This more than compensated for the increased upward fluxes of Q_E and Q_H in 1975. From mid-July to the end of the season, the atmospheric fluxes were comparable in both years. In the month of August, standard deviations of the mean atmospheric fluxes are shown for each wind condition. In spite of the great variability, it can be clearly seen that onshore winds, originating over the polar pack, result in heat losses by the system. Offshore winds, originating over the warmer continental land mass, cause heat input to the system.

Figure 19 shows the accumulated heat content due to the atmospheric fluxes starting from May 1. The large excess of accumulated heat absorbed by the system by mid-June 1975 remains about constant during the remainder of the study period.

The values obtained for the atmospheric fluxes in the Southeastern Beaufort Sea during the summers of 1974 and 1975 were compared to results obtained by Walmsley (1966) in Baffin

Bay for the period 1919-1942, and to the results obtained by Huyer and Barber (1970) for Barrow Strait in 1962 (Figure 20), which agree well with the present data. It can be seen that in general in the Arctic Seas, the atmospheric fluxes reach a maximum downward at about the same time as the maximum open water, usually shortly after the summer solstice.

D. OCEANIC HEAT FLUX (STORAGE CHANGE) Q_S

The storage change Q_s is defined in Equation (3) as the summation of the individual oceanic fluxes such that:

$$Q_S = Q_T + Q_W + Q_F + Q_I \qquad (3)$$

(see Section III.A for definition of terms). The accumulated storage heat $\overline{Q}_S$ equals the time integral of the sum of the oceanic fluxes such that:

$$\overline{Q}_S = \overline{Q}_T + \overline{Q}_W + \overline{Q}_F + \overline{Q}_I \qquad (16)$$

(see Section III.A for definition of terms). Each term will be discussed separately in the following sections. Figure 21 summarizes each flux term and Figure 22 summarizes the accumulated heat terms. Further references will be made to each of these figures in the applicable section.

1. Mackenzie River Heat Q_T

Mackenzie River water enters the Southeastern Beaufort Sea through three main channels [Davies, 1975]. About one-third of the flow enters Shallow Bay, about one-third enters

Kugmallit Bay, and the remainder stays in Middle Channel until it reaches Mackenzie Bay in the vicinity of Richard's Island. Figure 23 shows the annual variation for the year 1974/1975 of the thickness of landfast ice in Mackenzie Bay, the river temperature, and the river discharge volume. It can be seen that the landfast ice is about two meters thick in May and remains at about the same thickness until breakup in July, which follows closely after the peak freshet in early June. The maximum river water temperature does not occur until late July. The inter-annual variations in river-water temperature appear small [Fraker, 1979]. Discharge volumetric rates vary only slightly from year to year [Herlinveaux, 1976]. Since no discharge rates were available for the summer of 1975, the discharge rates for 1972, a similarly good ice year, were used.

The river's heat contribution, Q_T, was calculated by multiplying the net discharge volume between particular dates by the water temperature relative to the reference temperature of -1.5°C. These quantities were both reasonably well known. The river was assumed to be the only source of heat due to water mass advection across the boundaries of the study area. The deep water remains cold and contains little heat (if any) relative to -1.5°C. The surface currents within the area vary considerably but residual currents appear to be weak and would cause little heat change by advection.

Figure 21A shows the variation of Q_T during each summer season, and Figure 22 shows the accumulated heat contribution

$\bar{Q}_T$. The major heat input occurs with the combination of large discharge volumes and high temperatures about mid-July. The heat from the river varies little from year to year and remains about 2.2×10^{18} g cal in both 1974 and 1975.

2. The Heat Used to Warm the Water in the Upper Layer of the Ocean Q_W

The oceanographic data which were used in calculating the heat content of the upper layer of the sea were collected as part of the Beaufort Sea Project, a set of environmental studies carried out in the Southeastern Beaufort Sea in 1974 and 1975 [Herlinveaux, 1976]. During the summer of 1974, profiles of salinity, temperature and turbidity were obtained from MV THETA, an ice-strengthened vessel resembling a North Sea trawler. Sixty-three stations were occupied during the period August 12 to September 1, 1974 (Figure 24). In the summer of 1975, similar observations were made at forty-eight stations during the period 5-24 August 1975 (Figure 25). The water temperatures versus depth at each oceanographic station in these two years were used to determine the heat content of the water column in the study area.

The calculation of this term depends on the mean layer temperature above the -1.5°C isotherm and its depth. The calculations were based on recorded CTD casts [Herlinveaux, 1976]. The heat content of the water column was generally underestimated since it was assumed that the heat content below the deepest temperature reading was zero (Section III.B.7). In shallow water, where the temperatures were warm, considerable

error may have been introduced to a maximum of about 5% underestimate of the heat content at any one time.

The oceanographic observations were then grouped into Marsden sub-sub-squares (see Appendix I) and their respective heat contents were averaged to obtain a heat content for each sub-sub-square. These mean heat content values in each sub-sub-square were summed to obtain the total heat content of the study area at the time of the oceanographic observations in August of each year. The heat content of the water column in August 1974 was calculated at three different times corresponding to each of the three different wind regimes. The corresponding variation in $\bar{Q}_W$ is shown in Figure 22. From these accumulated values, the Q_W fluxes were determined by difference and are plotted in Figure 21B which shows that the heat flux indicates cooling of the water column during onshore winds and warming of the water column during offshore winds (refer to Figure 11 for wind vectors). A similar calculation could not be done for August 1975 because the entire period of oceanographic stations was considered as a single synoptic period for purposes of calculating the heat content $\bar{Q}_W$. Thus Figure 21B shows the flux $Q_W = 0$. In Figure 22, the accumulated heat $\bar{Q}_W$ in August of each year can be compared. It can be seen that the heat content of 4.4×10^{18} g cal in 1975 was much higher than the heat content $\bar{Q}_W$ of 1.0×10^{18} g cal in 1974. The change in accumulated heat $\bar{Q}_W$ between May 1 and the time of the first of the oceanographic measurements is unknown, and is not shown in Figure 22. Because of this, the heat budget equation (Equation

(4)) can only be solved during the period of oceanographic observations. Further information obtained concerning the distribution of heat in the water column is shown in Appendix D.

3. The Heat Due to Cooling or Warming of the Ice and its Subsequent Freezing or Melting in Place Q_F

The ice coverage in the study area was determined from available satellite imagery and ice charts. Satellite imagery provided a semi-monthly look at the ice cover from May 1 until the end of June, after which ice charts provided weekly information until the end of September.

The calculation of $\bar{Q}_F$ was based solely on the determination of the ice coverage and concentration to determine the amount of heat lost in melting a certain area of ice-in-place. Based on the assumption of Section III.B.8, the heat required to raise the temperature of the ice from -7°C to 0°C and subsequently to melt the ice is the latent heat of fusion of approximately 79 cal gm^{-1}. The heat required to melt 1 km^2 of two-meter thick ice would be 0.15×10^{15} g cal km^{-2}. Since the total study area is 46,794 km^2, the heat required to melt a given area of ice can be quickly determined from Figure 26, which shows the relationship between ice coverage in the study area and the heat content $\bar{Q}_F$. For example, if the ice coverage observed throughout the study area were six-tenths, the heat $\bar{Q}_F$ used to melt the ice to obtain that open-water area by melting-in-place would be 3.1×10^{18} g cal.

Errors may arise due to unobserved changes in the ice cover which would result in changes in the effective albedo

of the area. Another possible error is that the ice is assumed to melt-in-place. This means that a decrease in the ice cover observed from one ice report to the next was assumed to be the result of melting only. If these changes in the ice cover were instead due to ice advection, the error introduced in this term would be balanced by a change in the ice advection term $\overline{Q}_I$ (see Section III.D.4). For example, if the ice cover in consecutive ice reports was seen to change from three-tenths to one-tenth, it would be assumed that the change was strictly due to the melting of two-tenths ice-in-place, rather than any combination of melting and advection. Figure 21C shows the heat fluxes Q_F corresponding to the observed ice coverage throughout the season. It can be seen that early in the season in 1975 there is a long period of decreasing ice coverage which led to the good ice conditions of that year; whereas, in 1974 in late May and early June the ice coverage was still increasing.

The accumulated heat $\overline{Q}_F$ is shown in Figure 22 and corresponds directly to the plot of open water area shown in Figure 10. Because the area of open water was much greater in 1975, the heat used to melt the ice-in-place was also much greater in 1975. The peak open-water period in 1975 occurred in the latter part of July, after which predominant northwest winds imported ice at a rate which exceeded the melting rate so that the open-water area decreased until the end of the season. There was a time lag of about one week at the end of

August between the minimum value of $\bar{Q}_F$ and the minimum value of the heat content of the water column $\bar{Q}_W$.

In 1974, the time for the maximum open water did not occur until mid-September after a prolonged period of easterly winds had made more heat available to melt the ice and to export it from the study area.

4. Heat Due to Ice Advection Q_I

As was previously indicated in Section III.B.8.e., the ice advection term, Q_I, together with Q_F are determined by difference. Q_I therefore contains all of the errors in the other terms. Nevertheless, it will be seen that it is of plausible magnitude, consistent between the two years and properly correlated with wind effects. If Q_I is a positive flux, it represents a volume of ice being imported, since that represents a heat loss to the system in that the entire volume imported ice must be melted so that the ice coverage does not change. If Q_I is a negative flux, it represents a volume of ice being exported, since that represents a heat gain to the system such that the volume of exported ice did not require heat from the system to melt the ice to obtain the ice coverage observed. Figure 21D shows the calculated Q_I fluxes for the period of oceanographic observations in each year during which Equation (5) could be solved. It can be seen that in August of 1974, the rate of ice export increased during the month, accounting for the increase in open-water area. Figure 22 shows the values for accumulated heat due to ice advection $\bar{Q}_I$. It can be seen that in both years, there was a net import

of ice throughout the season. In August 1974, the $\bar{Q}_I$ term is diminishing corresponding to an export of ice, especially at the end of the month. This is to be expected since the known winds were blowing offshore at this time and were pushing ice out of the study area. In August, 1975, there was continuous ice import (Figure 21D), accounting for the decrease in open-water area. Also, the $\bar{Q}_I$ term (Figure 22) is increasing corresponding to ice import. Thus the onshore direction of the winds during most of the latter part of August 1975 seems to have imported ice to the area.

The two curves of $\bar{Q}_I$ (Figure 22) cross each other in the last week of August at about the same time that the plot of open water (Figure 10) shows equal ice coverage in the study area. This occurs in spite of a vastly greater area of open water in July/August of 1975. Therefore there must have been a rapid import of ice during August 1975 due to the prevailing northwesterly winds (Figure 11).

The values obtained for $\bar{Q}_I$ represent a volume of advected ice. Using a calculation similar to that done in Section III.D.3 to calculate the heat of fusion of ice, 0.15×10^{15} g cal represents the advection of 1 km^2 of two-meter thick ice. Table 2 shows the estimated ice areas advected based on the calculation of Q_I.

E. SUMMARY OF THE HEAT BUDGET EQUATION

An example heat budget calculation was done for August 15 of the years 1974 and 1975 based on the values of the heat

TABLE 2

	$\bar{Q}_I$ g cal $\times 10^{18}$	change in $\bar{Q}_I$ g cal $\times 10^{18}$	ice area advected $km^2 \times 10^3$
1974 August 12	11.5	-2.1	-13.0
August 31	9.4		
1975 August 5	7.6	+3.2	+20.0
August 24	10.8		

(-) export of ice
(+) import of ice

budget terms assuming that all the heat started accumulating on May 1. The resulting heat budget equation is shown in Figure 27.

The greatest difference in the heat inputs from May 1 to August 15 was the net radiation term $\bar{Q}^*$. The appearance of open water and subsequent wind-mixing early in the season in 1975 during the period of maximum insolation allowed large quantities of radiation heat to be absorbed by the water column. This in turn made more heat available to the system to be used to melt ice ($\bar{Q}_F$). With more open water in 1975, the river heat, $\bar{Q}_T$, was allowed to spread over a larger area, rather than being dammed up by the ice as it was in 1974. The sensible heat, $\bar{Q}_H$, and the latent heat $\bar{Q}_E$ were about the same in each year and were roughly equal to the input of heat from the

Mackenzie River. The energy loss due to conversion of energy into stored heat in the upper layer of the ocean, $\bar{Q}_W$, was larger in 1975 as shown by the deep warm surface layer (see Appendix D). In 1974, the heat was restricted to a thin layer about 5-10 meters deep. A difference was that in 1975 increased turbulent mixing early in the season allowed the heat to be absorbed to much greater depths. The remaining ice advection term, $\bar{Q}_I$, used to balance the equation shows net ice import in both years. In spite of the import of ice in 1975, there was sufficient heat excess to keep the study area mainly ice-free throughout the month of August, thus making it a good ice year, in contrast to 1974 when there was insufficient heat in the water column to keep the area ice-free, thus making it a severe ice year.

IV. CONCLUSIONS

Data gathered during the Beaufort Sea Project in the summer of 1974 (a severe ice year), and in the summer of 1975 (a good ice year) were displayed and analyzed with special attention to the heat budget terms and the related heat fluxes. The heat budget equations were computed for each summer period and comparisons made to determine the relative importance of the various fluxes. The following conclusions resulted:

A. The major source of heat to the study area, regardless of the severity of the ice, is the contribution from solar radiation. However, the net radiation was a factor of two greater in 1975 (a good ice year) than in 1974 (a severe ice year) due principally to the much larger area of open water in 1975.

B. The wind pattern in early spring is critical in the final outcome of the heat budget. Offshore winds will produce an early breakup, allowing the large fluxes of incident solar radiation to be absorbed in the sea. Onshore winds (primarily from the northwest) press the pack-ice nearer the shore, causing most of the incident solar radiation to be reflected by the ice cover.

C. The wind patterns later in the summer are the major factor in determining the ice coverage by controlling its advection. Persistent offshore winds in the latter part of

August 1974 were responsible for a greater open-water area in September 1974 than was observed at the same time of year in 1975.

D. The heat contribution from the Mackenzie River varies little from year to year and is only about 10% to 20% of the heat input due to the net radiation. The river heat is responsible for local breakup in the vicinity of the Delta, but has negligible impact beyond the shelf.

APPENDIX A

SUMMARY OF MARINE SURFACE OBSERVATIONS

Figures 28 through 33 summarize the observations of air temperature, water temperature, dew point temperature, cloud amount, wind speed and wind direction as provided in the marine meteorological records obtained from the National Weather Records Center at Asheville, North Carolina.

The reader is reminded that these observations were from vessels operating on their preferred routes in the study area and that sequential observations may have been reported by different vessels operating at opposite ends of the study area under different meteorological conditions. Changes in water temperature, for example, are as likely due to a change of location of a vessel as an actual change in temperature at one location. Wind speed and wind direction tend to be consistent throughout the study area as supported by observations from drill ships in the Southeastern Beaufort Sea in later years [Milne, 1980].

APPENDIX B

DETERMINATION OF DAILY FLUXES IN AUGUST

The calculated atmospheric fluxes of sensible heat Q_H, latent heat Q_E, net radiation Q^*, the resultant atmospheric flux Q_A, and the relationship of atmospheric flux Q_A to wind direction are shown in Figures 34 through 39 for August of 1974 and in Figures 40 through 45 for August of 1975. Figure 46 summarizes the daily average atmospheric fluxes Q_A for August of each year. Figure 47 compares the accumulated atmospheric heat $\overline{Q}_A$ for August of each year showing the effects of ice cover on $\overline{Q}_A$.

1. Assumptions

The meteorological observations of Appendix A provided the raw data for calculating the atmospheric fluxes using Equations (7) through (15) as discussed in Section III.C. Three different assumptions were made, resulting in three sets of curves.

a. Open Water

It was assumed that the marine observations were taken in open water and that the calculated fluxes represent those which would have existed under the given environmental conditions if no ice were present.

b. Ice Covered

It was assumed that the marine observations were taken over an ice surface; that is, in effect a sheet of ice

was simply slid into place with no modification of the air mass overlying it.

c. Averaged over the Entire Area

During the study period, there was a known ice coverage in the study area at any given time. It was not known, however, what ice concentration existed at the reporting point. Since it was assumed that the observation was representative of the conditions over the entire study area at that time, the effects of ice had to be considered. This was done in each case with Equation (17) (similar to Equation (13)), where Q represents any atmospheric flux term.

$$Q = Q(\text{ice})(\text{CONC}) + Q(\text{water})(1 - \text{CONC}) \qquad (17)$$

2. Results

The main features of the graphs of atmospheric fluxes were consistent regardless of the source of the radiation values.[1] A summary for each element of the atmospheric flux term Q_A based on each of the above assumptions follows.

a. Sensible Heat Flux Q_H

Over open water, Q_H is directed upward (+) representing a heat loss to the system. Over ice, the flux is directed downward (-) representing a heat gain to the system

[1]Similar graphs were drawn based on observations at Sachs Harbor and Inuvik. These are not included in the discussion since no new information was gleaned from them. They showed the same directions of fluxes and same trends, although the magnitudes differed slightly.

whenever T_a is greater than 0°C (which it is for most of August). When averaged over the entire area, the direction of flux turns out to be dependent on the wind direction: Onshore winds cause upward Q_H; offshore winds cause downward Q_H. During onshore winds, cold, dry air blows across the ice towards the open water of Mackenzie Bay. If air temperatures are only slightly above freezing, very little air mass modification will take place until the winds blow over the water, at which time the cold air will warm and absorb large quantities of heat from the water column. When offshore winds blow, warm, continental air moves over the water. The air mass near the surface cools quickly to the water temperature to produce a stable, saturated air column which inhibits the sensible heat transfer, and results in a small downward transfer of sensible heat (a heat gain by the ocean).

b. Latent Heat Flux Q_E

Over open water Q_E is generally directed upward (+) (a heat loss from the system). Over ice, the flux is directed downward (-) as condensation occurs over the ice surface. When averaged over the entire area, the direction of flux again appears to be dependent primarily on wind direction: onshore winds cause evaporation and upward Q_E; offshore winds cause condensation and downward Q_E. The reasoning is similar to that given above.

c. Net Radiation Flux Q*

Over open water, Q* is generally directed downward because of the low albedo of the water. Over ice, it tends

to be directed upward because of the high albedo of the ice. When averaged over the entire area in August 1974, except when the cloud cover was less than three-tenths, Q* was directed upward because of the extensive ice coverage. In contrast, in August 1975, there was a greater open water area, and as a result, the curves for the open-water case and the entire area were very similar showing a general downward direction decreasing in magnitude as the season progressed and the incident solar radiation K↓ decreased.

d. Atmospheric Flux Q_A

These curves are the summation of each of the three previous curves for any particular case. The most striking feature is the dependence of direction of flux on wind direction which shows up in all cases. With onshore winds, Q_A is directed upward (heat loss from the ocean); with offshore winds Q_A is directed downward (heat gain by the ocean). This dependence is pictured more graphically in Figures 39 and 45 which plot heat flux Q_A versus wind direction for August 1974 and August 1975 respectively. To the left of the zero line represents a heat gain by the ocean. Notice that the major heat gains occur for offshore winds. The major heat losses occur during onshore winds, most notably northwesterly winds.

3. Summary

The results obtained for the atmospheric flux Q_A are summarized in Figure 46, showing the curves based on two of the assumptions, 1a, and 1c. (Since few observations were

likely taken in total ice cover, this case, 1b, is not shown.) Two features should be noted:

a. the heat losses are almost always greater over open water than averaged over the entire area, probably because the water is warmer and has more heat to lose;

b. the direction of heat loss is determined by wind direction (onshore or offshore).

The calculated daily fluxes for August were summed to obtain the net accumulated heat $\bar{Q}_A$ for each day of the month, using the first day of observations in each year as the zero point. The following features of Figure 47 are noted:

a. the accumulated heat loss over water is greater than that averaged over the entire area;

b. in August of both years there was a net loss during the month over the open-water area but a net gain of heat through the ice which resulted in a net gain of heat over the entire area; and

c. although the open-water area in August 1974 was less than in 1975, the loss of heat through that area was greater due to cooler air temperatures.

APPENDIX C

EXTREME VALUES OF HEAT FLUXES AND ASSOCIATED ENVIRONMENTAL CONDITIONS

Tables 3 through 6 inclusive list extreme values of atmospheric heat fluxes and the conditions that existed when they occurred.

1. Maximum Upward Fluxes

Table 3 summarizes the maximum upward fluxes as calculated over open water. Maximum sensible heat losses occurred during northwest winds, with cold polar air blowing over warmer water, and clear skies. The maximum latent heat losses were also found during northwest winds but in this case cloud amounts were moderately high at 7/10. The maximum net radiation flux also occurred during northwest winds and overcast skies. Finally, the maximum atmospheric flux Q_A occurred under identical conditions to the maximum latent heat loss, suggesting that the latent heat flux was a major contributing factor to high heat losses at the surface.

Table 4, summarizes the maximum upward fluxes as averaged over the entire area, taking into account the ice coverage at the time. Because of the small upward fluxes over ice, the extreme values over the entire area were generally less than those over open water alone. The exception is the net radiation where the high albedo of the ice cover increased the upward radiation flux.

TABLE OF EXTREME VALUES OF UPWARD FLUXES OVER WATER ONLY

TABLE 3	Flux (ly/day)	Date	Location by Marsden subsquare	Wind Dir.	Wind Speed (knots)	Air Temp. (°C)	Dew Point (°C)	Water Temp. (°C)	Cloud Cover (tenths)	Ice Cover (tenths)
SENSIBLE HEAT										
1974	223	15 Aug 74	230 974	320	4	0.0	0.0	7.4	1	8
1975	166	21 Aug 75	230 964	300	12	2.4	2.0	7.6	0	3
LATENT HEAT										
1974	281	17 Aug 74	230 972	310	13	4.1	0.0	8.4	7	8
1975	442	10 Aug 75	230 982	300	34	1.9	-2.0	4.2	7	2
NET RADIATION										
1974	19	22 Aug 74	230 982	330	6	0.0	0.0	0.9	9	6
1975	23	12 Aug 75	266 090	350	14	3.0	-2.0	7.5	9	2
ATMOSPHERIC FLUX Q_A										
1974	392	17 Aug 74	230 972	310	13	4.1	0.0	8.4	7	8
1975	477	10 Aug 75	230 982	300	34	1.9	-2.0	4.2	7	2

TABLE OF EXTREME VALUES OF UPWARD FLUXES OVER THE ENTIRE AREA

TABLE 4	Flux (ly/day)	Date	Location by Marsden subsquare	Wind Dir.	Wind Speed (knots)	Air Temp. (°C)	Dew Point (°C)	Water Temp. (°C)	Cloud Cover (tenths)	Ice Cover (tenths)
SENSIBLE HEAT										
1974	45	15 Aug 74	230 974	320	4	0.0	0.0	7.4	1	8
1975	133	07 Aug 75	266 040	330	11	1.2	0.0	6.2	8	1
LATENT HEAT										
1974	111	20 Aug 74	230 974	300	32	0.0	-1.0	2.5	8	7
1975	379	10 Aug 75	230 982	300	34	1.9	-2.0	4.2	7	2
NET RADIATION										
1974	30	22 Aug 74	230 982	330	6	0.0	0.0	0.9	9	6
1975	28	21 Aug 75	266 052	260	13	2.4	2.0	7.6	8	3
ATMOSPHERIC FLUX Q_A										
1974	153	20 Aug 74	230 974	300	32	0.0	-1.0	2.5	8	7
1975	397	10 Aug 75	230 982	300	34	1.9	-2.0	4.2	7	2

2. Maximum Downward Fluxes

Table 5 summarizes the maximum downward fluxes as calculated over open water. Maximum sensible heat gains occurred when winds blew offshore from 120° to 190° at fairly high speeds (23-32 knots), blowing warm, dry air from the land over the colder water. The sensible heat fluxes under these conditions seemed to be independent of the cloud amount. The maximum latent heat gains occurred under the identical conditions as the largest values of downward sensible heat flux. The maximum net radiation flux occurred under clear skies. Finally, the maximum atmospheric flux Q_A occurred under the identical conditions as the maxima of sensible and latent heat fluxes above. This indicates that the warm, dry, continental air was a major factor affecting the heat budget of the Southeastern Beaufort Sea.

Table 6 summarizes the maximum downward fluxes as averaged over the entire area, taking account of the ice coverage at the time. Because of the large downward fluxes over the ice, the magnitudes of the extreme values were generally greater than those over open water. The exception is the net radiation where high albedo of the ice cover increased the upward radiation flux.

TABLE OF EXTREME VALUES AT DOWNWARD FLUXES OVER WATER ONLY

TABLE 5	Flux (ly/day)	Date	Location by Marsden subsquare	Wind Dir.	Wind Speed (knots)	Air Temp. (°C)	Dew Point (°C)	Water Temp. (°C)	Cloud Cover (tenths)	Ice Cover (tenths)
SENSIBLE HEAT										
1974	-12	30 Aug 74	266 040	120	23	8.4	8.3	6.0	7	7
1975	-39	26 Aug 75	230 974	190	32	10.0	7.0	4.4	3	4
LATENT HEAT										
1974	-140	30 Aug 74	266 040	120	23	8.4	8.3	6.0	7	7
1975	-233	26 Aug 75	230 974	190	32	10.0	7.0	4.4	3	4
NET RADIATION										
1974	-181	26 Aug 74	230 964	150	17	8.8	8.0	6.6	0	6
1975	-268	6 Aug 75	266 040	260	4	4.8	4.0	6.4	0	1
ATMOSPHERIC FLUX Q_A										
1974	-262	26 Aug 74	230 964	150	17	8.8	8.0	6.6	0	6
1975	-387	26 Aug 75	230 974	190	32	10.0	7.0	4.4	3	4

TABLE OF EXTREME VALUES OF DOWNWARD FLUXES OVER THE ENTIRE AREA

TABLE 6	Flux (ly/day)	Date	Location by Marsden subsquare	Wind Dir.	Wind Speed (knots)	Air Temp. (°C)	Dew Point (°C)	Water Temp. (°C)	Cloud Cover (tenths)	Ice Cover (tenths)
SENSIBLE HEAT										
1974	-135	31 Aug 74	230 944	090	10	6.7	6.0	7.4	6	7
1975	-100	20 Aug 75	230 944	180	4	11.2	10.0	11.3	6	3
LATENT HEAT										
1974	-369	30 Aug 74	266 040	120	23	8.4	8.3	6.0	7	7
1975	-360	26 Aug 75	230 974	190	32	10.0	7.0	4.4	3	4
NET RADIATION										
1974	- 68	26 Aug 74	230 964	150	17	8.8	8.0	6.6	0	6
1975	-248	6 Aug 75	266 040	260	4	4.8	4.0	6.4	0	1
ATMOSPHERIC FLUX Q_A										
1974	-383	30 Aug 74	266 040	120	23	8.4	8.3	6.0	7	7
1975	-475	26 Aug 75	230 974	190	32	10.0	7.0	4.4	3	4

APPENDIX D

DISTRIBUTION OF HEAT IN THE STUDY AREA

1. Summer of 1974

As discussed previously, the 1974 data has been divided into three groups corresponding to the three synoptic conditions encountered during the study period; northwest winds from August 9 to 20; post-northwest winds from August 20 to 24; and easterly winds from August 25 to September 1. The following observations are noted.

a. Northwest Winds

During northwest winds, the pack-ice was pressed toward shore by the wind. Also, the surface currents close to shore tended to flow east following the coastline as shown in Figure 48 [MacNeill and Garrett, 1975]. The ice edge advanced southward into Mackenzie Bay south of Herschel Island. The heat content was highest at the mouth of the river as might be expected (Figure 49). Surface temperatures during this period ranged as high as 8°C in places. The maximum heat content of 6 kg cal cm^{-2} was located midway between Herschel Island and Pullen Island (Figure 49). The reason for this concentration of heat is unknown. However, it appears that this area of maximum heat content would have been the optimum position between the shallow, shelf waters which were bottom-limited in gaining more heat from the river and the deeper water near the ice-edge where heat was extracted from

the water in melting the ice. The river plume is well marked by the contours of the heat content. Figure 50 shows that the mean layer temperature was over 3°C near the river mouth. Figure 51 shows how the depth of the -1.5°C isotherm increases to seaward. Toward shore, in the shallow water over the shelf, the -1.5°C isotherm was bottom-limited.

b. Post-northwest winds

In the short period after the northwest winds stopped blowing, a relaxation seems to have taken place. For example, the surface currents immediately north of Richard's Island completely reversed direction form northeast to southwest (Figure 52). There was also a relatively strong westward flowing surface current from Shallow Bay to Herschel Island. The ice edge retreated slightly, especially in the vicinity of the warm core mentioned in the previous section. The contours of heat content moved shoreward, pushing the available heat in the water closer to shore (Figure 53). The mean temperature of the layer (not shown) had been similarly changed with the 0°C mean layer temperature paralleling the ice edge.

This short period of three days represents a transition stage between the northwest winds and the easterly winds. Figure 54 shows the onshore and offshore movement of Mackenzie River water due to these wind conditions. Because of the time lag in the water column, the heat content during this post-northwest wind period more closely resembles the situation during northwest winds in Figure 54 with the warmer

Mackenzie River water pressed near the shore. The corresponding heat content under conditions of easterly winds is discussed in the following section.

c. Easterly Winds

During the period of easterly winds from August 25 to September 1, the surface currents all flow westward (Figure 55) as might be expected [MacNeill and Garrett, 1975]. The heat content of the water (Figure 56) reflected the shifting of the upper five meters of warmer, less saline water as it slid over the deeper, colder, more saline water in response to the wind. There was a significant change in the edge of the ice pack as it retreated seaward north of Herschel Island. The Mackenzie River plume re-asserted itself to the northwest of Shallow Bay and a second tongue of warm water extended north of Richard's Island. The residual cold water was concentrated in a small area near Kay Point where the temperature of the surface water was less than 1°C.

Another feature not observed before lies north of Atkinson Point on the Tuktoyaktuk Peninsula. A tongue of warm water extended into the study area from Amundsen Gulf. This is believed to have been due to solar heating of the open-water area in the vicinity of the Bathurst Polynya. This area was ice-free much earlier in the season and was heated by solar radiation and wind-mixed to a greater depth than elsewhere. The easterly winds also tended to move this feature westward. This concept is supported by the depth of the -1.5°C isotherm shown in Figure 57. North of Atkinson Point, although

the mean layer temperature (Figure 58) is less than 0°C, the depth of the -1.5°C isotherm was over twenty-five meters so that there was a thick layer of cool water containing more heat than the thin layer of warmer water in the Delta area. The plumes of river water are readily identified in Figure 58 by the contours of mean layer temperature.

2. Summer of 1975

The data for 1975 are presented in a similar manner to that above. First, the month of August is examined in three different wind conditions: strong northwest winds from August 5 to 13; variable winds from August 13 to 19; and light northwest winds from August 20 to 24. Finally, the data from August 5 to 24 is looked at in total as a synoptic picture of the study area.

a. Strong Northwest Winds

During strong northwest winds, the surface currents flowed about the same as in August 1974 under similar wind conditions (Figure 48). In 1975, however, there was a much greater expanse of open water and more mixing occurred in the water column. Figure 59 shows the heat content in the study area during this wind condition. The pack-ice edge was on the northern boundary of the study area. The greatest heat content in the water was in the eastern portion of the study area. This supports the hypothesis made earlier that solar radiation incident on the large open-water area north of Cape Bathurst was responsible for early heating of the water column. Even though the upper layer temperatures were not high, the warm

water was deeply mixed giving it a high heat content. Figure 60 shows the mean layer temperatures, which were warmest near the river mouth, and gradually cooling as the ice edge approached.

b. Variable Winds

With the cessation of the northwest winds, there was a relaxation similar to that seen during the post-northwest period of August 1974. A similar current pattern was also established [MacNeill and Garrett, 1975]. The edge of the ice pack retreated to the north. The limit of open water also retreated to the north except in the west where it moved into Mackenzie Bay from west of Herschel Island (Figure 61). The greatest heat content in the water was north of Atkinson Point near the ice edge, but covering a much smaller area than during the northwest winds the week before. Figure 62 shows the mean layer temperature contours which roughly parallel the ice edge. The warmest water was near the river mouth in Kugmallit Bay but because it is so shallow, its heat content was less than that in the northeast part of the study area.

c. Light Northwest Winds

Light northwest winds brought a rapid drop in the air temperature resulting in the advection of ice into the area and reduced ice melting. The heat content of the water was greatly reduced from the previous period as it was chilled by imported ice (Figure 63). The river plume is clearly marked in Figure 64 by the 6°C contour of mean layer temperature.

Unfortunately, there were no data during this time period in the eastern half of the study area.

d. Synoptic Picture of August 1975

Figure 65 shows the heat content of the study area based on all available oceanographic data between August 5 to 24, 1975. The southern boundary of the polar ice-pack is marked by a series of X's. The average August position of the northerly limit of ice free water is marked with a dashed line. Two warm cores stand out. One is in the east and was probably a result of early season heating in the Bathurst Polynya. The second was northeast of Herschel Island and was probably caused by river run-off.

The mean layer temperature contours shown in Figure 66 confirm that the plume of warm river water contributes to the core of heat northeast of Herschel Island. As might be expected, the mean layer temperature decreases as one moves north from the coast to the ice-edge.

The depth of the -1.5°C isotherm is shown in Figure 67. Where waters are shallow closer to shore, temperatures of -1.5°C are not reached so that the depths shown are the depths of the deepest temperature measurements which were used in calculating heat content. The 25-meter and 30-meter depth contours of the -1.5°C isotherm exhibit an undulation northwest of Richard's Island. This feature is caused by a cold intrusion of Arctic surface water which will be discussed further. The greatest depths to the -1.5°C isotherm are found in the vicinity of the highest heat content, indicating significant

absorption of solar radiation and probably substantial wind-mixing in the open-water area to carry the heat to such great depths.

Figures 68, 69, 70 and 71 show temperature contours at depths of 5m, 10m, 15m, and 20m respectively which exhibit features of the heat distribution at those depths. At a depth of 5 meters (Figure 68), a plume of 8°C water extended northeast from Shallow Bay and another plume of 8°C water extended from Kugmallit Bay, also in a northeasterly direction. These high temperatures were from river water flowing out of the various channels of the Mackenzie River. In fact, in the river itself, temperatures reach as high as 20°C. Also in Figure 68, a core of cold water is evident just north of Richard's Island indicating that upwelling had occurred and that there was an inshore movement on the shelf of cold Arctic surface water from beyond the continental shelf. (The appearance of this feature is based on a single observation at Station 38, is not supprted by any additional observations, and may be a bogus feature.)

Figure 69 shows the temperature contours at a depth of 10 meters with features similar to those described at the 5-meter depth. Figure 70 shows the temperature contours at a depth of 15 meters and reveals several new features. A plume of 4°C water extended northeast of Shallow Bay associated with the 8°C plume at 5-meters depth. A second 4°C plume north of Kugmallit Bay is associated with the 8°C plume found

there. The 4°C contour continues to the far northeastern sector of the study area and reflects the existence of the warm water area north of Atkinson Point associated with early season heating in the Bathurst Polynya. Figure 70 also shows a core of cold water (less than -1.5°C) northwest of Richard's Island. This core of cold water could be a possible source of the cold water core seen at 5-meters depth north of Pullen Island. The reasons for its existence are not yet clear, but studies of bottom currents in the vicinity support an on-shelf motion at this depth [Milne, 1980].

Figure 71 shows the temperature contours at 20 meters depth. A large portion of the study area is bottom-limited at this depth. The warm plumes of river water noted above are barely discernible at this depth. The core of cold water (less than -1.5°C) northwest of Richard's Island is even clearer at this depth. Figure 71 also shows the extent of the warming of the water column in the northeastern part of the study area. Even at 20 meters, the temperature exceeded 4°C.

3. Comparison of Heat Distribution, 1974 and 1975

a. The surface current regime during northwest winds was similar in both years.

b. The surface current regime after northwest winds showed a similar relaxation in both years.

c. The heat content of the water was much higher in 1975, a good ice year, than in 1974, a severe ice year.

d. A warm water core in the vicinity of 70°N, 138°W existed in both years and with a comparable heat content.

e. A core of warmer water north of Atkinson Point apparently associated with the Bathurst Polynya was evident in both years.

f. The depth of the -1.5°C isotherm was a maximum of 15 meters in 1974, but extended to a depth of over 50 meters in 1975.

g. The maximum observed sea surface temperature in 1974 was 8.08°C at Station 11 on 17 August east of Herschel Island (Figure 24). In 1975, the maximum observed sea surface temperature was 8.70°C at Station 39 on 20 August north of Richard's Island (Figure 25). Both Stations were on the continental slope in about 60 meters of water. In spite of the great difference in severity of the ice, there was little difference in the maximum observed sea surface temperatures.

h. The thickness of the surface wedge of fresh, warm water was greatest near the Delta and decreased as the ice edge was approached.

APPENDIX E

SELECTED PROFILES AND CROSS-SECTIONS

1. Temperature, Density, and Salinity Profiles

Figure 72A shows the temperature, density and salinity profiles at Station 12 (see Figure 24 for location) which is typical of profiles seen in August 1974. Note that the thermocline, the halocline, and the pycnocline all lie between five and ten meters depth. There was a warm, fresh layer of water overlying the very cold saline water below. This thin layer of fresh water contained virtually all of the heat in the water column and carried it about under the direct influence of the winds and the river water movement. There was apparently very little mixing across the interface. Using the reference temperature of -1.5°C as the base depth of the layer for the purposes of calculating heat content, the layer depth at Station 12 in 1974 was 15 meters. That is, all the heat was in the top 15 meters of the water column.

This is in marked contrast to Figure 72B which shows the profiles at Station 13 (see Figure 25 for location) typical of a good ice year. The water at the surface was more saline and the gradients of temperature, density and salinity were more gradual. The heat had been mixed to a much greater depth. Using the reference temperature of -1.5°C as the base depth of the layer, the layer depth in 1975 was 27 meters, almost twice as deep as in a severe ice year.

2. Cross-section A

Figure 73 shows the location of cross-section A comprising Stations 20, 23, 24, 25, 26, and 27 during the period of August 21 to 23, 1974. The cross-section itself is shown in Figure 74. Along the coast, southeast of Herschel Island the water was still very cold (below 1°C) right up to the surface. Then to the east, a tongue of warmer, lower salinity water was encountered with surface temperatures up to 1.68°C. Further east, a tongue of much warmer and fresher water (4.43°C) was encountered. At Station 29, still further east (not included in the cross-section) warm water with surface temperatures over 6°C was encountered in the shallow inshore regions of eastern Mackenzie Bay. Below seven meters there was very little change in temperature except as the bottom shoals toward the east. At Station 28, the deepening of the -1.5°C isotherm can be easily seen. The density cross-section shows a marked pycnocline at eight to ten meters where the sigma-t rapidly changed from 5 to 20 due to the layer of fresher water (from river run-off and ice melt) overlying the oceanic water. The density structure was well-stratified.

3. Cross-section B

Figure 73 shows the location of cross-section B north of Richard's Island comprising Stations 41, 53, 54 and 57 taken during the period from August 25 to 30, 1974. The cross-section itself is shown in Figure 75; it shows the changes from close inshore off Richard's Island (depth 10 m)

northwest across the shelf to the edge of the continental slope. In the upper five meters, the effects of river run-off can be seen. The surface temperature at Station 41 was 5.18°C, gradually decreasing to almost 0°C at Station 54 near the ice edge. The most notable feature is the large mound or intrusion of water colder than -1.5°C between Station 53 and Station 57. This water appears to be Arctic surface water originating from the continental slope region of the Southeast Beaufort Sea.

The fresh-water effects can be seen in the density cross-section to diminish as the distance from shore increases. This near fresh-water layer was about eight meters deep at Station 41 and only about two meters deep at Station 57. The density contour (sigma-t = 24) follows very closely the temperature contour (T = -1.5°C) to outline the mound of cold water.

4. Cross-section C

Figure 73 shows the location of cross-section C north of Tuktoyaktuk Peninsula comprising Stations 44, 45, 46, 47, 48, 49, 50, and 51 taken during a twenty hour period of August 26 to 27, 1974. The cross-section itself is shown in Figure 76. Because of the large number of stations taken over a relatively short time span, this cross-section provides a reasonably synoptic picture of the water column. Two shallow tongues of warm, relatively fresh water can be seen centered on Stations 45 and 51 respectively, but with a thickness of only a few meters. The 0°C isotherm is almost horizontal at

five-meters depth. The -1.5°C isotherm slopes with the bottom contours to a depth of about 20 meters. The density structure shows a fresh-water wedge gradually shoaling to the north. There was a marked pycnocline at a depth near five meters.

5. Cross-section D

Figure 77 shows the location of cross-section D east of Herschel Island comprising Stations 45, 46, 47 taken during the period of August 21 to 22, 1975. The cross-section itself is shown in Figure 78, as it starts near the coast and goes northward to the deep water on the continental slope. It can be seen that mixing was greater than in cross-section A of 1974 (Figure 74). The wedge of warm water extended both deeper and further seaward. Also the heat content of the water was much greater. The density cross-section shows deep mixing compared to 1974. The surface water, although fairly fresh, had a sigma-t of almost twelve. The wedge of near-fresh water is still noticeable, but not as obviously as in 1974.

6. Cross-sections E, F, G

As in 1974, there is similar evidence of cold Arctic water intruding toward Richard's Island in the summer of 1975. Used in the foloowing description are three vertical cross-sections, each of temperature and density, from locations shown in Figure 76.

a. Cross-section E

Figure 79 shows cross-section E comprising Stations 41, 42 and 43 taken on August 20 and 21, 1975. The warm river

water extended a considerable distance seaward. Sea surface temperatures decreased from 8.61°C at Station 43 to 3.65°C at Station 41. There was a steep thermocline at about five meters depth where the temperature decreased from 7°C to 4°C. In shallow water, it appears that considerable mixing occurred right to the bottom, where the temperatures exceeded 3°C. The density cross-section also shows the mixing in shallow water. Surface sig_{ma}-t values were about 10-12 with a weak pycnocline at about seven meters. Cold, dense sea-water had intruded onto the shelf to a depth of about 25 meters. The cold intrusion of Arctic water does not manifest itself in this cross-section.

b. Cross-section F

Figure 80 shows cross-section F comprising Stations 11, 12, and 13 taken on August 13 and 14, 1975. This cross-section slices through the cold water intrusion discussed above. A wedge of warm water extended seaward and cooled from 6.90°C to 4.97°C at the surface. The warm water was well-mixed to a depth of about 20 meters to a position midway between Stations 11 and 12. Here, there appears to have been a sharp thermocline where the temperature decreased from 4°C to -1.5°C. The cold, dense mound of sea-water is seen to have pushed its way onto the shelf between Stations 12 and 13. Its position coincided with the position of the cold intrusion identified in cross-section B of 1974 (Figure 75).

The density structure shows that there was considerable downward mixing of the near-fresh water layer. The

AD-A096 387 NAVAL POSTGRADUATE SCHOOL MONTEREY CA F/G 8/3
HEAT BUDGETS OF THE SOUTHEAST BEAUFORT SEA FOR THE YEARS 1974 A--ETC(U)
SEP 80 E L TUMMERS

UNCLASSIFIED NL

2 OF 3
AD-A096387

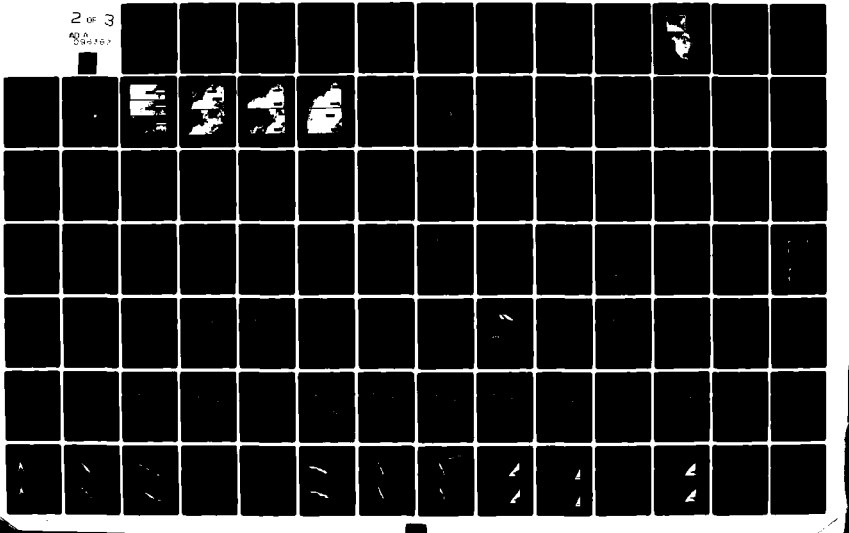

minimum sigma-t was 10. The sigma-t equals 25 contour was almost coincident with the -1.5°C isotherm and formed a distinct boundary to the cold water intrusion.

c. Cross-section G

Figure 81 shows cross-section G comprising Stations 38, 39, and 40 taken on August 20, 1975. This cross-section is from stations occupied a week later than for those of cross-section F and also intersects the cold water intrusion. Surface temperatures show a reversal in that they increase as one proceeds seaward. The temperatures at Station 38 (just north of Richard's Island) were much cooler than those further seaward. At Station 39, a surprising maximum of 8.70°C marked the southern edge of a large shallow tongue of 8°C water (see Figure 68). The cold intrusion is also seen located between Station 39 and 40. Directly above the cold intrusion is a sharp thermocline where the temperature dropped from 8°C to 1°C in a depth increase of less than three meters.

The density structure does not reflect the features mentioned above. The water column was strongly but evenly stratified showing an almost horizontal sigma-t contour of 10 at about four-meters depth with no concentration of isopycnals.

7. Cross-sections H, I, J, K

These four cross-sections (Figure 77) are used to examine more closely an area of high heat content north of the Tuktoyaktuk Peninsula in the vicinity of the Bathurst

Polynya (Figure 65). These cross-sections are for a region of open water that was ice-free early in the season (as hinted by the profile at Station 5) so that solar radiation was absorbed to heat the water column. Later, as air temperatures dropped, the surface layers would cool first possibly leaving a warm, interstitial layer; however, it is more likely that the temperature inversions described below were due to surficial cooling by ice.

a. Cross-section H

Figure 82 shows cross-section H comprising Stations 22, 23, 24, 25 taken during the period of August 16, 17, 1975. It marks the westernmost limit of the thick warm water feature. At station 24; a lens of warm 6°C water can be seen to begin. It will be seen in the following cross-sections that this feature extends northeastward from there. Only a hint of the deep mixing exists at Station 24 where 6°C water extends from five to eighteen meters depth.

b. Cross-section I

Figure 83 shows cross-section I comprising Stations 27, 28, 29, and 30 taken on August 17 and 18, 1975. Stations 28 and 29 intersect the feature showing clearly a deep layer of 5°C water at about 15 meters depth with colder water above and below it. Even at Station 27, close to the ice edge, a layer of warm water, albeit only 3°C, existed between 15 and 20 meters deep. Surface cooling had apparently occurred during the week to reduce the surface temperatures above the warm water layer. An atmospheric cooling trend

is also seen in the records of the 5-day mean temperature beginning on August 16, 1975 (Figure 89 of Appendix H).

c. Cross-section J

Figure 84 shows cross-section J comprising Station 5, taken on August 8, 1975 and Stations 31, 32, and 33 taken on August 18, 1975. At Station 5, the water was warmer than 5°C to a depth of about 16 meters. The remaining Stations, taken ten days later, show the effects of the surface cooling which had occurred, leaving a warmer, deep layer of water at about 15 meters deep.

d. Cross-section K

Figure 85 shows cross-section K comprising Stations 34, 35, 36 taken on August 18 and 19, 1975. This cross-section approximately marks the eastern boundary of the feature. The water temperature gradually warmed as the distance to shore decreased. The river water apparently formed a narrow wedge of warmer, less saline water along the entire length of the Tuktoyaktuk Peninsula.

In each of the above cross-sections, the density structure was relatively simple with no indication of the complex temperature patterns in the water mass.

APPENDIX F

SELECTED OCEANOGRAPHIC TIME-SERIES

1. Station 11, August 15 to 18, 1974

Figure 86 shows great variability in the temperature of the upper 5 meters of the water column over a period of several days at the same location. Surface temperatures ranged from 5.09°C to 8.08°C, whereas at 10 meters the temperature was almost constant at -1°C. There was a steep thermocline between 5 and 10 meters depth throughout the time series which was typical of most temperature profiles taken during August, 1974. A result is that the heat content also changed rapidly with time as the surface layer temperature changed.

2. Station 48, August 23 to 24, 1975

Figure 87 shows the variability of the temperature versus depth in the water column over a period of several days at the same location. At the far left in the temperature versus time plot is a profile taken a week earlier on August 15, 1975 at Station 19 very close to the position of Station 48. During the following week (August 15-23) there was considerable warming of the top 10 meters of the water column. Surface temperatures increased from 5.52°C to 7.33°C. At the very end of the time series, advection of cold water is noticeable as the temperature contours bend sharply upward, especially between 5 and 10 meters.

APPENDIX G

COMPARISON OF SURFACE SALINITIES

Figure 88 shows surface salinities and the polar ice-pack boundary for the summer of 1974 and the summer of 1975 [Herlinveaux, 1976]. The surface distribution of salinity indicates that if the pack-ice is offshore, as it was in 1975, low salinity water from the Mackenzie River generally moves eastward under the influence of the Coriolis effect. If the pack-ice is unusually close to the shore, as it was in the summer of 1974, much of the river flow is confined south of the ice barrier and low-salinity surface water is seen to accumulate over the Mackenzie Delta.

APPENDIX H

SURFACE AIR TEMPERATURES AT BARTER ISLAND AND CAPE PARRY

Barter Island is located about 120 km west of the westernmost edge of the study area. Cape Parry is in Amundsen Gulf about 200 km east of the easternmost edge of the study area. Surface air temperatures on a five-day running mean were available from each of these stations for 1974 and 1975, as well as mean temperatures based on climatology. These temperatures are plotted in Figure 89.

1. General

Cape Parry is generally 2°C warmer than Barter Island, indicating the greater prevalence of continental air masses moving over Cape Parry into the Southeastern Beaufort Sea.

2. Summer of 1974

a. At both locations, the air temperatures were much colder than normal until mid-July;

b. Both locations had their extreme temperatures almost simultaneously; and

c. It was warmer at Cape Parry until mid-August after which it was warmer at Barter Island.

3. Summer of 1975

a. At both locations, air temperatures were much warmer than normal until mid-July, corresponding to the time of maximum open-water area;

b. The peak temperature of 14°C at Cape Parry corresponded to a minimum temperature of 0°C at Barter Island on August 23, 1975;

c. The September cooling trend was the same at both locations but the absolute temperatures at Barter Island were much lower; and

d. With two exceptions, July 19 and August 2, 1975, this was a consistently warmer summer than 1974.

APPENDIX I

EXPLANATION OF MARSDEN SQUARE GRID SYSTEM

1. Marsden Squares

Each Marsden square describes a 10° square of the earth's surface. The numbering starts at 0°N, 0°W and numbers the squares westward in a belt moving around the equator. The numbers increase north and south from the equator. The Marsden Squares of interest in this study are 230 and 266.

2. Marsden Sub-squares

Each Marsden square is divided into 100 1° sub-squares which are always oriented so that the lowest number is nearest the intersection of the Greenwich meridian and the equator. In Marsden Square 230, the sub-squares of interest are 90-99; and in Marsden Square 266, the sub-squares of interest are 00-12. The corresponding latitude and longitude can be determined by knowing the positions of the Marsden Square and the number of the sub-square. For example, Marsden square 230 is the 10° square whose lower right corner intersects 60°N and 130°W. Marsden sub-square 95 then would be the sub-square whose lower right corner intersects 69°N and 135°W. Similarly, Marsden square 266 is the Marsden square whose lower right corner intersects 70°N and 130°W. Marsden sub-square 11 refers to that sub-square whose lower right corner intersects 71°N and 131°W. Note the first digit of the Marsden sub-square

refers to the increment in latitude and the second digit refers to the increment in longitude.

3. Marsden Sub-sub-squares

In temperate regions, the Marsden sub-squares are approximately square. At high latitudes, such as in the Beaufort Sea, a 1° square becomes rectangular with a height of 60 nm but a width of only about 20 nm. To preserve the square appearance of the box, the idea of a Marsden sub-sub-square is introduced. This makes each square about 40 km in each direction. The number of the Marsden sub-sub-square is a single digit number indicating the point the lower right corner of the square intersects the minutes of latitude. Each Marsden sub-square is divided into three sub-sub-squares numbered '0', '2', '4'. For example, Marsden sub-sub-square 266 110 indicates the square whose lower right corner is 71°0'N and 131°0'W. Similarly, 112 would indicate 71°20'N and 131°0'W (see Figure 90).

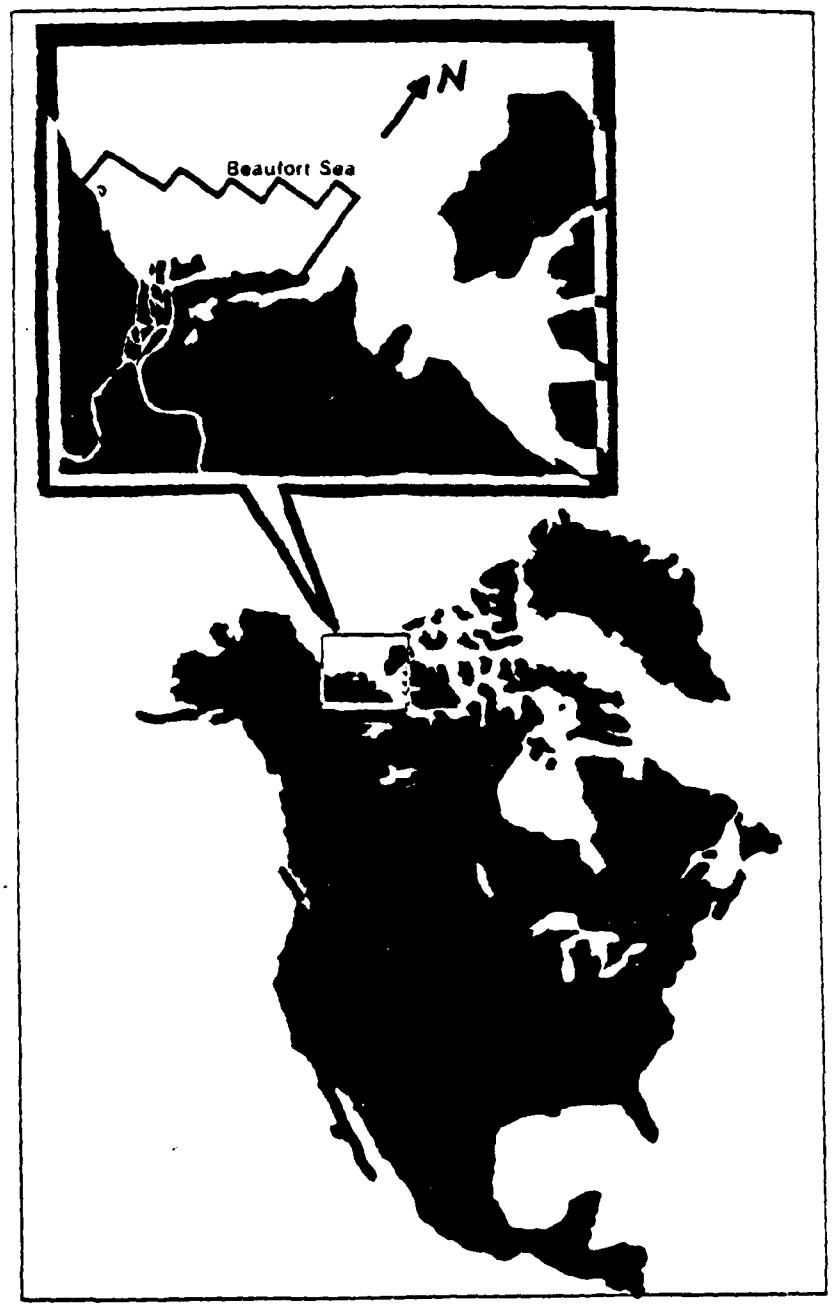

Figure 1: The study area in the Southeastern Beaufort Sea.

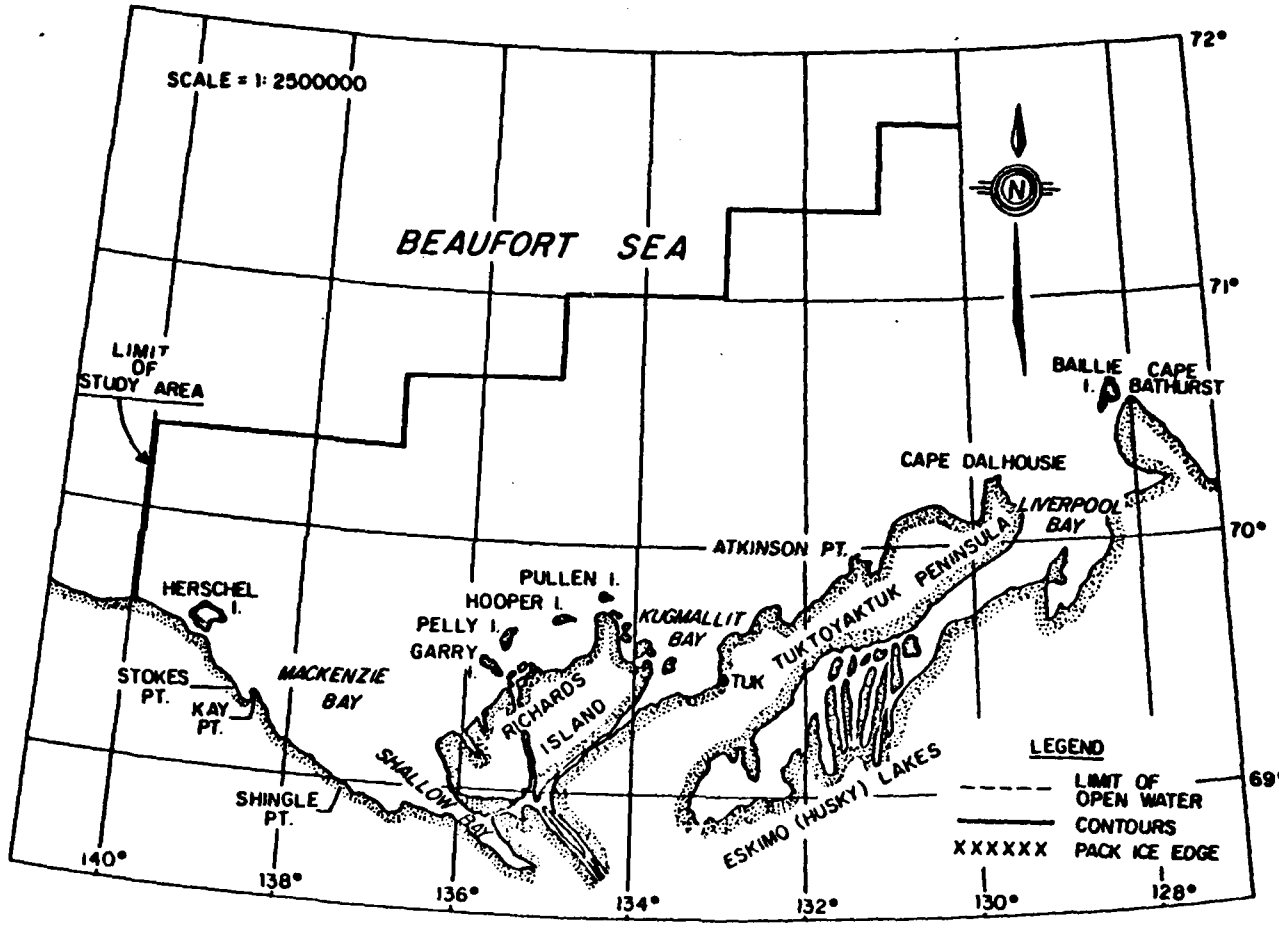

Figure 2: Place names in the study area.

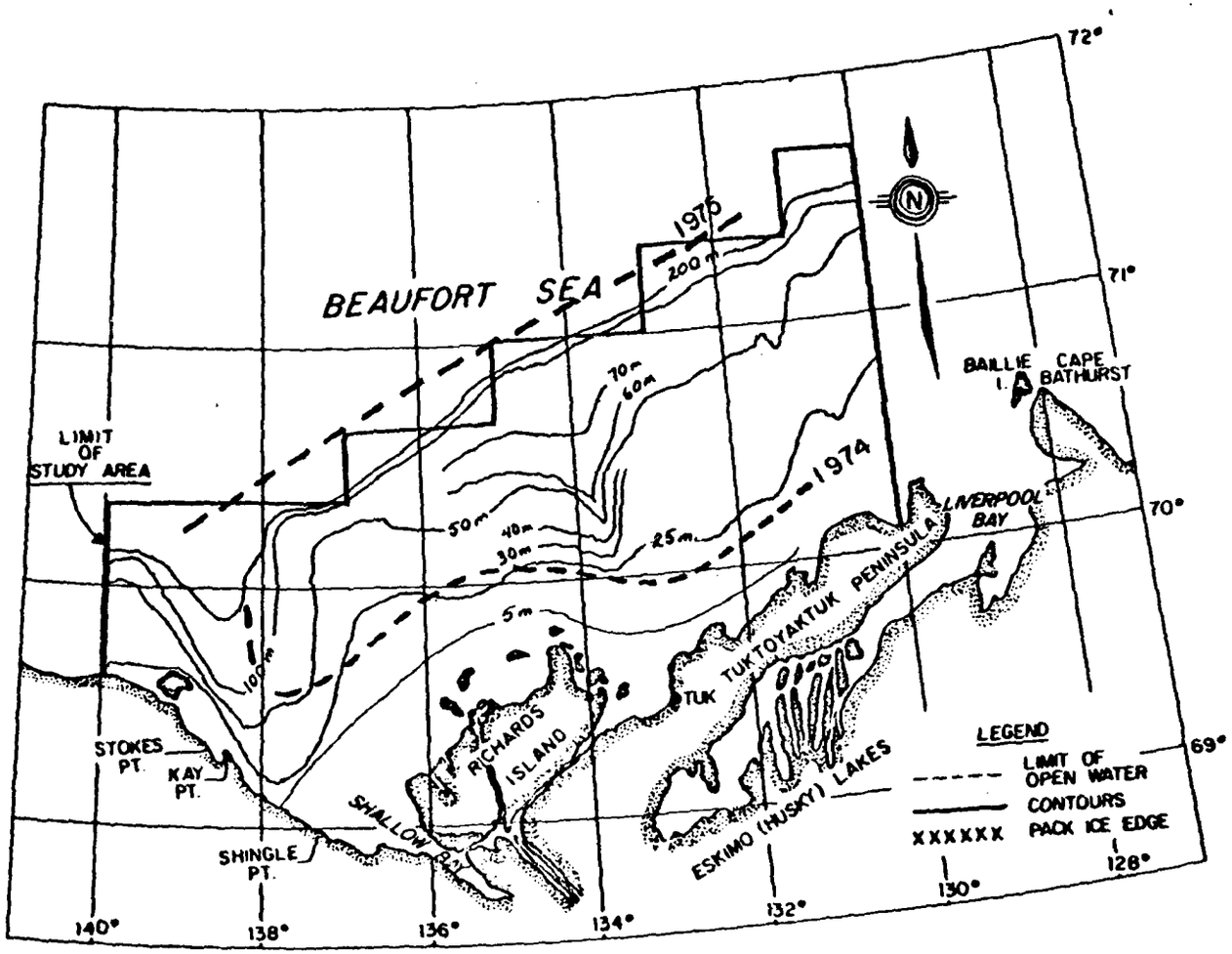

Figure 3: Bathymetry of the study area, and comparison of maximum extent of open water in each year.

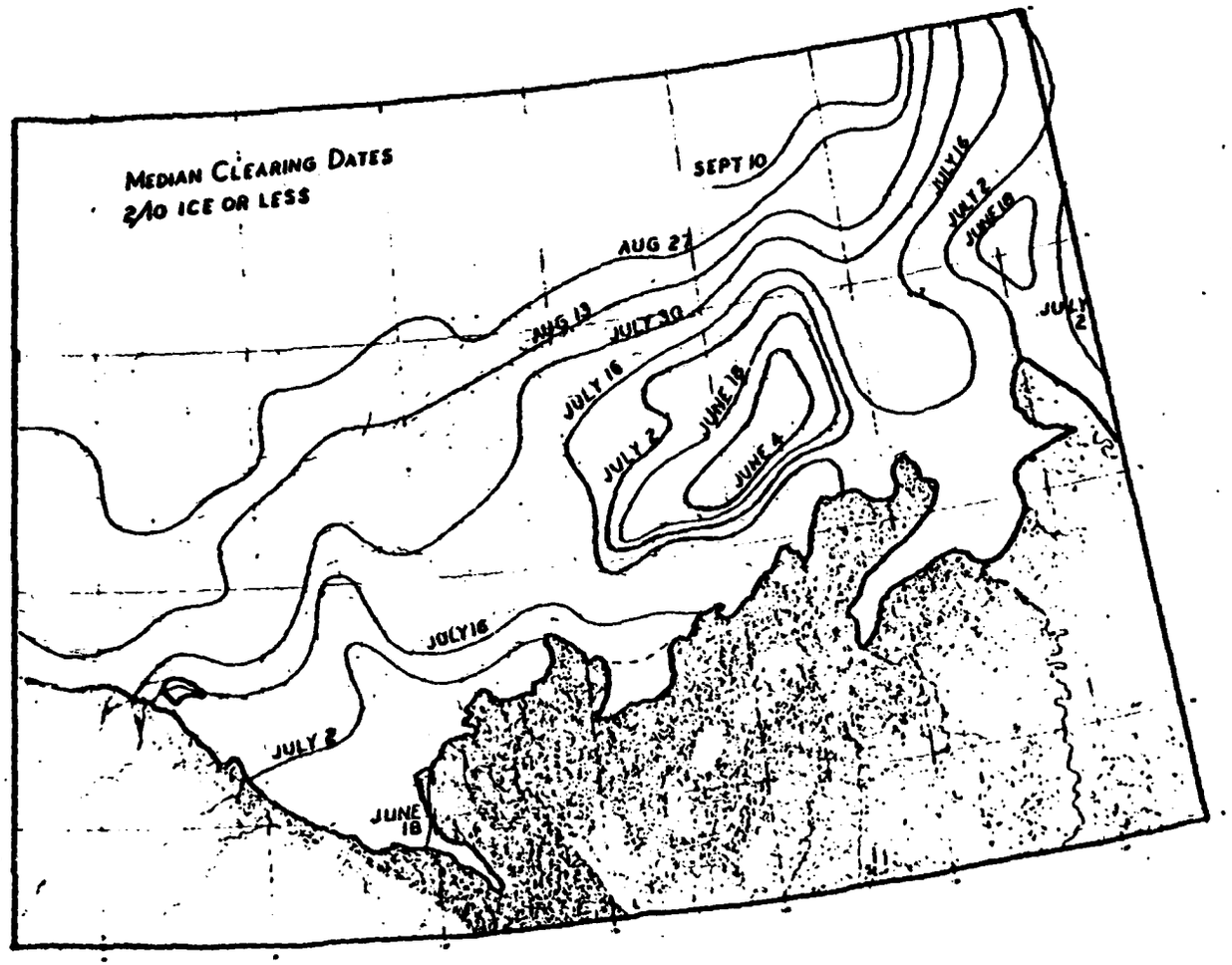

Figure 4: Map of Median Clearing Dates - 2/10 ice or less.

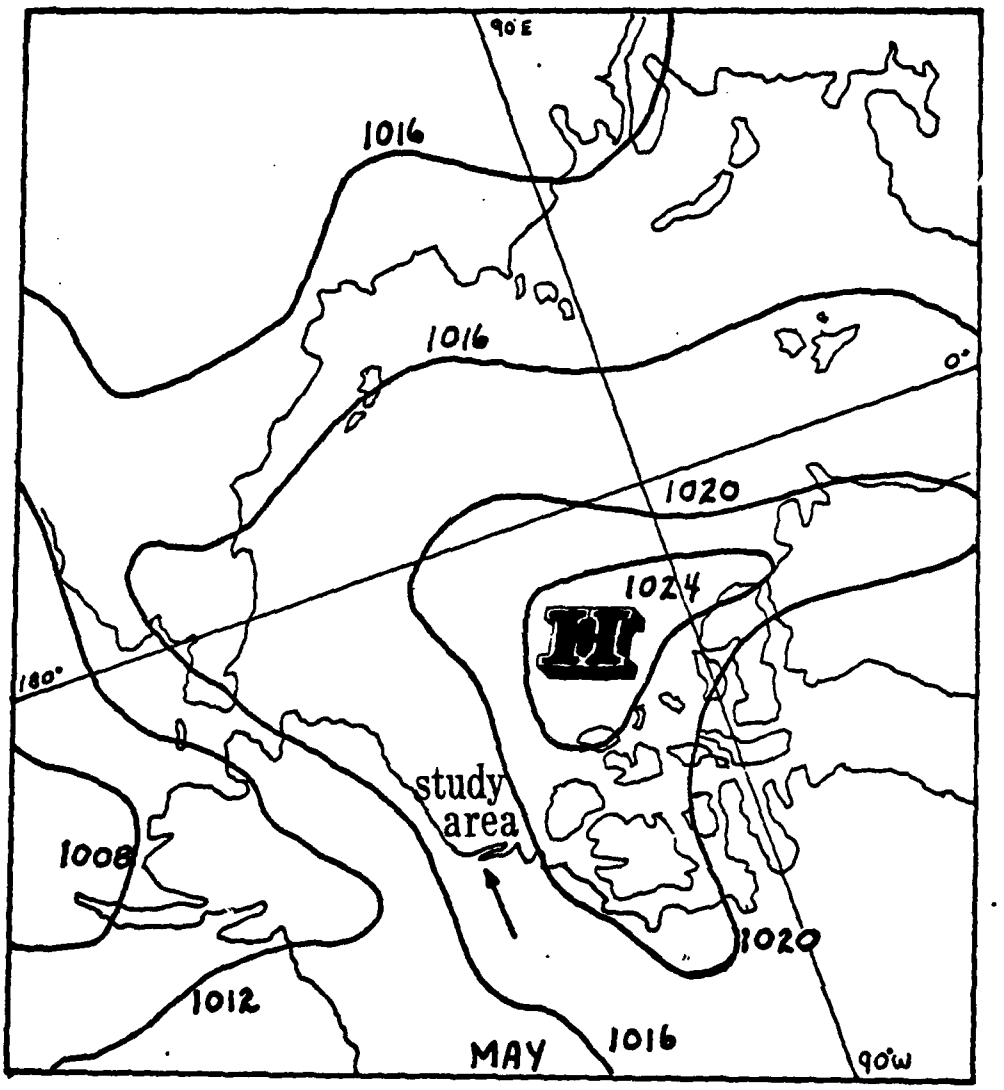

Figure 5: Mean Sea Level Atmospheric Pressure Chart for May.

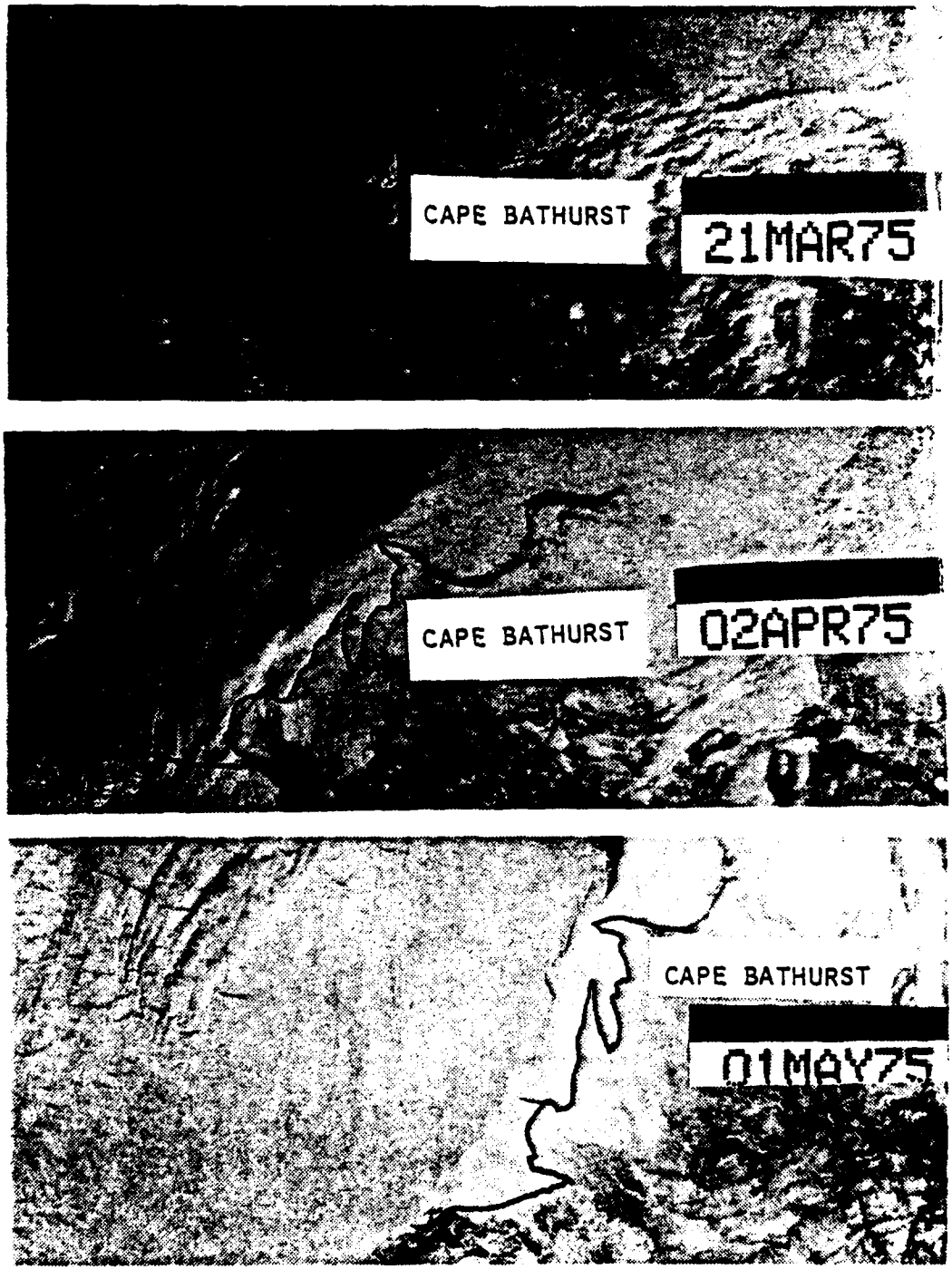

Figure 6: A time sequence showing three stages of the spring breakup in 1975.
a. There was a large open-water area seaward of the edge of the landfast ice on 21 Mar 75.
b. The offshore lead increased in width by 2 Apr 75.
c. Southward advection of the polar pack reduced the open-water area by 1 May 75.

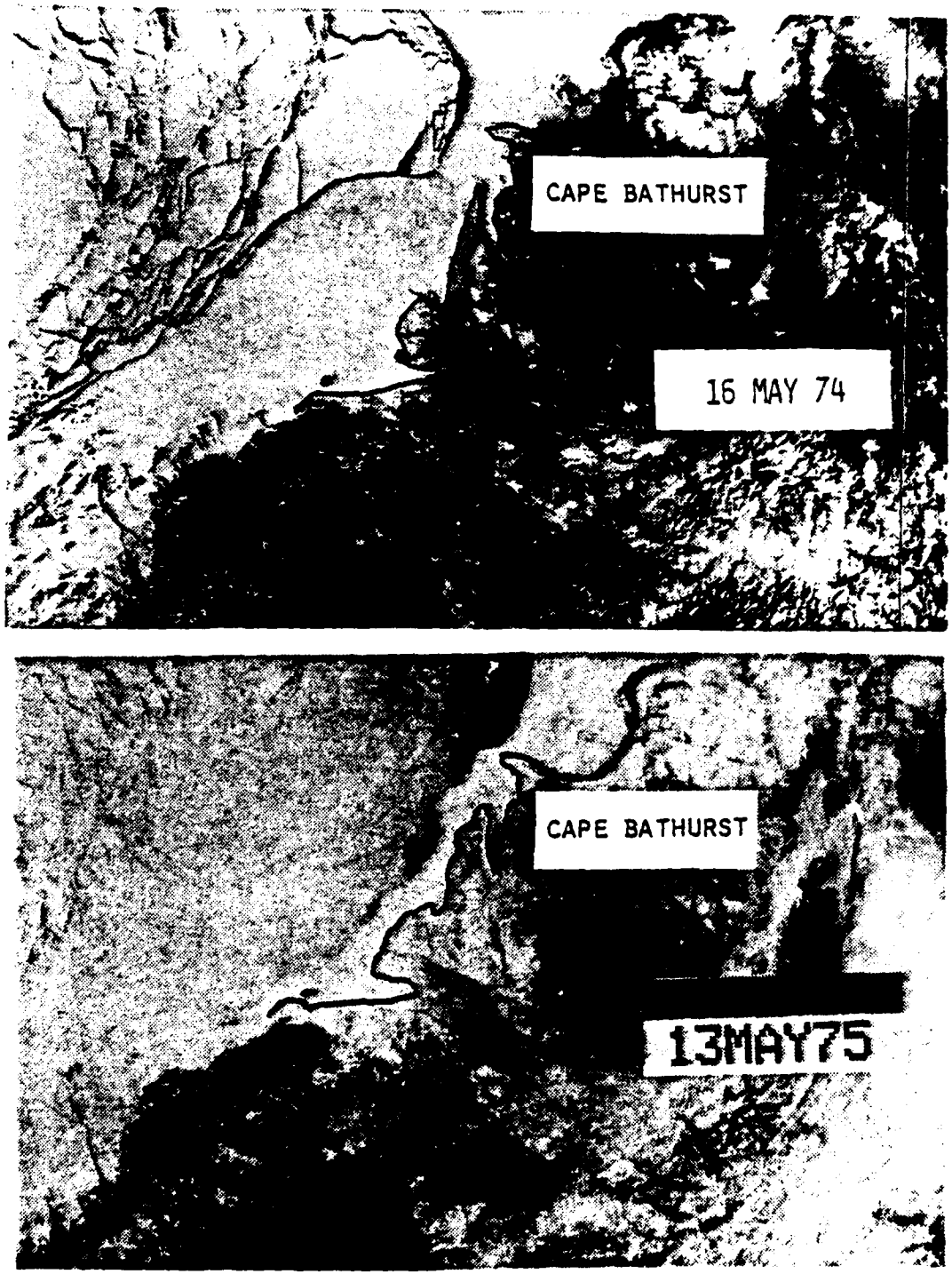

Figure 7: Comparison of open-water area on 13 May 75 and on 16 May 74.

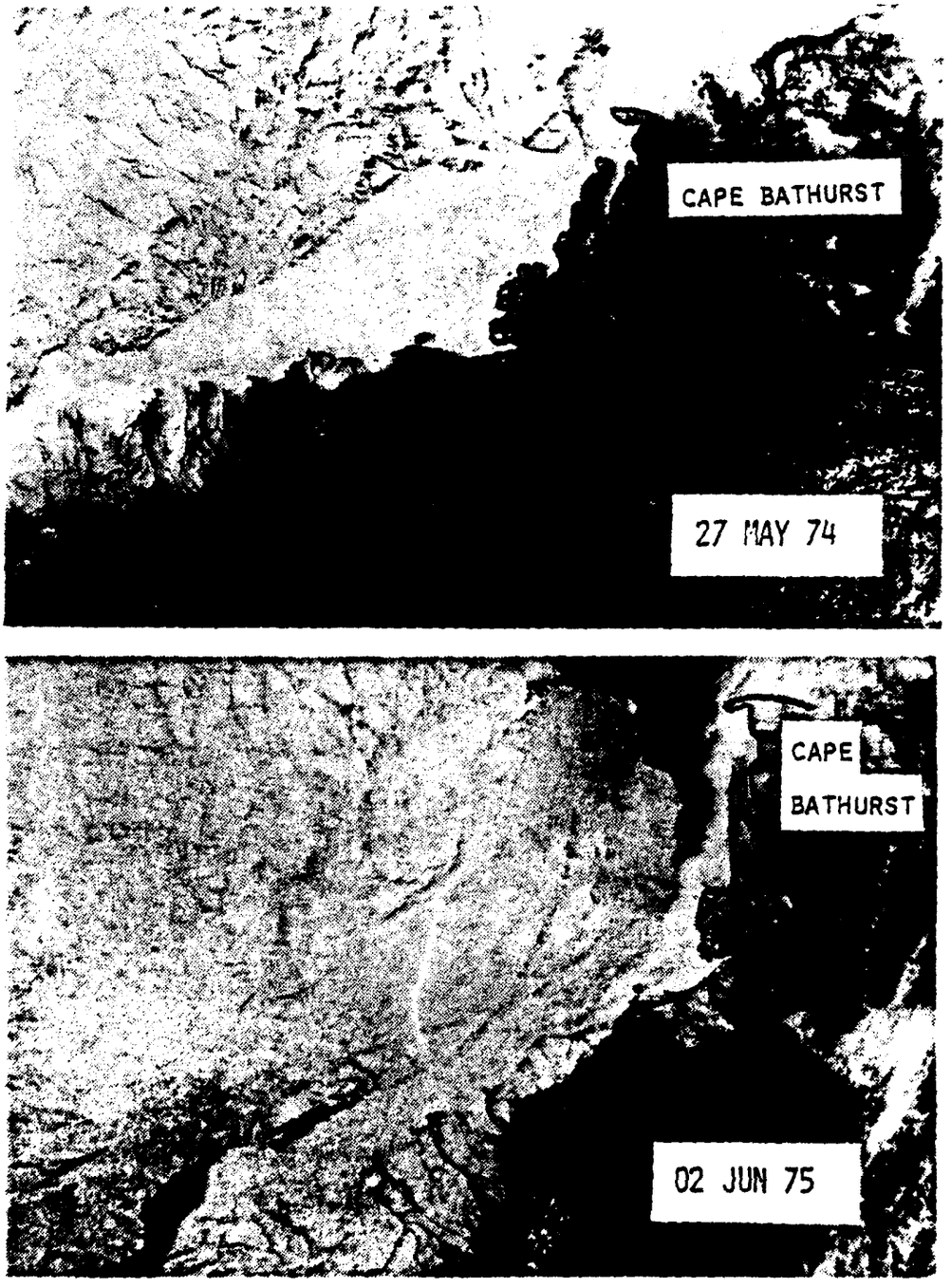

Figure 8: Comparison of open-water area on 27 May 74 and 02 June 75.

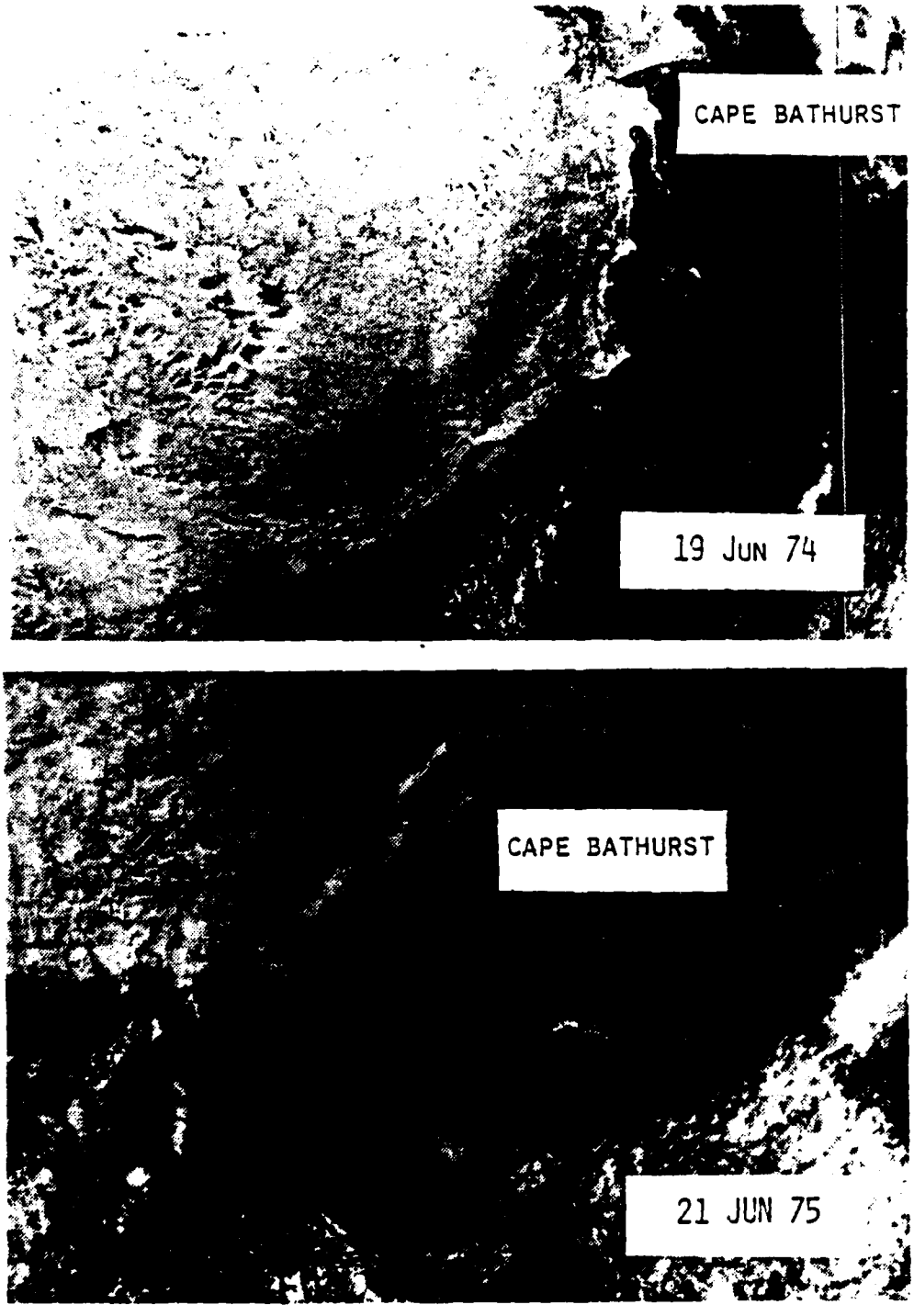

Figure 9: Comparison of open-water area on 19 Jun 74 and 21 Jun 75.

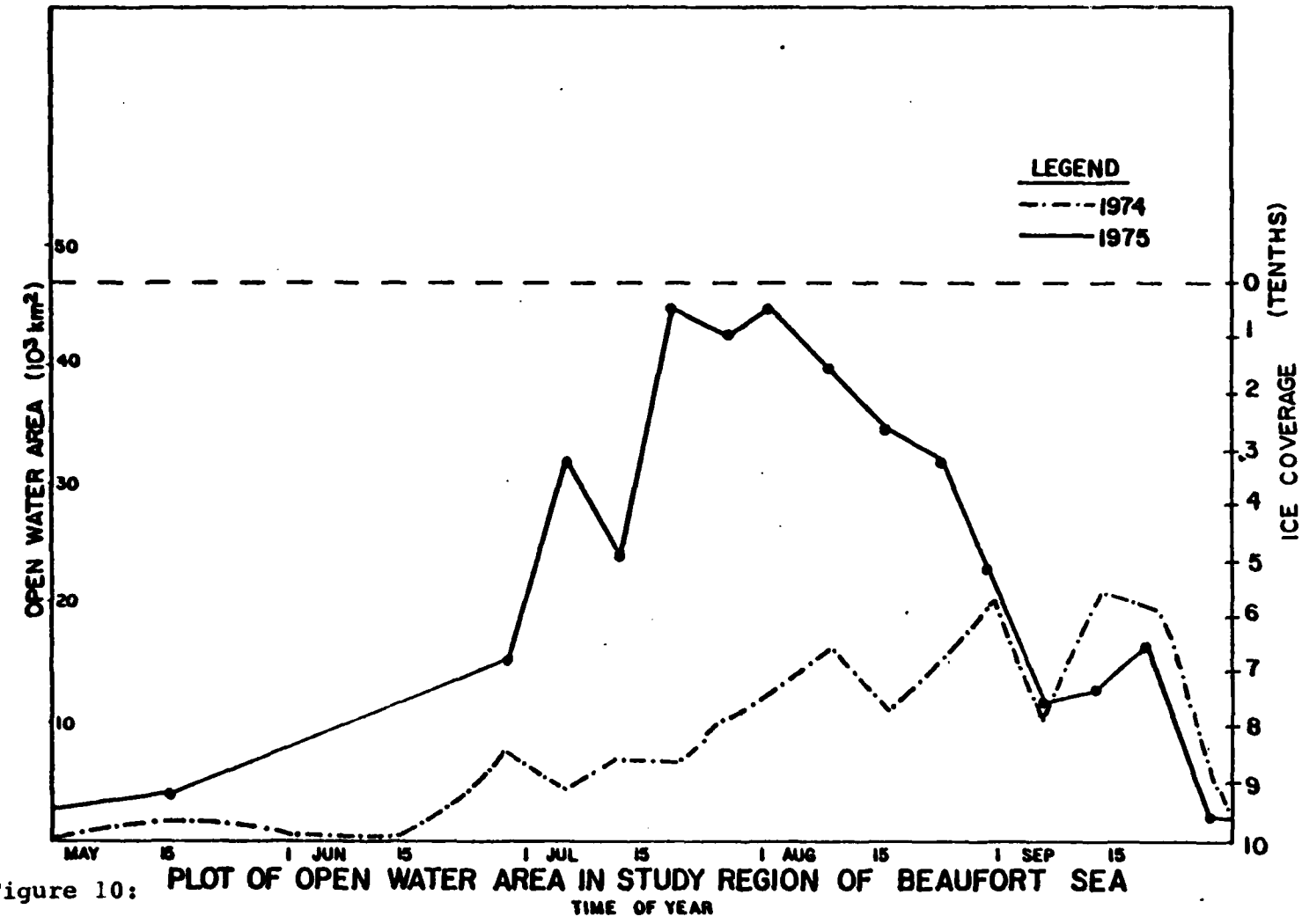

Figure 10: PLOT OF OPEN WATER AREA IN STUDY REGION OF BEAUFORT SEA

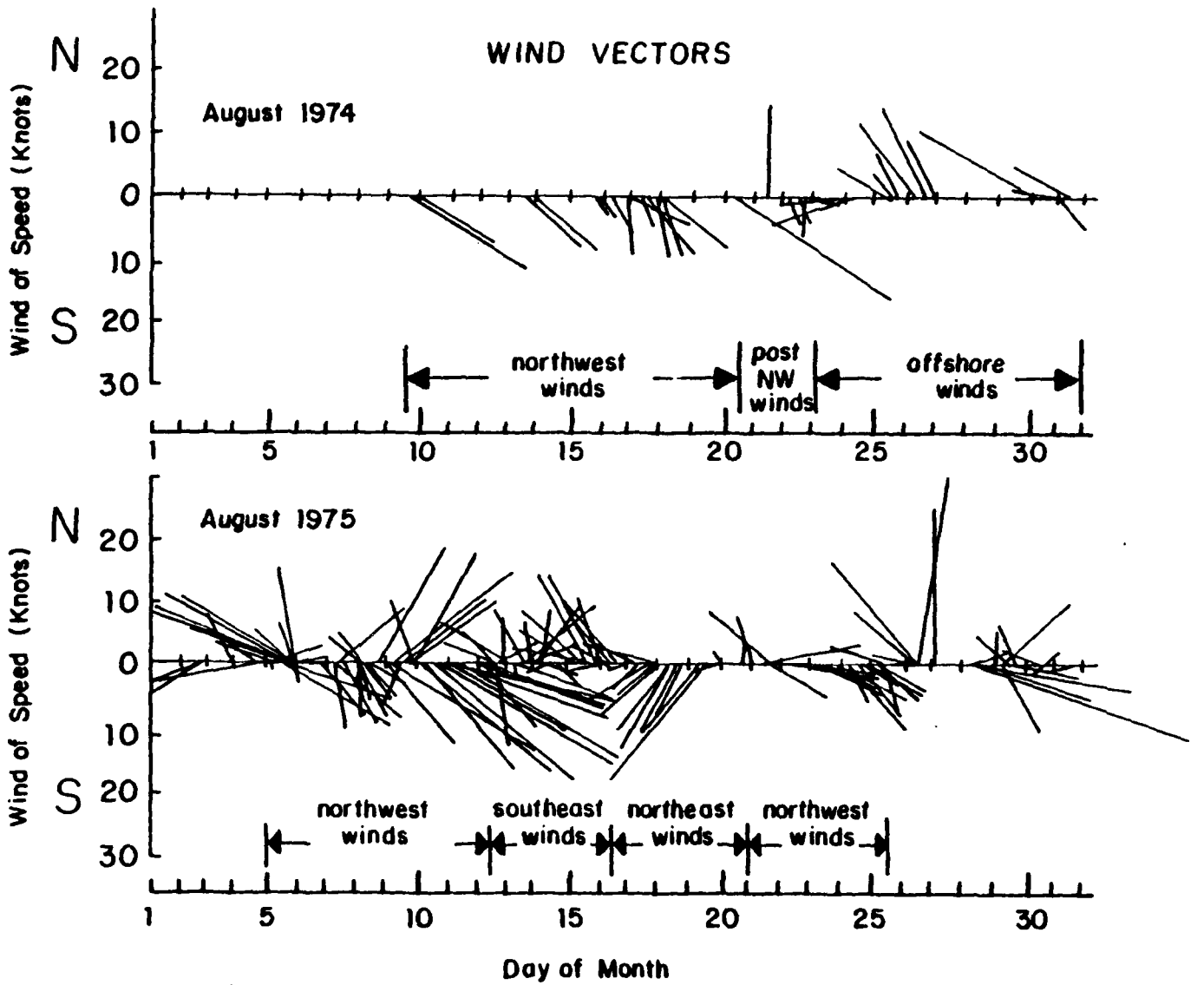

Figure 11: Wind vectors and division into wind periods for August 1974 and 1975.

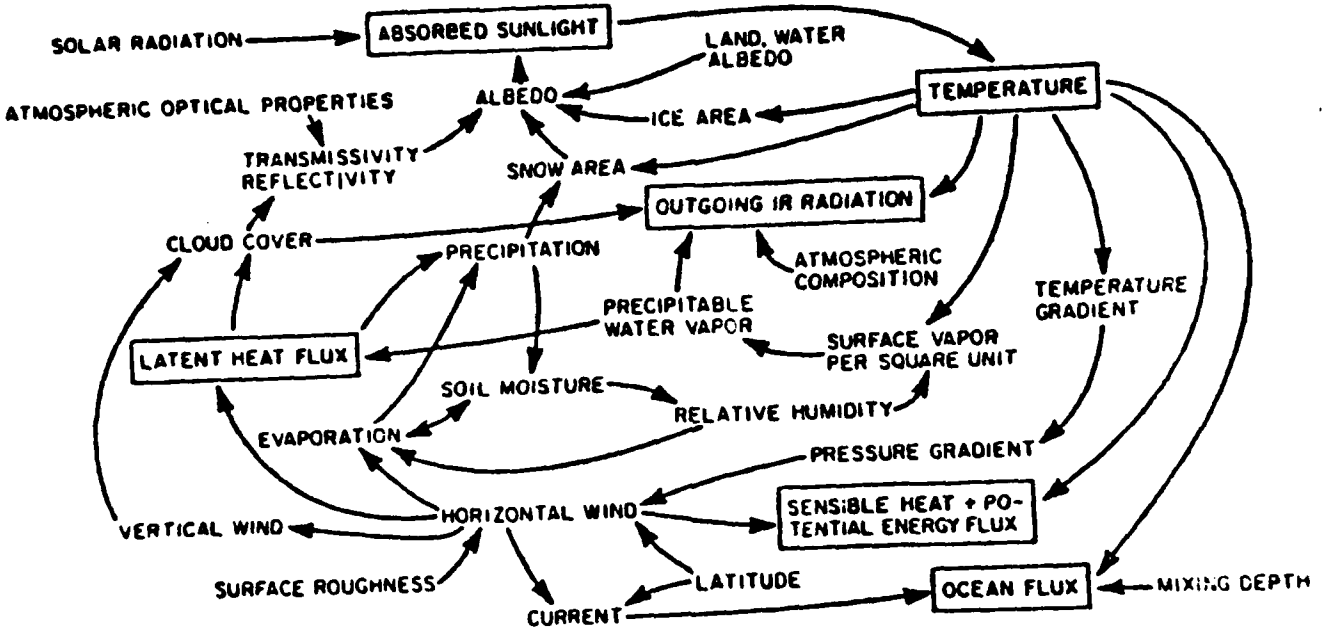

Figure 12: Climatic feedback linkages IR, infrared, (after Kellogg and Schneider 1974).

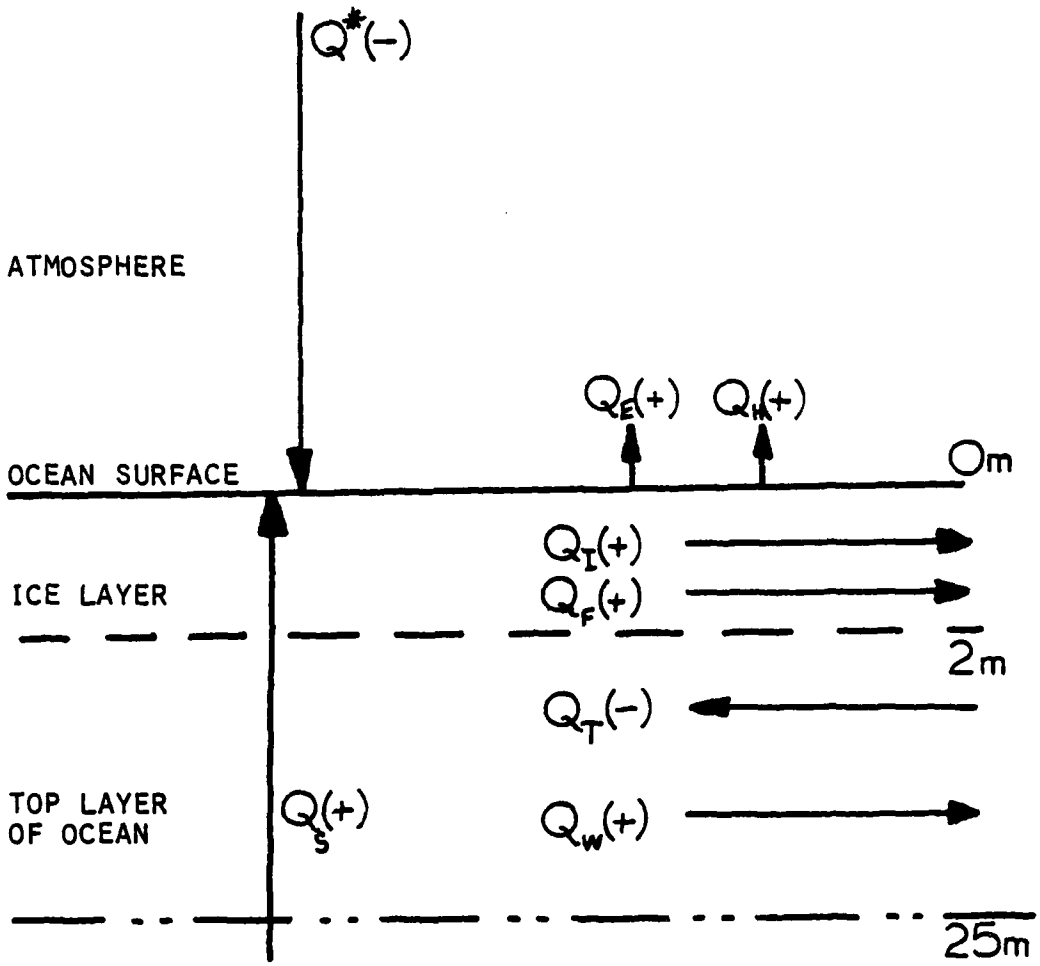

FIGURE 13. TYPICAL SUMMER FLUXES IN THE SE BEAUFORT SEA (SIGN IS INDICATED IN BRACKETS)

Q* (-): THE NET RADIATION DOWN
QE (+): THE HEAT LOSS DUE TO EVAPORATION
QH (+): THE UPWARD TRANSFER OF SENSIBLE HEAT
QA (-): THE RESULTANT DOWNWARD ATMOSPHERIC FLUX
QT (-): THE INPUT OF THE MACKENZIE RIVER
QW (+): THE HEAT USED TO WARM THE TOP LAYER
QF (+): THE HEAT USED TO MELT ICE-IN-PLACE
QI (+): THE HEAT USED TO MELT IMPORTED ICE
QS (+): THE STORAGE CHANGE

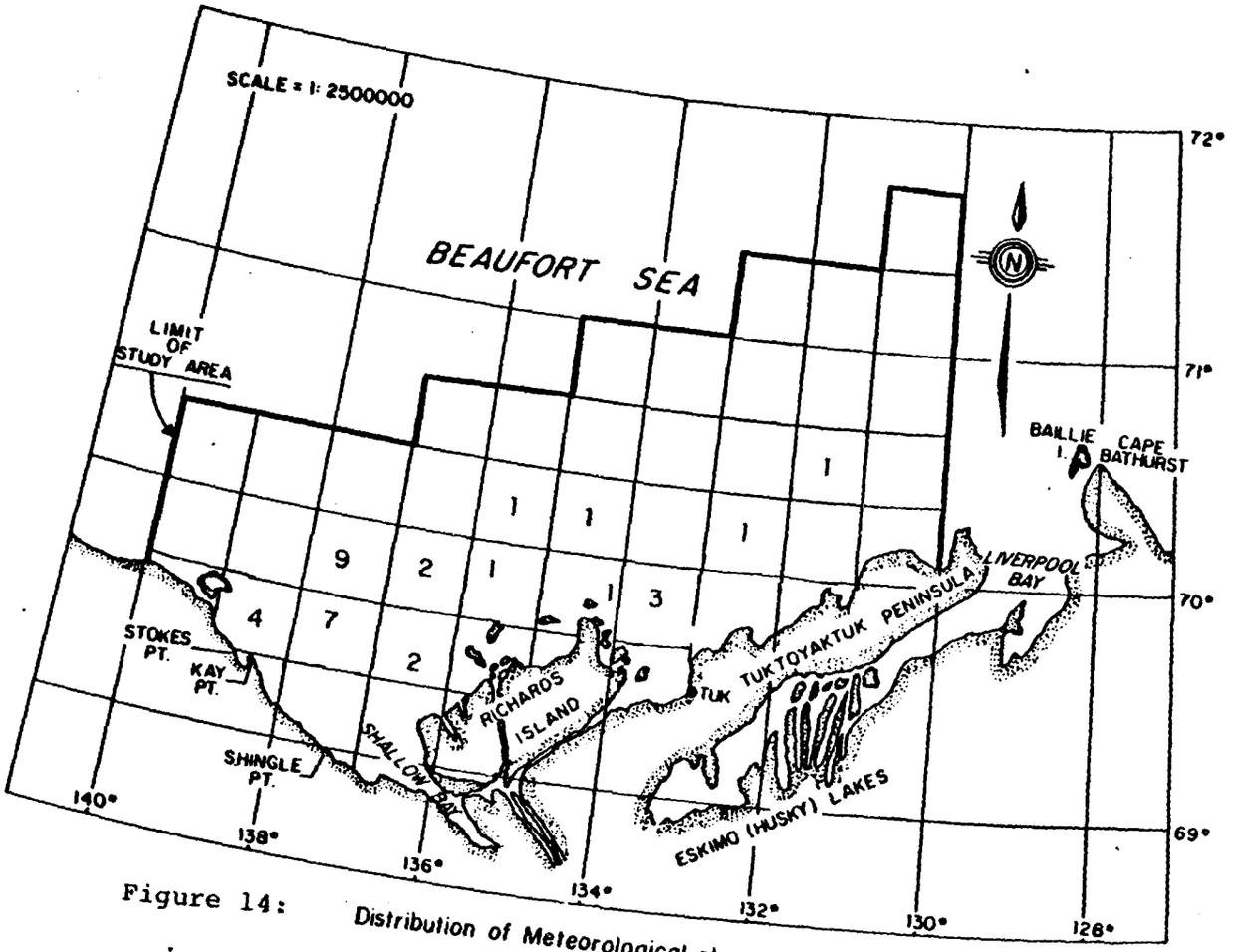

Figure 14: Distribution of Meteorological observations
August 1974
by Marsden sub-sub square

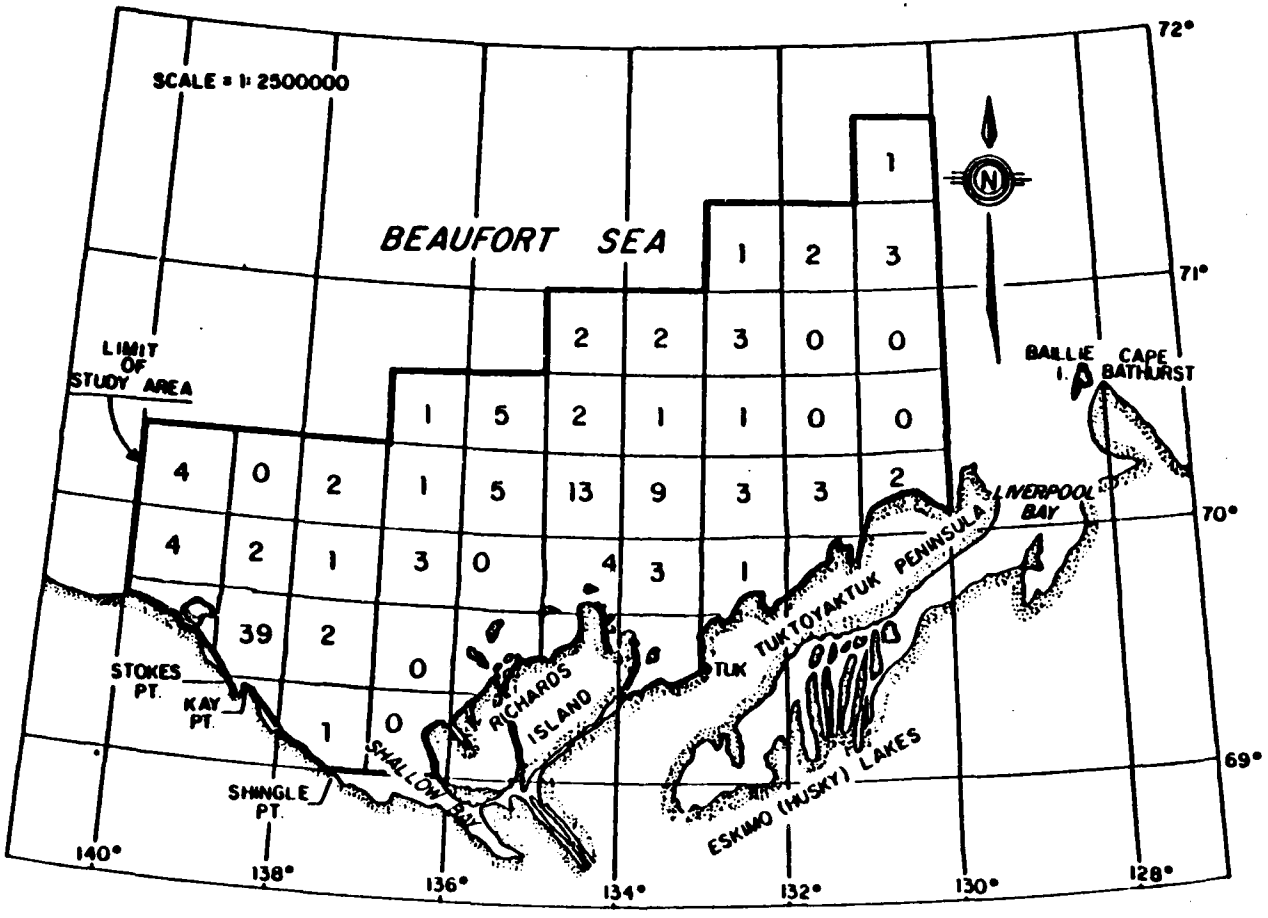

Figure 15: Distribution of Meteorological observations
August 1975
by Marsden sub-sub square

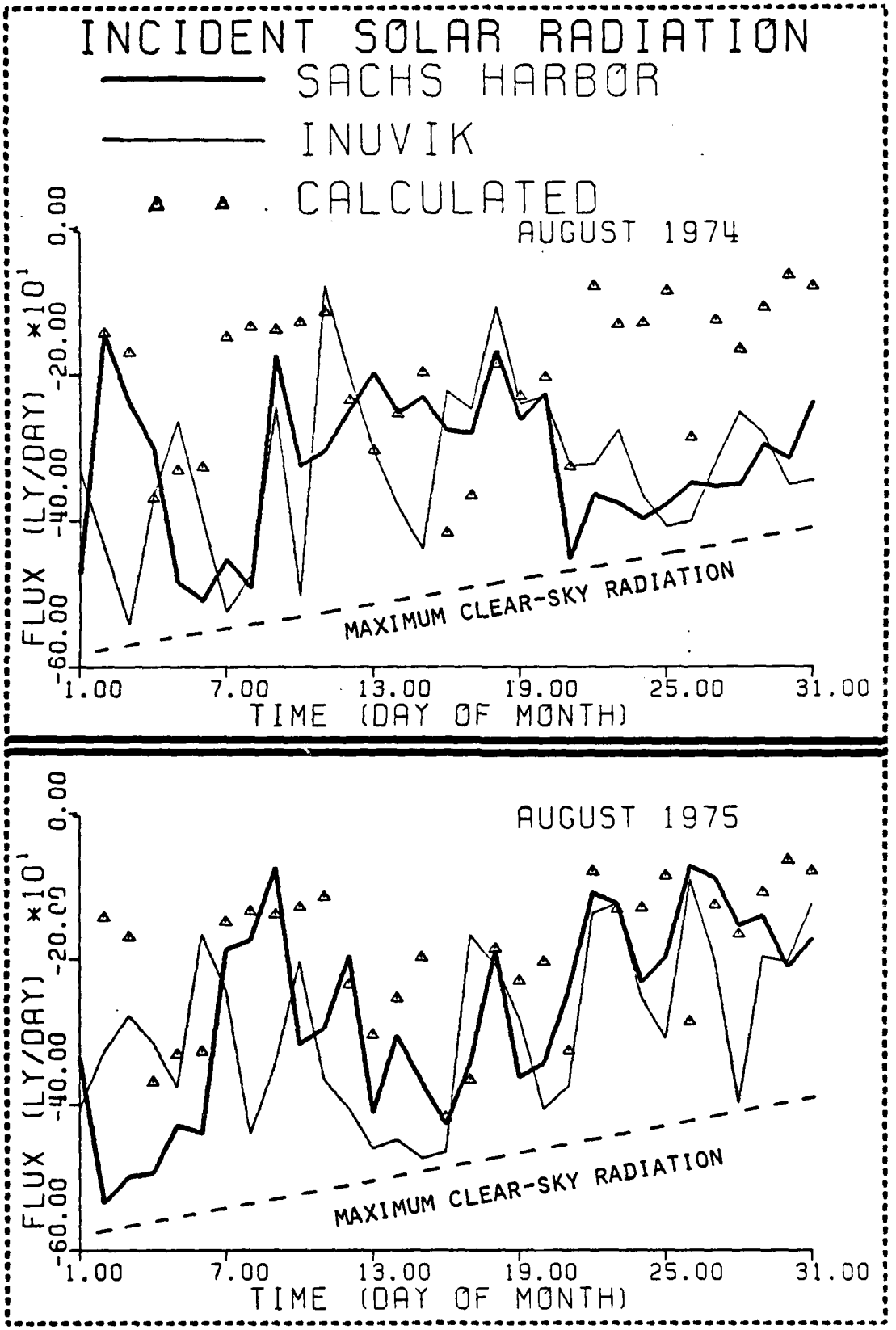
INCIDENT SOLAR RADIATION
SACHS HARBOR
INUVIK
CALCULATED
AUGUST 1974
FLUX (LY/DAY) *10¹
0.00
-20.00
-40.00
-60.00
MAXIMUM CLEAR-SKY RADIATION
1.00
7.00
13.00
19.00
25.00
31.00
TIME (DAY OF MONTH)
AUGUST 1975
FLUX (LY/DAY) *10¹
0.00
-20.00
-40.00
-60.00
MAXIMUM CLEAR-SKY RADIATION
1.00
7.00
13.00
19.00
25.00
31.00
TIME (DAY OF MONTH)

Figure 16

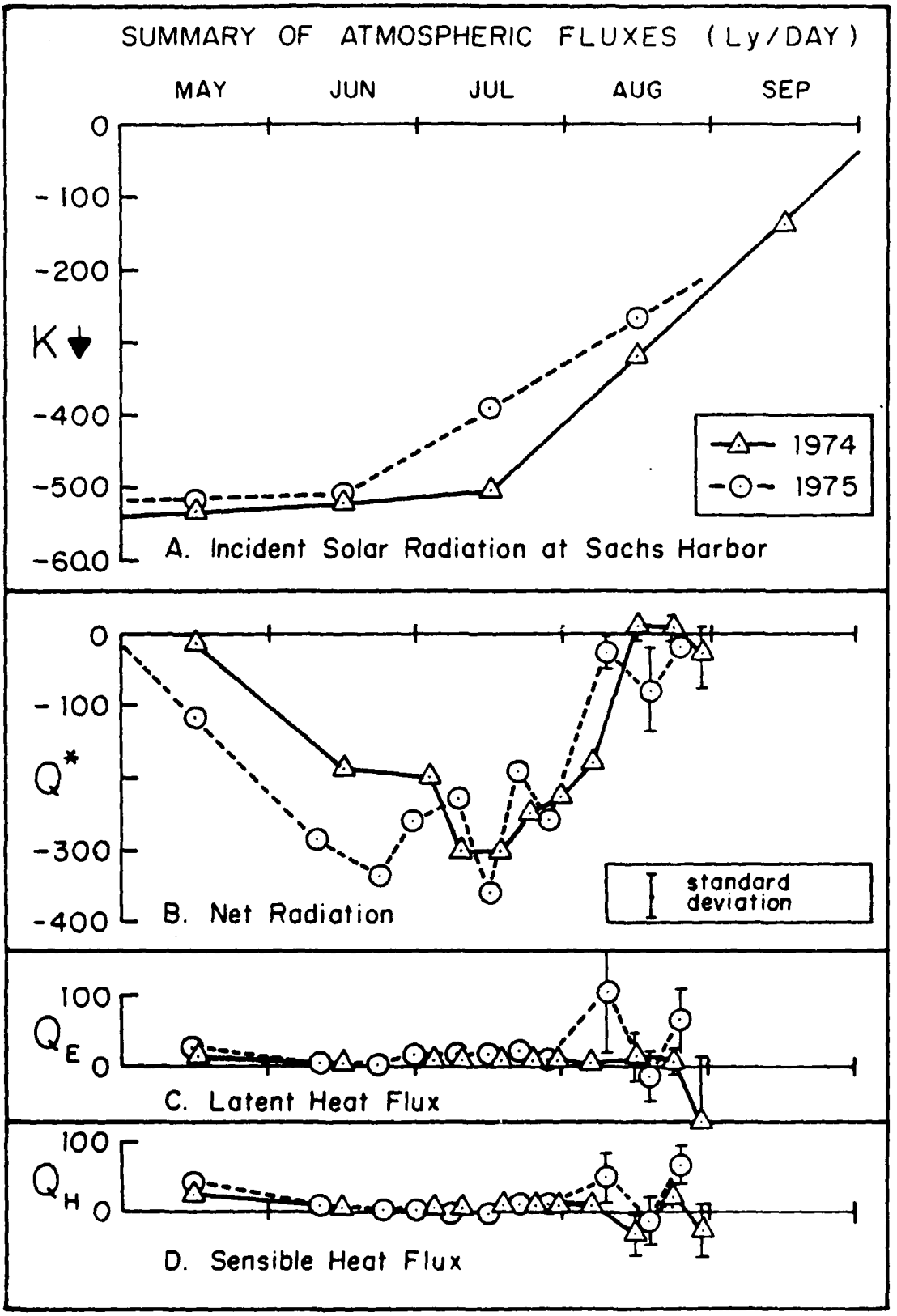
SUMMARY OF ATMOSPHERIC FLUXES (Ly/DAY)
MAY
JUN
JUL
AUG
SEP
0
-100
-200
K↓
-400
-500
-600
1974
1975
A. Incident Solar Radiation at Sachs Harbor
0
-100
Q*
-300
-400
standard deviation
B. Net Radiation
100
Q_E
0
C. Latent Heat Flux
100
Q_H
0
D. Sensible Heat Flux

Figure 17

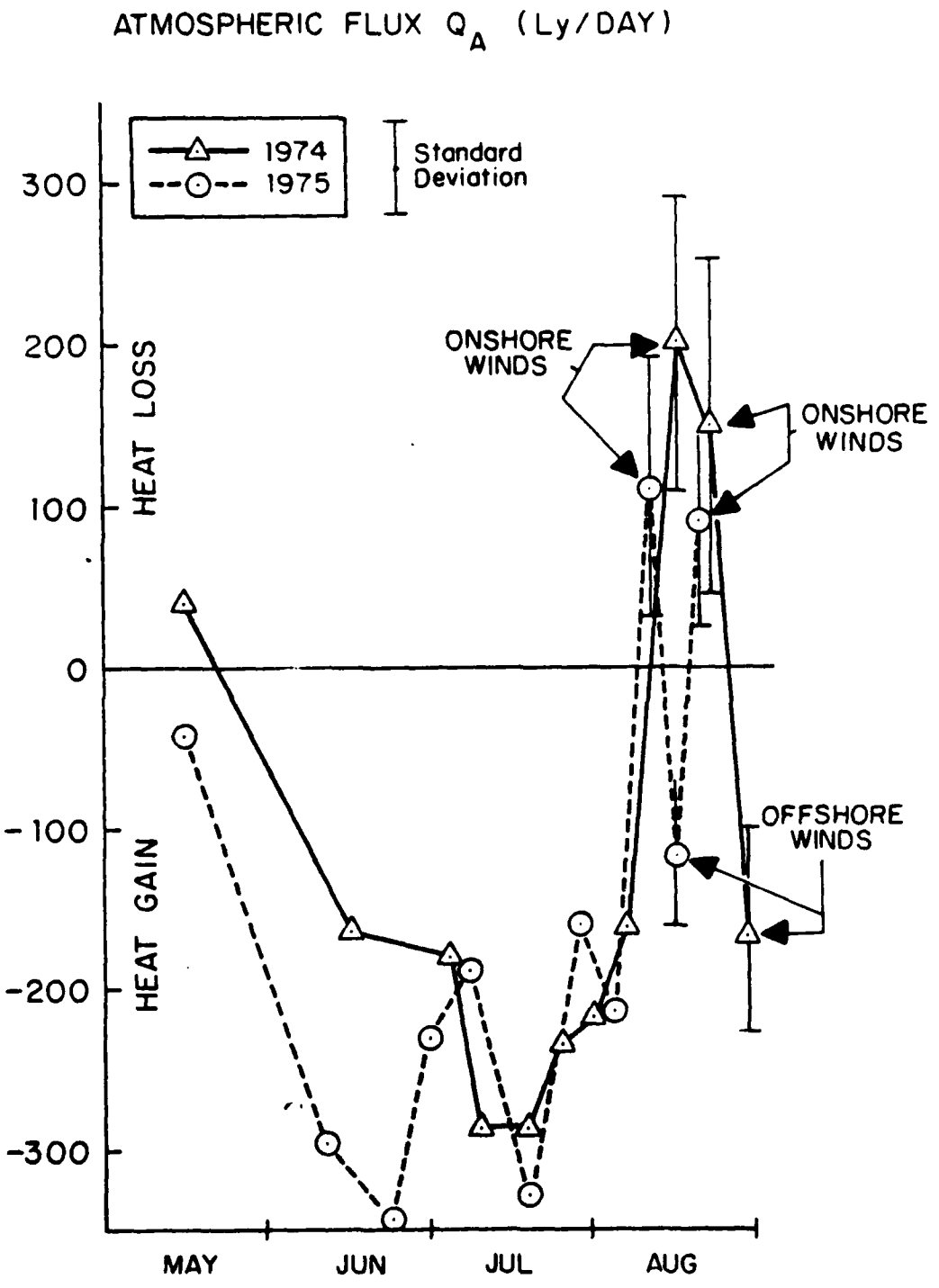
ATMOSPHERIC FLUX Q_A (Ly/DAY)
1974
1975
Standard Deviation
300
200
100
0
-100
-200
-300
HEAT LOSS
HEAT GAIN
ONSHORE WINDS
ONSHORE WINDS
OFFSHORE WINDS
MAY
JUN
JUL
AUG

Figure 18

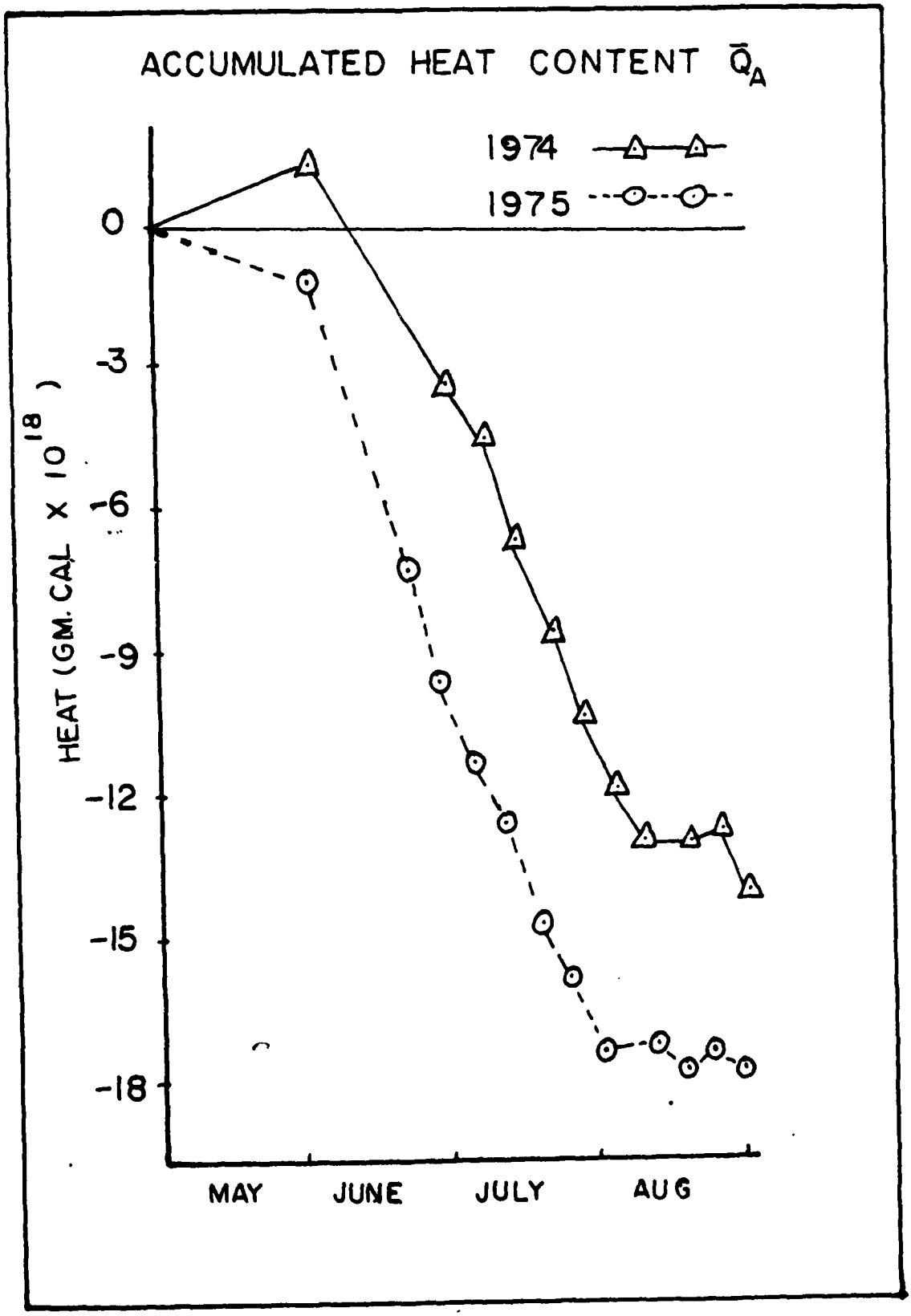
ACCUMULATED HEAT CONTENT $\bar{Q}_A$
1974
1975
0
-3
-6
-9
-12
-15
-18
HEAT (GM. CAL X 10^{18})
MAY
JUNE
JULY
AUG

Figure 19

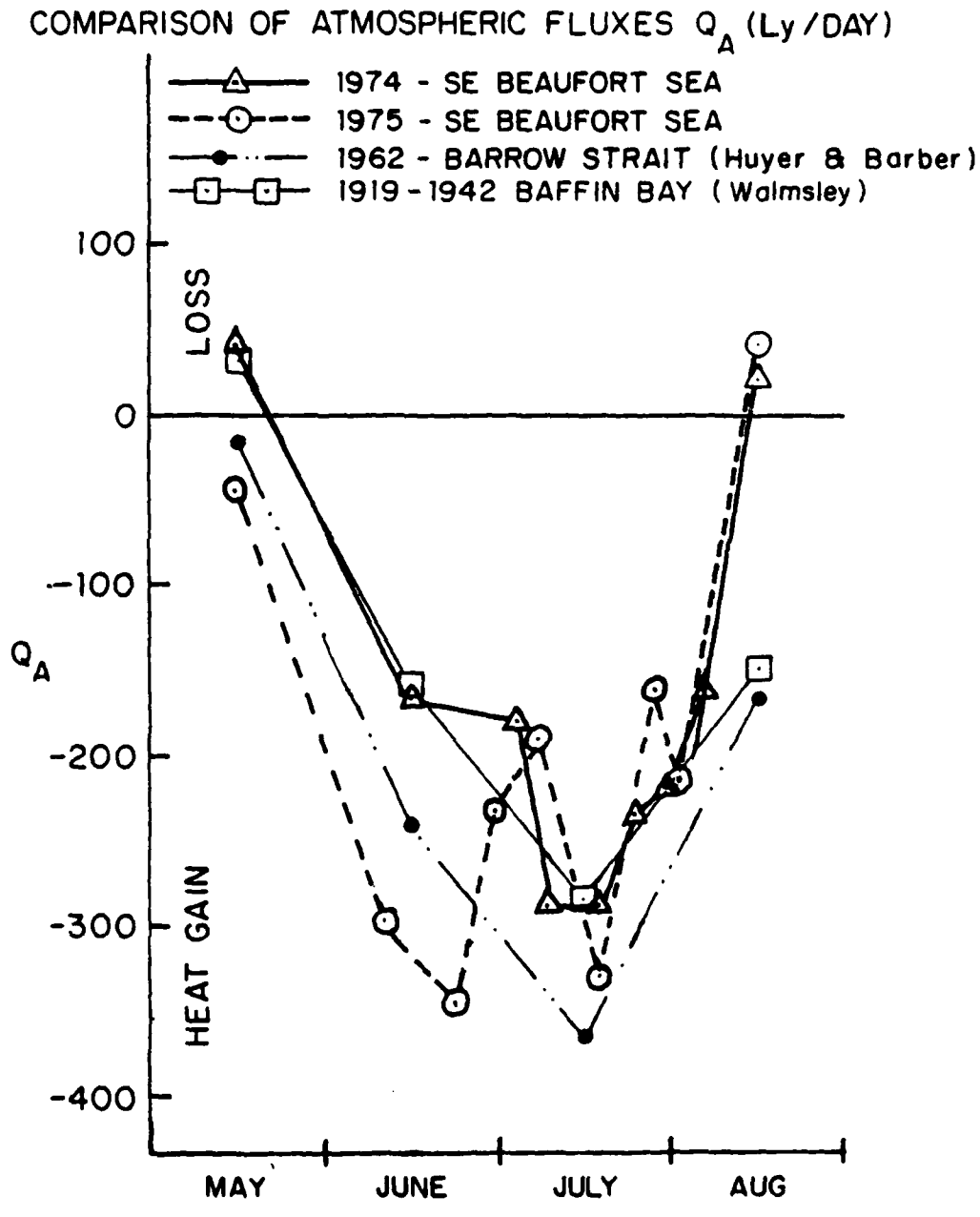
COMPARISON OF ATMOSPHERIC FLUXES Q_A (Ly/DAY)
1974 - SE BEAUFORT SEA
1975 - SE BEAUFORT SEA
1962 - BARROW STRAIT (Huyer & Barber)
1919-1942 BAFFIN BAY (Walmsley)
100
0
-100
-200
-300
-400
Q_A
LOSS
HEAT GAIN
MAY
JUNE
JULY
AUG

Figure 20

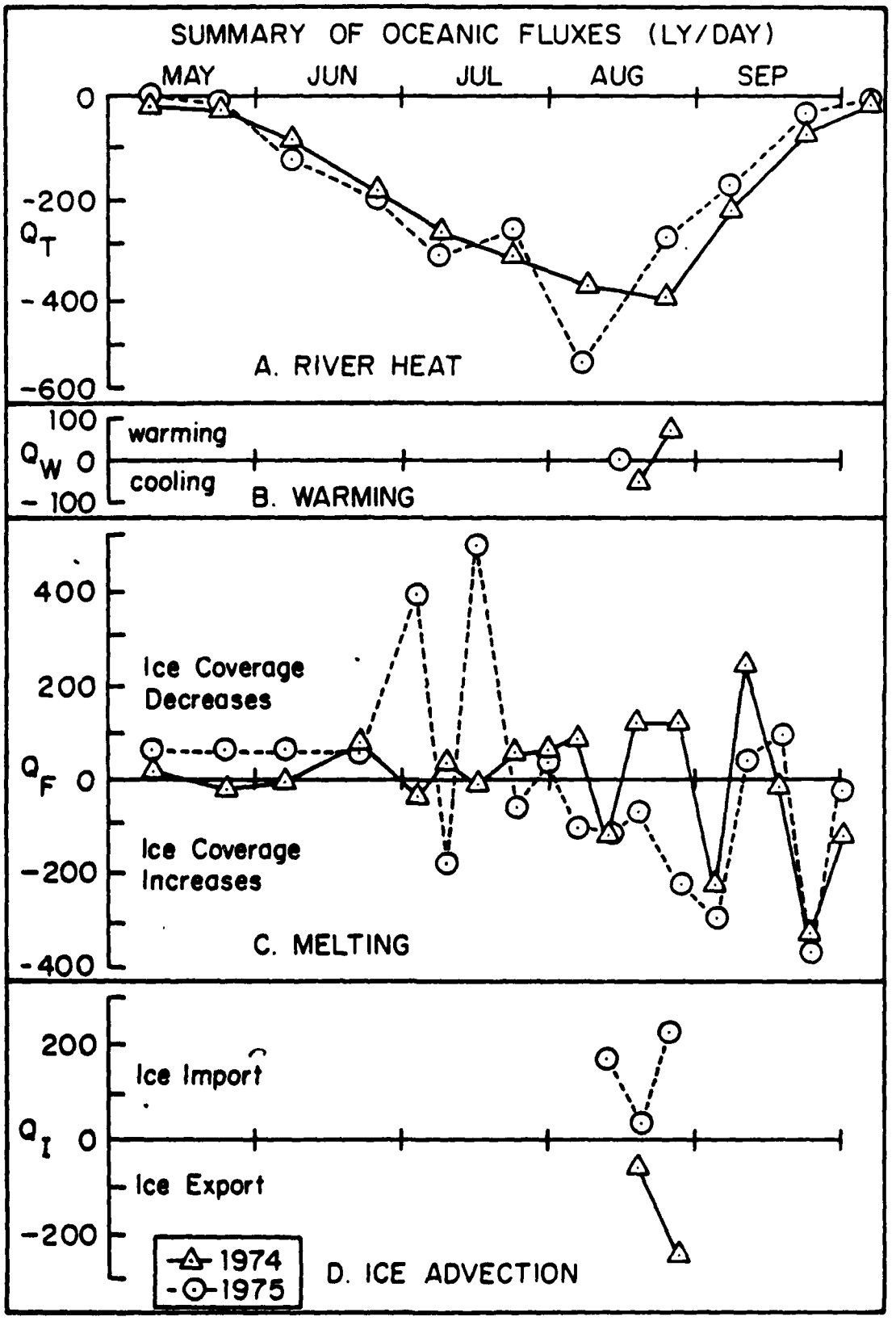
SUMMARY OF OCEANIC FLUXES (LY/DAY)
MAY
JUN
JUL
AUG
SEP
0
-200
Q_T
-400
-600
A. RIVER HEAT
100
Q_W 0
-100
warming
cooling
B. WARMING
400
200
Q_F 0
-200
-400
Ice Coverage Decreases
Ice Coverage Increases
C. MELTING
200
Q_I 0
-200
Ice Import
Ice Export
1974
1975
D. ICE ADVECTION

Figure 21

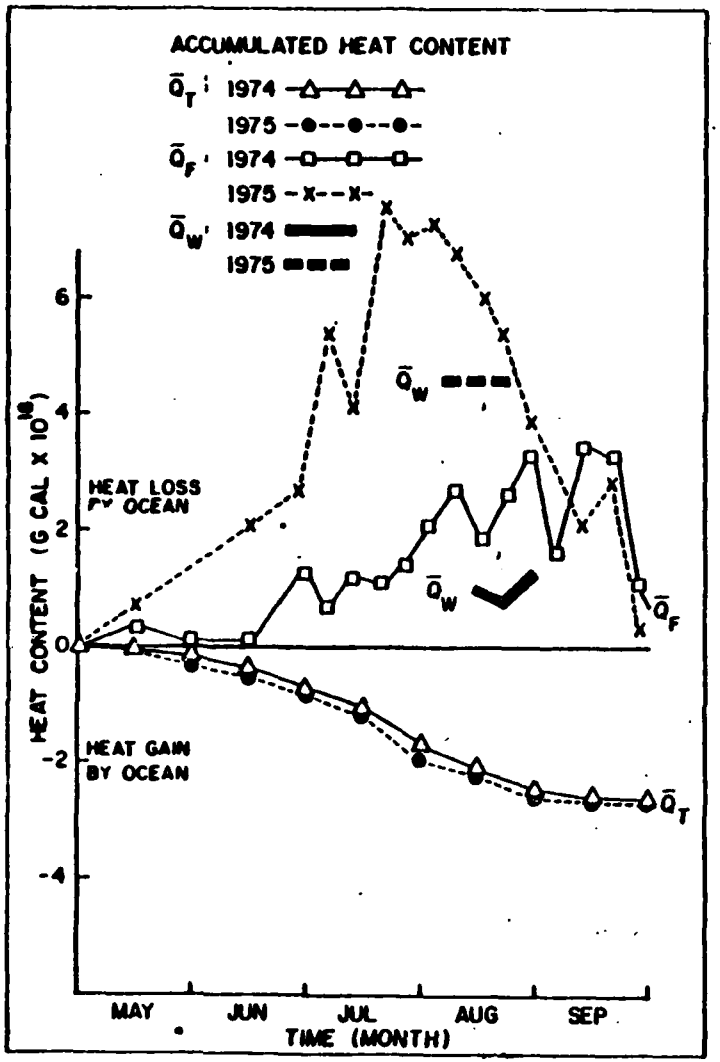
ACCUMULATED HEAT CONTENT
$\bar{Q}_T$ 1974
1975
$\bar{Q}_F$ 1974
1975
$\bar{Q}_W$ 1974
1975
HEAT LOSS BY OCEAN
HEAT GAIN BY OCEAN
HEAT CONTENT (G CAL X 10^{18})
6
4
2
0
-2
-4
MAY
JUN
JUL
AUG
SEP
TIME (MONTH)

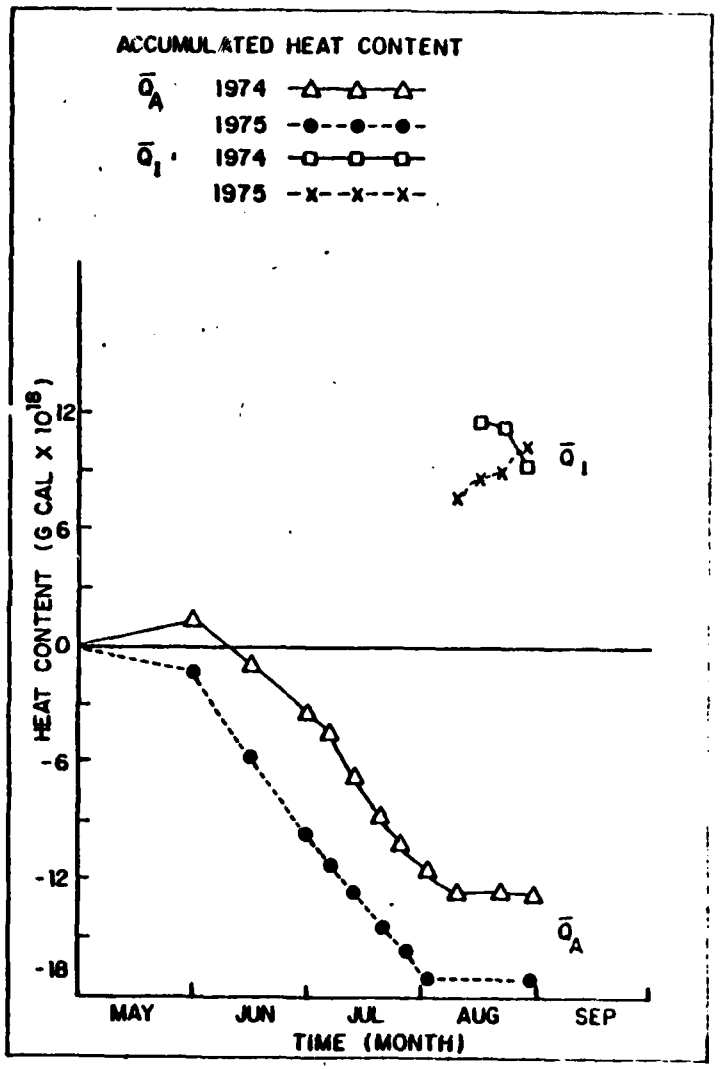
ACCUMULATED HEAT CONTENT
$\bar{Q}_A$ 1974
1975
$\bar{Q}_I$ 1974
1975
HEAT CONTENT (G CAL X 10^{18})
12
6
0
-6
-12
-18
MAY
JUN
JUL
AUG
SEP
TIME (MONTH)

Figure 22

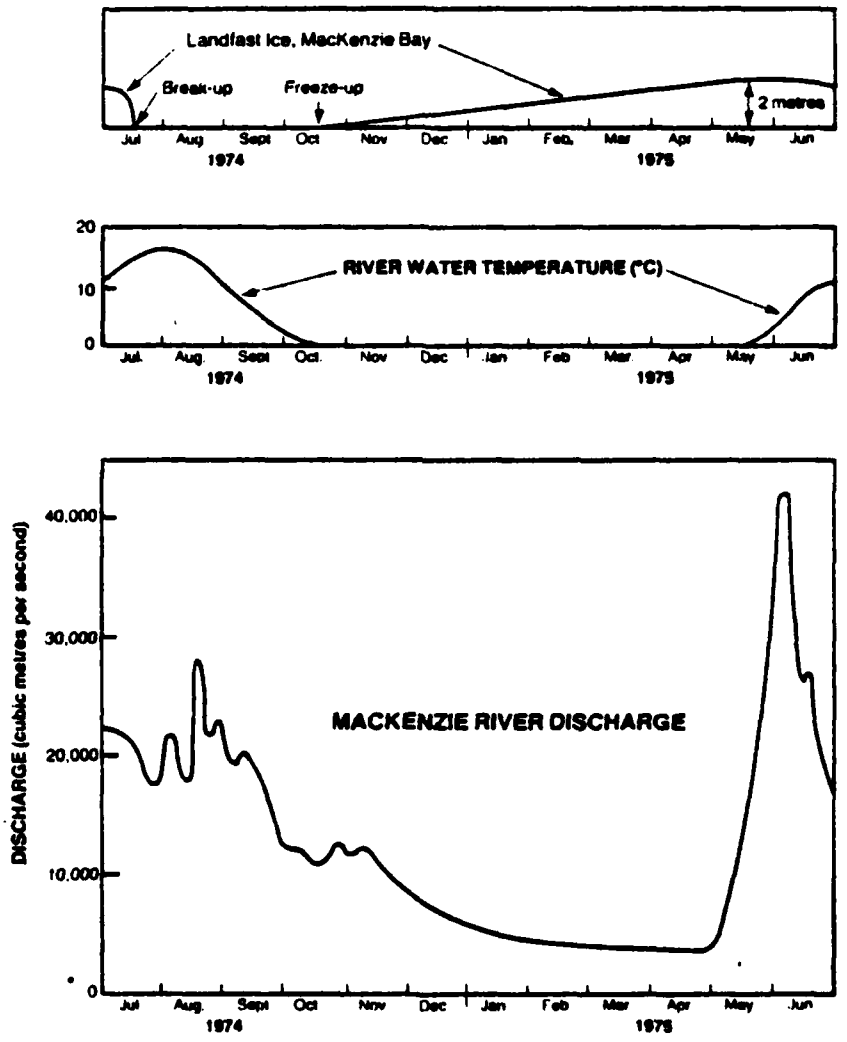

Figure 23: Mackenzie River discharge volume and temperature and the relationship to breakup and freeze-up of landfast ice in Mackenzie Bay.

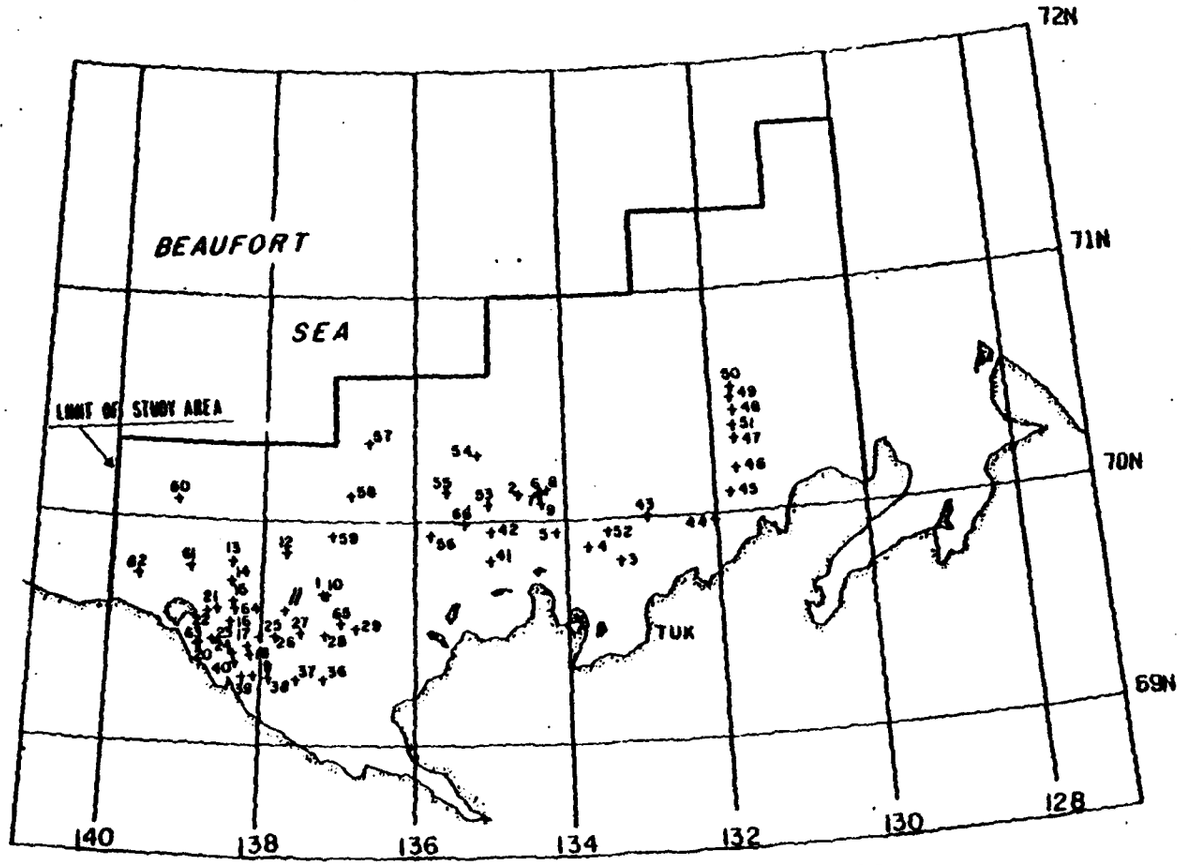

Figure 24: Oceanographic stations, 1974 summer (stations 30 to 35 were for bottom samples only and were not plotted)

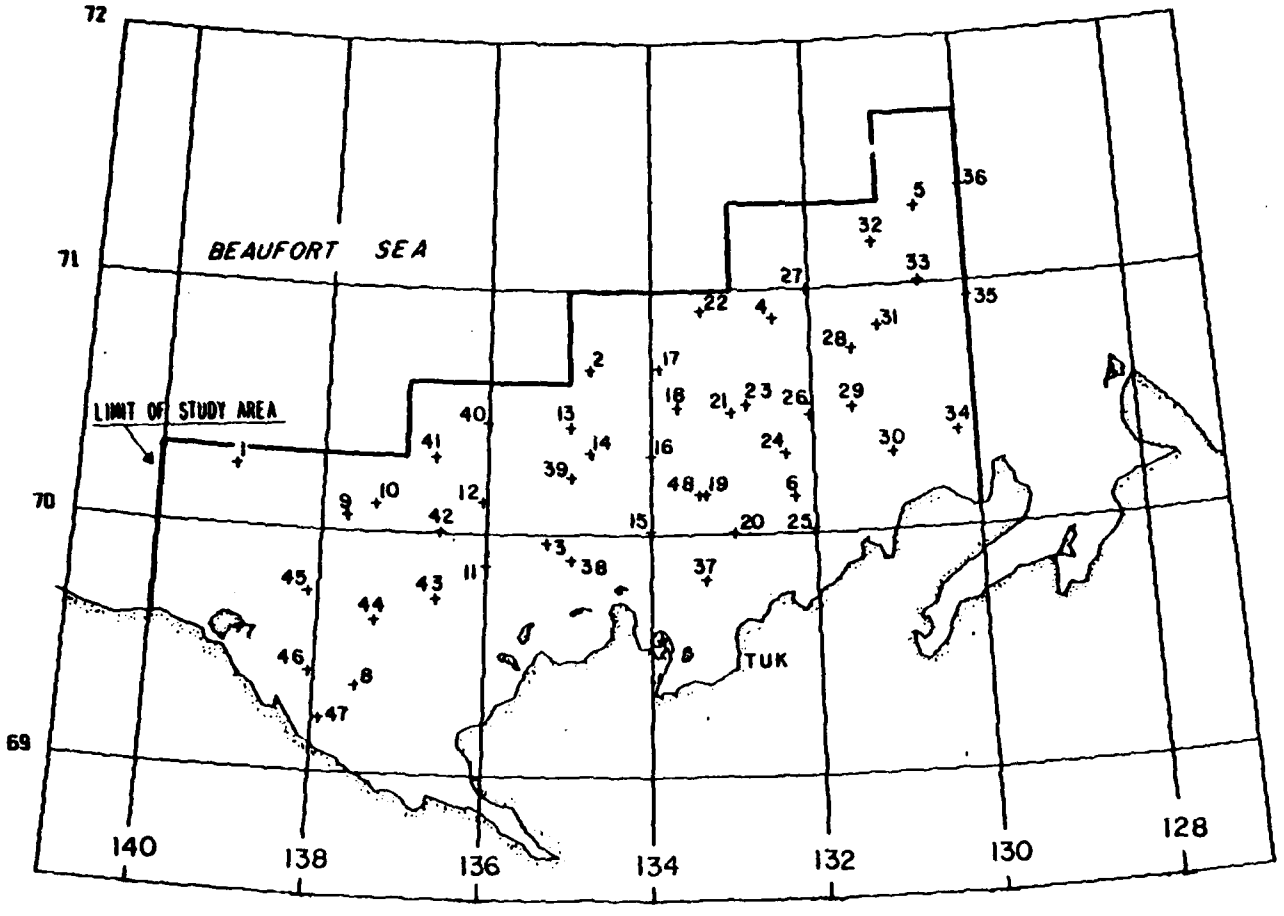

Figure 25: Oceanographic stations, 1975 summer

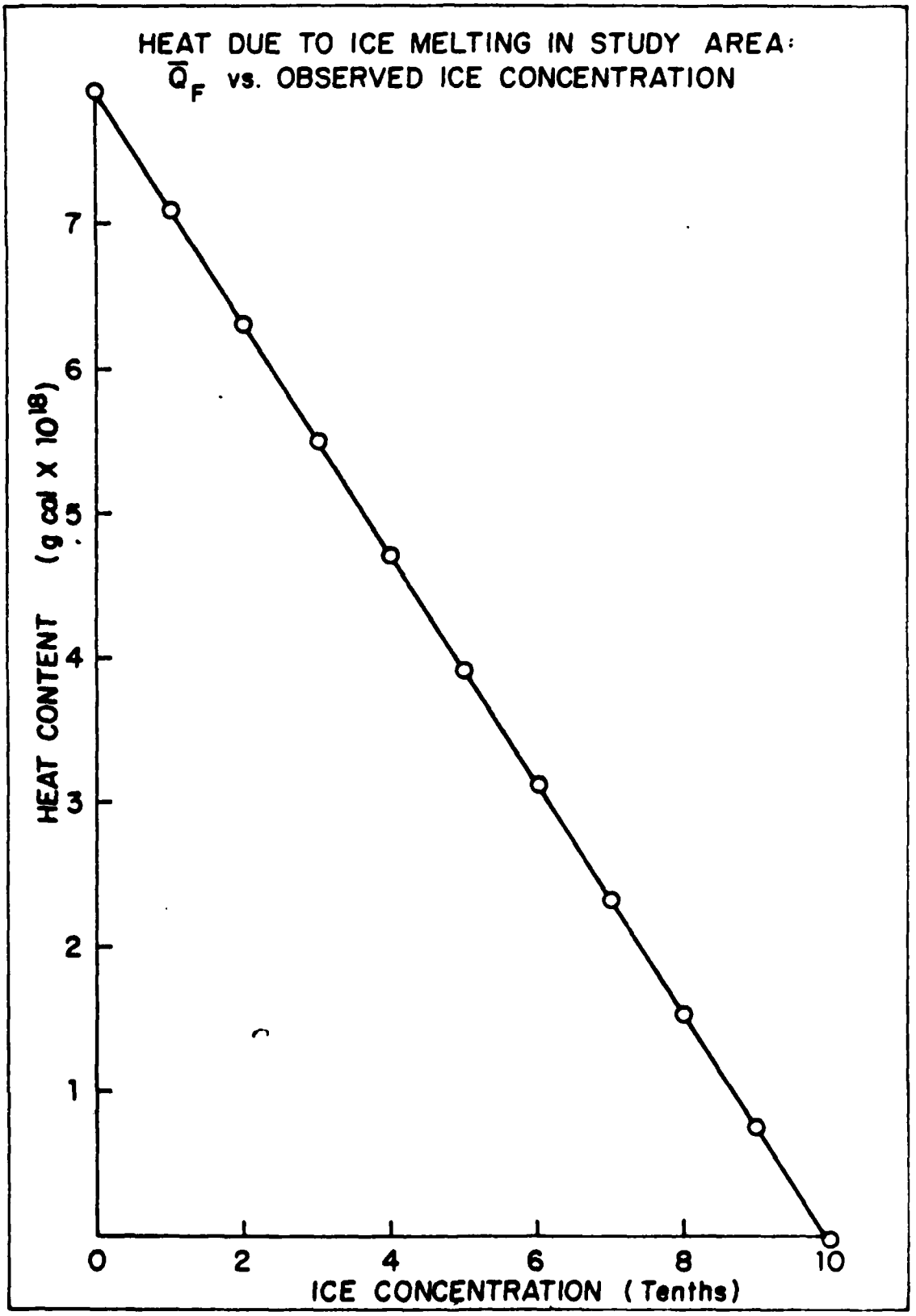
HEAT DUE TO ICE MELTING IN STUDY AREA:
$\bar{Q}_F$ vs. OBSERVED ICE CONCENTRATION
HEAT CONTENT (g cal X 10^{18})
1
2
3
4
5
6
7
0
2
4
6
8
10
ICE CONCENTRATION (Tenths)

Figure 26

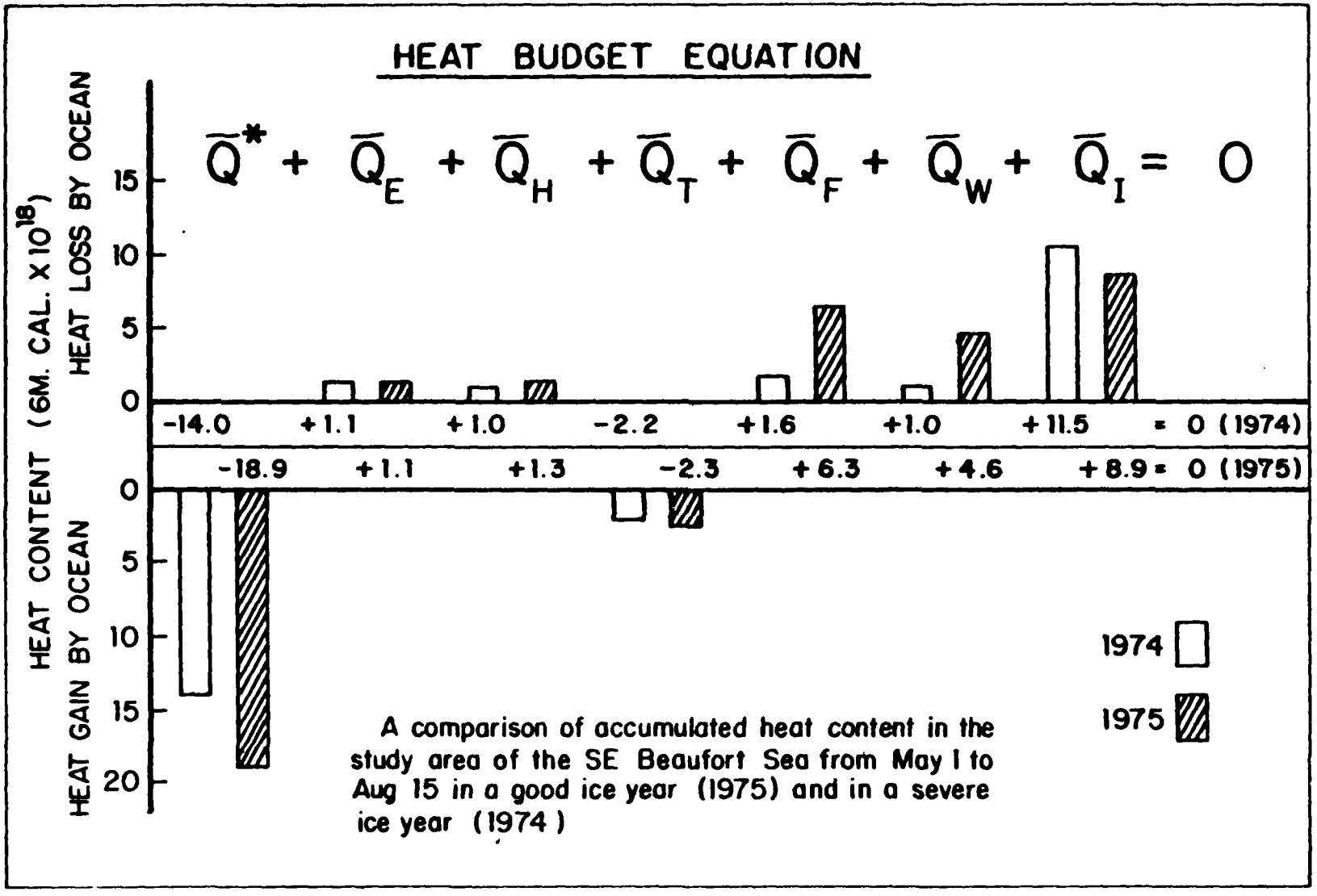
HEAT BUDGET EQUATION
$\bar{Q}^* + \bar{Q}_E + \bar{Q}_H + \bar{Q}_T + \bar{Q}_F + \bar{Q}_W + \bar{Q}_I = 0$
HEAT CONTENT (6M. CAL. X 10^{18})
HEAT LOSS BY OCEAN
HEAT GAIN BY OCEAN
15
10
5
0
-14.0 +1.1 +1.0 -2.2 +1.6 +1.0 +11.5 = 0 (1974)
-18.9 +1.1 +1.3 -2.3 +6.3 +4.6 +8.9 = 0 (1975)
0
5
10
15
20
1974
1975
A comparison of accumulated heat content in the study area of the SE Beaufort Sea from May 1 to Aug 15 in a good ice year (1975) and in a severe ice year (1974)

Figure 27

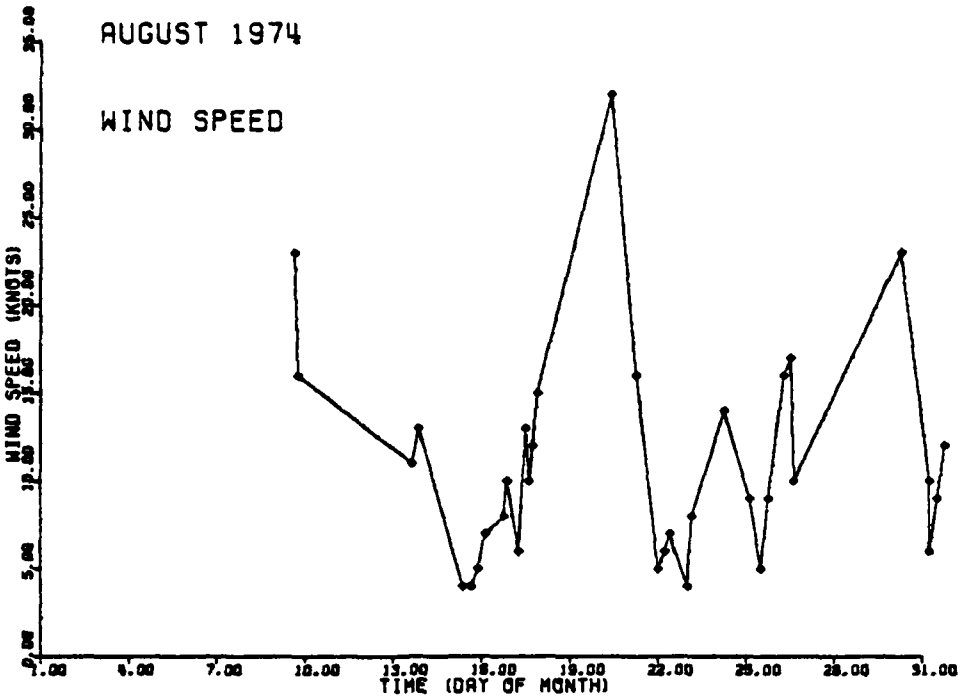

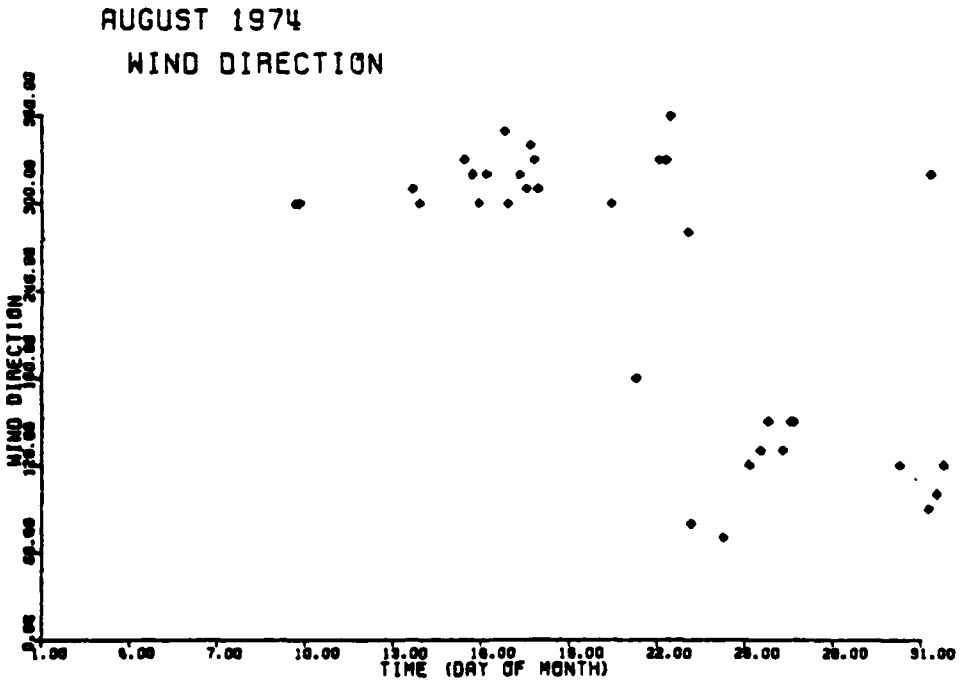

Figure 28: Wind speeds and wind direction versus time during August 1974 from marine observations.

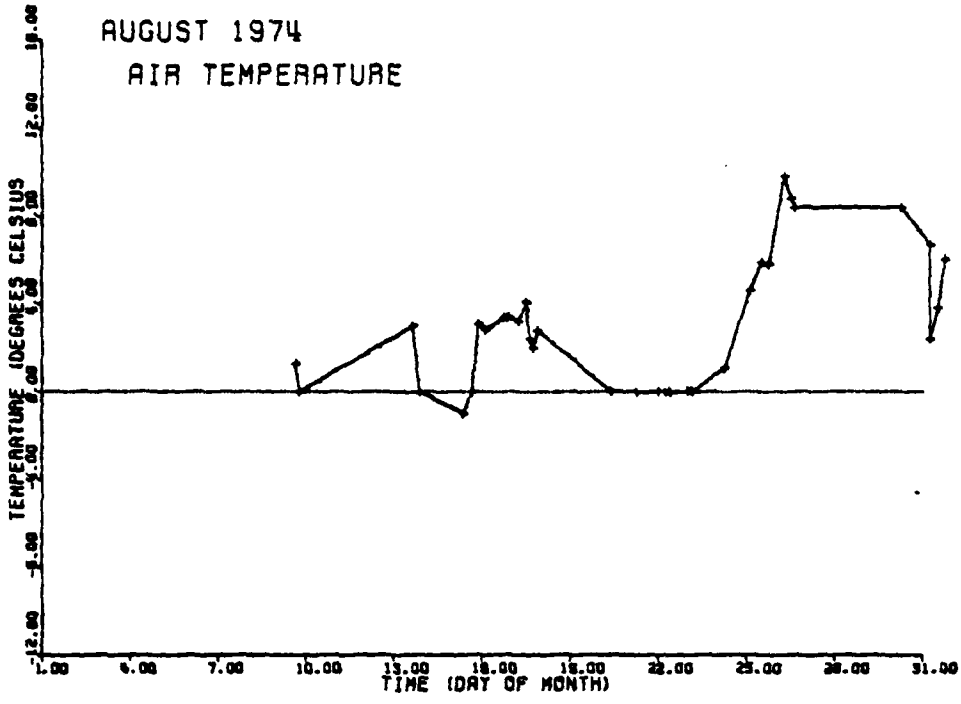

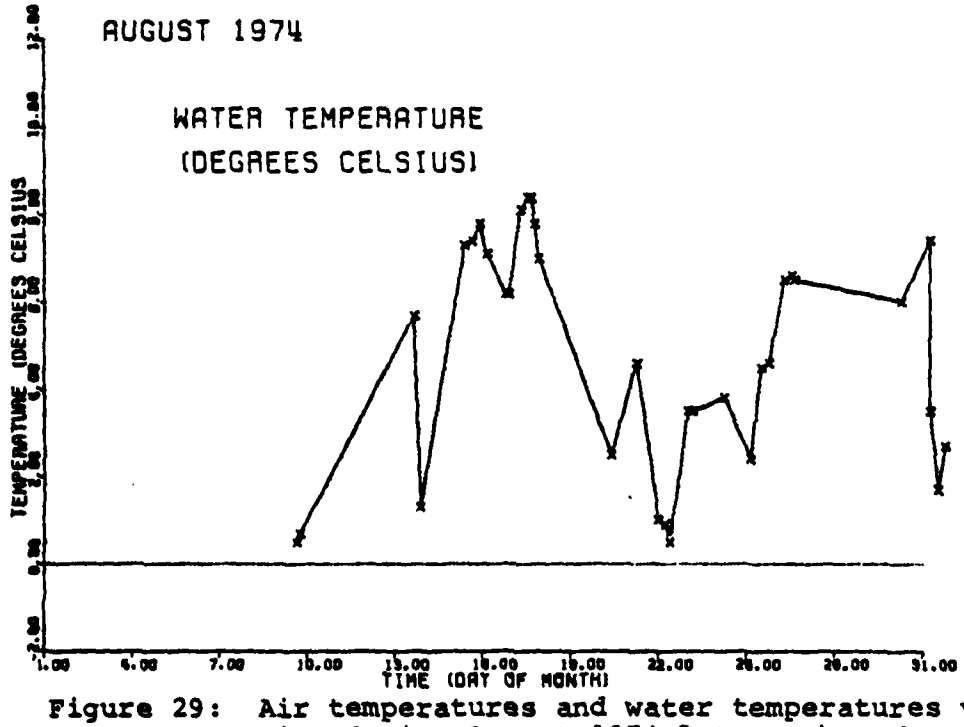

Figure 29: Air temperatures and water temperatures versus time during August 1974 from marine observations.

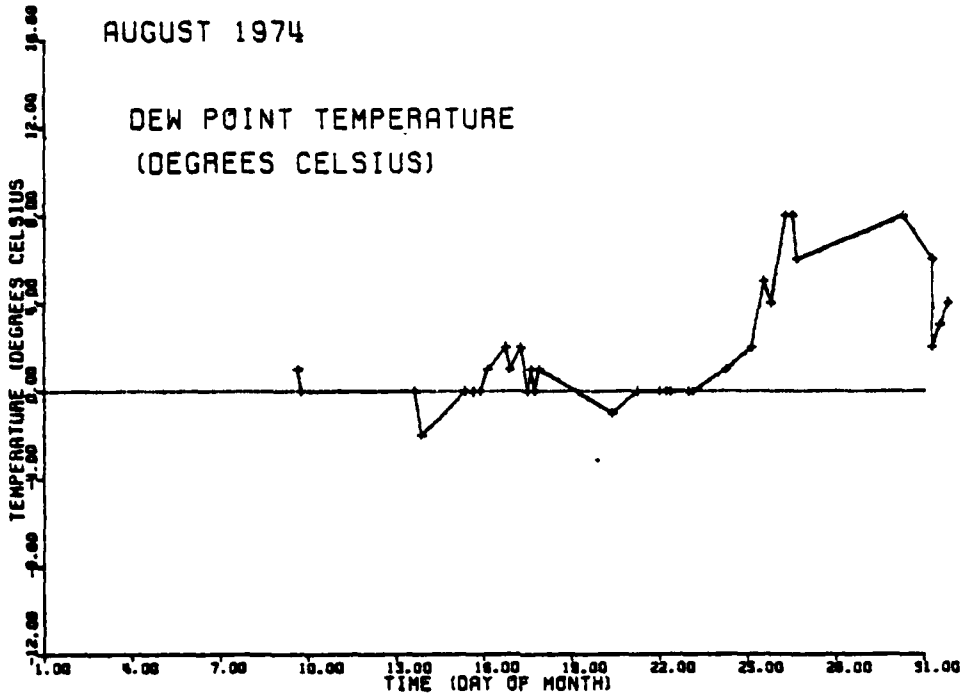

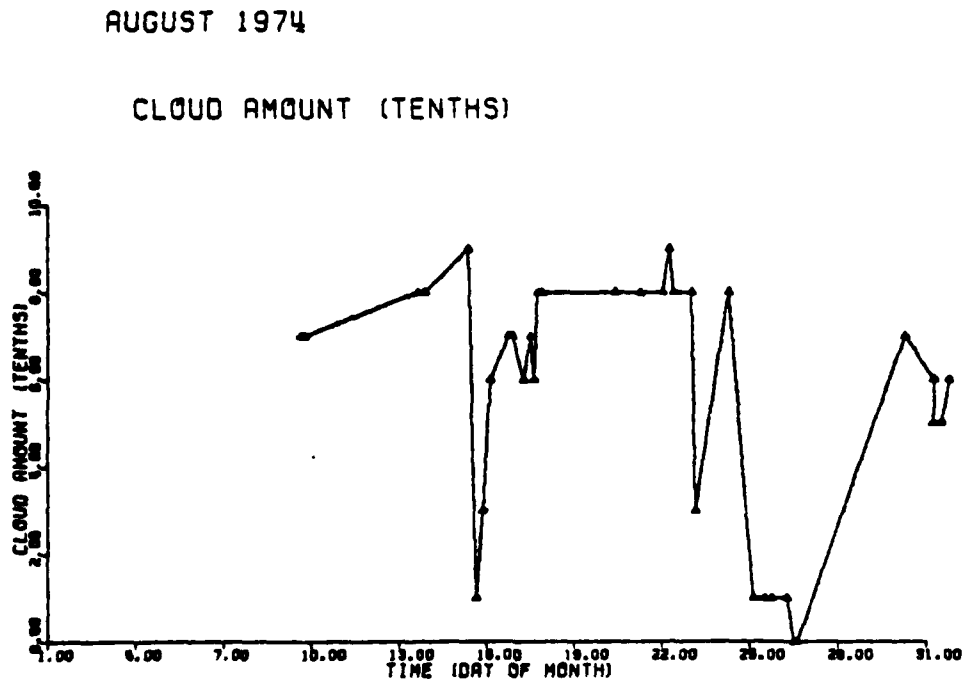

Figure 30: Dew point temperatures and cloud amounts versus time during August 1974 from marine observations

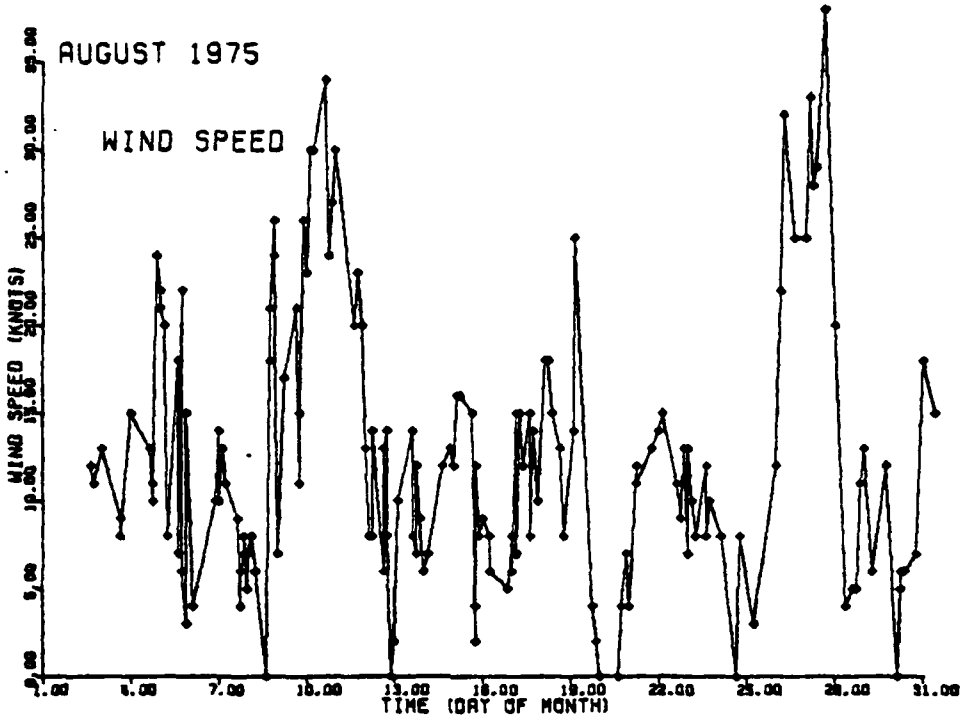

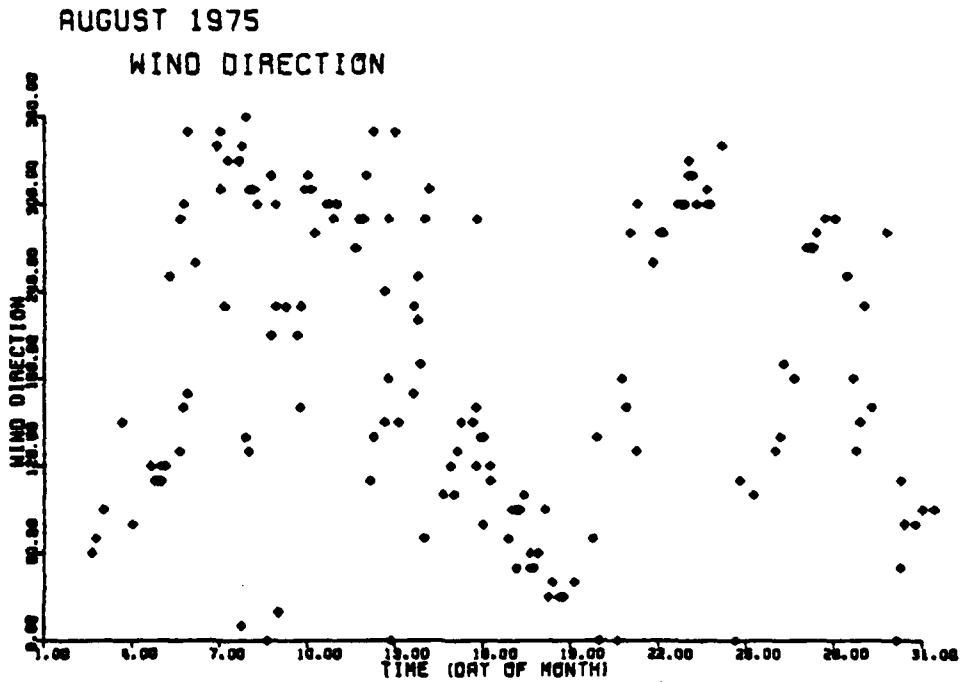

Figure 31: Winds speeds and wind direction versus time during August 1975 from marine observations.

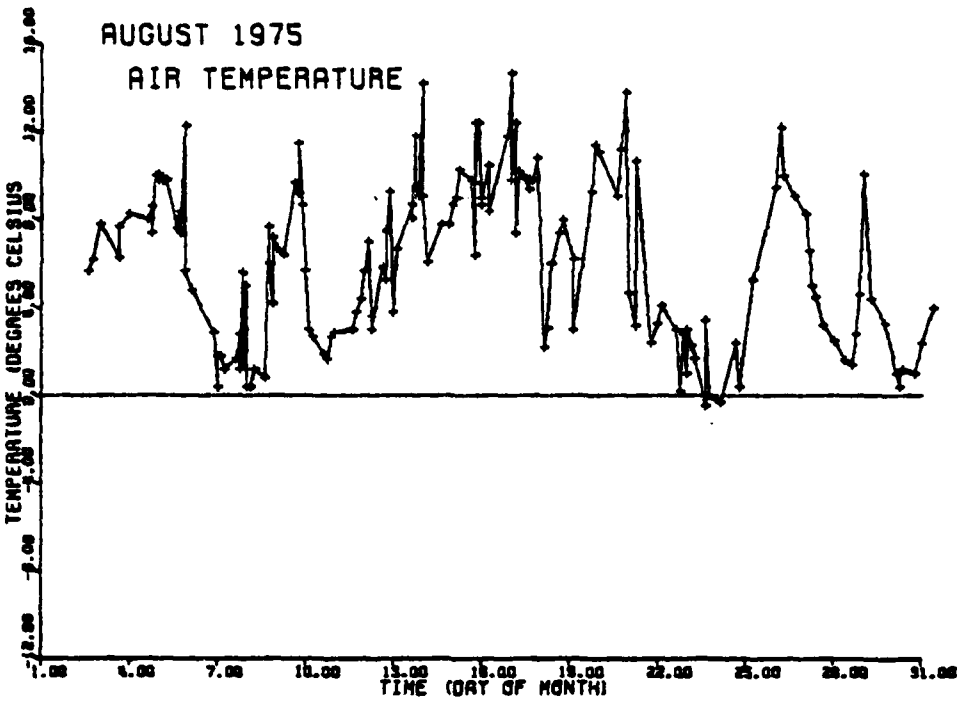

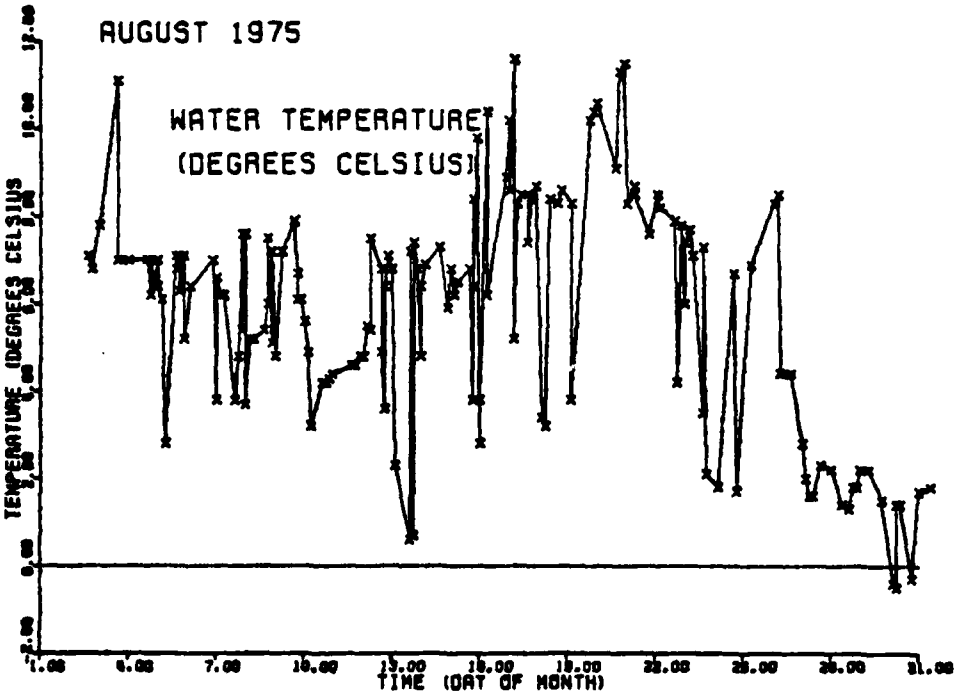

Figure 32: Air temperatures and water temperatures versus time during August 1975 from marine observations.

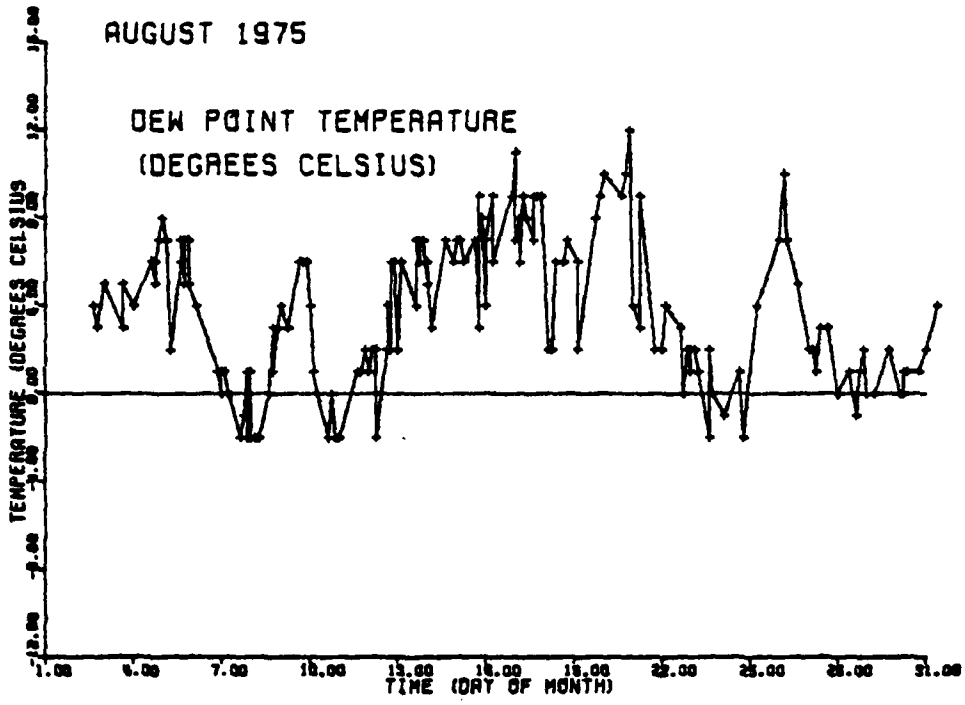

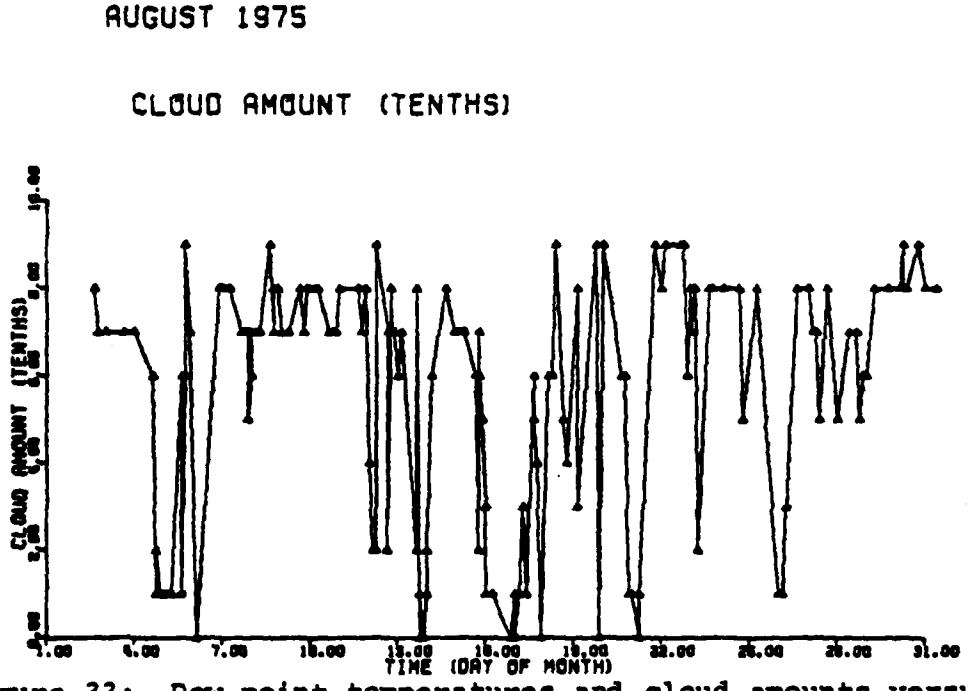

Figure 33: Dew point temperatures and cloud amounts versus time during August 1974 from marine observations.

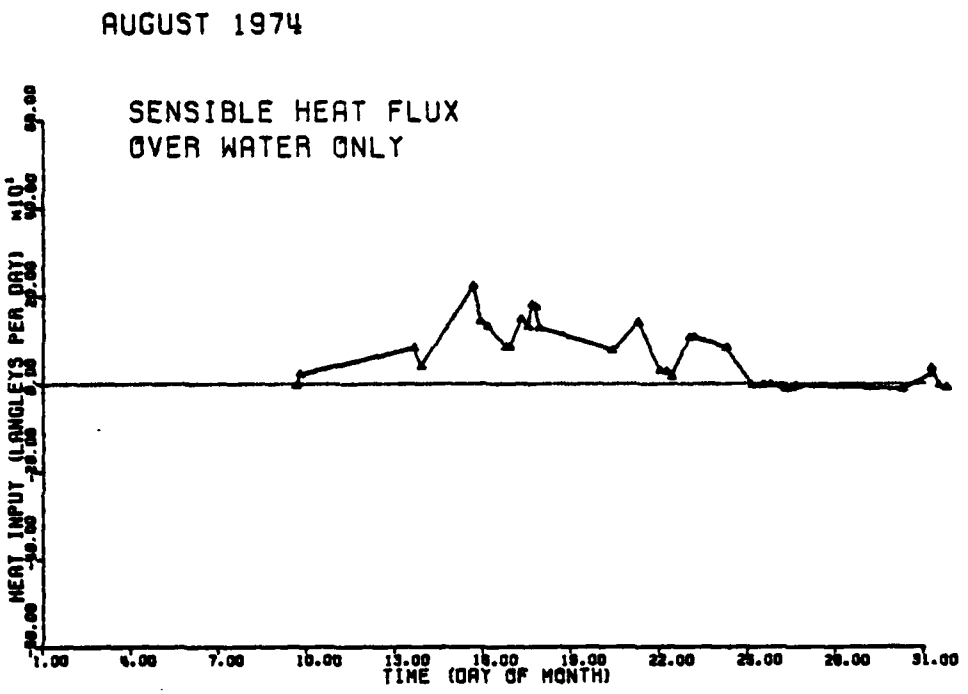

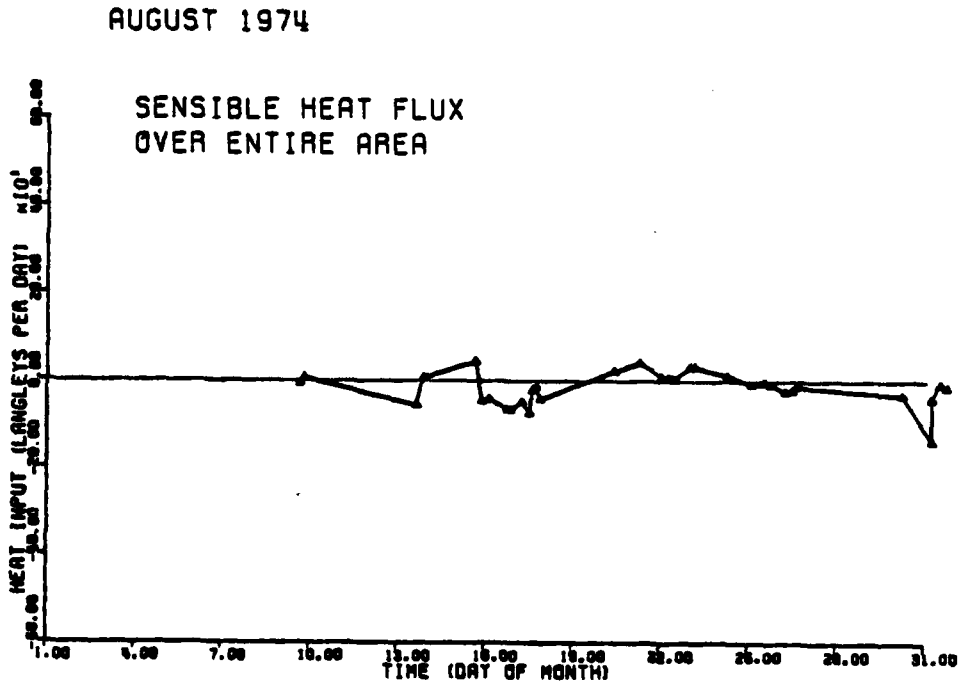

Figure 34: Sensible heat flux versus time in August 1974.

AUGUST 1974

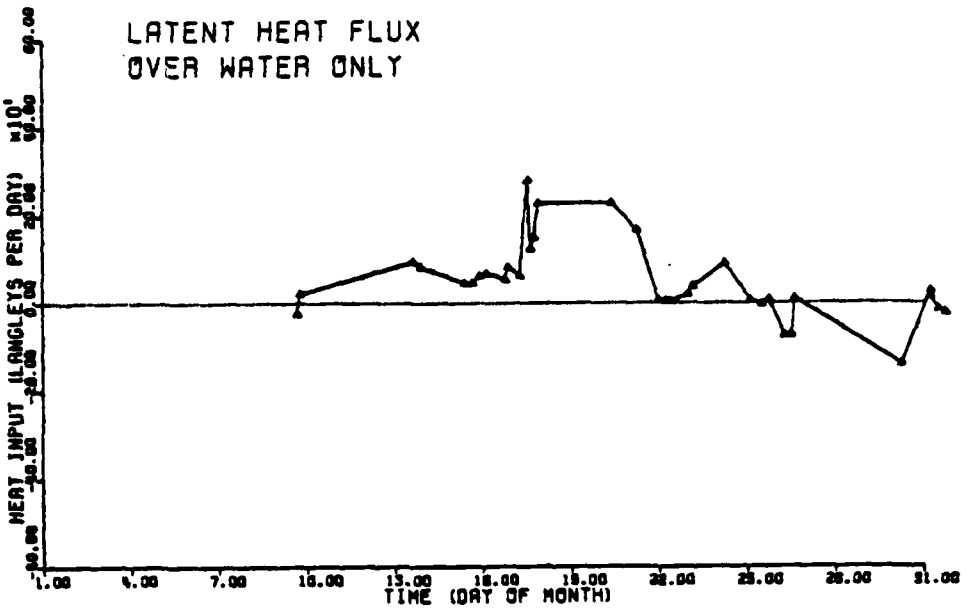

AUGUST 1974

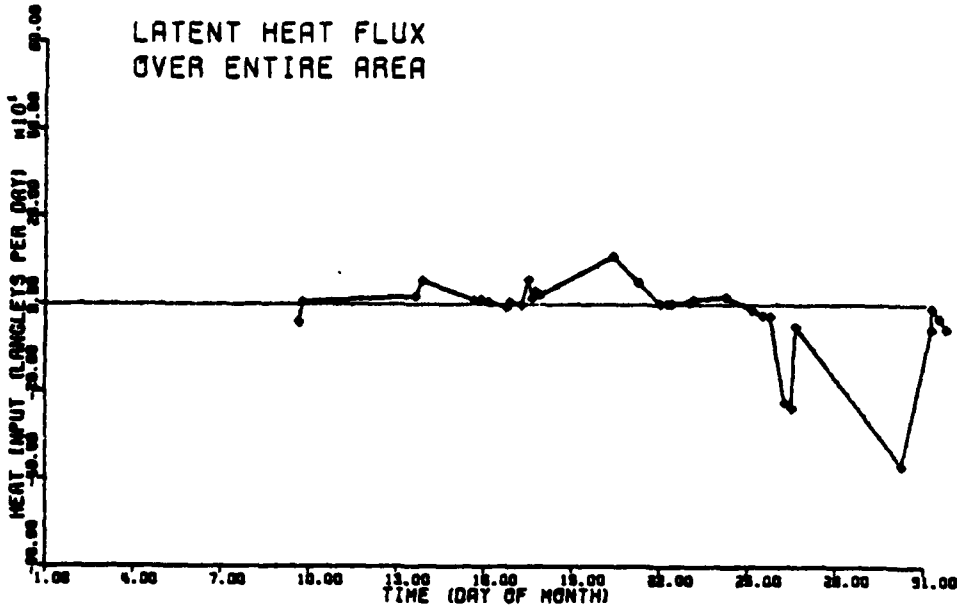

Figure 35: Latent heat flux versus time in August 1974.

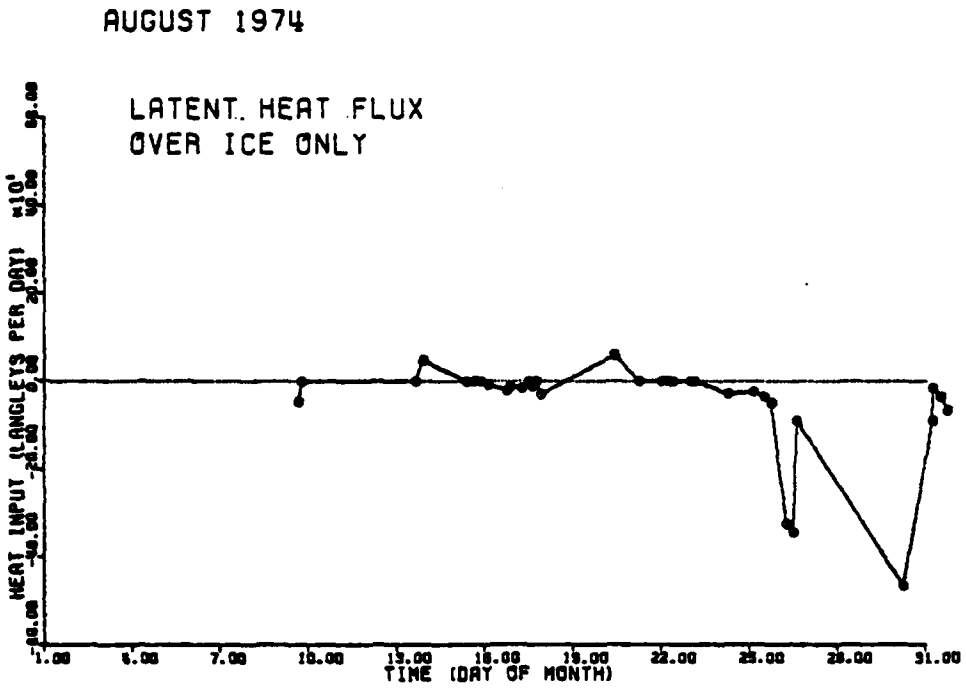

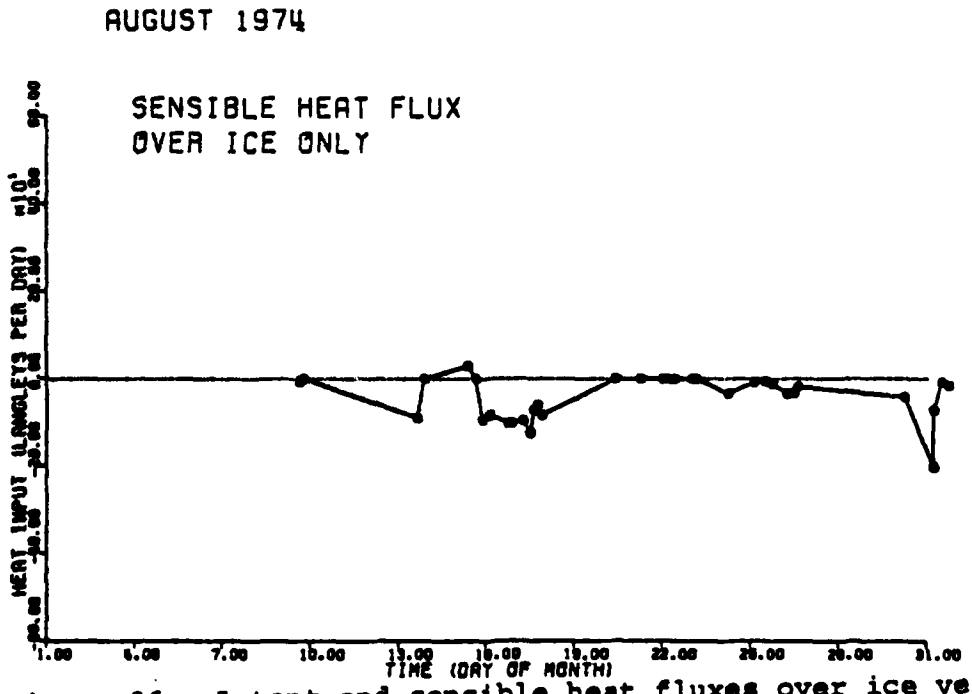

Figure 36: Latent and sensible heat fluxes over ice versus time in August 1974.

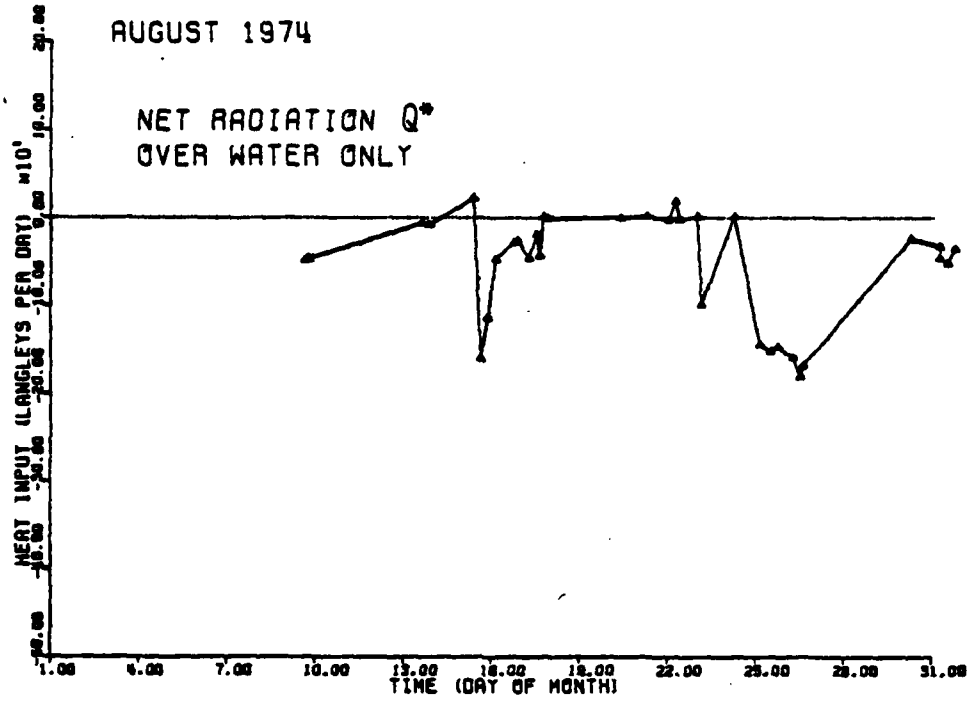

BASED ON CALCULATED RADIATION FLUX

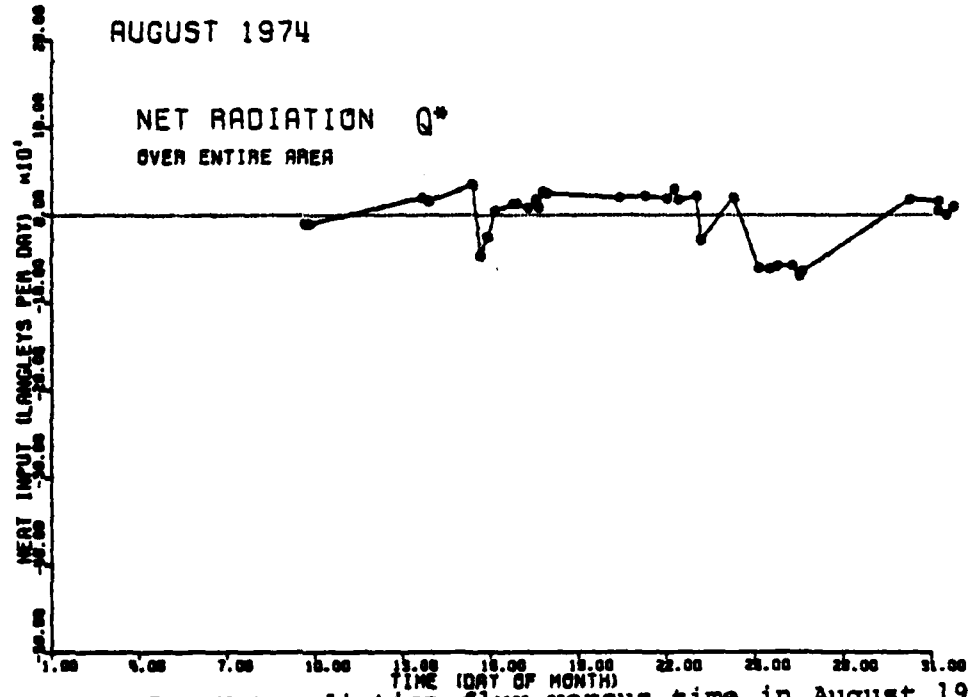

Figure 37. Net radiation flux versus time in August 1974.

AUGUST 1974

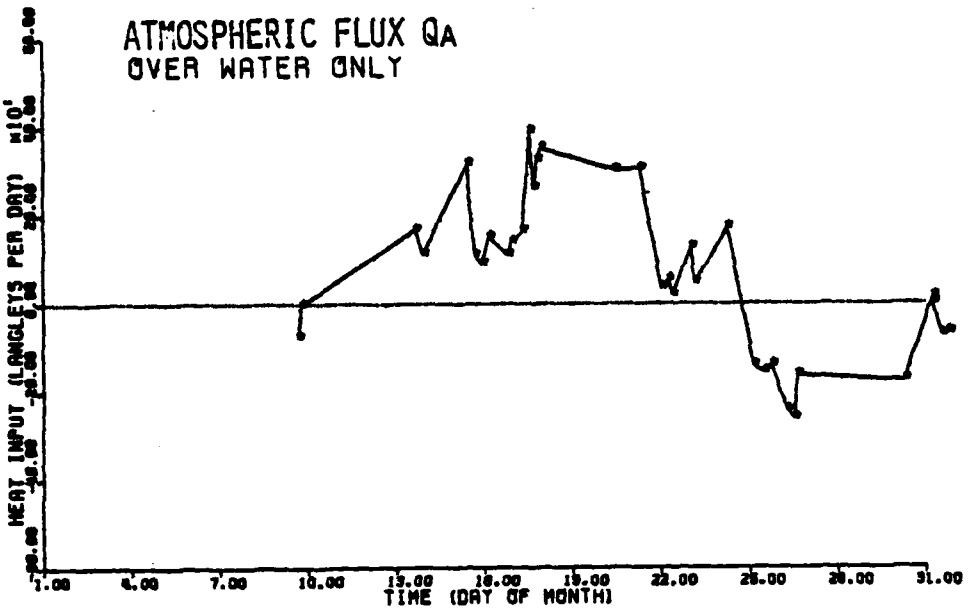

BASED ON CALCULATED RADIATION FLUX

AUGUST 1974

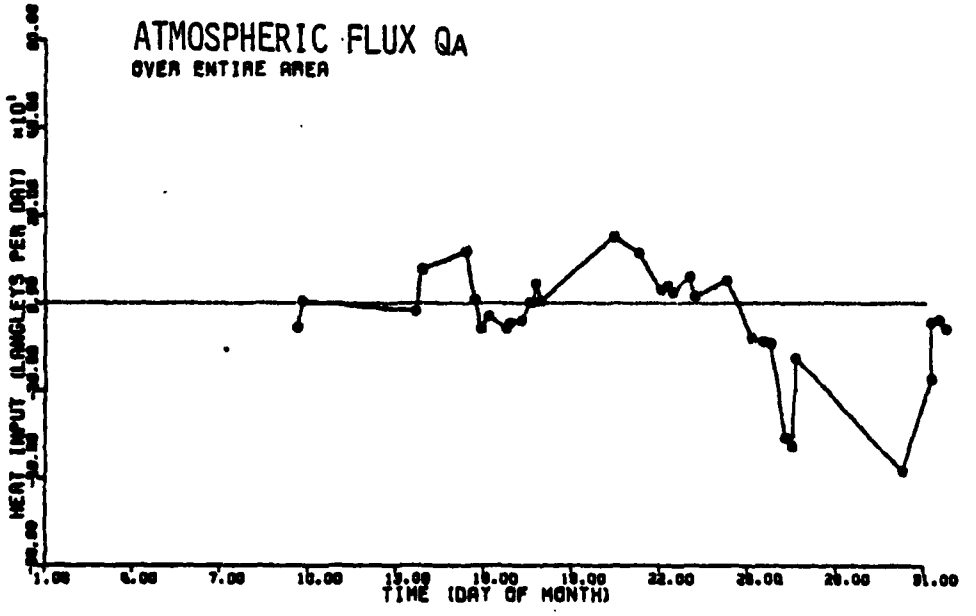

Figure 38: Atmospheric flux versus time in August 1974.

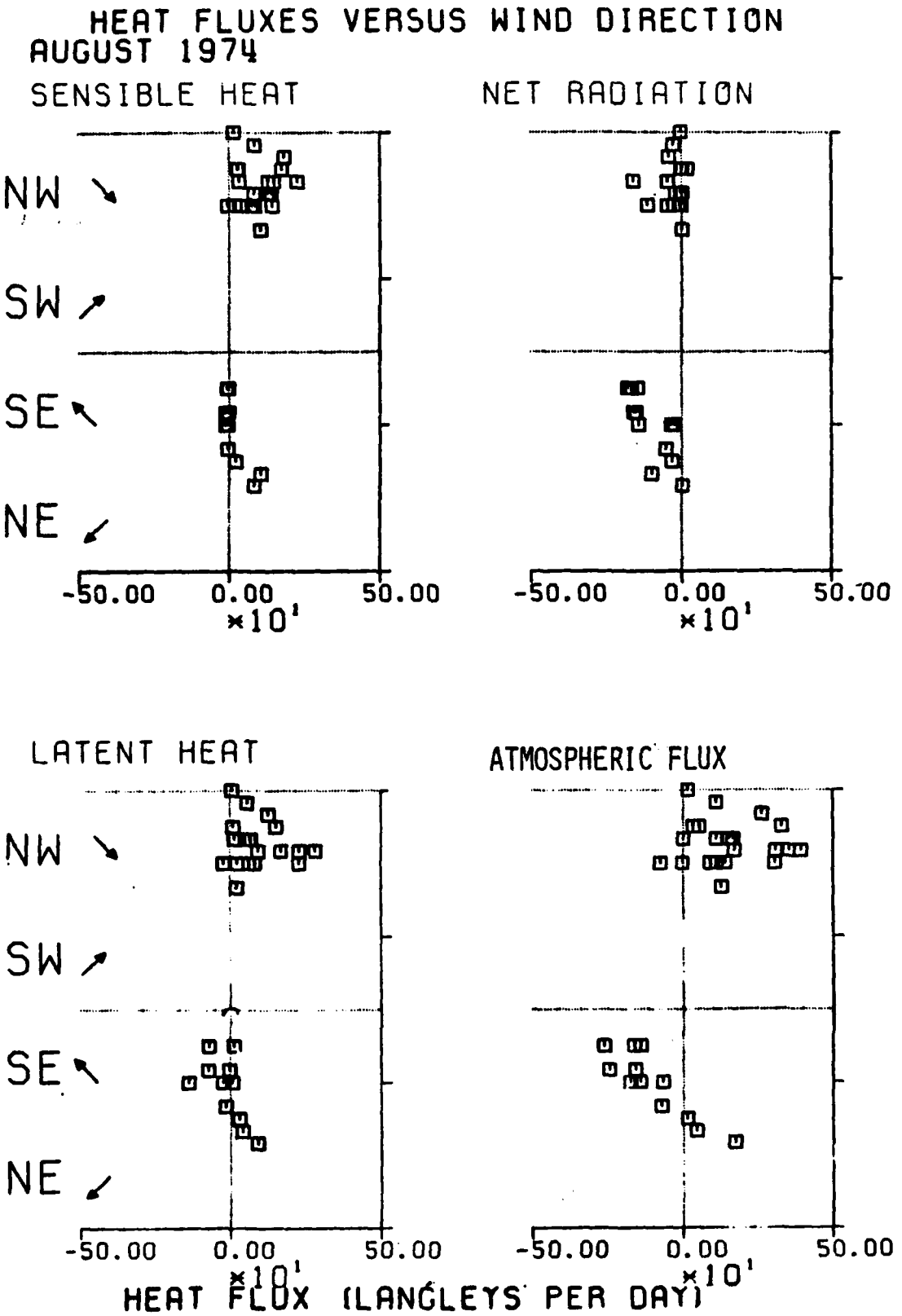
HEAT FLUXES VERSUS WIND DIRECTION
AUGUST 1974
SENSIBLE HEAT
NET RADIATION
LATENT HEAT
ATMOSPHERIC FLUX
NW
SW
SE
NE
-50.00
0.00
50.00
×10¹
HEAT FLUX (LANGLEYS PER DAY)

Figure 39

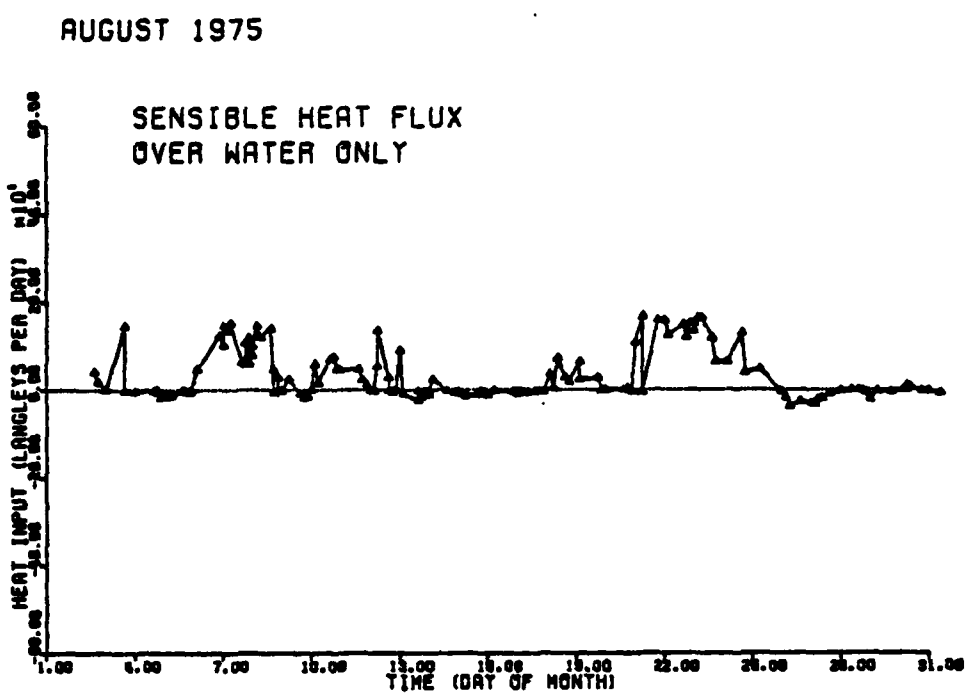

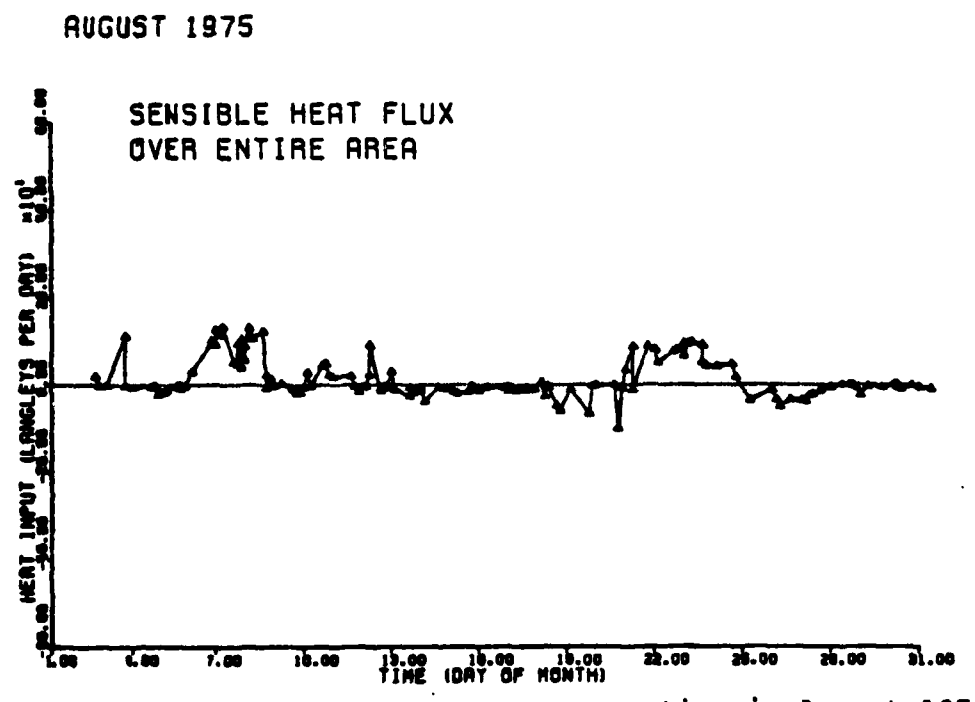

Figure 40: Sensible heat flux versus time in August 1975.

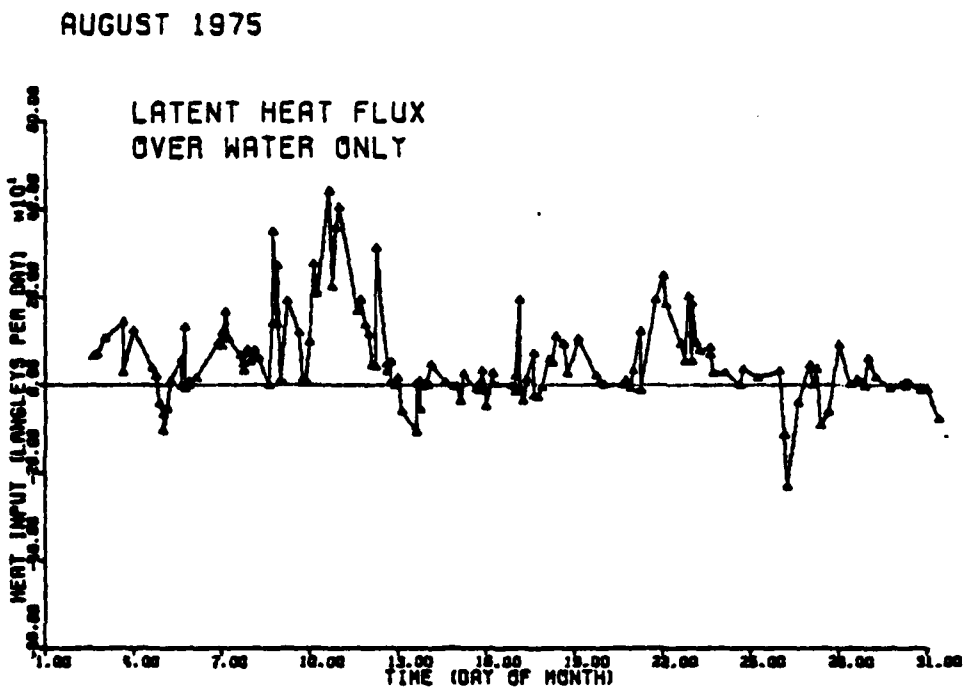

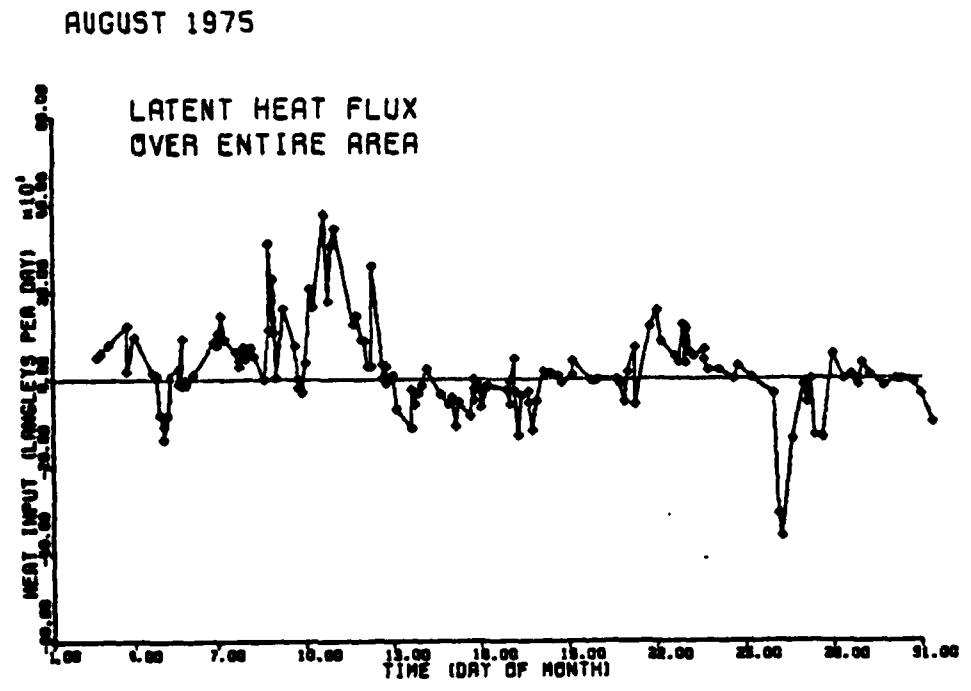

Figure 41: Latent heat flux versus time in August 1975

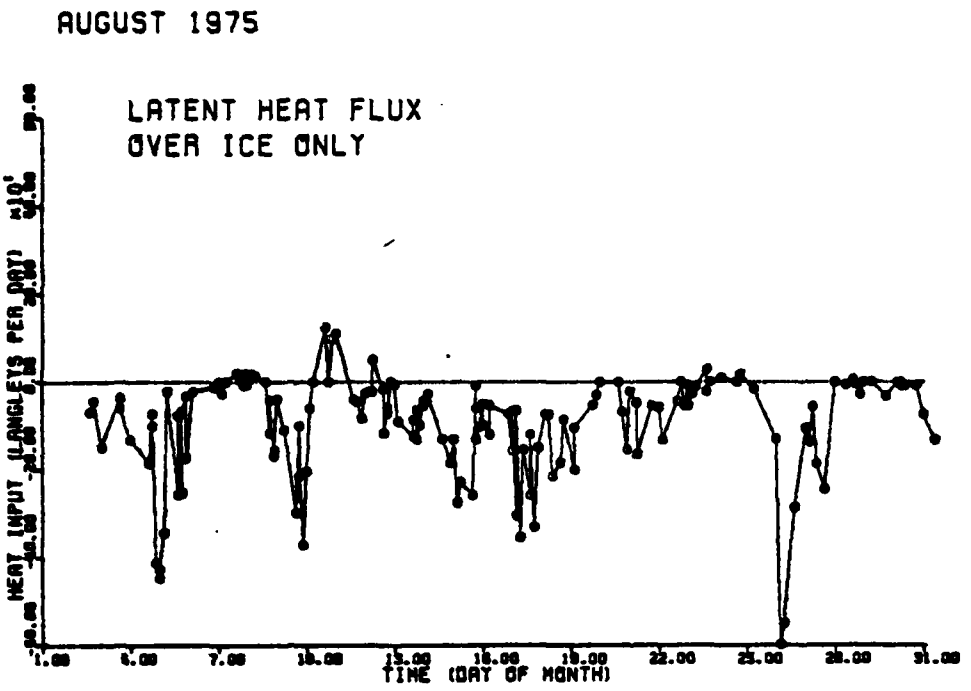

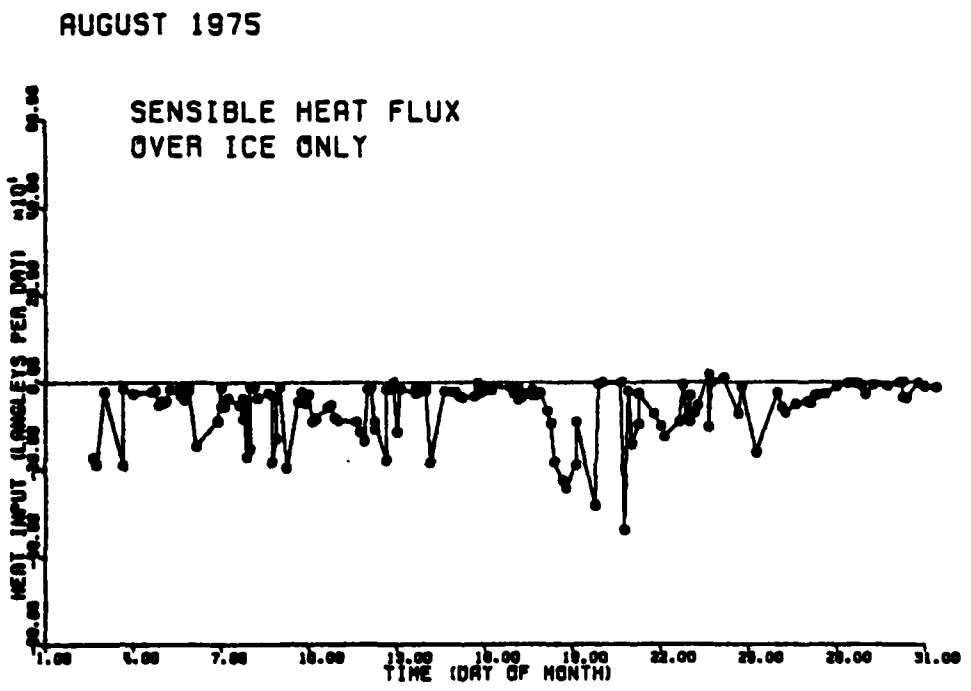

Figure 42: Latent and sensible heat fluxes over the ice versus time in August 1975.

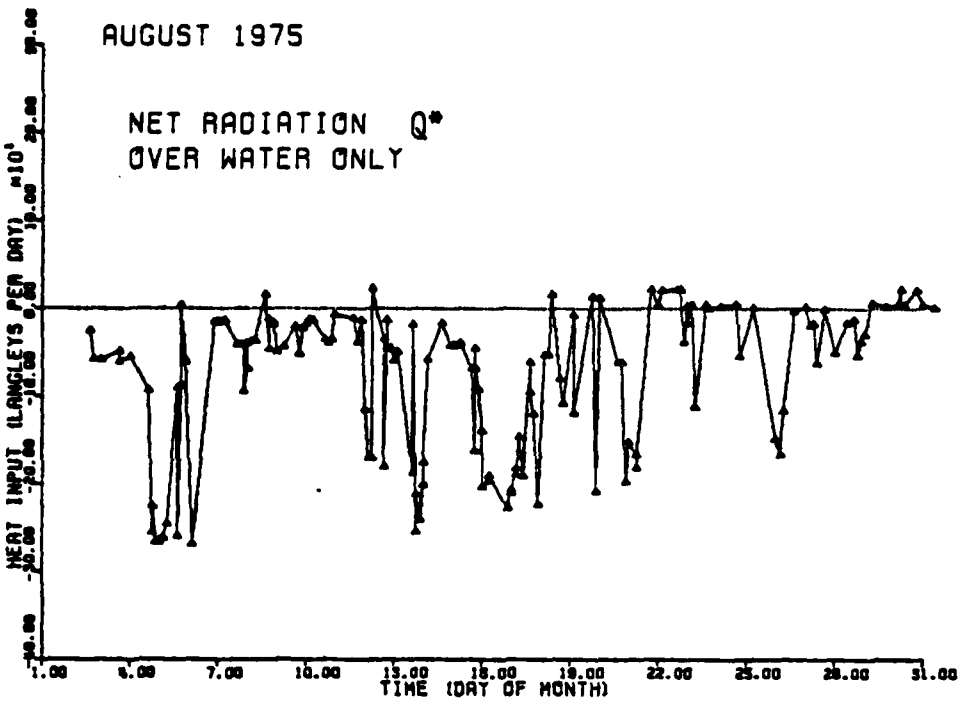

BASED ON CALCULATED RADIATION FLUX

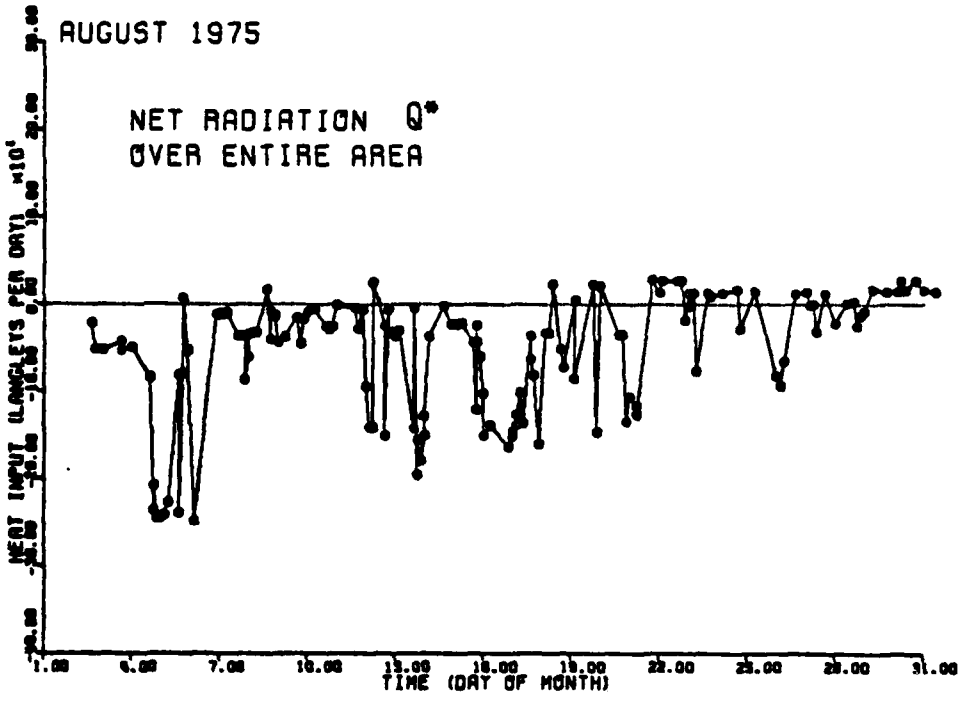

Figure 43: Net radiation flux versus time in August 1975.

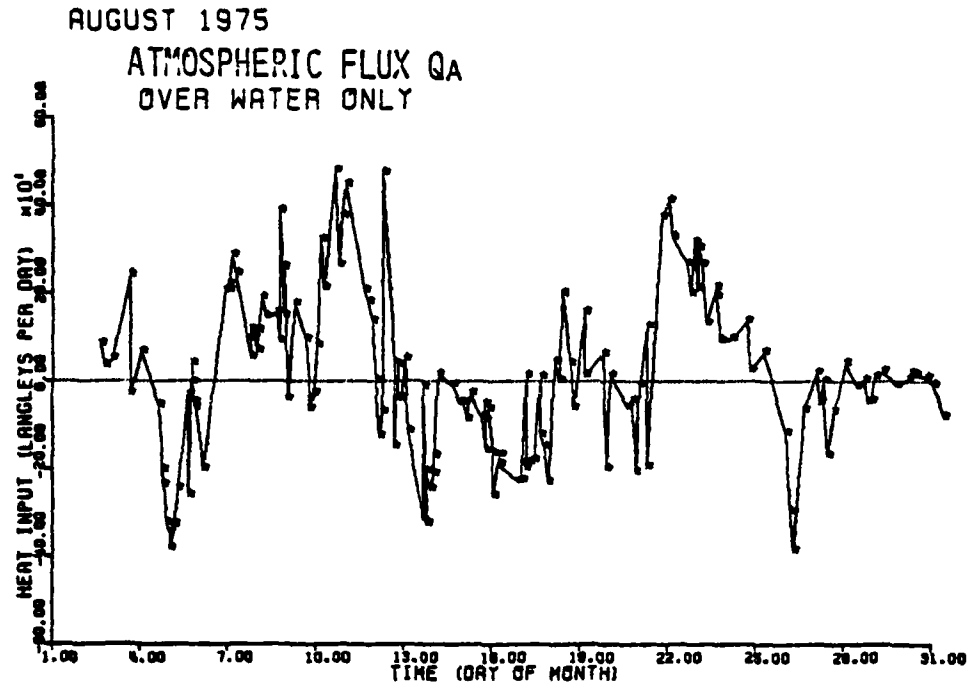

BASED ON CALCULATED RADIATION FLUX

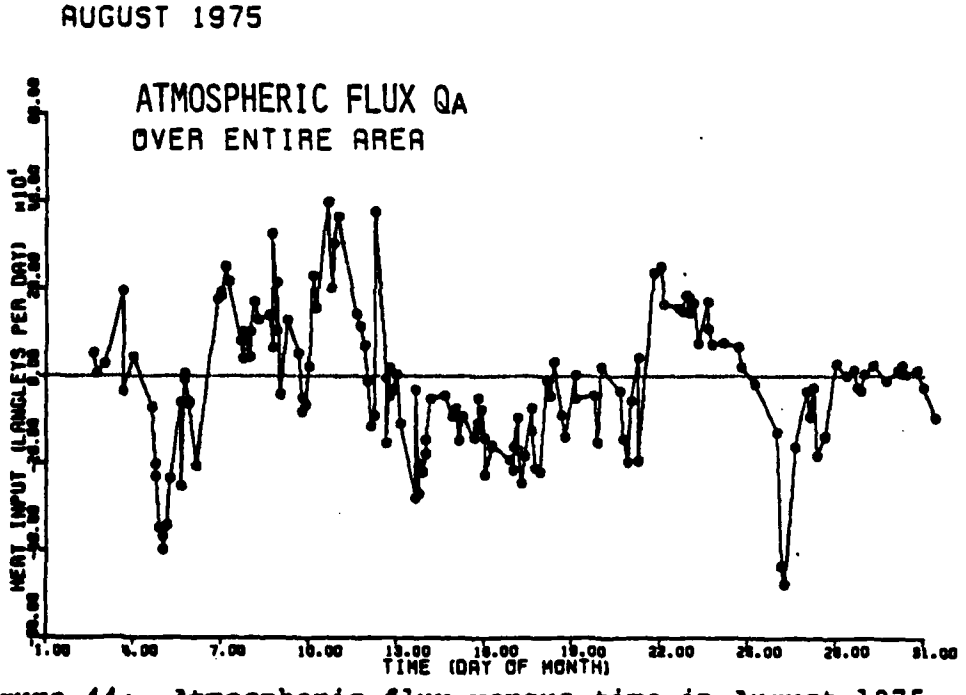

Figure 44: Atmospheric flux versus time in August 1975.

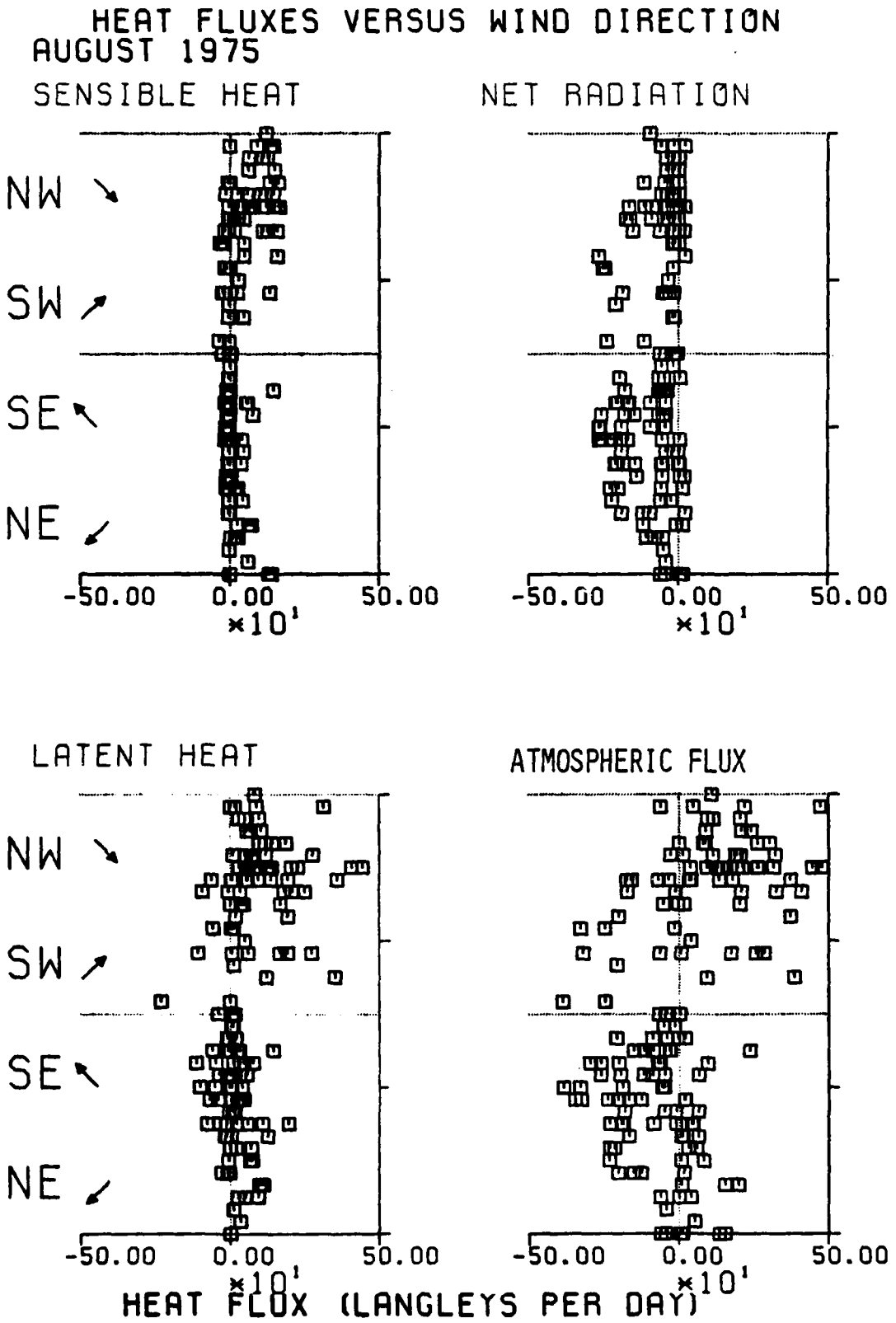
HEAT FLUXES VERSUS WIND DIRECTION
AUGUST 1975
SENSIBLE HEAT
NET RADIATION
LATENT HEAT
ATMOSPHERIC FLUX
NW
SW
SE
NE
-50.00
0.00
50.00
×10¹
HEAT FLUX (LANGLEYS PER DAY)

Figure 45

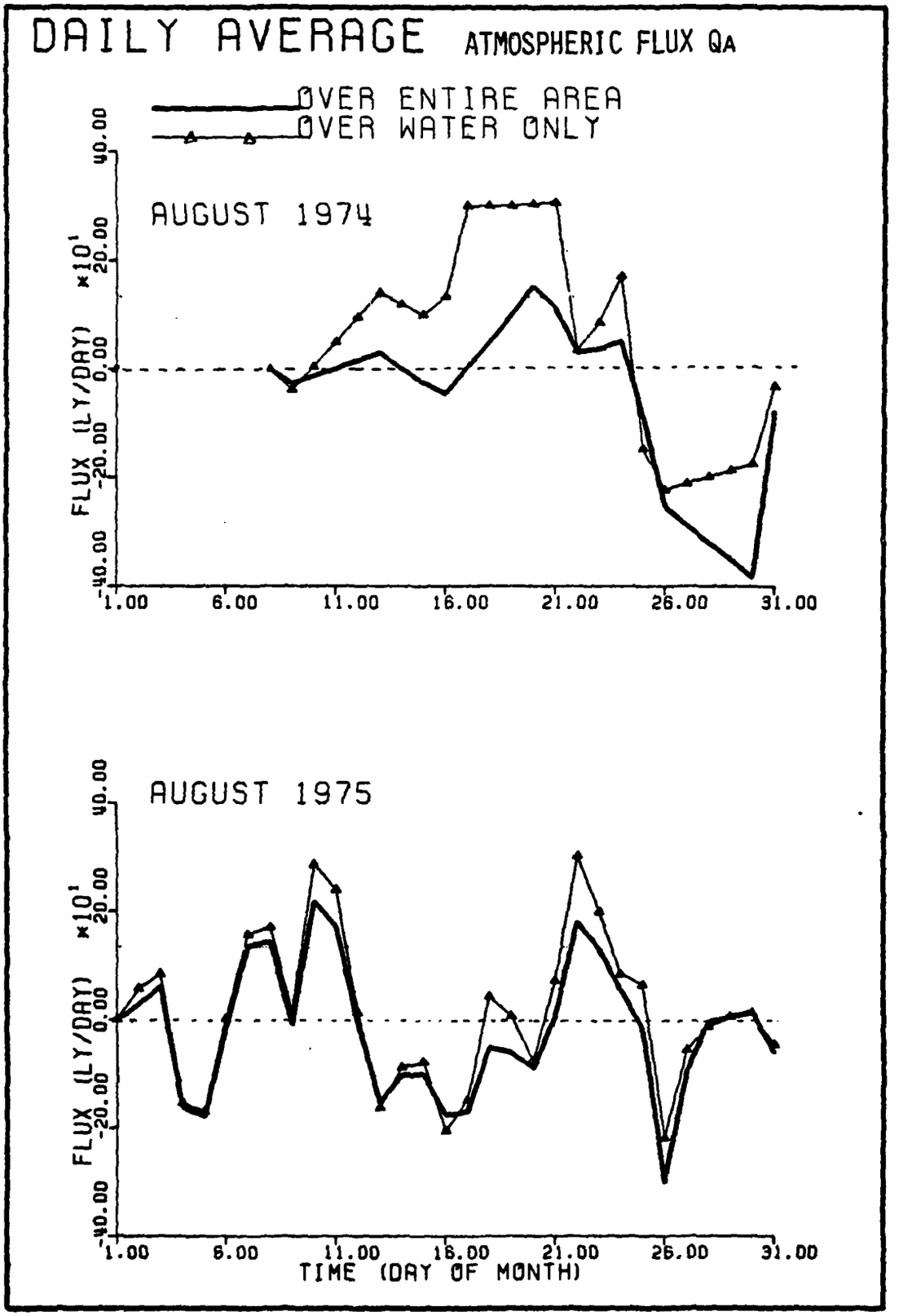
DAILY AVERAGE ATMOSPHERIC FLUX QA
OVER ENTIRE AREA
OVER WATER ONLY
AUGUST 1974
FLUX (LY/DAY) ×10¹
40.00
20.00
0.00
-20.00
-40.00
1.00
6.00
11.00
16.00
21.00
26.00
31.00
AUGUST 1975
TIME (DAY OF MONTH)

Figure 46

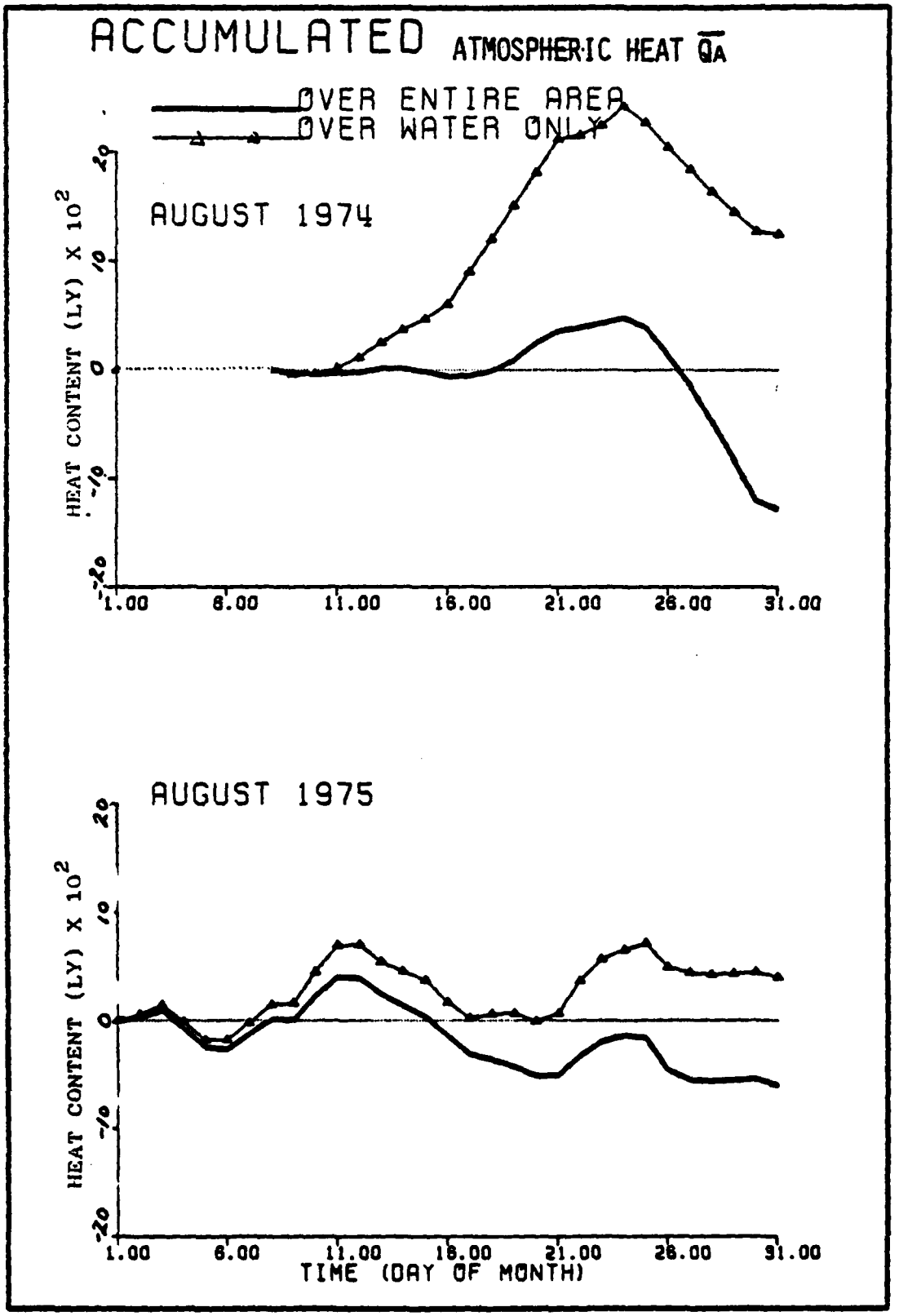
ACCUMULATED ATMOSPHERIC HEAT $\overline{Q_A}$
OVER ENTIRE AREA
OVER WATER ONLY
AUGUST 1974
HEAT CONTENT (LY) X 10^2
20
10
0
-10
-20
1.00
6.00
11.00
16.00
21.00
26.00
31.00
AUGUST 1975
HEAT CONTENT (LY) X 10^2
20
10
0
-10
-20
1.00
6.00
11.00
16.00
21.00
26.00
31.00
TIME (DAY OF MONTH)

Figure 47

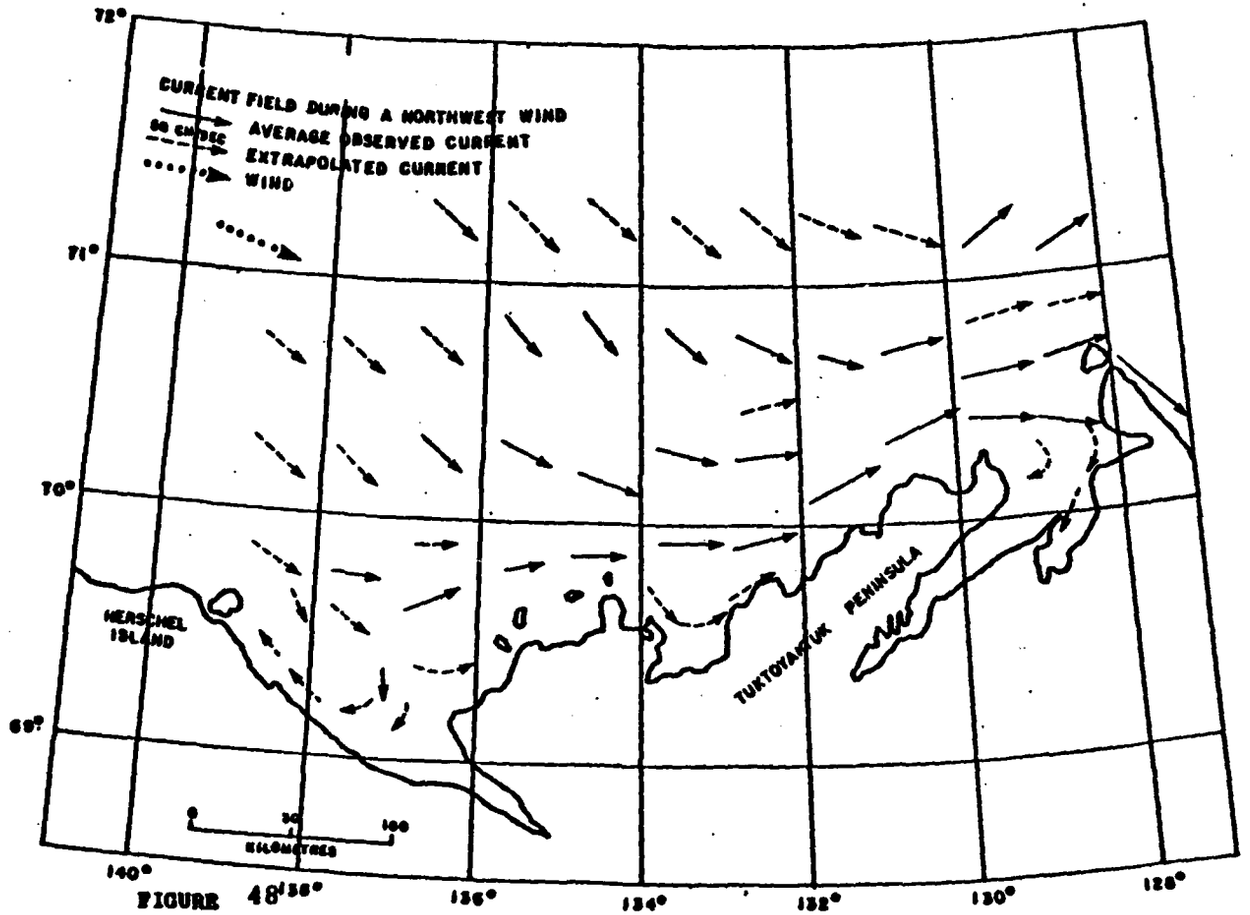
CURRENT FIELD DURING A NORTHWEST WIND
AVERAGE OBSERVED CURRENT
EXTRAPOLATED CURRENT
WIND
72°
71°
70°
69°
HERSCHEL ISLAND
TUKTOYAKTUK PENINSULA
0
50
100
KILOMETRES
140°
138°
136°
134°
132°
130°
128°

FIGURE 48

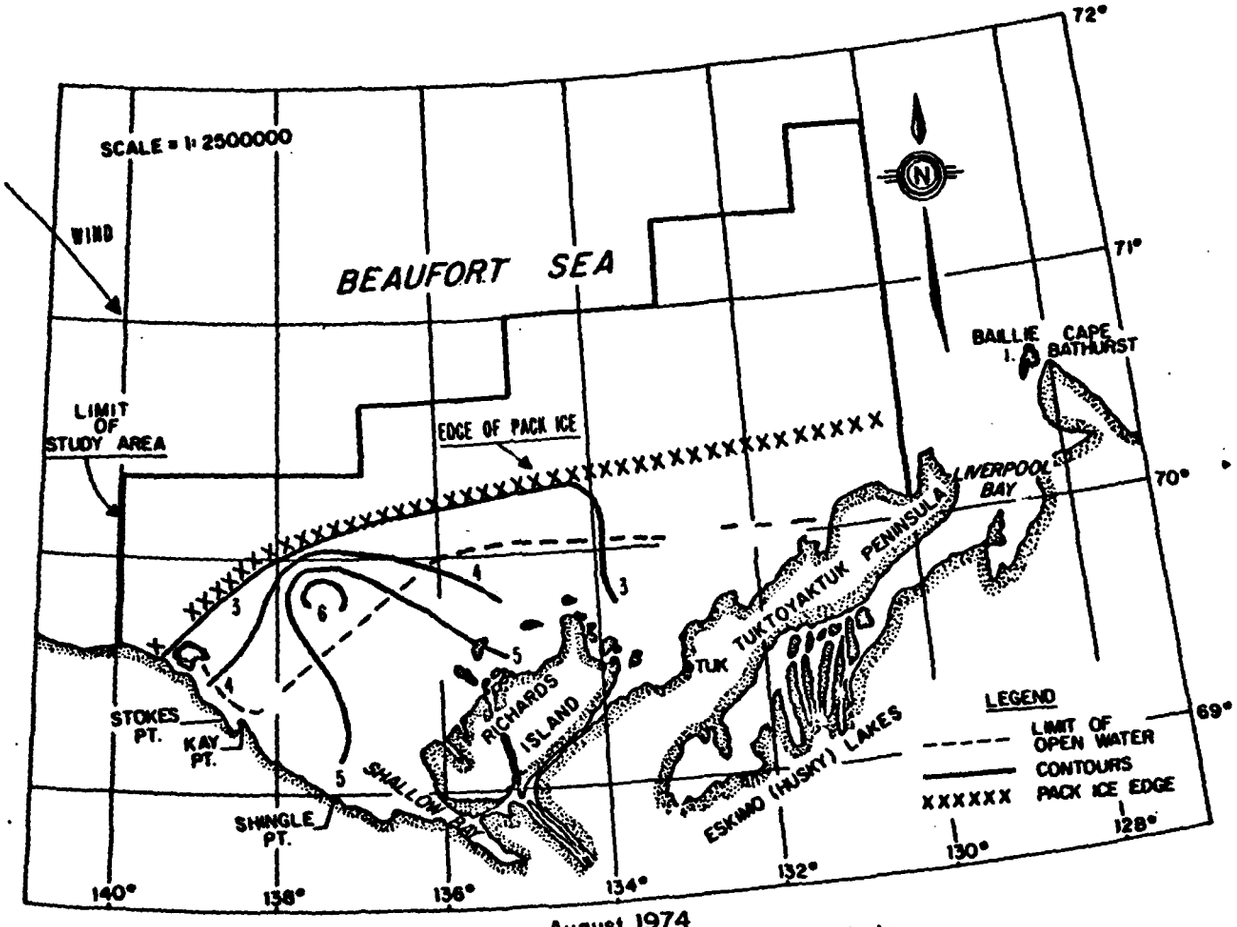

Figure 49: August 1974
Heat content (kgcal/cm^2) during NW winds
12-20 Aug

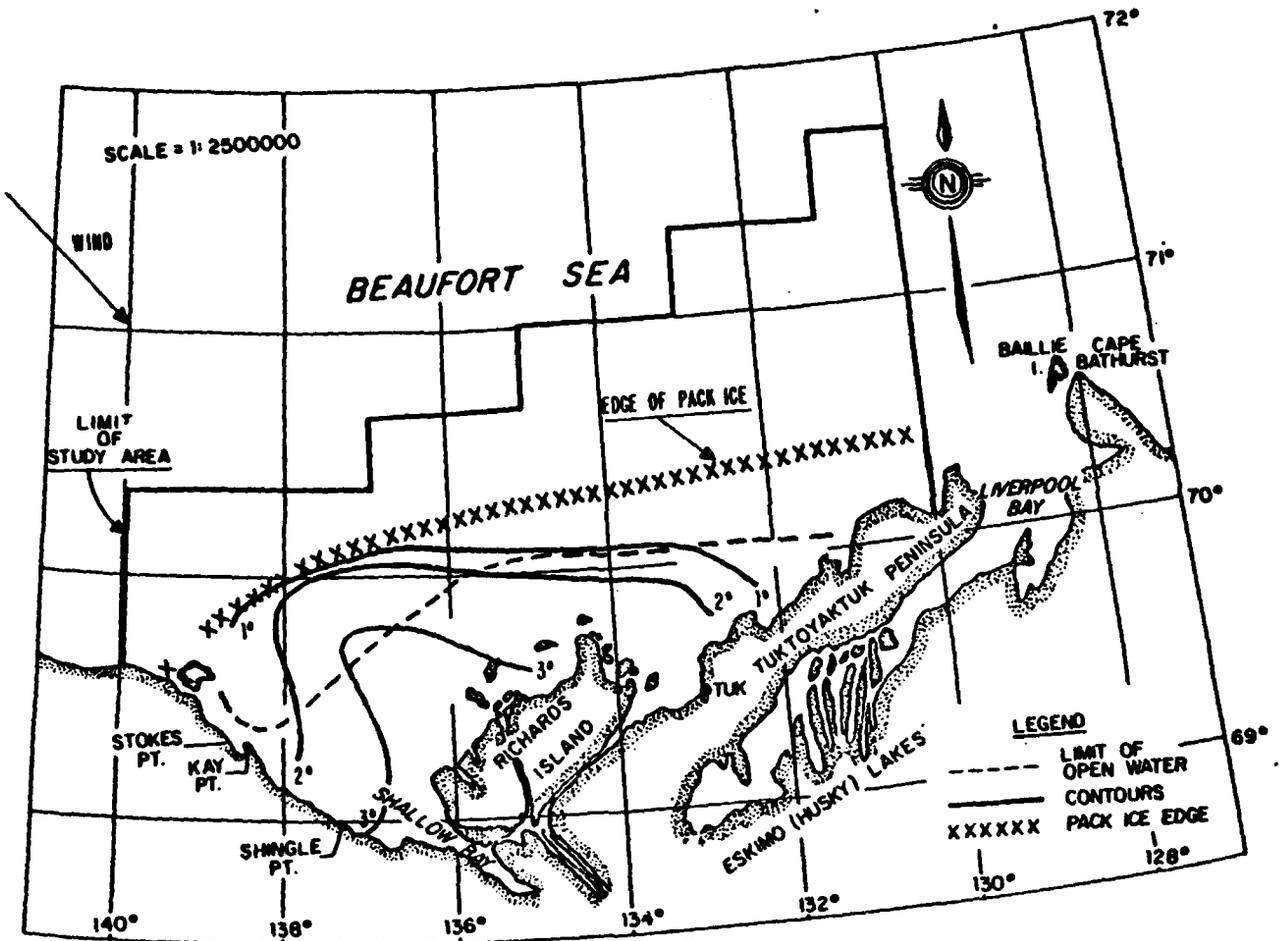

August 1974

Figure 50: Mean layer temp (°C) during NW winds
12-20 Aug

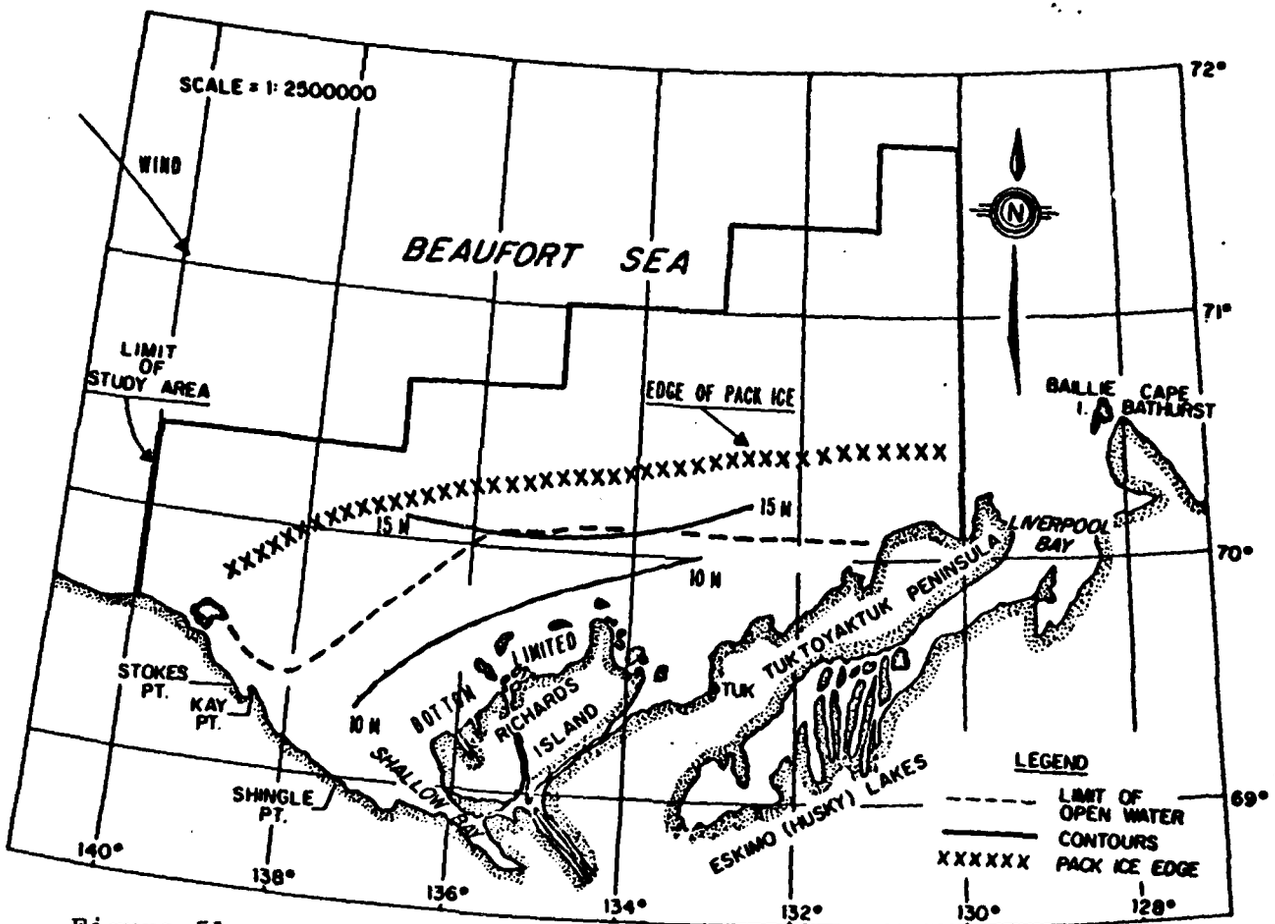

Figure 51: August 1974
Depth of -1.5°C isotherm (meters) during NW winds
12 - 20 Aug

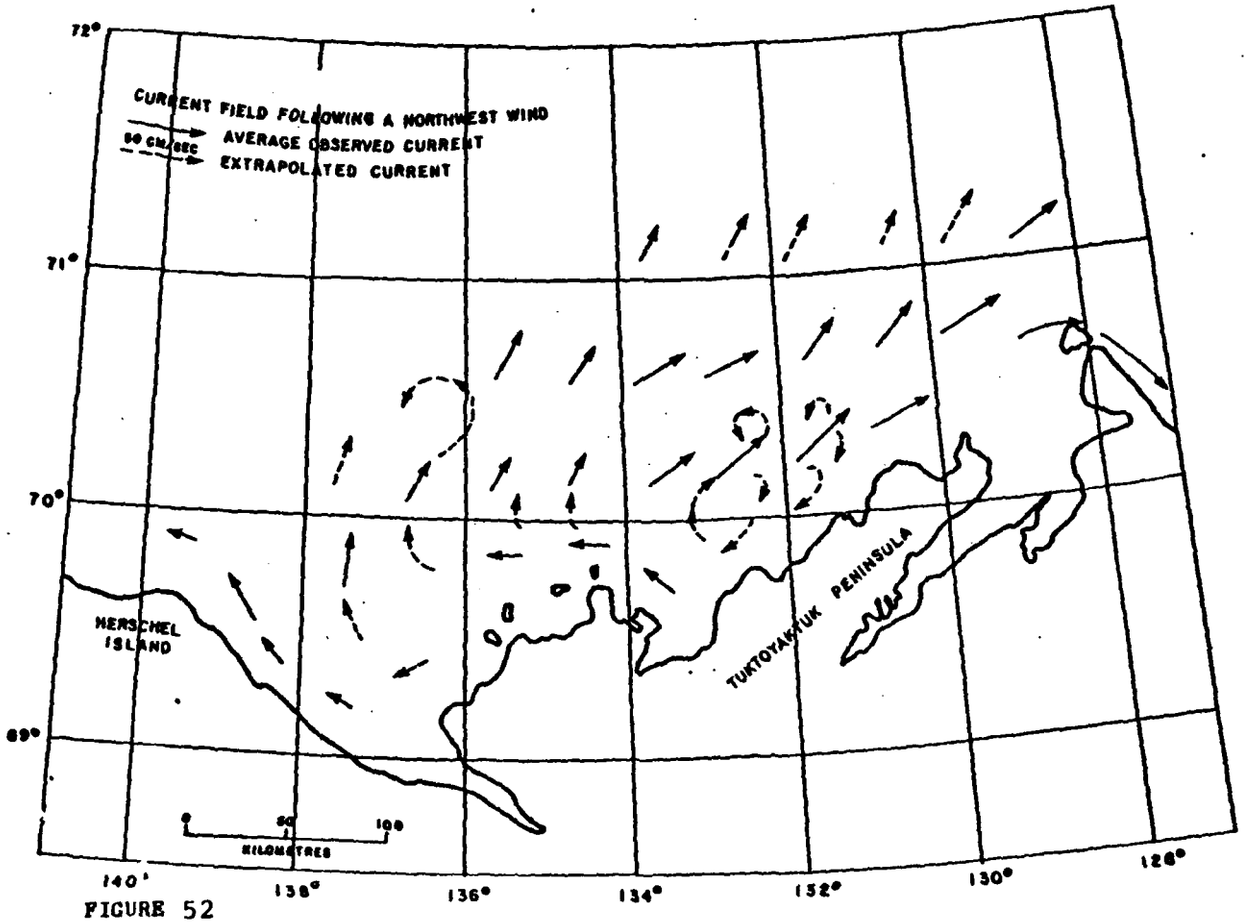
CURRENT FIELD FOLLOWING A NORTHWEST WIND
50 CM/SEC
AVERAGE OBSERVED CURRENT
EXTRAPOLATED CURRENT
72°
71°
70°
69°
HERSCHEL ISLAND
TUKTOYAKTUK PENINSULA
50
100
KILOMETRES
140°
138°
136°
134°
132°
130°
128°

FIGURE 52

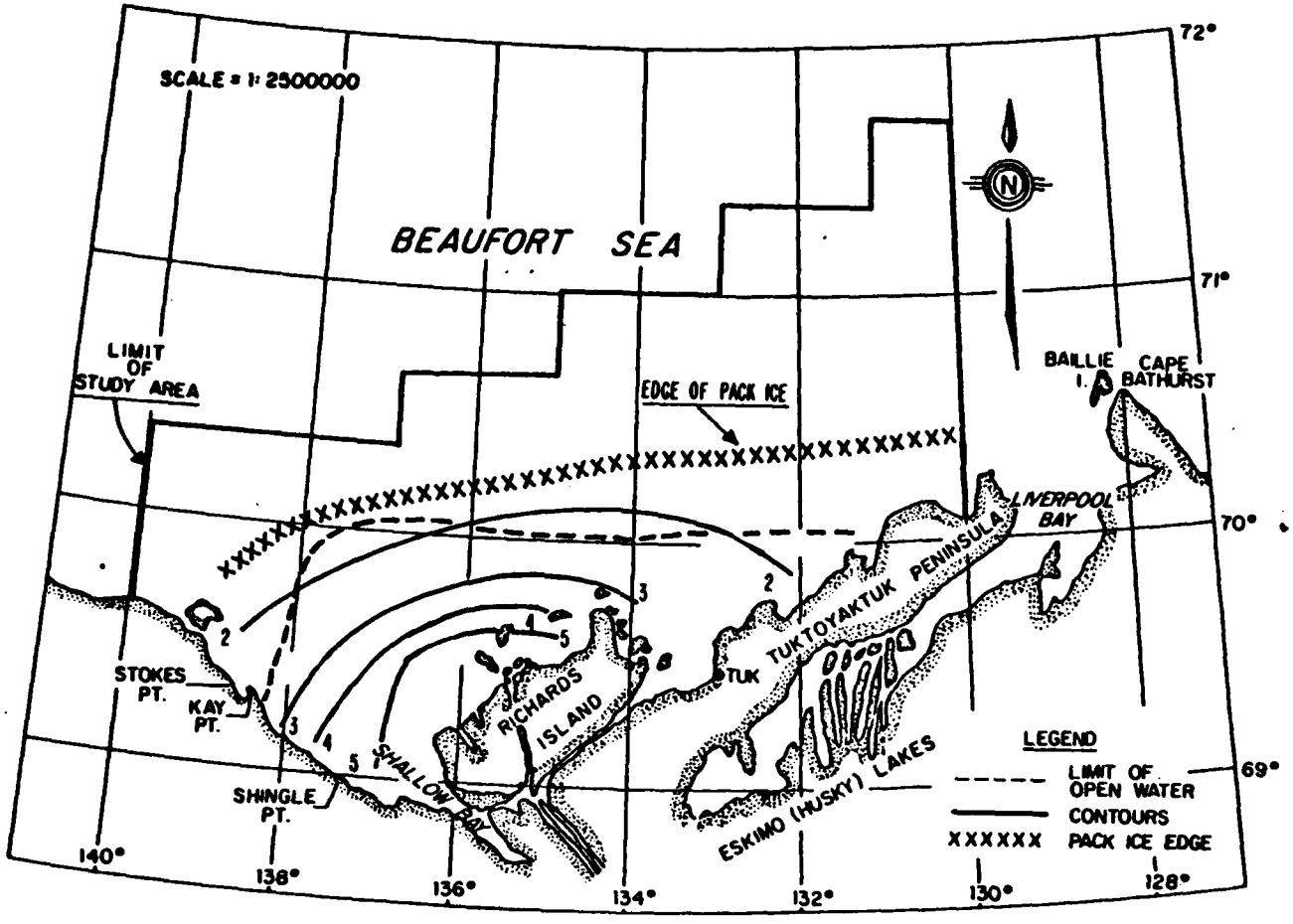

Figure 53: August 1974
Heat content (kgcal/cm^2) post NW winds
20 - 23 Aug

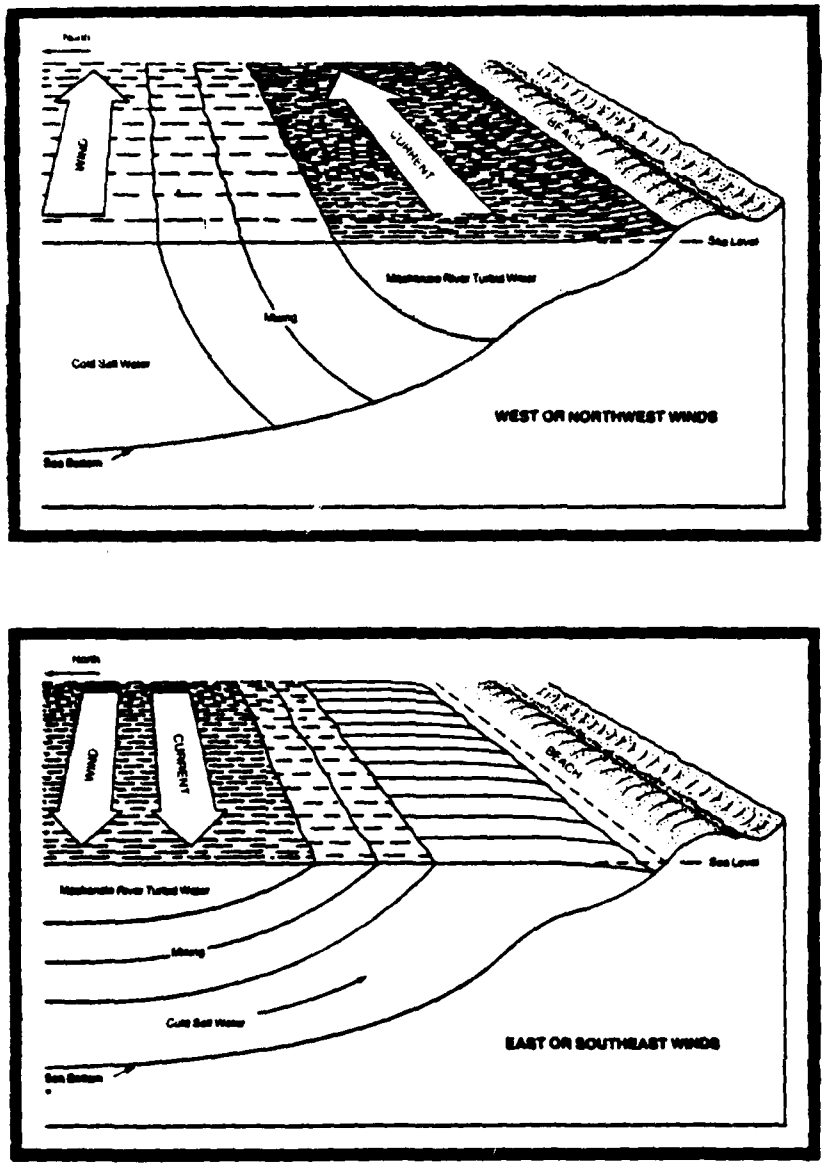

Figure 54 Onshore and offshore movement of Mackenzie River water due to wind.

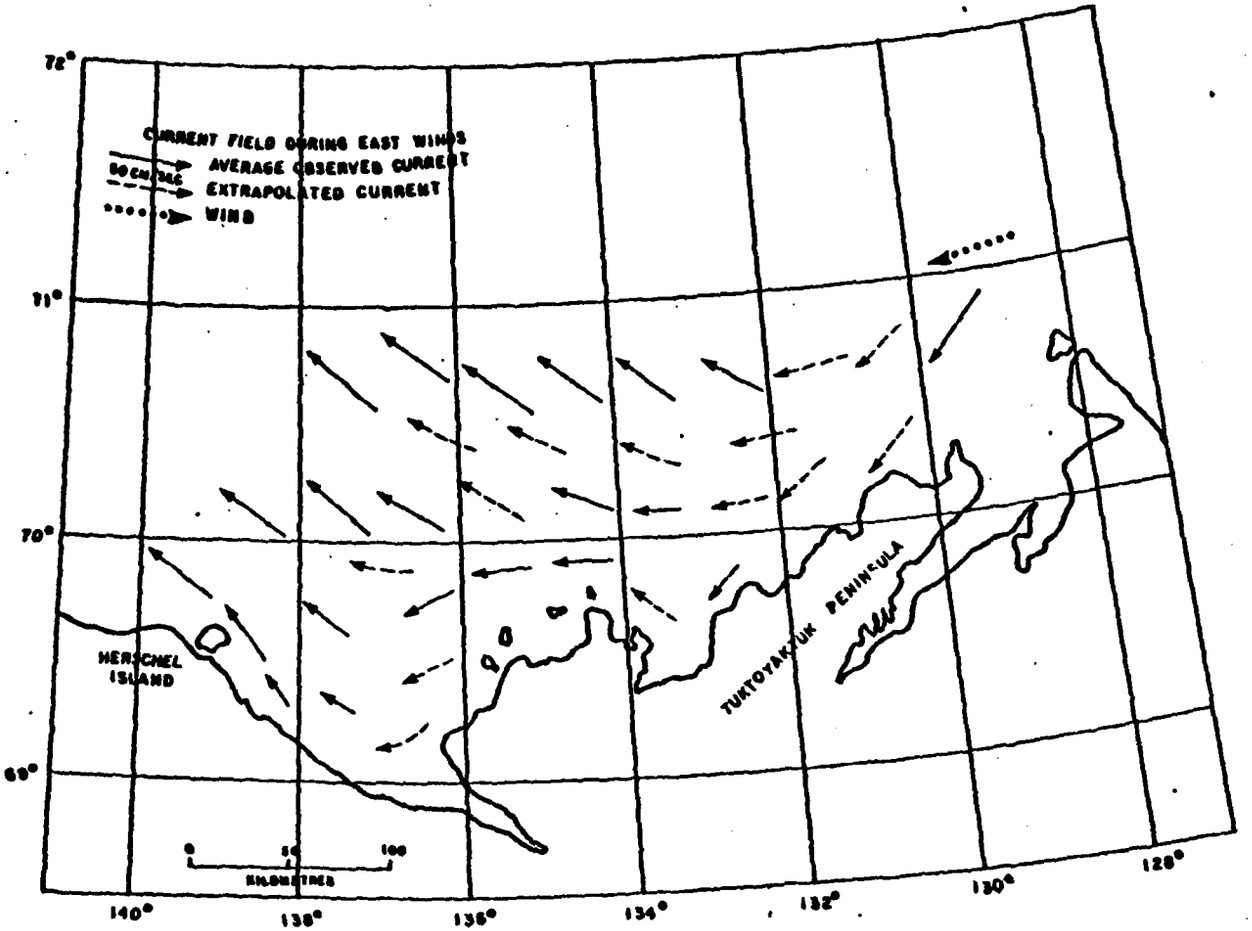
72°
71°
70°
69°
CURRENT FIELD DURING EAST WINDS
AVERAGE OBSERVED CURRENT
EXTRAPOLATED CURRENT
WIND
HERSCHEL ISLAND
TUKTOYAKTUK PENINSULA
0
50
100
KILOMETRES
140°
138°
136°
134°
132°
130°
128°

FIGURE 55

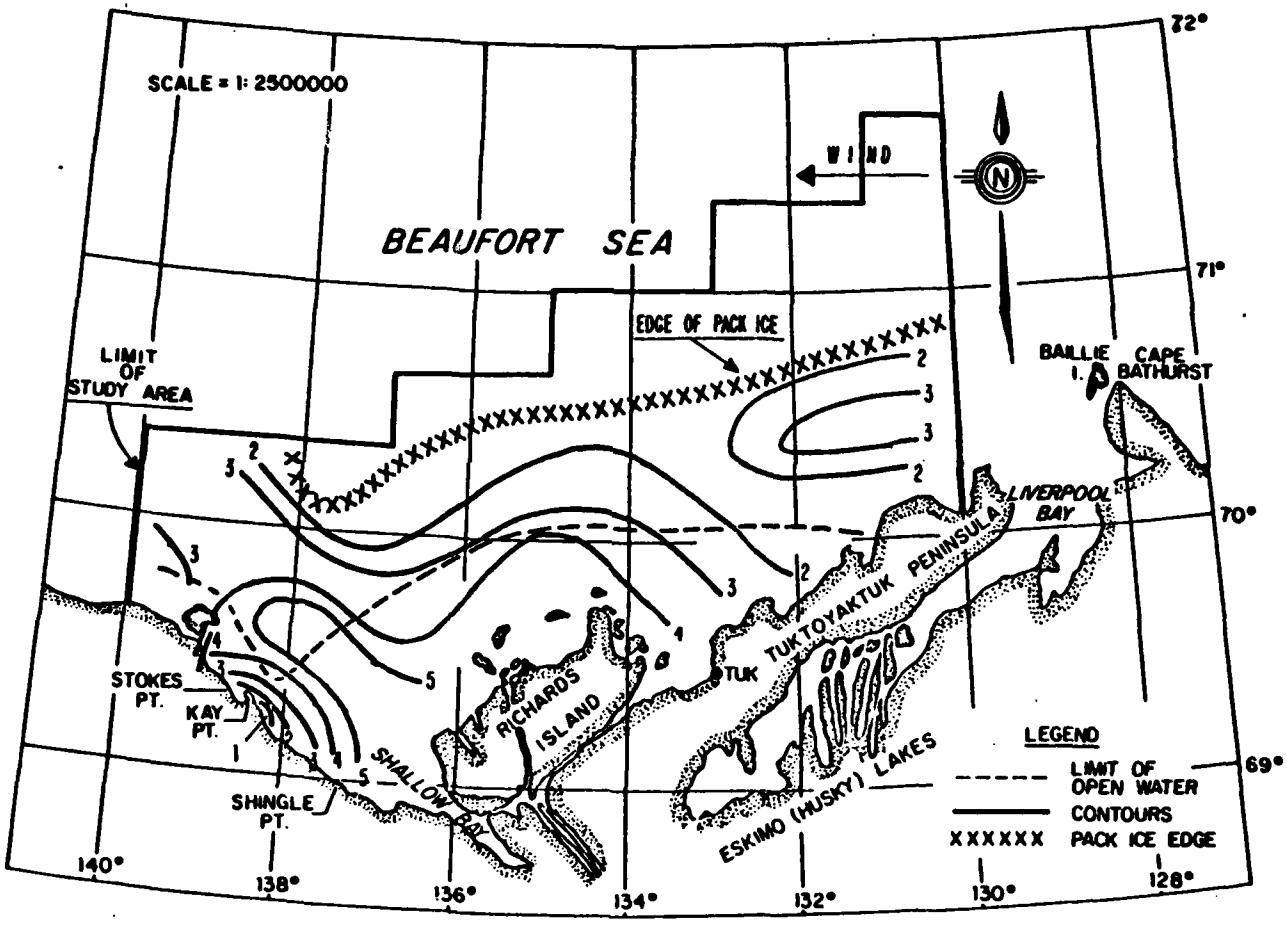

Figure 56: August 1974
Heat content (kqcal/cm^2) during easterly winds
25 Aug-1Sep

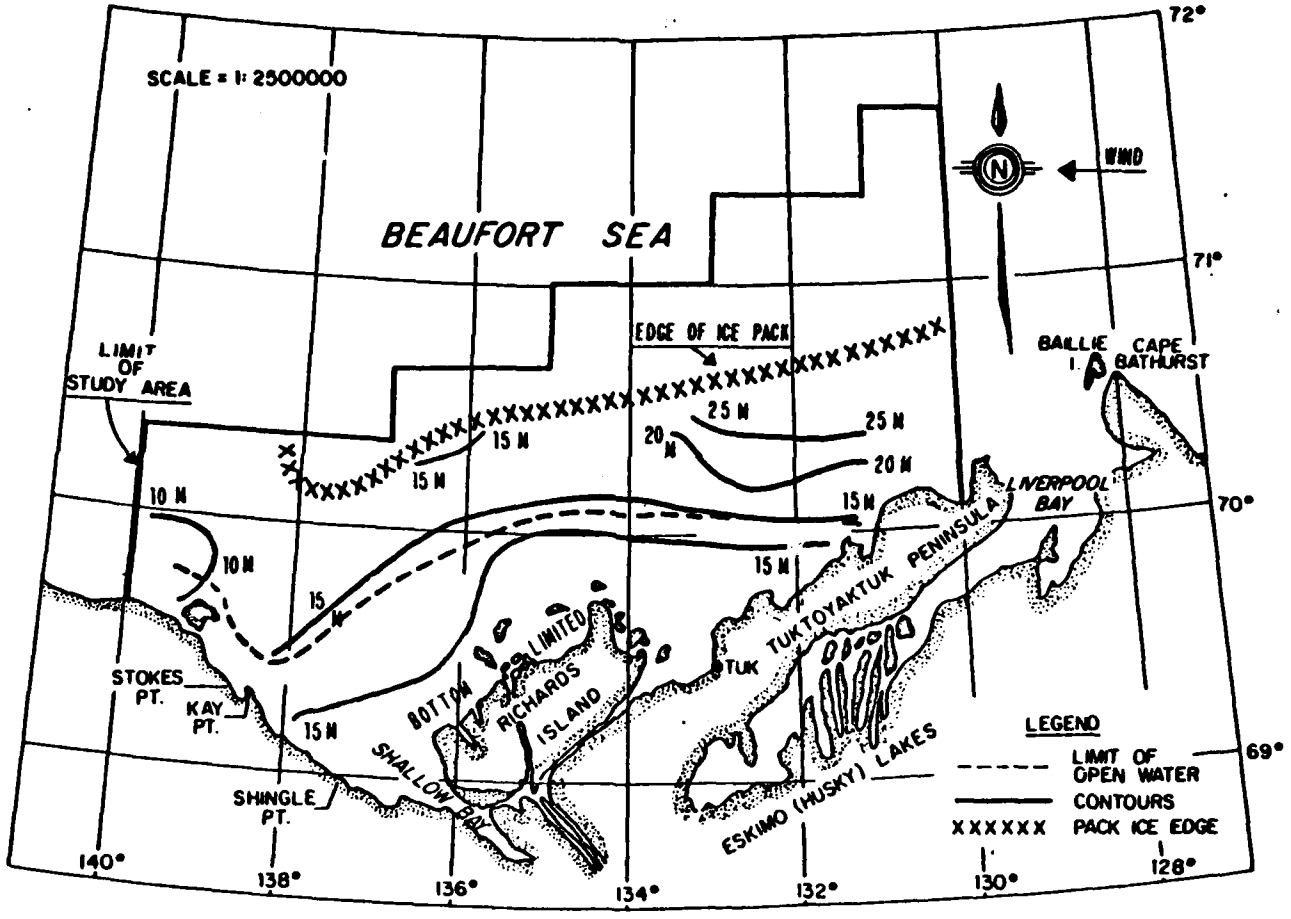

Figure 57: August 1974
Depth of -1.5° C isotherm (meters) during easterly winds
25 Aug – 1 Sep

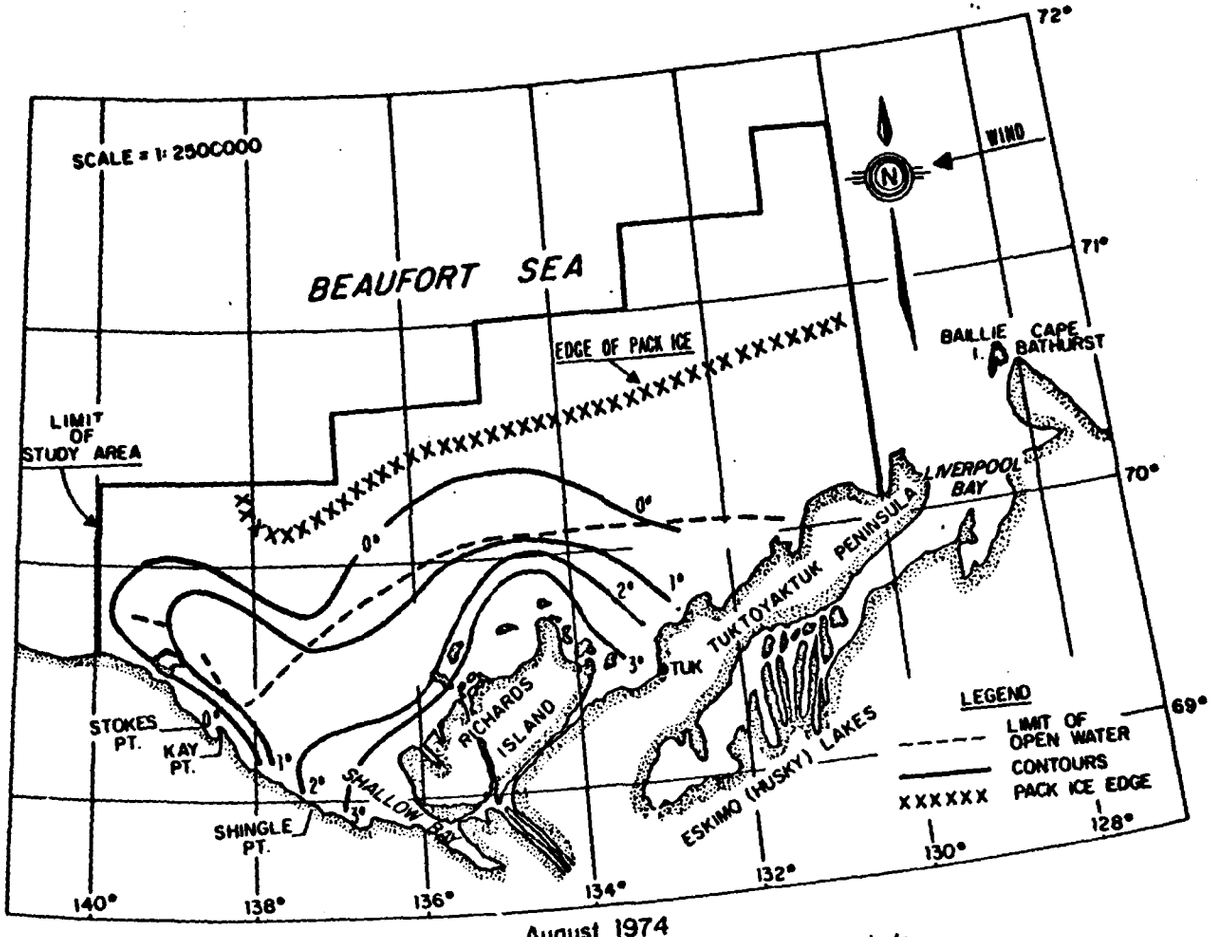

August 1974

Figure 58: Mean layer temperature (°C) during easterly winds
25 Aug-1 Sep

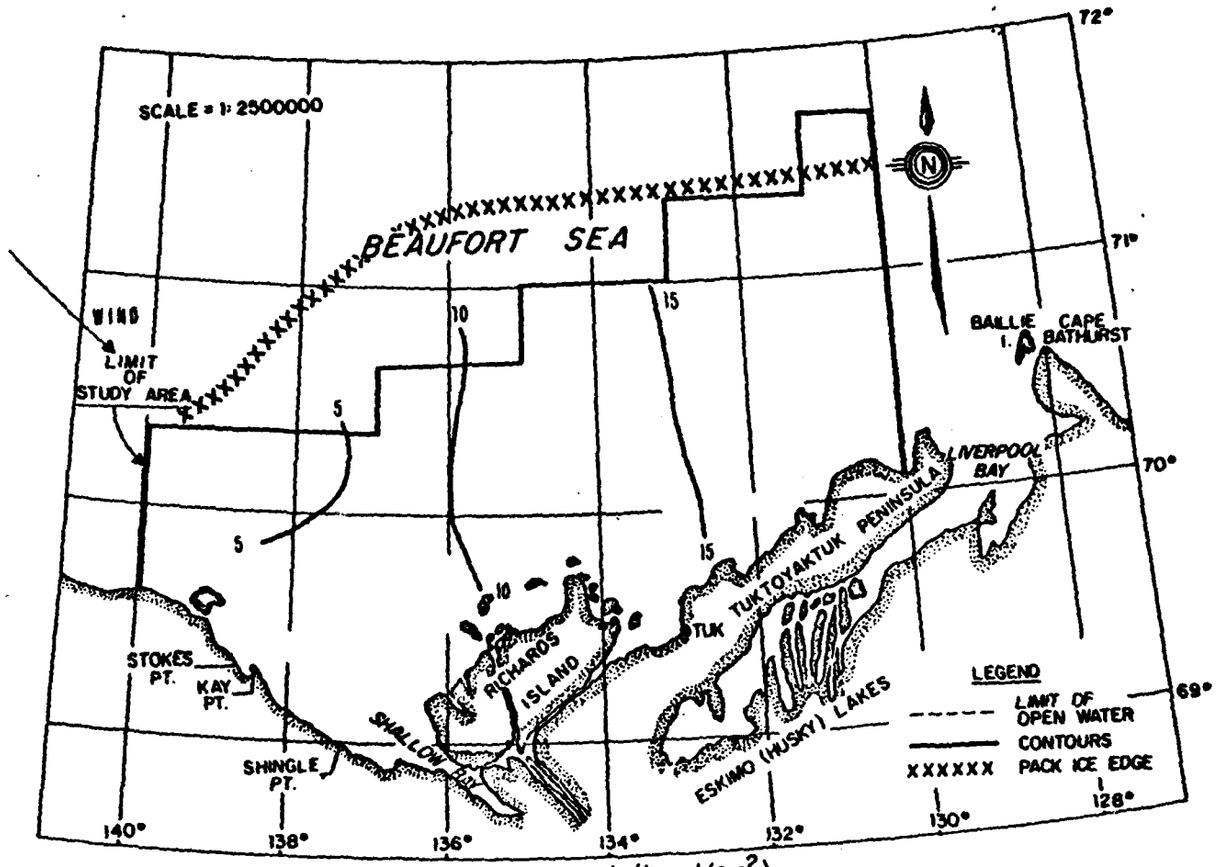

Figure 59: Heat content (kgcal/cm^2)
5-13 Aug 1975
during strong NW winds

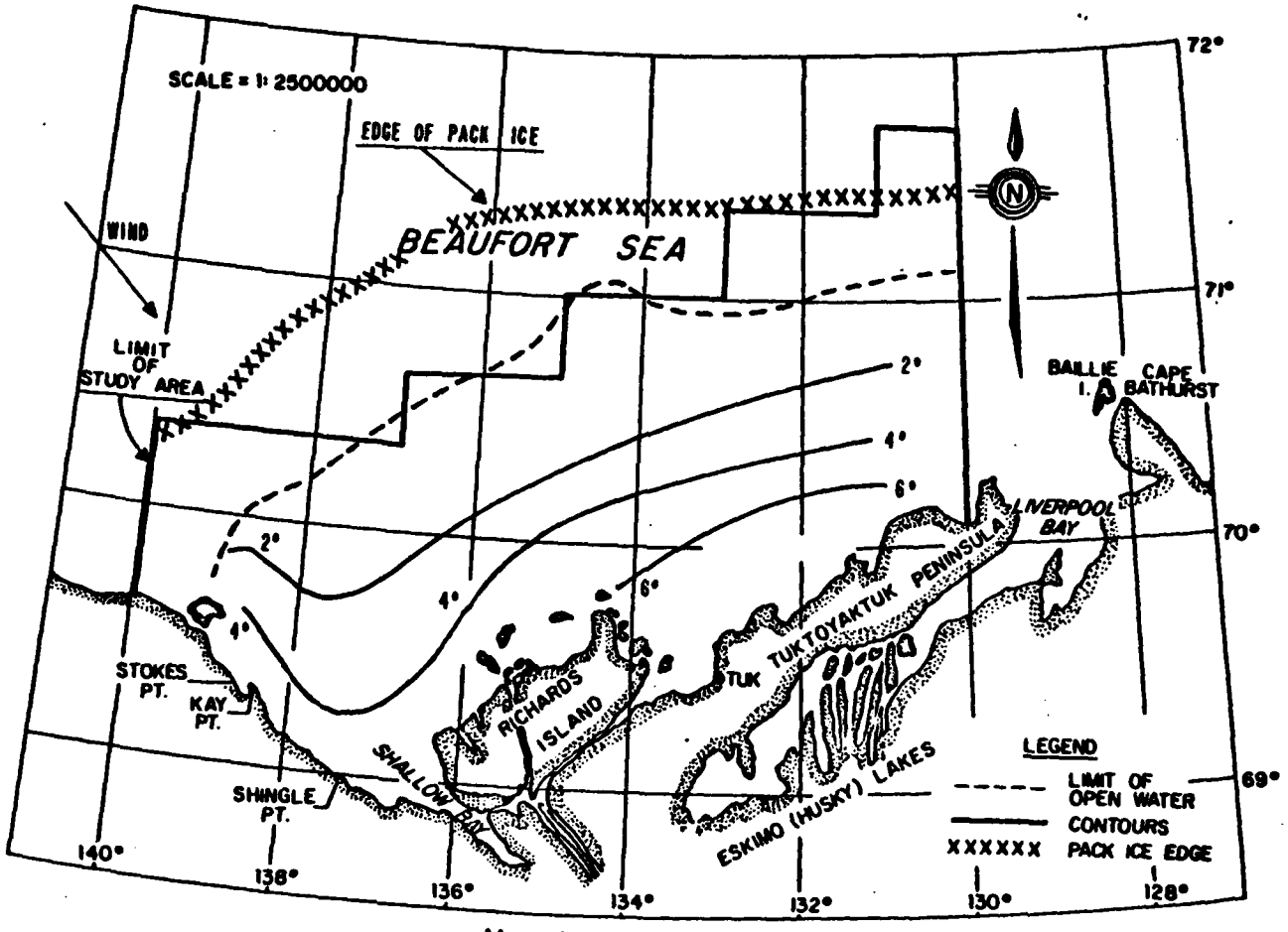

Figure 60: Mean layer temperature (°C)
5-13 Aug 1975
during strong NW winds

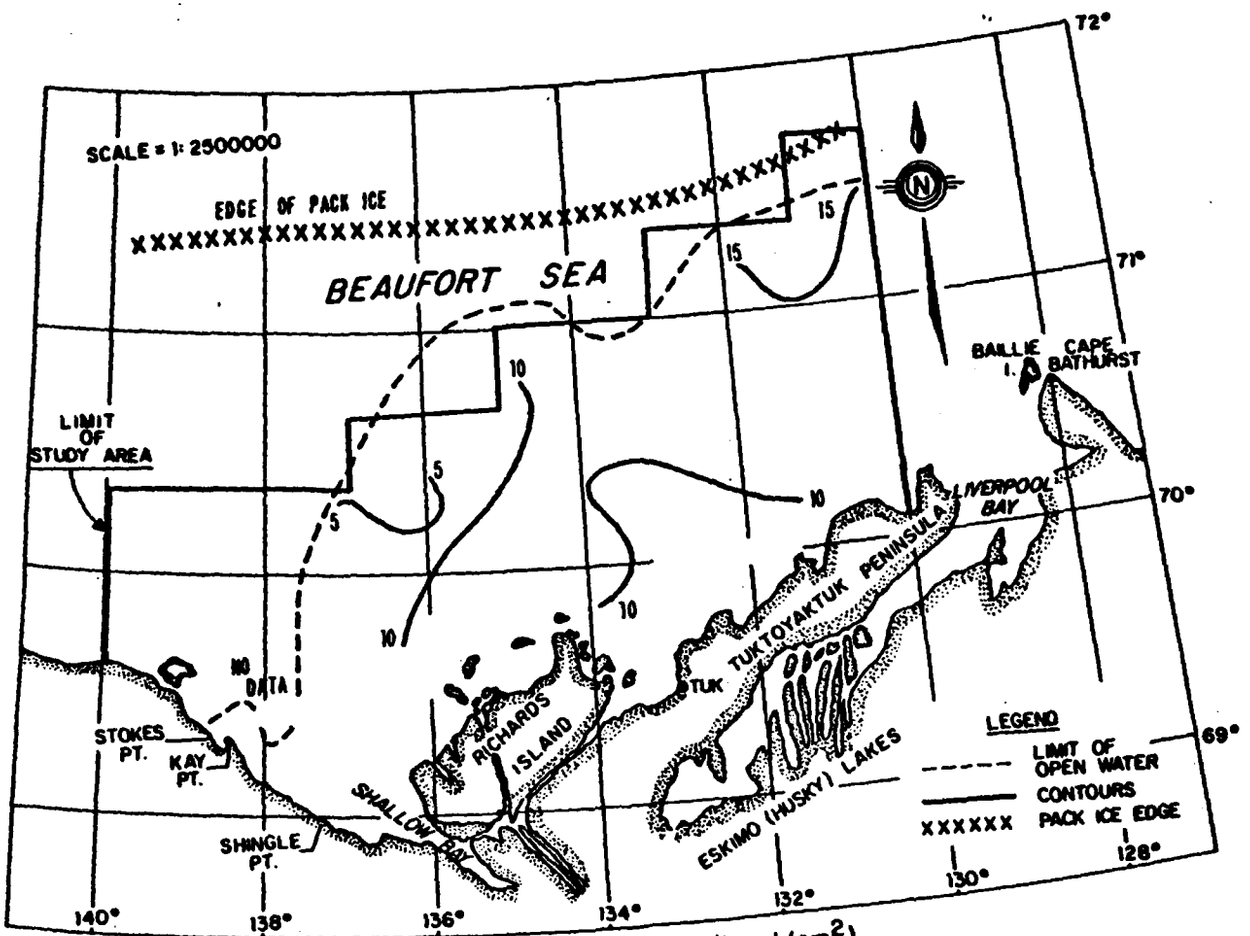

Figure 61: Heat content of water (kgcal/cm^2)
13-19 Aug 1975
during variable winds

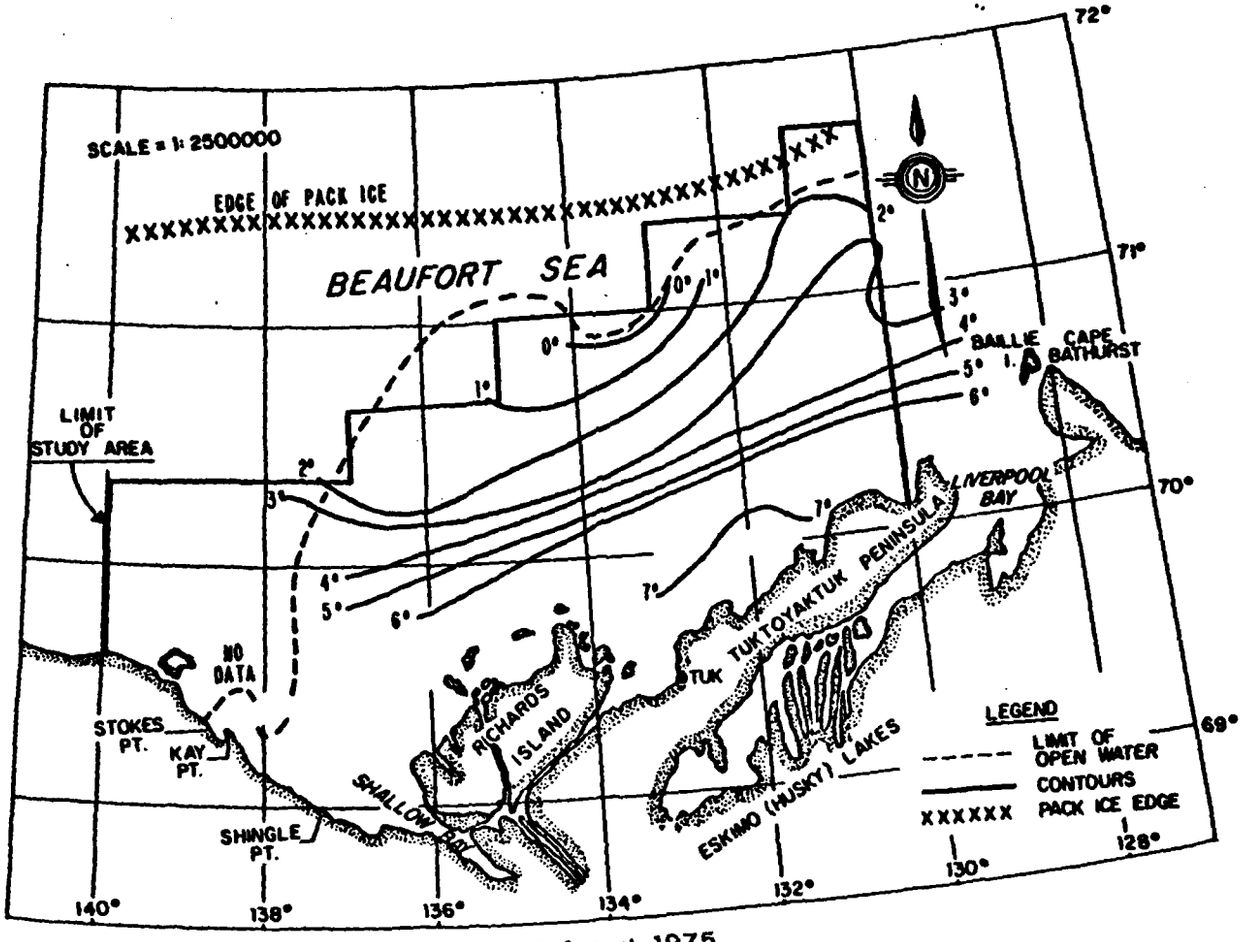

13-19 August 1975

Figure 62: Mean layer temperature (°C) during variable winds

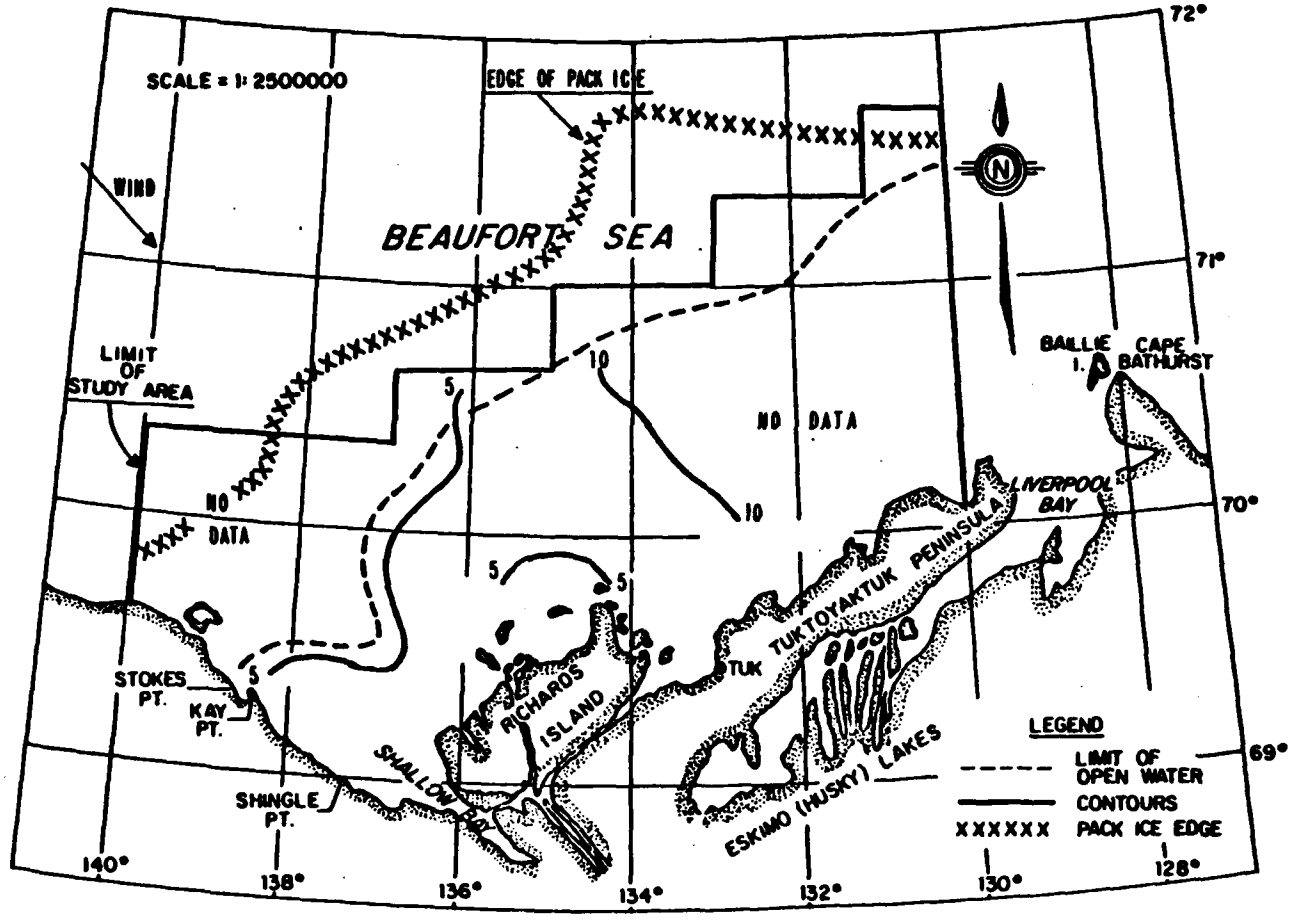

Figure 63: Heat content (kgcal/cm^2)
20-24 Aug 1975
during light NW winds

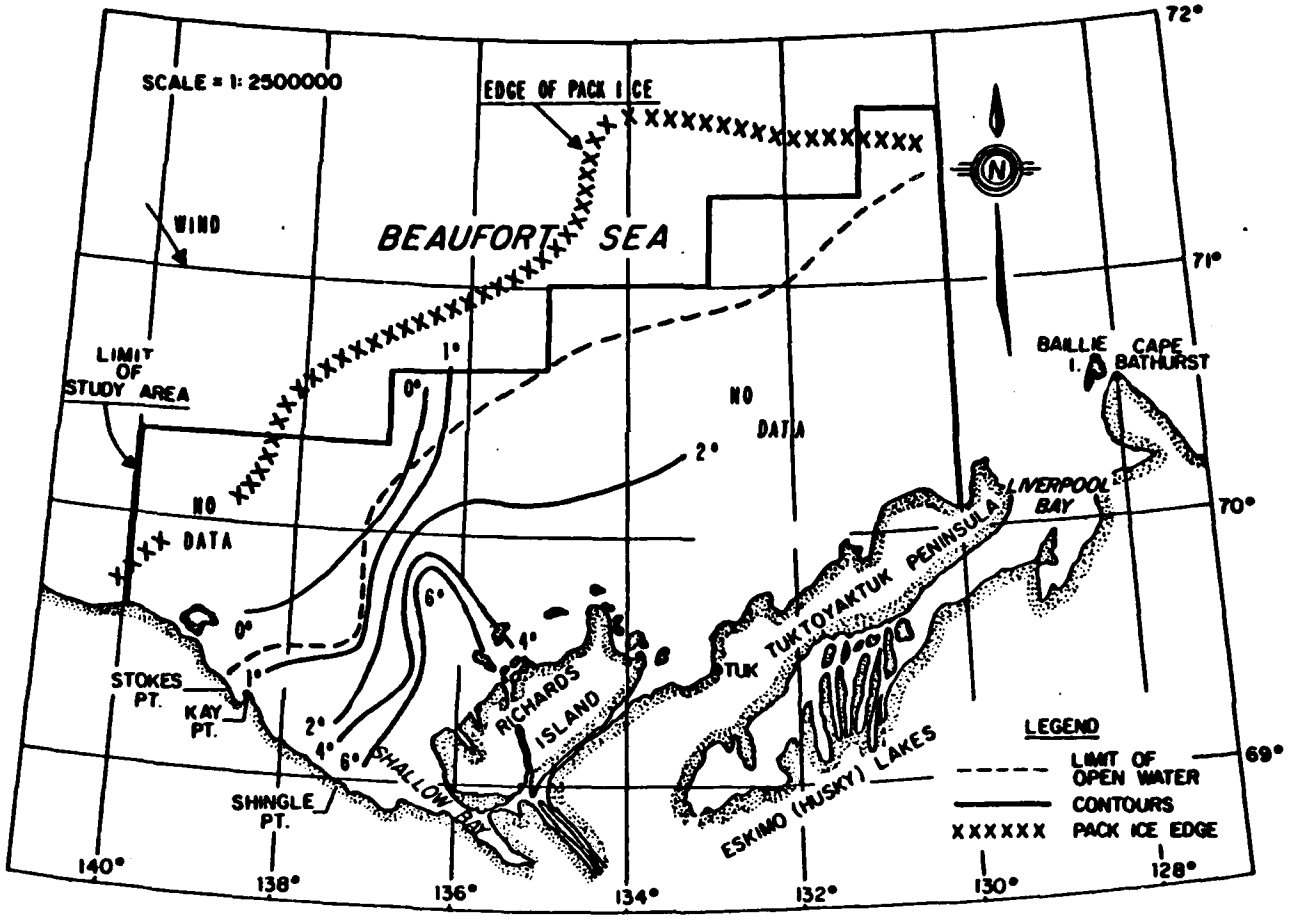

Figure 64: Mean layer temperature (°C)
20-24 Aug 1975
during light NW winds

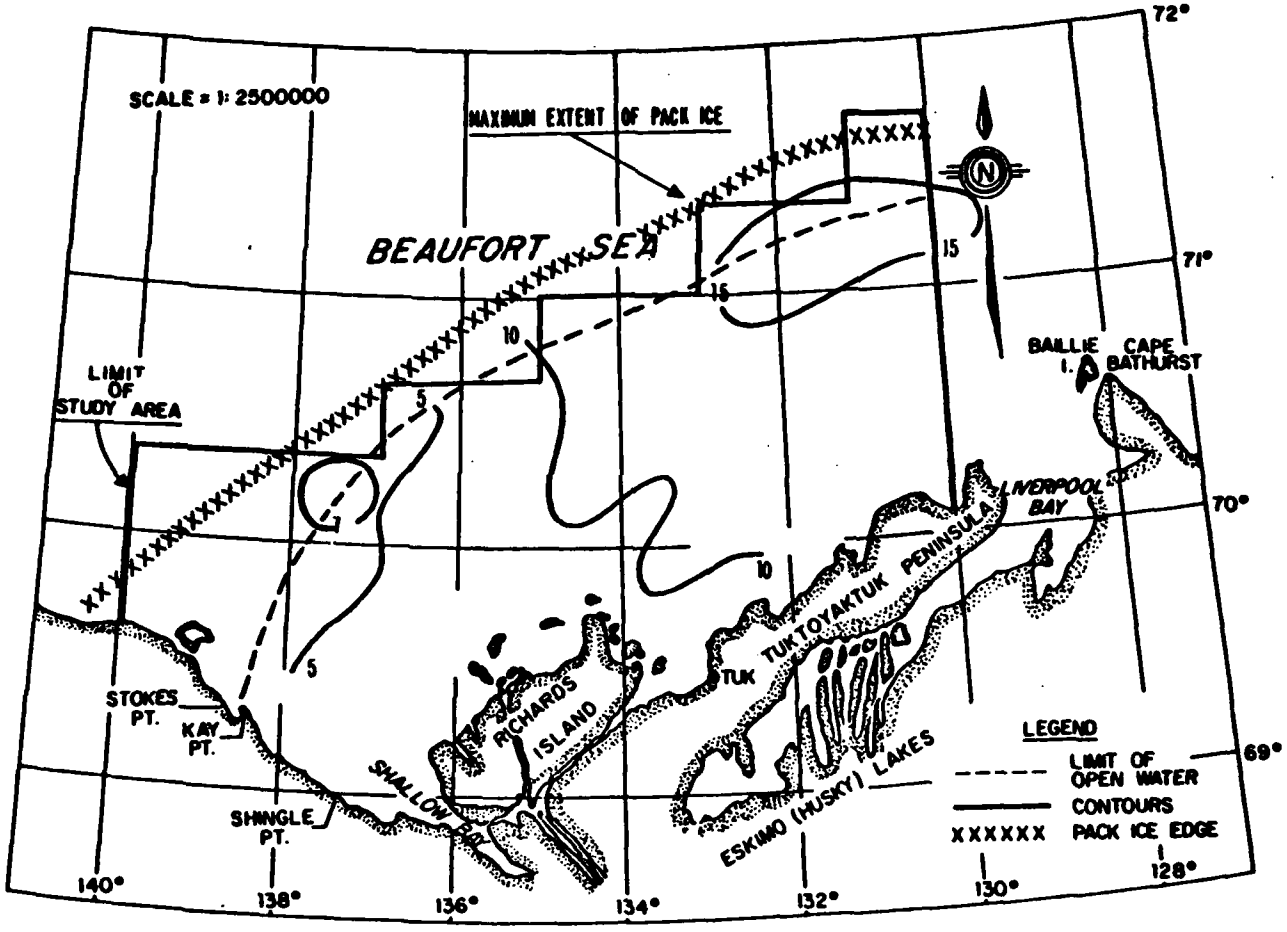

Figure 65: August 1975
Heat content (kgcal/cm^2)
Aug 5-24

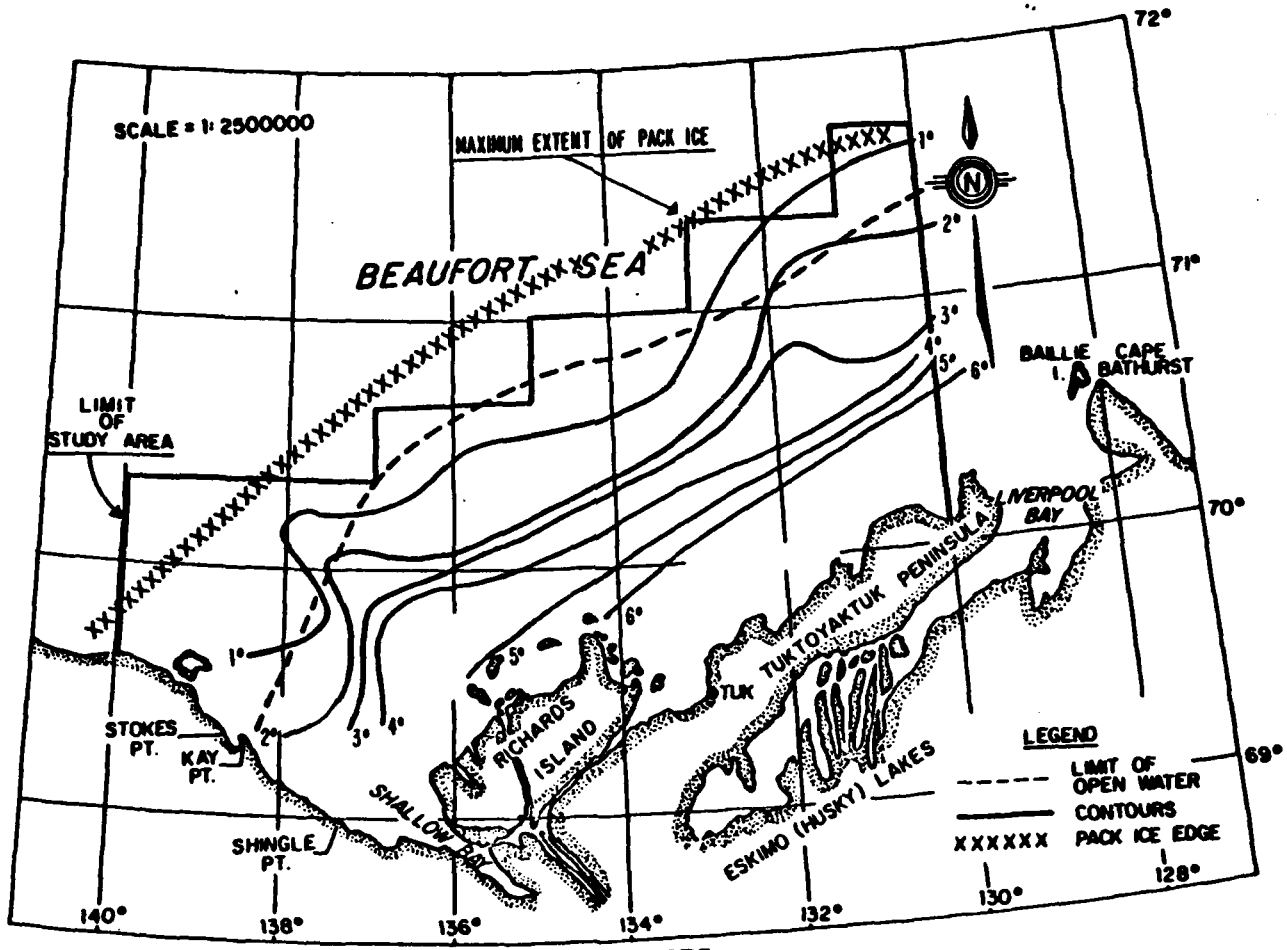

Figure 66: August 1975
Mean layer temperature (°C)
Aug 5 - 24

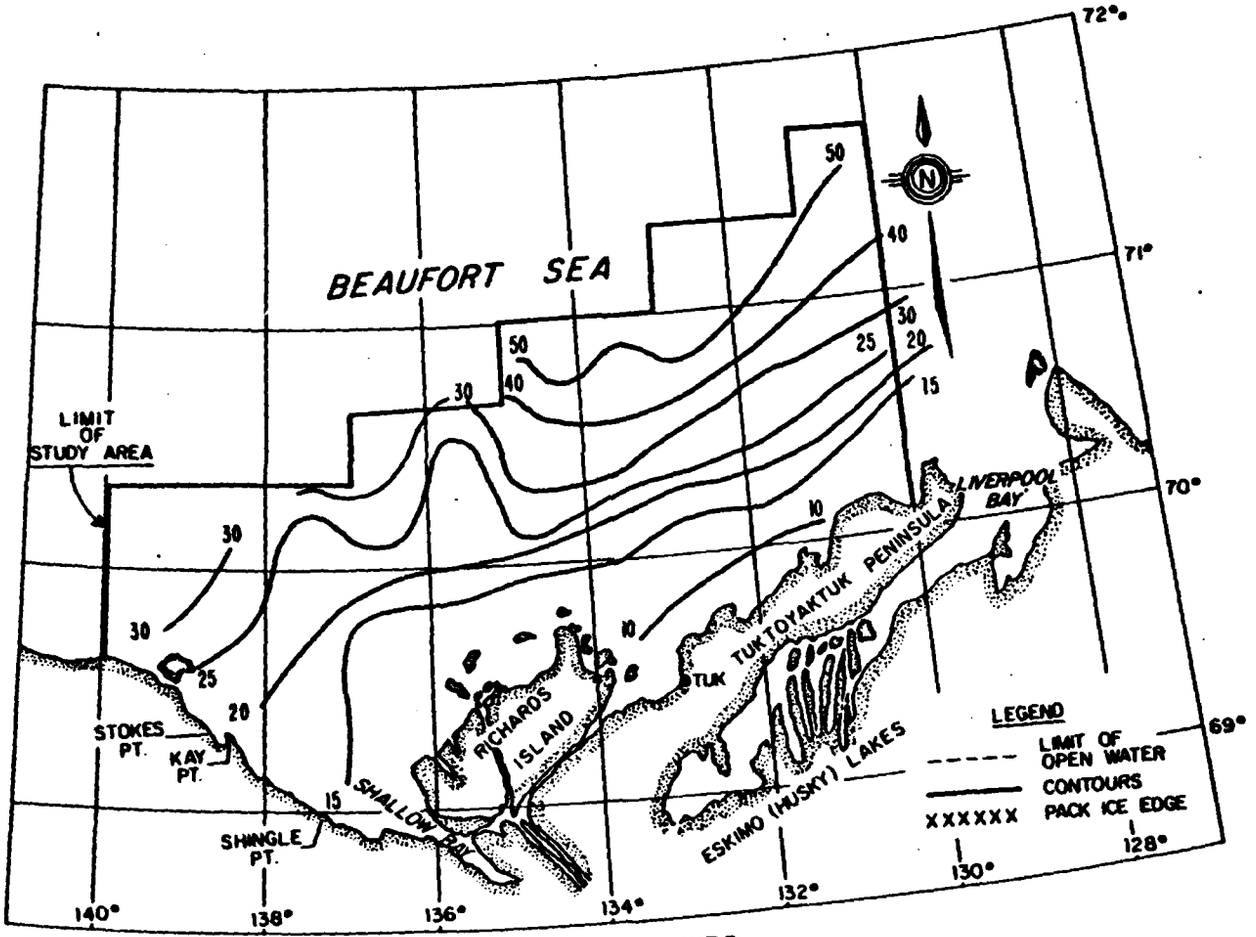

Figure 67: Summer of 1975
Depth of -1.5°C isotherm (meters)
(or deepest observation)

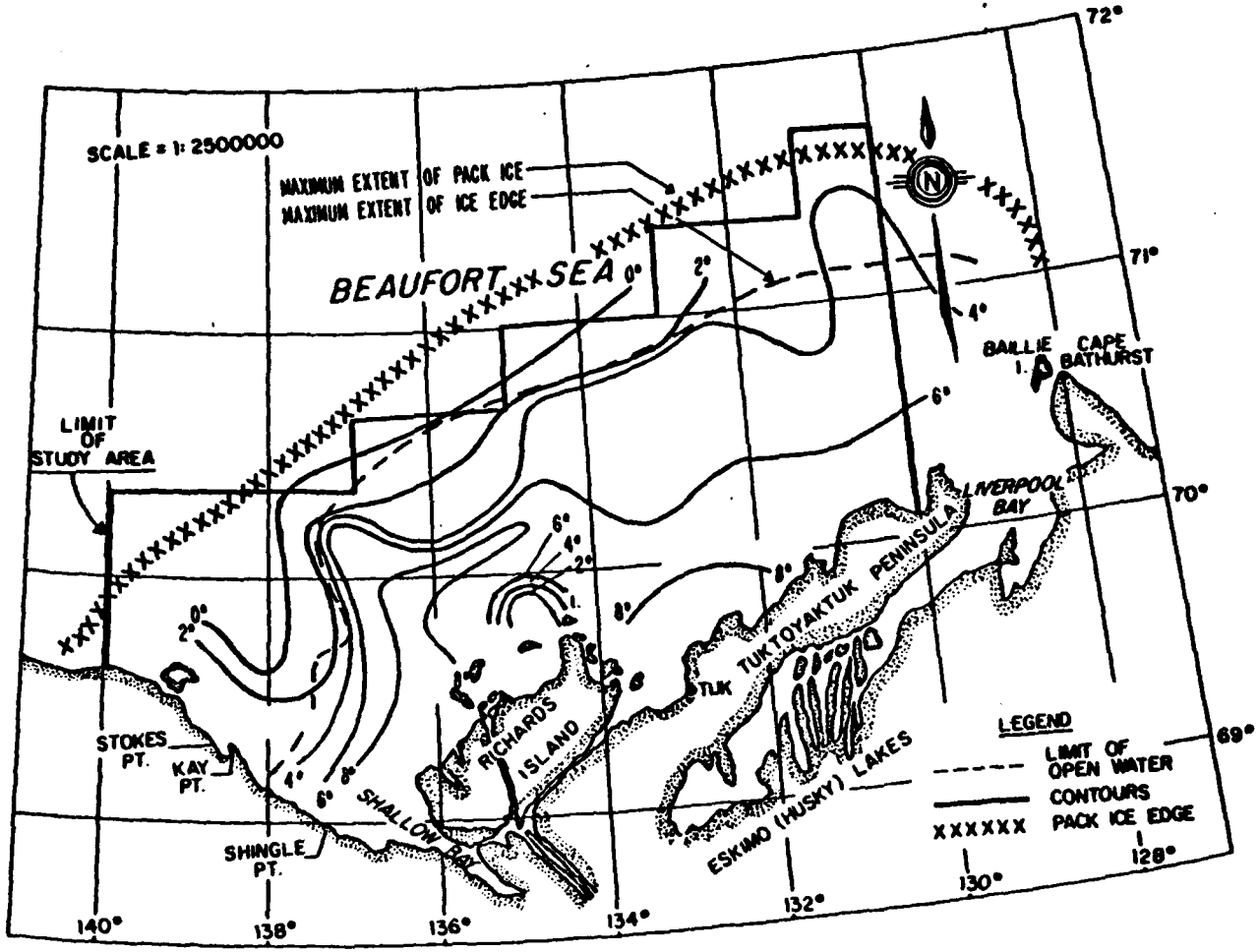

August 1975

Figure 68: Temperature contours at 5 meter depth

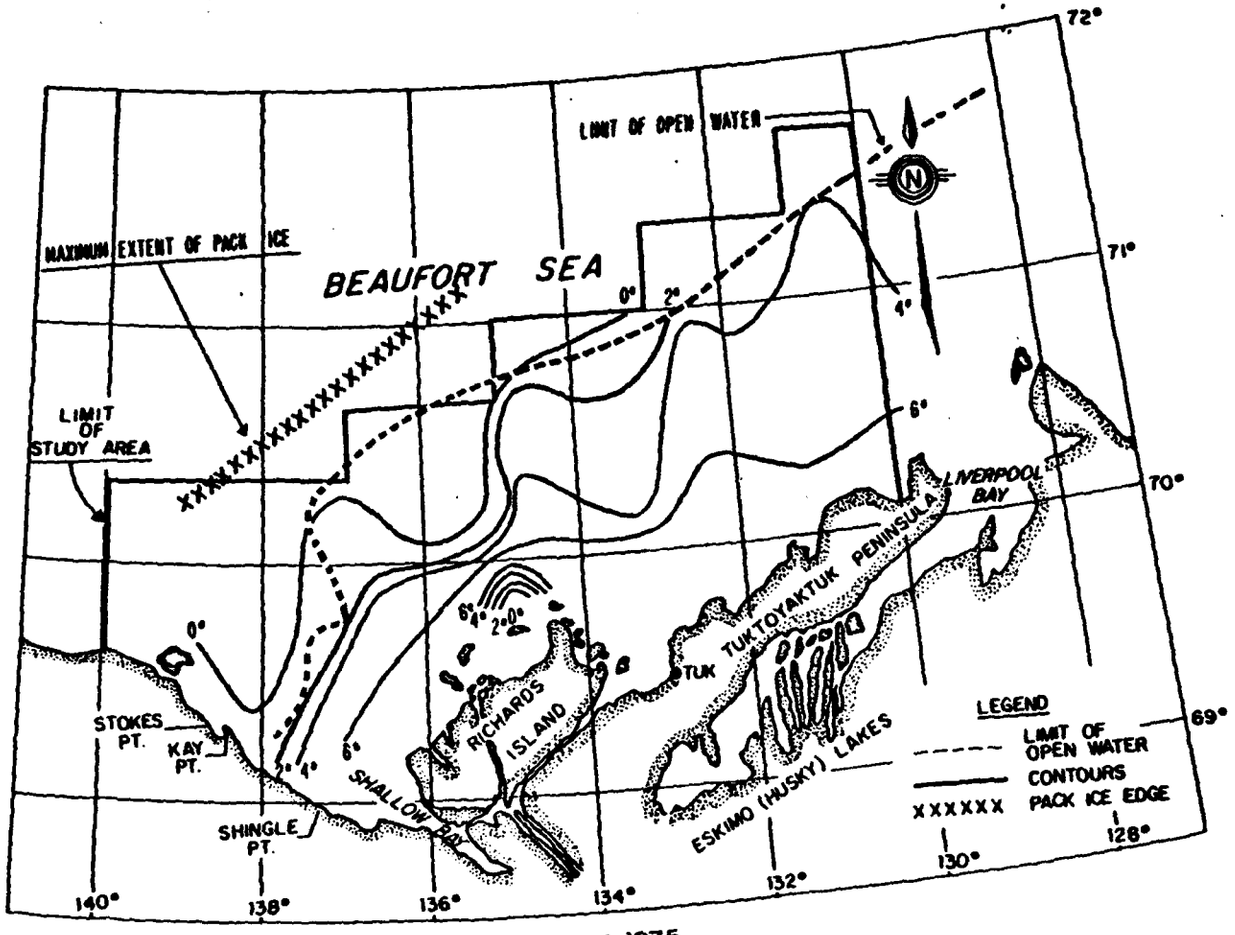

Figure 69: August 1975
Temperature contours at 10M depth

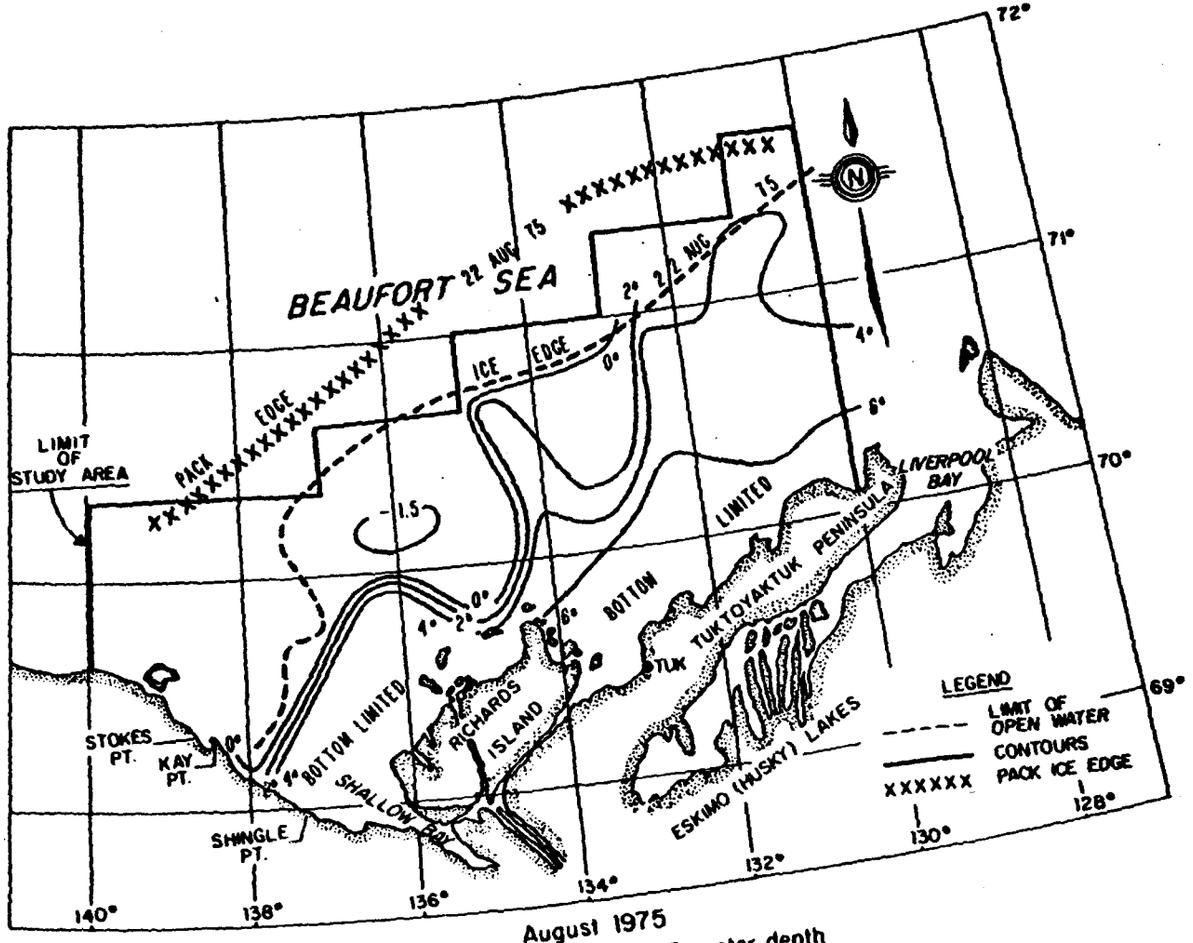

August 1975

Figure 70: Temperature contours at 15 meter depth

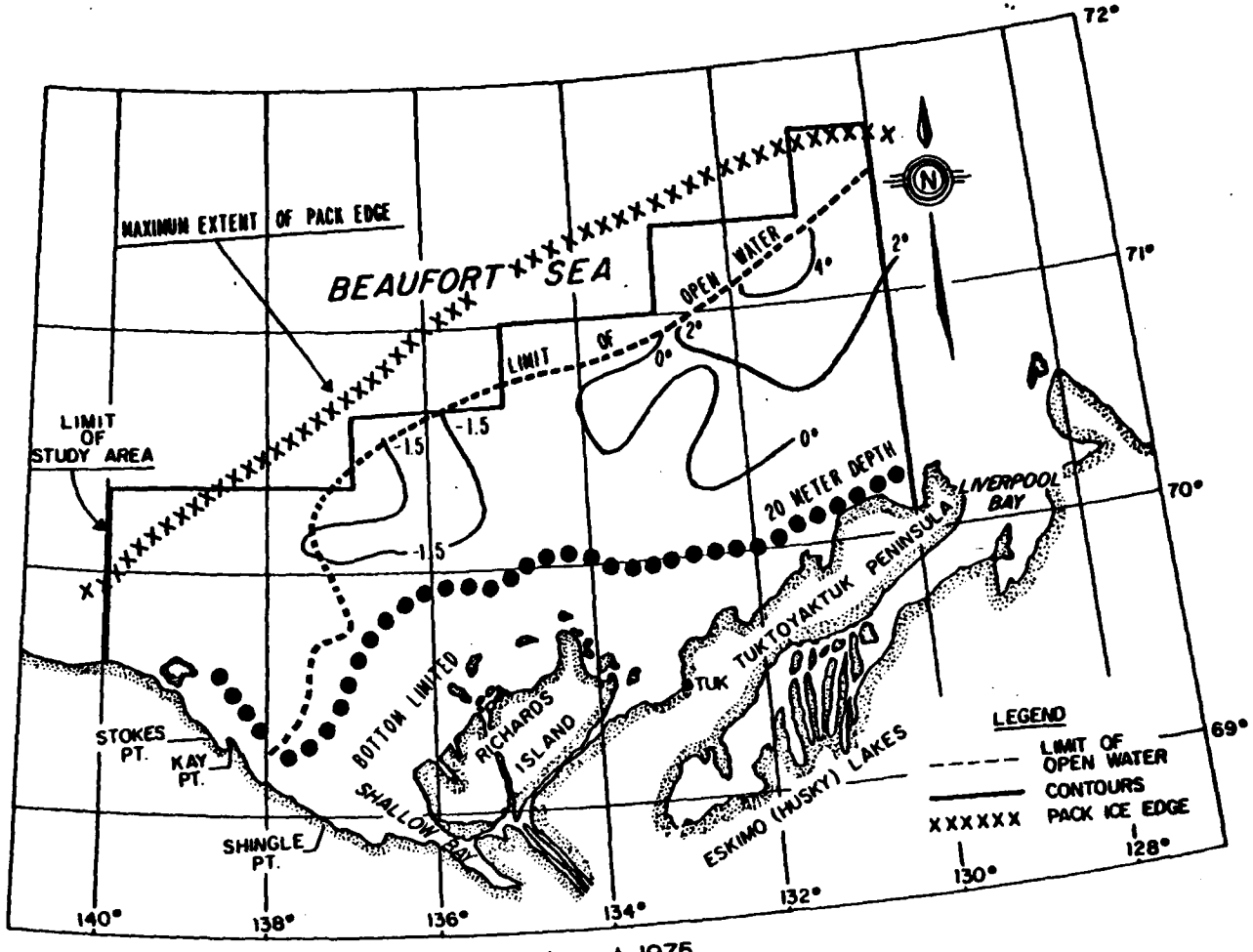

Figure 71: August 1975
Temperature contours at 20M depth

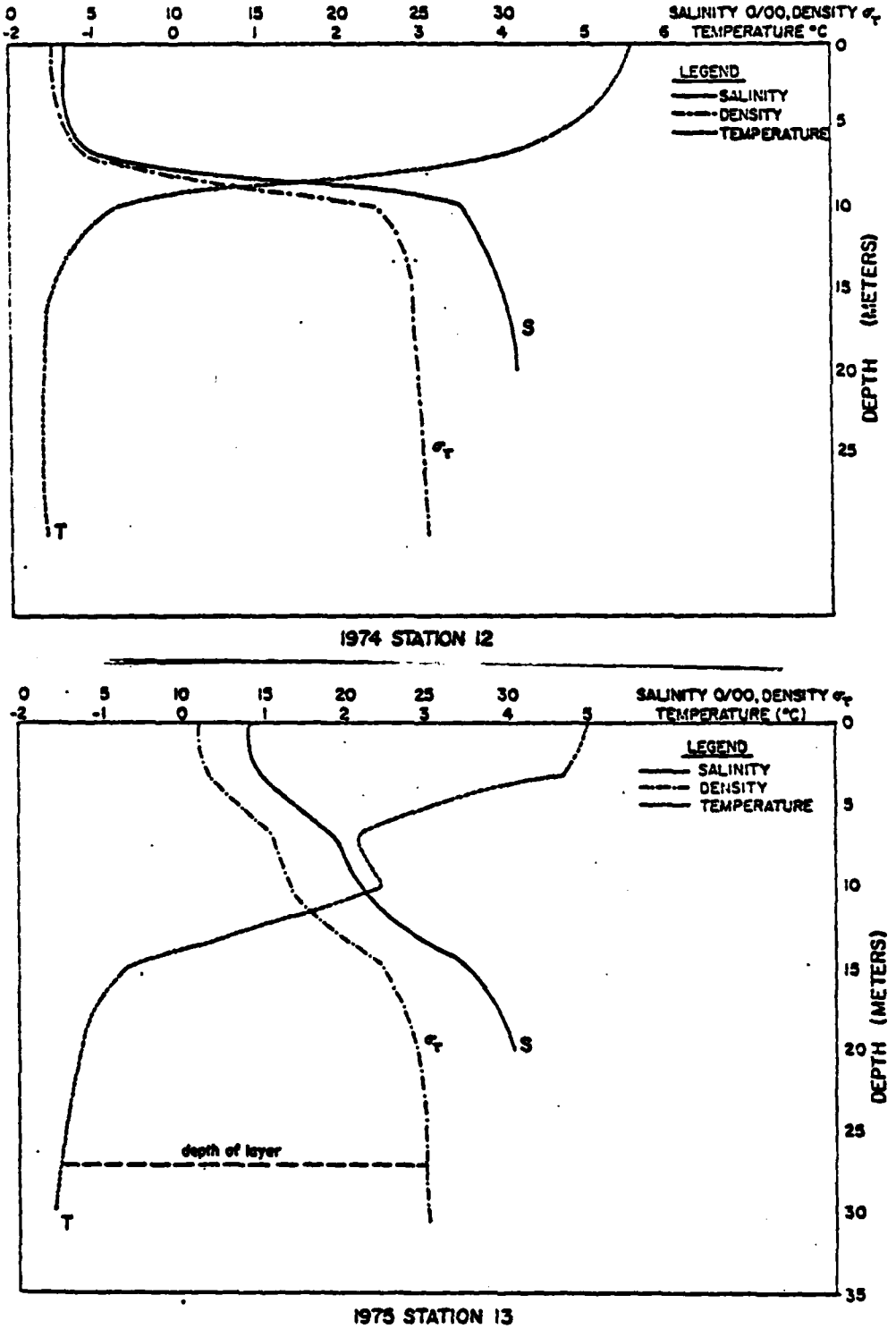

Figure 72: Salinity, density, and temperature versus depth at Station 12, August 18, 1974 and at Station 13, August 14, 1975.

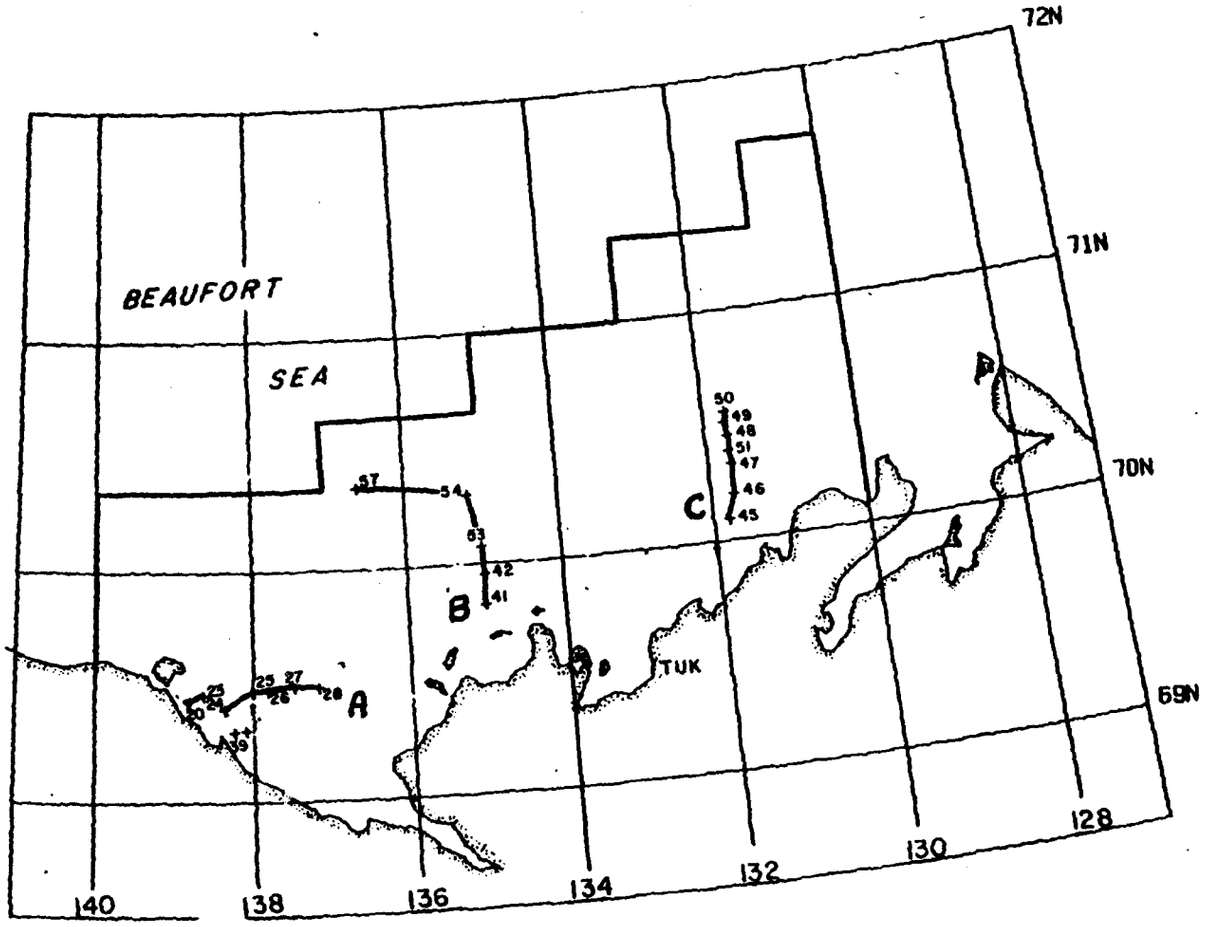

Figure 73: Location of oceanographic vertical cross-sections A, B, and C in the study area during August 1974.

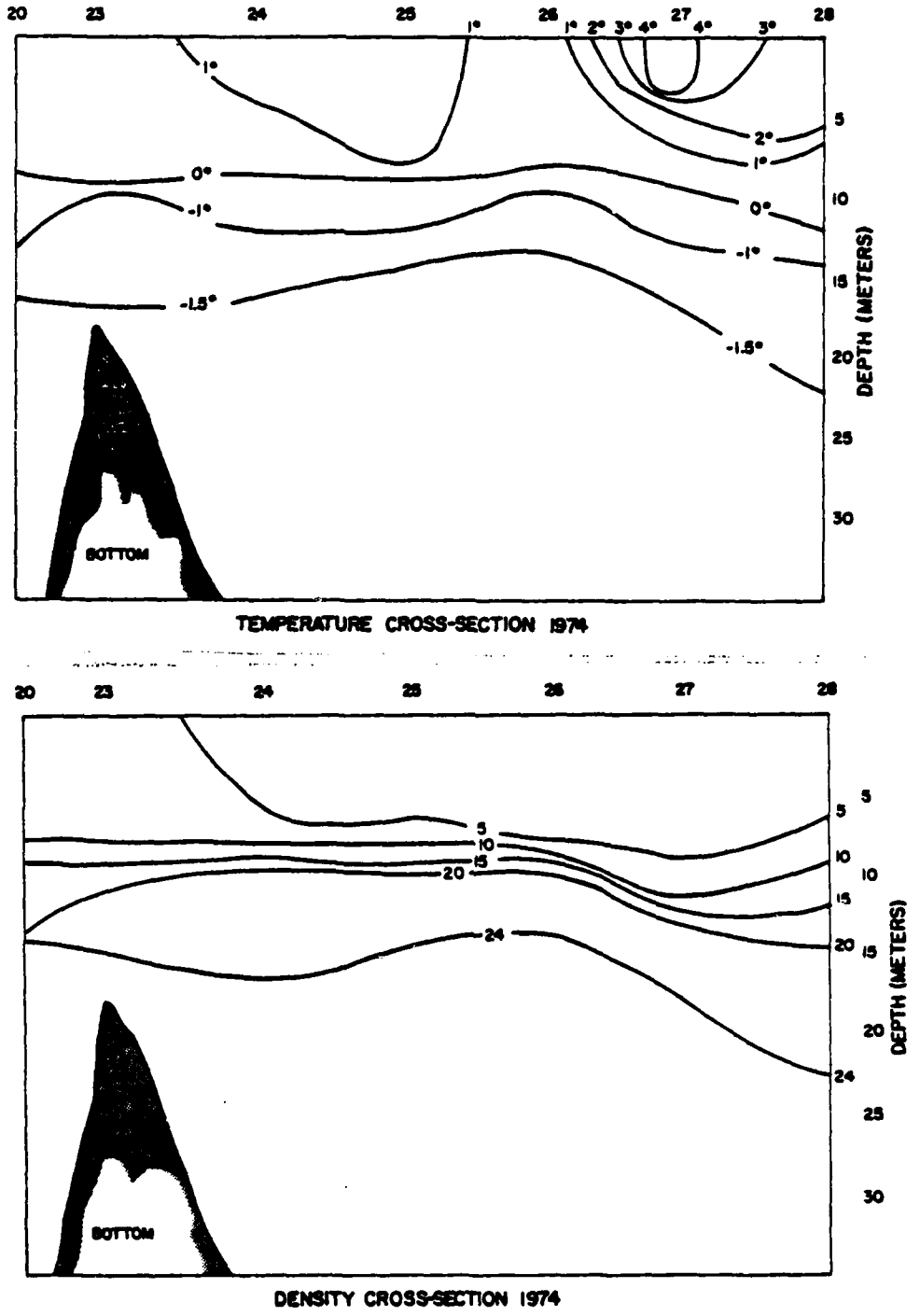

Figure 74: Temperature and density cross-section A.

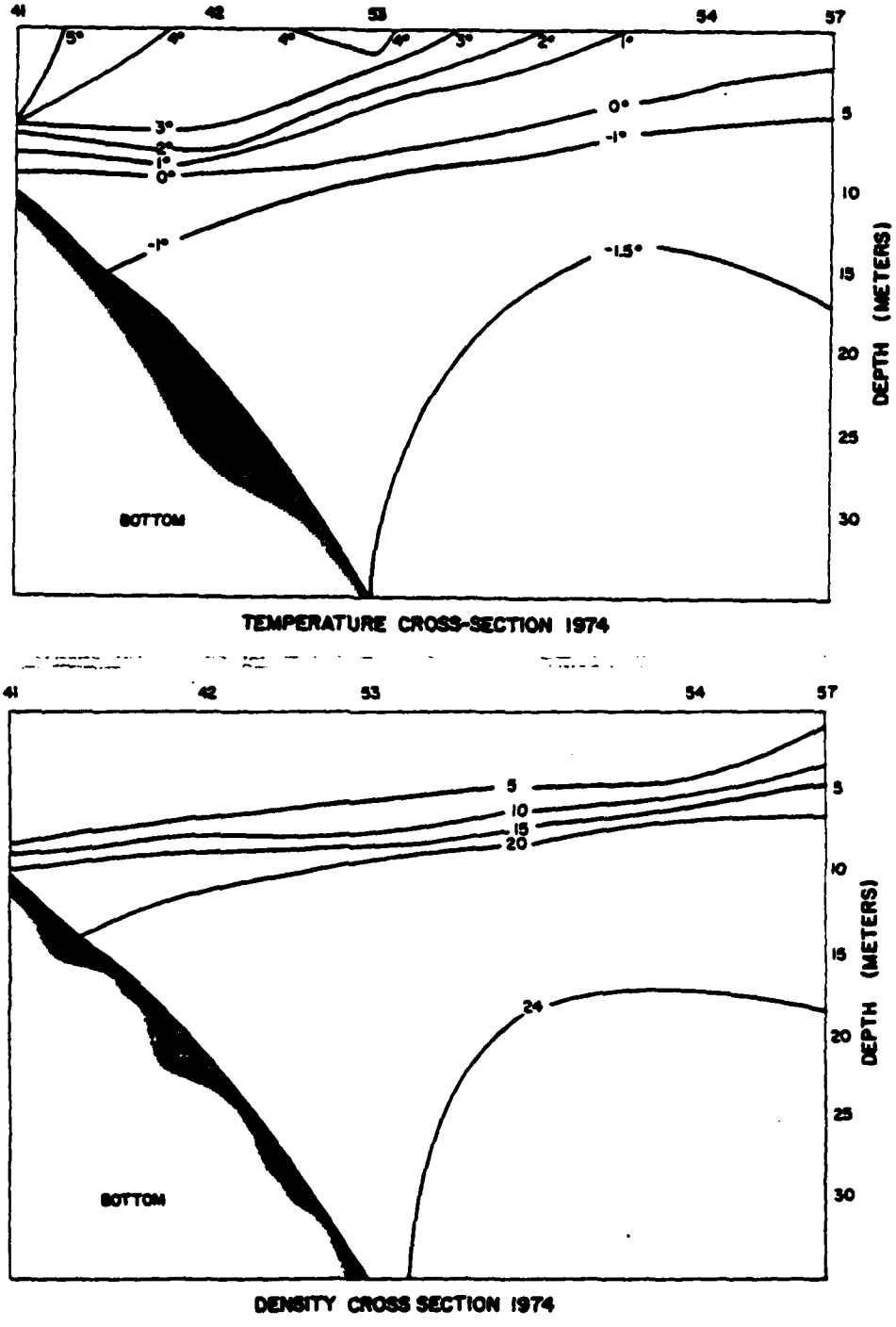

Figure 75: Temperature and density cross section B. A cold water intrusion is outlined by the -1.5°C isotherm.

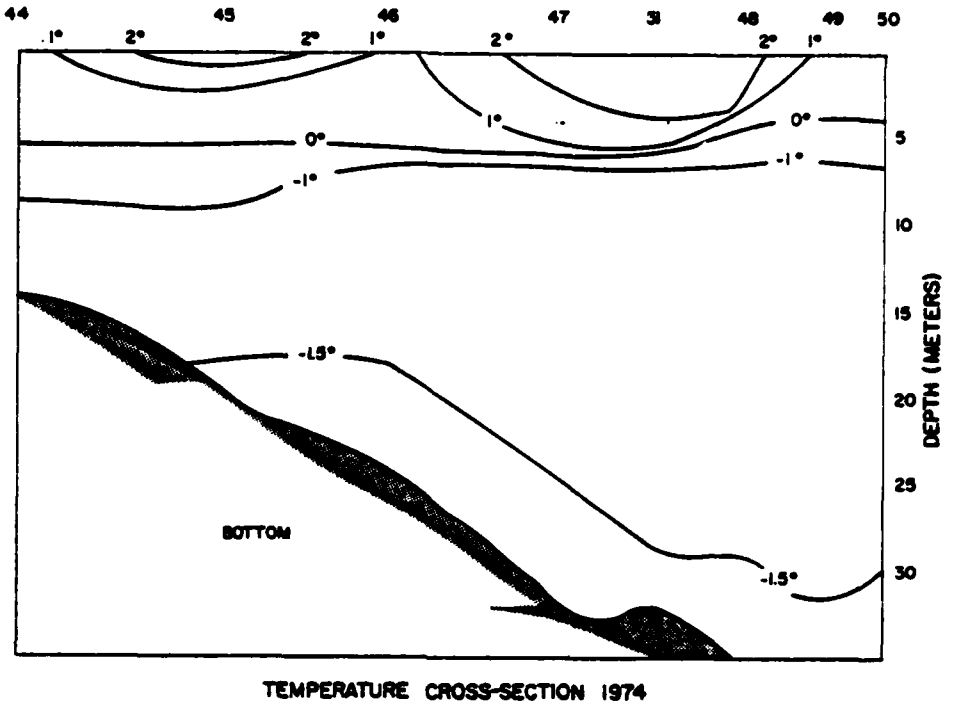

TEMPERATURE CROSS-SECTION 1974

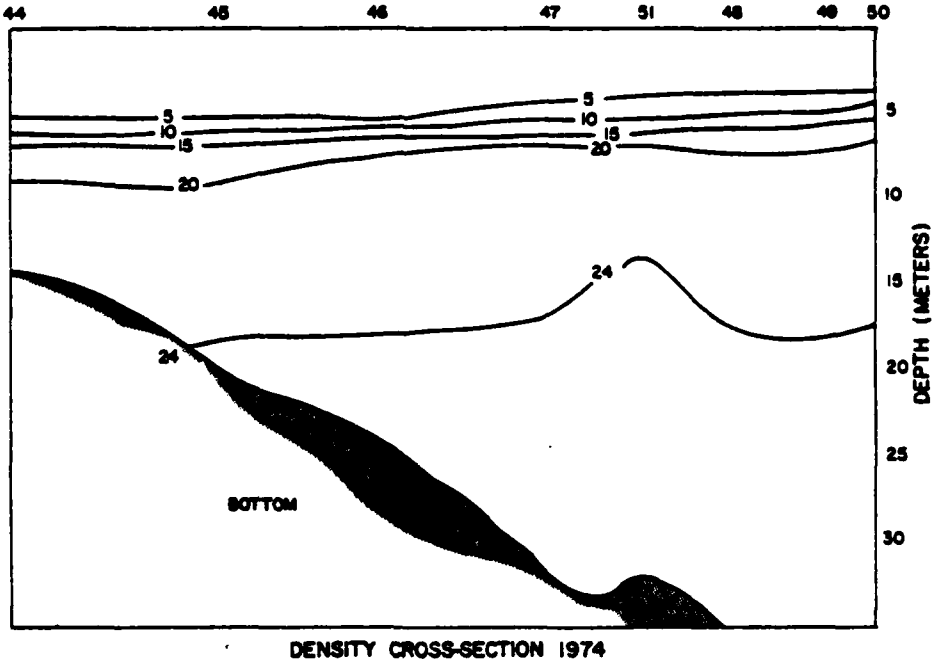

DENSITY CROSS-SECTION 1974

Figure 76: Temperature and density cross-section C. Shown are two tongues of warm water at the surface and a cold intrusion riding up the continental shelf.

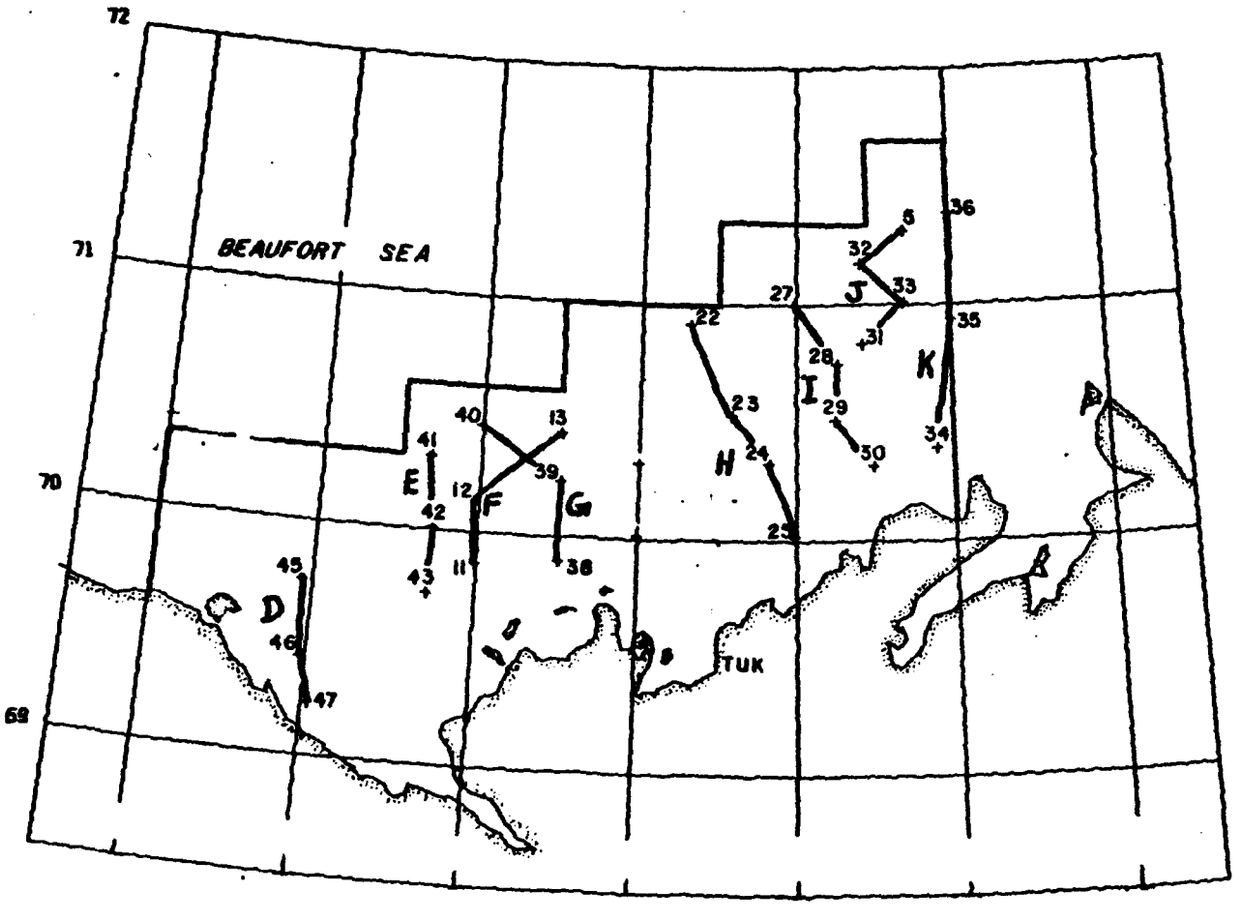

Figure 77: Location of oceanographic vertical cross-sections D, E, F, G, H, I, J, K in the study area during August 1975.

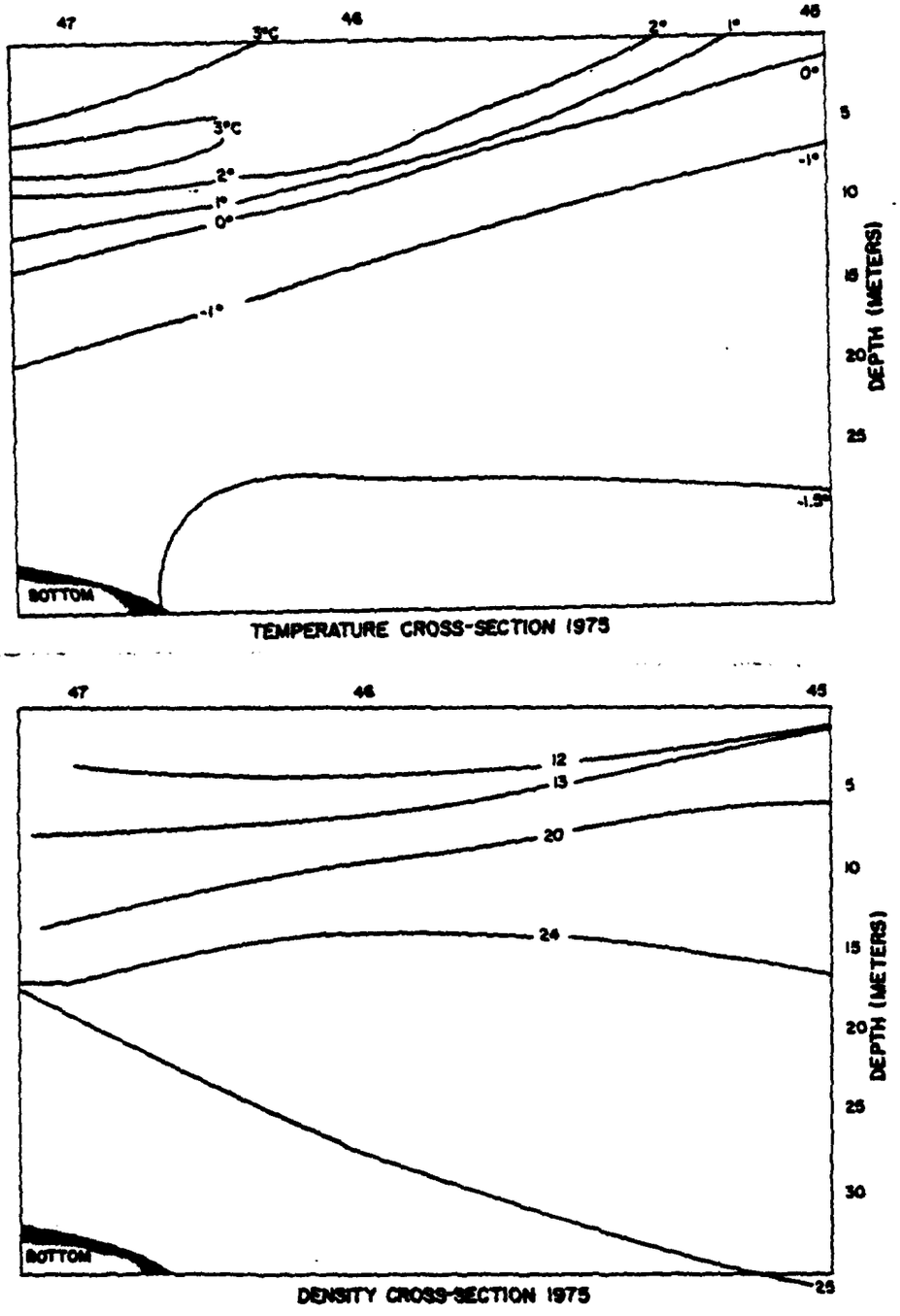

Figure 78: Temperature and density cross-section D. A wedge of warm water at the surface decreases in depth with the distance seaward, and cold water is seen along the continental slope at a depth of about 25 meters.

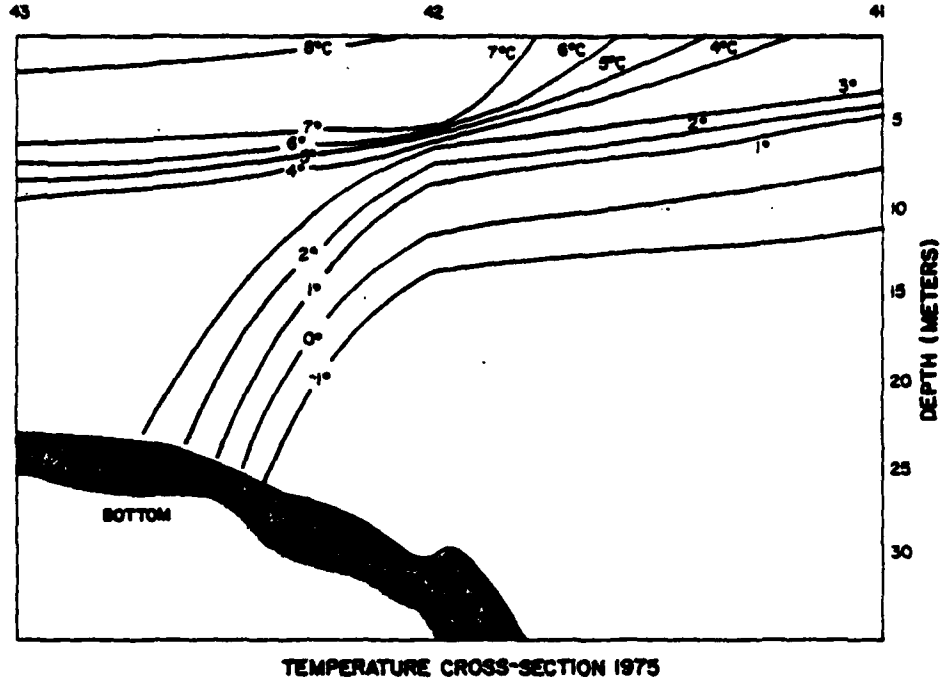

TEMPERATURE CROSS-SECTION 1975

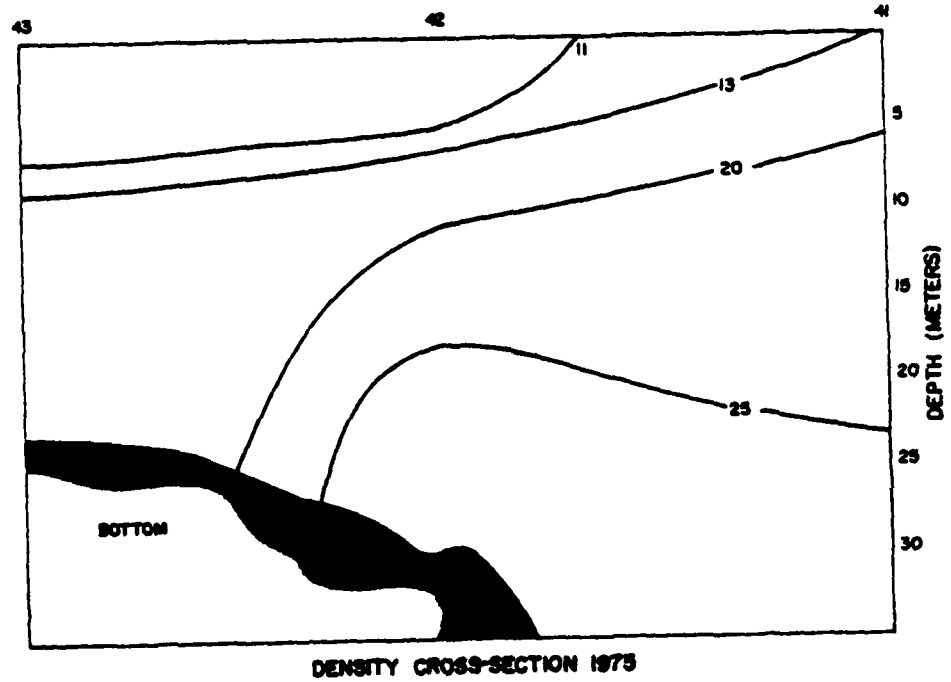

DENSITY CROSS-SECTION 1975

Figure 79: Temperature and density cross-section E. A wedge of warm water decreases in thickness with the distance seaward.

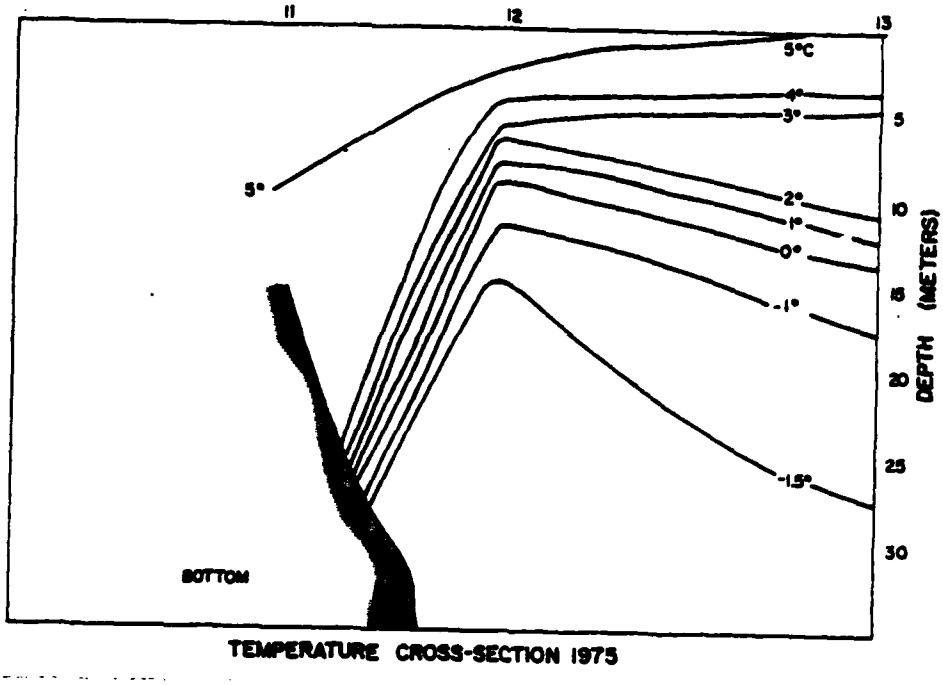

TEMPERATURE CROSS-SECTION 1975

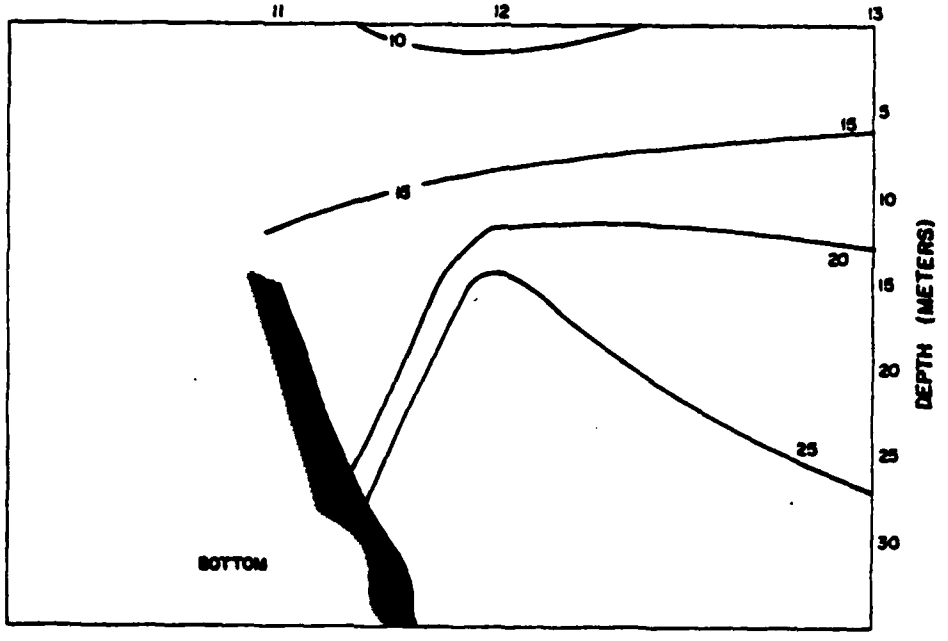

DENSITY CROSS SECTION 1975

Figure 80: Temperature and density cross-section F. An intrusion of cold water rises inshore to a depth of 15 meters along the continental slope.

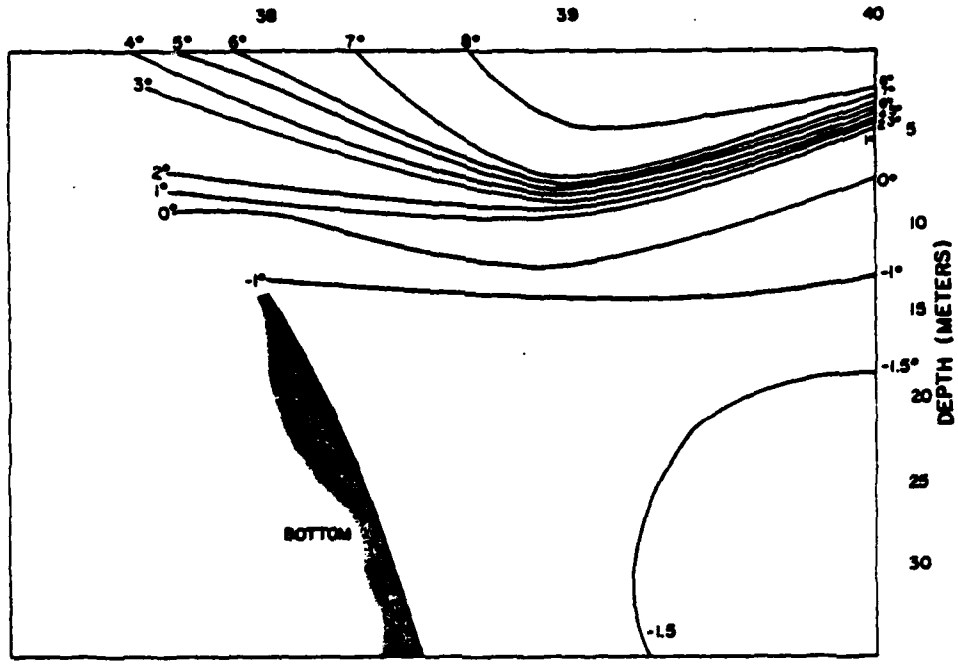

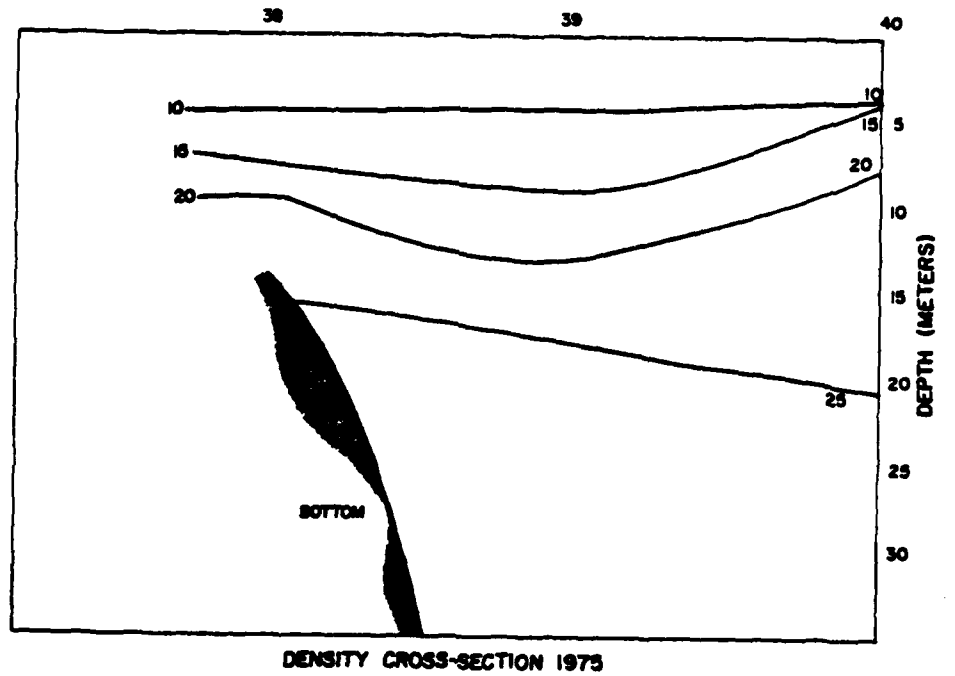

Figure 81: Temperature and density cross-section G. An intrusion of cold water is seen along the continental slope to a depth of about 18 meters. Also shown is an upwelling of cold water north of Richard's Island indicated by the decreasing water surface temperatures between Station 39 and the shore.

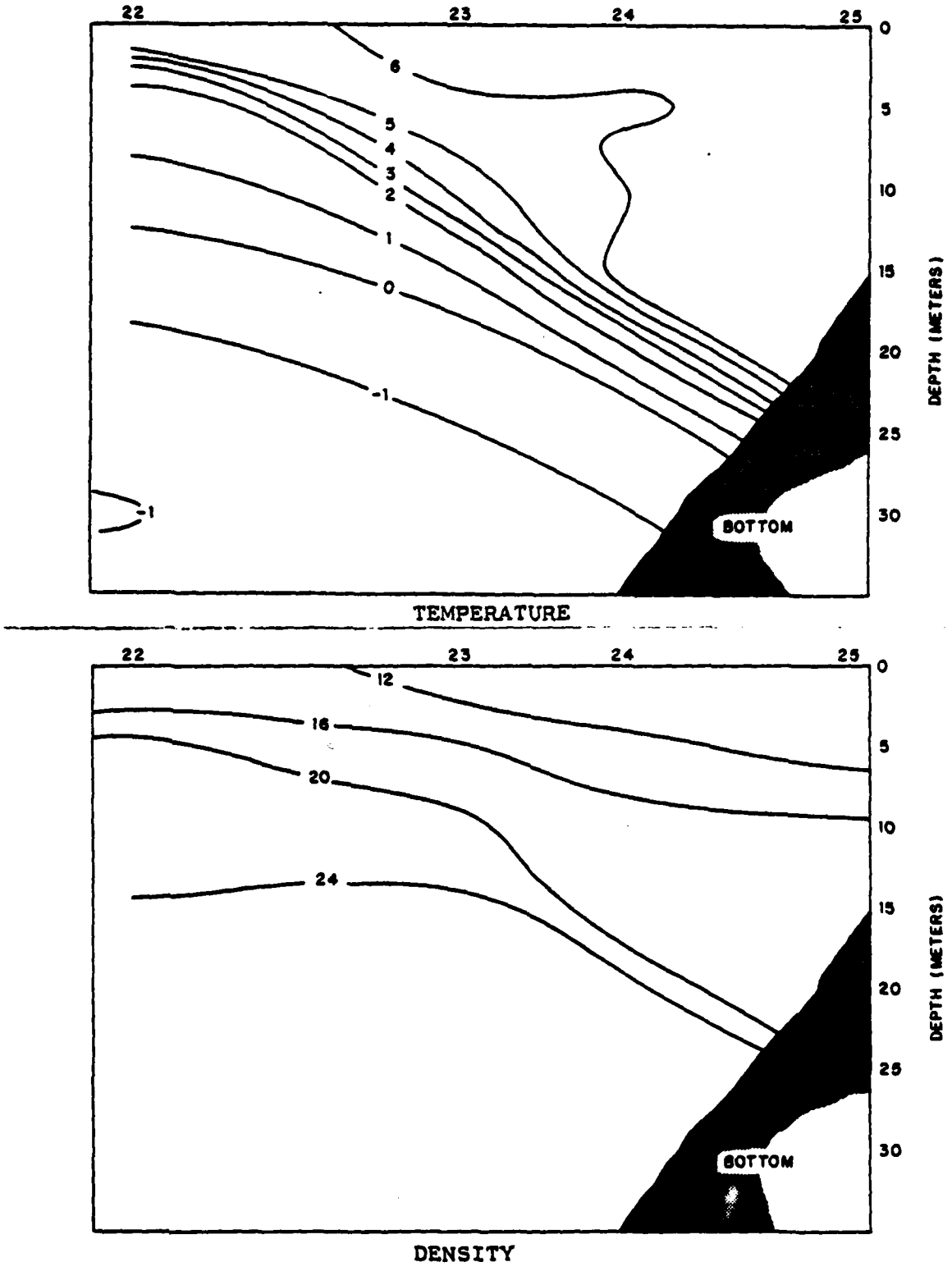

Figure 82: Temperature and density cross-section H. There was a warm wedge which thinned as the distance seaward increased.

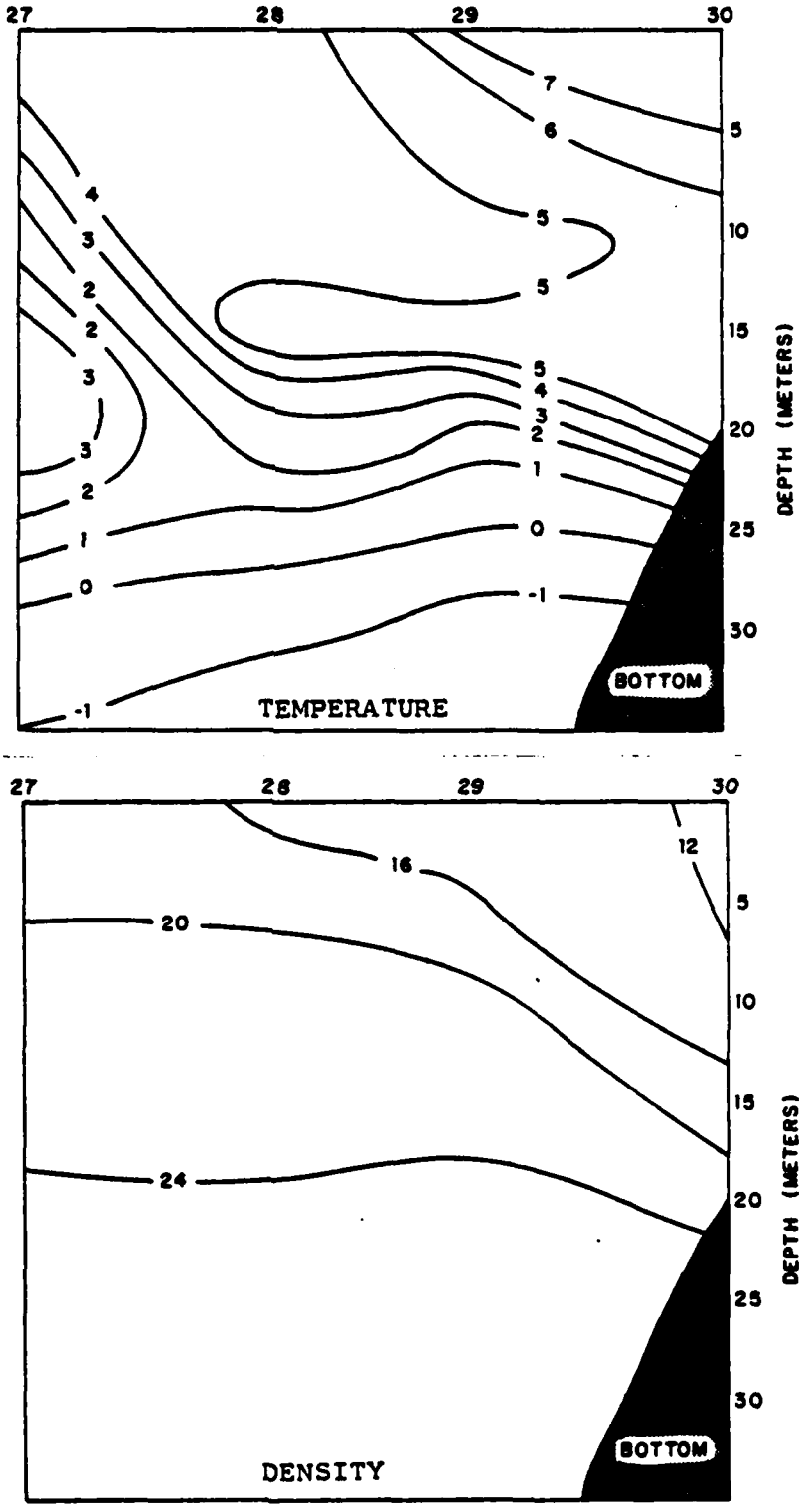

Figure 83: Temperature and density cross-section I. There was a well-mixed layer of 5°C water to a depth of 15 meters between Station 27 and 29 and a core of warmer 3°C water at 20 meters below Station 27.

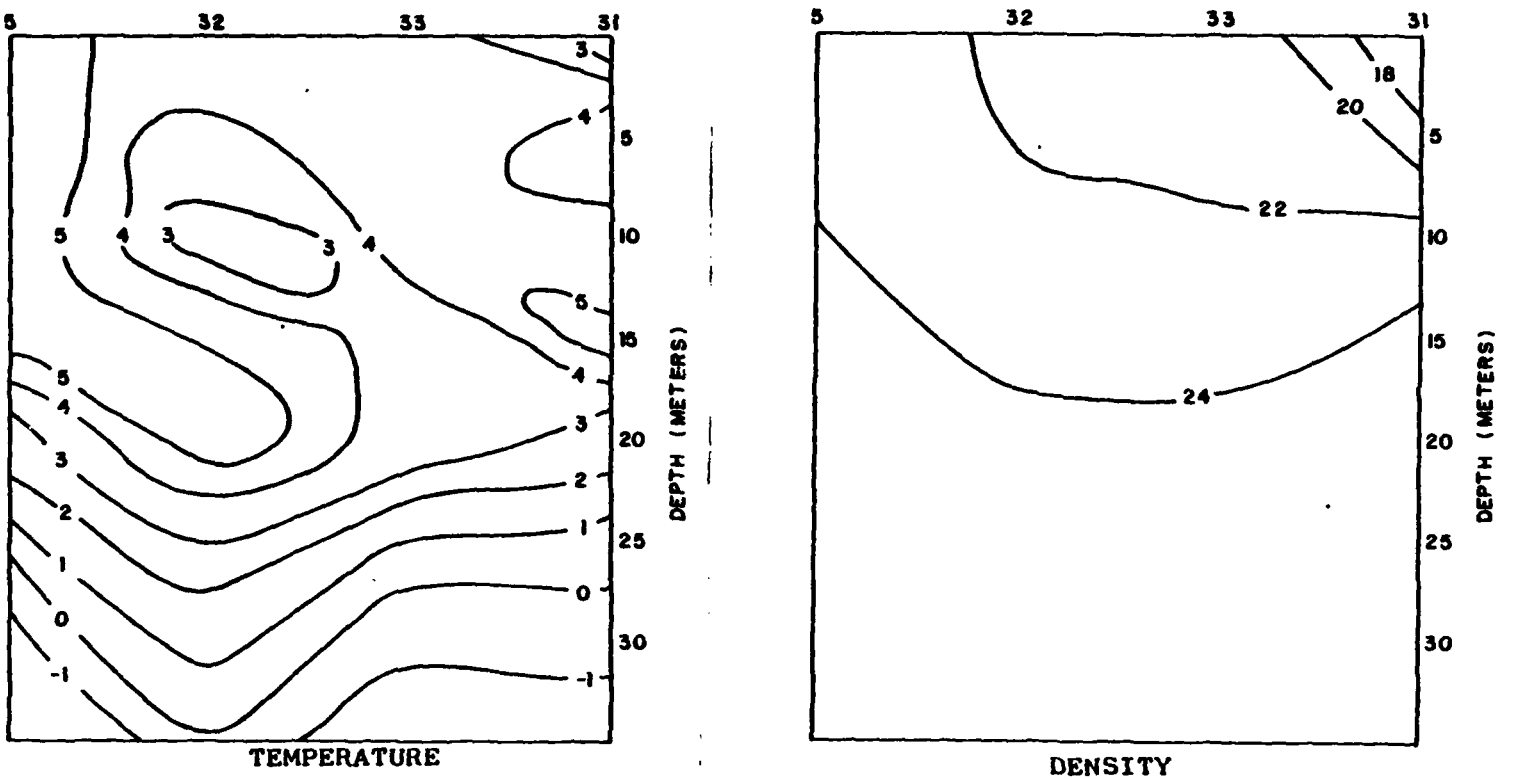

Figure 84: Temperature and density cross-section J. This shows the complex temperature structure north of Tuktoyaktuk Peninsula in the vicinity of the area where the first open water appeared beyond the landfast ice early in the season. Station 5 was occupied almost two weeks before Station 32 and it is seen that cooling occurred during northwest winds and there was subsequent heating of the upper 10 to 15 meter thick layer.

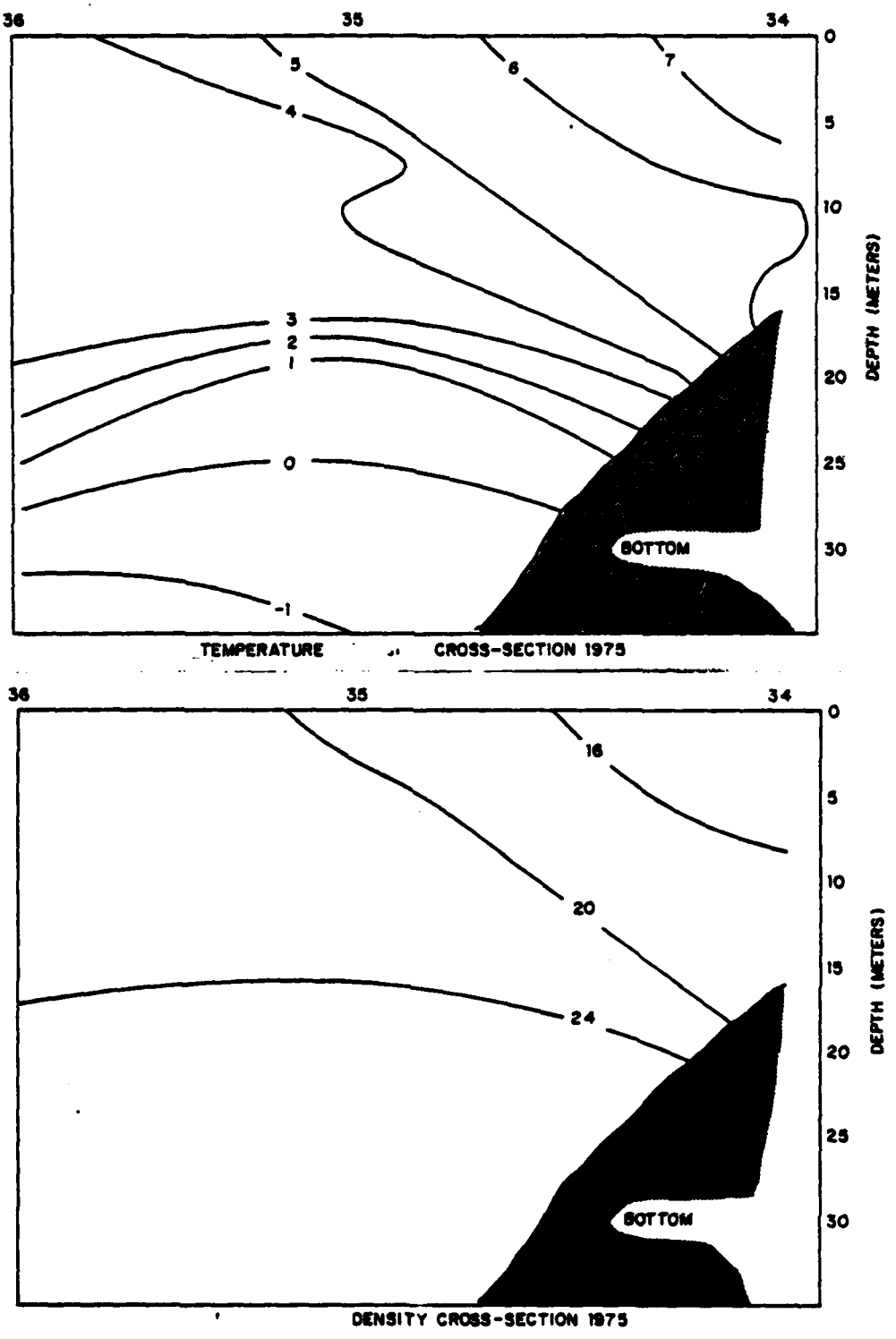

Figure 85. Temperature and density cross-section K. There was a relatively simple temperature structure with a decreasing thickness of a warm wedge as the distance seaward increased.

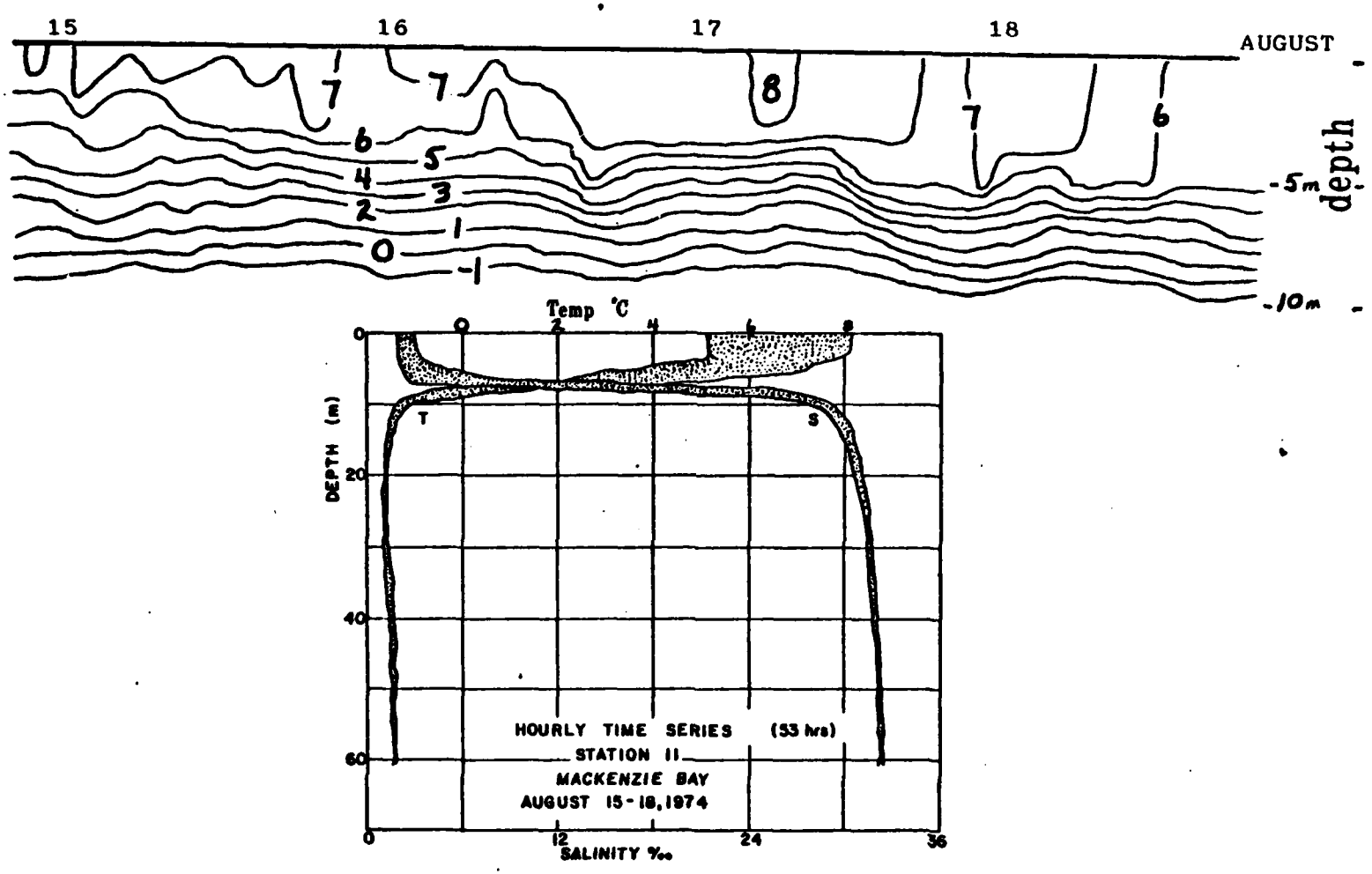

Figure 86: Hourly time series taken at Station 11, Mackenzie Bay 15-18 August 1974.

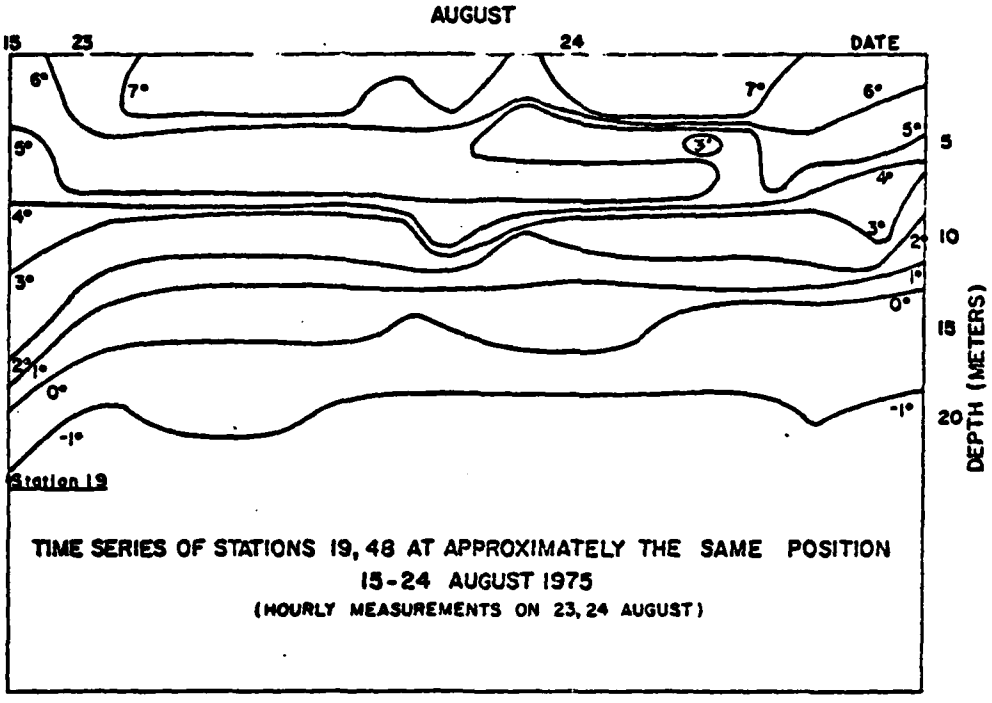

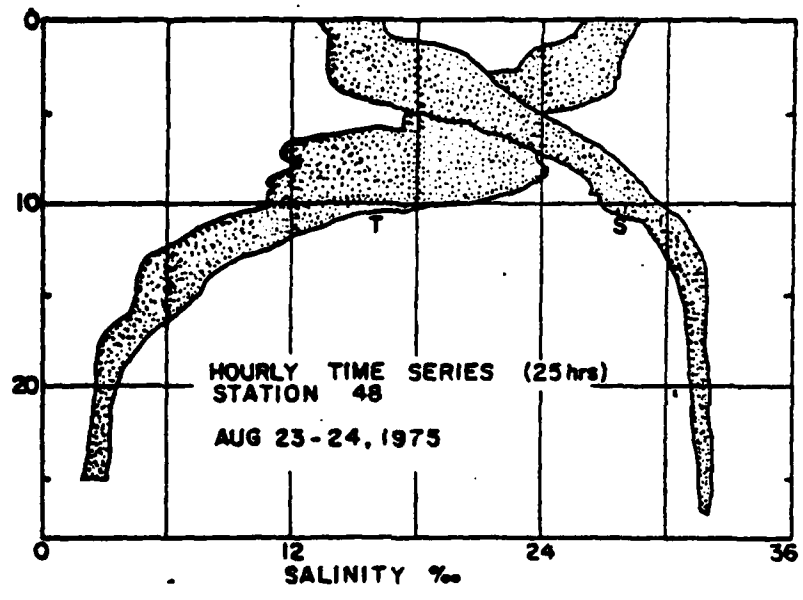

Figure 87: Hourly time series taken at Stations 19 and 48, north of Tuktoyaktuk, August 23-24, 1975.

AD-A096 387 NAVAL POSTGRADUATE SCHOOL MONTEREY CA F/G 8/3
HEAT BUDGETS OF THE SOUTHEAST BEAUFORT SEA FOR THE YEARS 1974 A--ETC(U)
SEP 80 E L TUMMERS

UNCLASSIFIED NL

3 OF 3
AD A 096387

END
DATE FILMED
4-81
DTIC

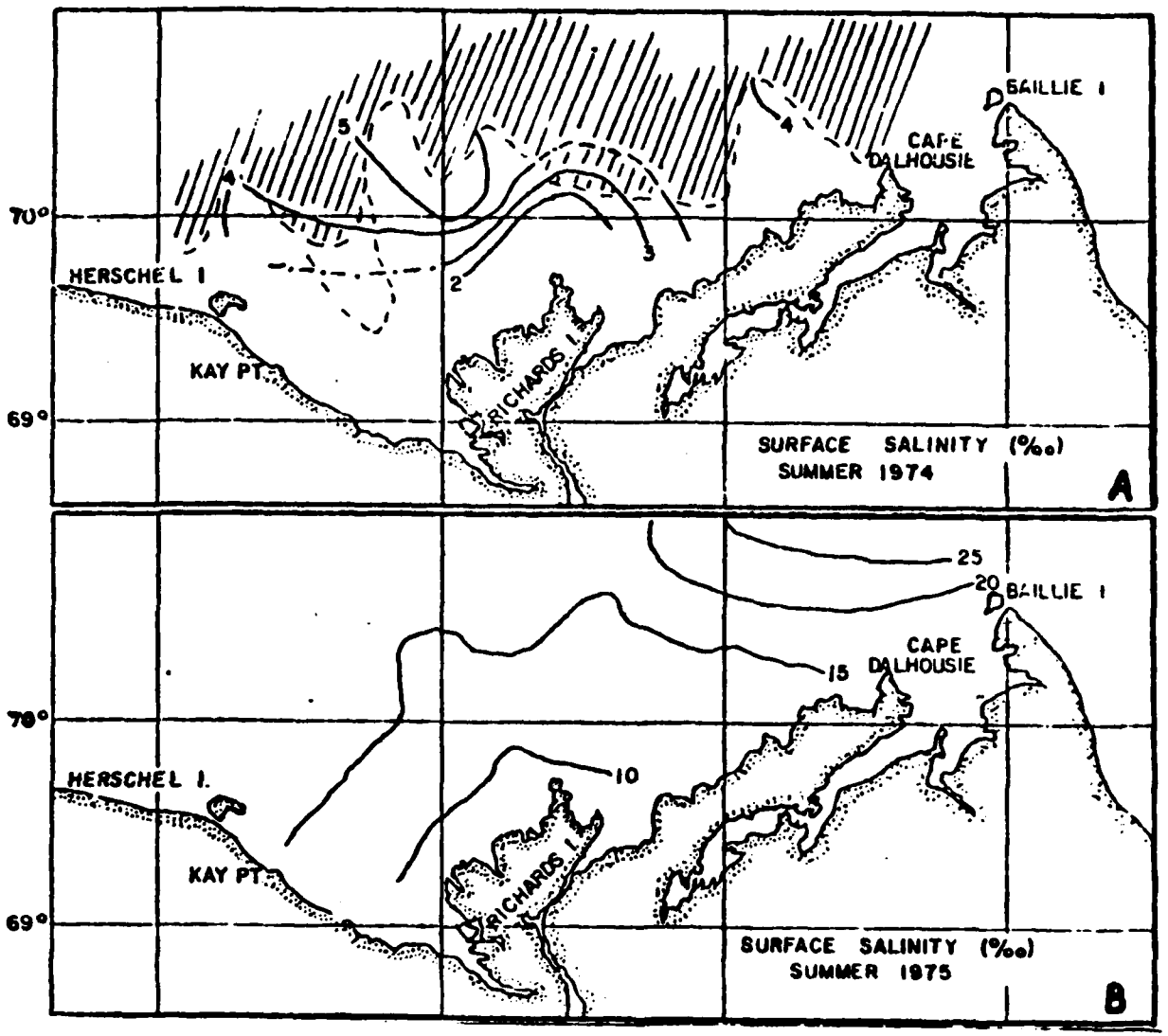

Figure 88: Comparison of surface salinities: summers of 1974 and 1975.

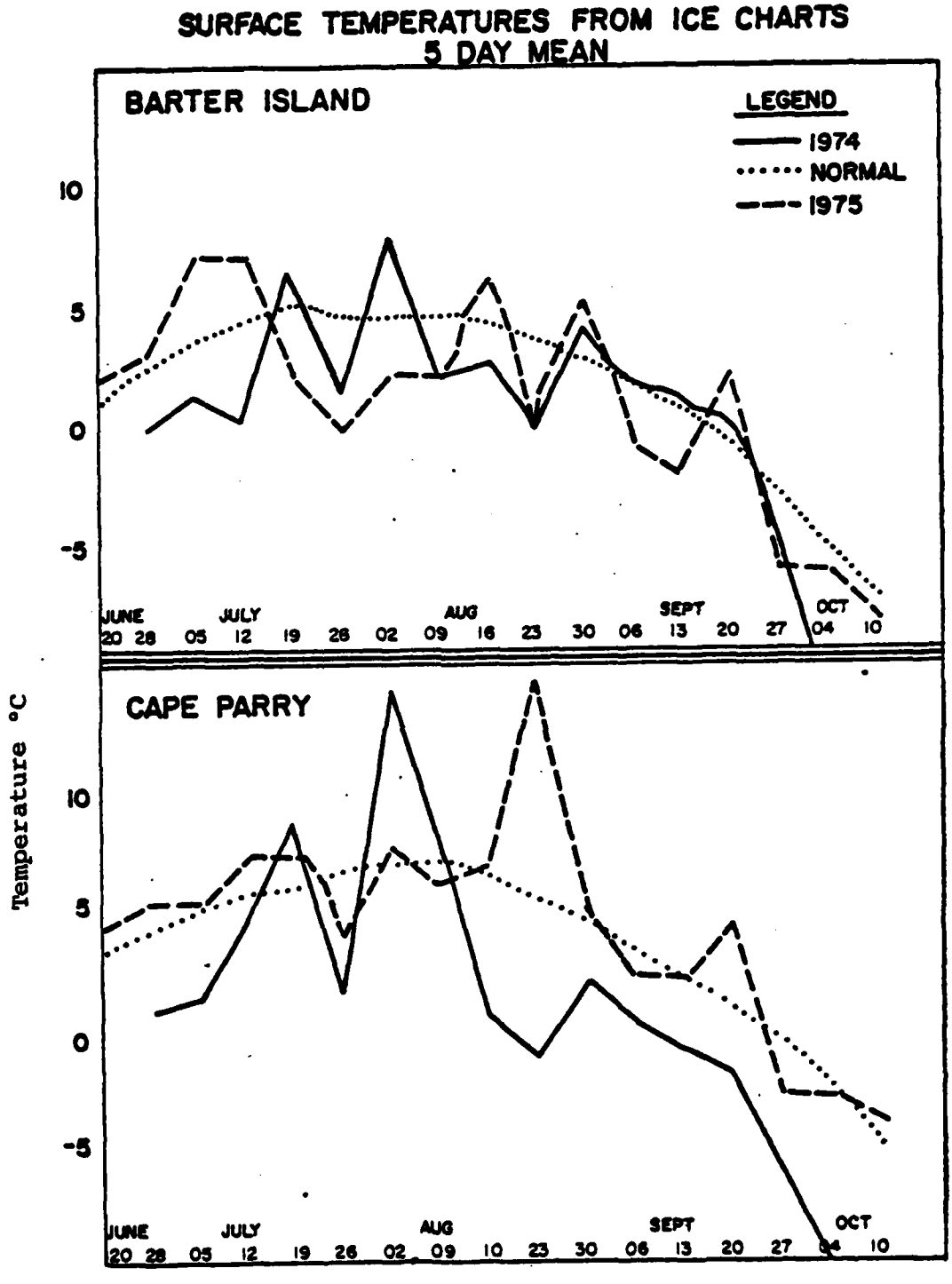

Figure 89: Comparison of surface air temperatures at Barter Island and Cape Parry based on 5-day mean temperatures in 1974 and 1975 from June 20 to October 10 of each year.

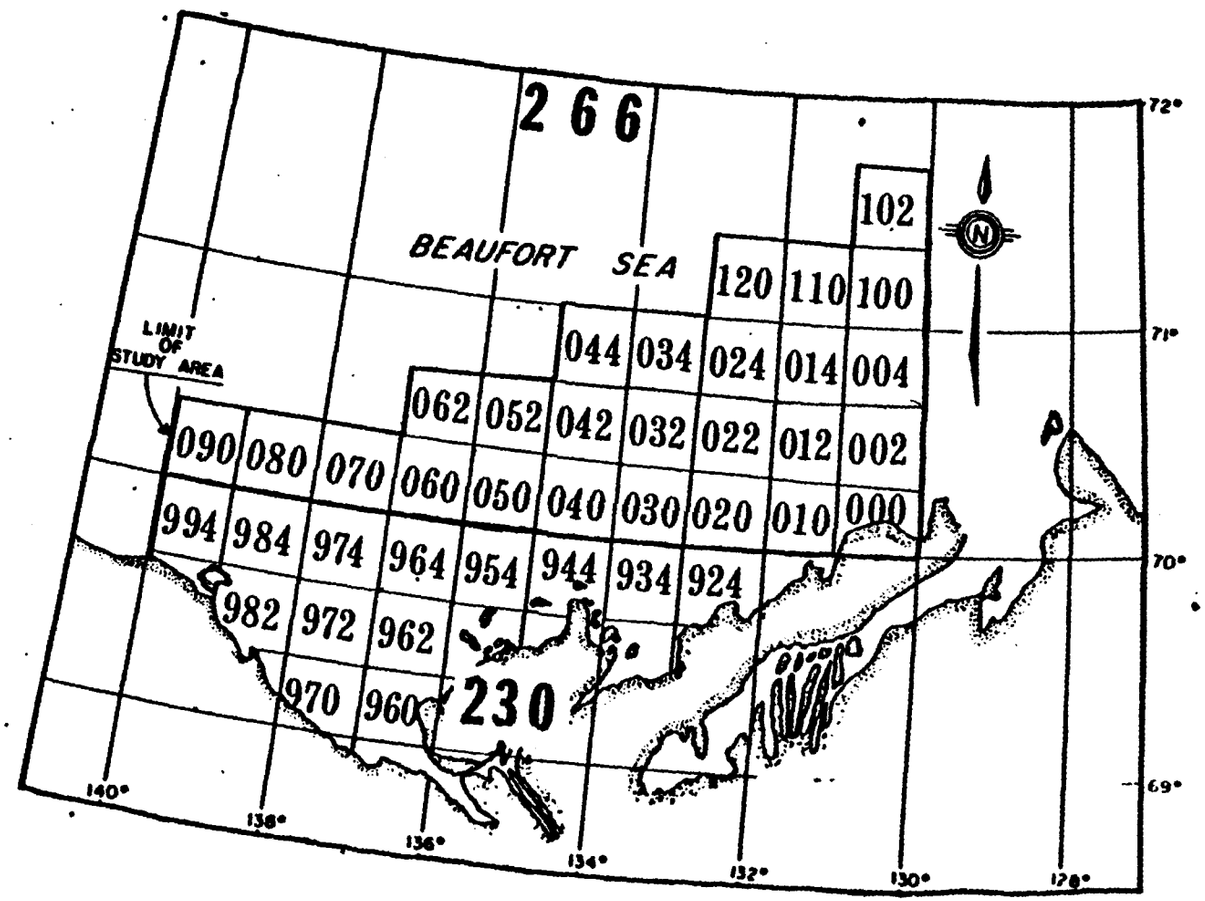

Figure 90: The study area showing the Marsden sub-sub-square grid.

LIST OF REFERENCES

Badgely, F.I., Heat Budget of the Surface of the Arctic Ocean, Proceedings of the Symposium on the Arctic Heat Budget and Atmospheric Circulation 31 Jan-4 Feb 1966, National Science Foundation Memorandum RM-5233-NSF December 1966, pp 269-277.

Burns, B.M., The Climate of the Mackenzie Valley - Beaufort Sea, Information Canada, Ottawa, Volume 1, 1973, Volume 2, 1974.

Davies, K.F., Mackenzie River Input to the Beaufort Sea, Beaufort Sea Technical Report #15, Department of the Environment, Victoria, BC, December, 1975.

Fraker, M.A., Gordon, C.D., McDonald, J.W., Ford, J.K., and Cambers, G., White Whale Distribution and Abundance and the Relationship to Physical and Chemical Characteristics of the Mackenzie Estuary, Fisheries and Marine Science Technical Report No. 863, Department of Fisheries and the Environment, Winnipeg, Dec 1979.

Gresswell, R., and Huxley, A., Standard Encyclopedia of the World's Rivers and Lakes, G.P. Putnam and Sons, New York, 1965.

Herlinveaux, R.H., de Lange Boom, B.R., Wilton, G.R., Salinity, Temperature, Turbidity and Meteorological Observations in the Beaufort Sea: Summer 1974, Spring and Summer 1975, Unpublished Manuscript, Institute of Ocean Sciences, Patricia Bay, Victoria, B.C., December, 1976.

Huyer, A., and Barber, F.G., A Heat Budget of the Water in Barrow Strait for 1962, Manuscript Report Series No. 12, Marine Sciences Branch, Department of Energy, Mines and Resources, The Queen's Printer for Canada, Ottawa, 1970.

Langleben, M.P., Albedo of Ice-Infested Waters in the Channels of the Canadian Archipelago, pp. 134-142, Energy Fluxes over Polar Surfaces, Proceedings of the IAMAP/IAPSO/SCAR/ WMO Symposium, Moscow, 3-5 August 1971, Technical Note No. 129, World Meteorological Organization, Geneva, Switzerland, 1973.

Laevastu, T., Factors Affecting the Temperature of the Surface Layer of the Sea, Merentut kimuslaitoksen Julkaisu Havsforskningsinstitutets Skrift, No 195, Helsinki, 1960.

MacNeill, M.R., and Garrett, J.F., Open Water Surface Currents, Beaufort Sea Technical Report #17, Department of the Environment, Victoria, B.C., December, 1975.

Markham, W.E., Ice Climatology of the Beaufort Sea, Beaufort Sea Technical Report #26, Department of the Environment, Victoria, B.C., December, 1975.

Matheson, K.M., The Meteorological Effect on Ice in the Gulf of St. Lawrence, Manuscript Report No. 3, Marine Sciences Center, McGill University Montreal, September, 1967.

Maykut, G.A., and Grenfell, T.C., The Spectral Distribution of Light Beneath First-Year Sea-Ice in the Arctic Ocean, pp. 554-563, Limnology and Oceanography 20, 4, 1975.

Milne, A.R., Personal Communication.

O'Neill, A.D.J., and Gray, D.M., Solar Radiation Penetration Through Snow, pp. 227-241, I Proceedings of the Banff Symposium, September, 1972, on the Role of Snow and Ice in Hydrology, IAHS Publication 107, Volume 1, UNESCO/ WMO/IAHS, 1972.

Orvig, S., Climates of the Polar Regions, World Survey of Climatology, Volume 14, p370, 1970.

Sellers, W.D., Physical Climatology, p272, U. of Chicago Press Chicago, 1965 (Quoted in Walker, 1975).

Shuleikin, V.V., Molecular Physics of the Sea, Physics of the Sea Part VIII, pp727-786, 1953 (USHO Translation, Washington, 1957) (Quoted in Walmsley, 1966).

Sverdrup, H.U., Johnson, M.W., Fleming, R.H., The Oceans, Their Physics, Chemistry and General Biology, Prentice Hall, Inc., Englewood Cliffs, N.J., 1942.

Swinbank, W.C., Evaporation from the Oceans, Scientific Report No. 12, A.F.C.R.C., TN-60-211 (Quoted in Walmsley, 1966).

Untersteiner, N., On the Mass and Heat Budget of Arctic Sea Ice, Arch. Meteor. Geophys. Biokl. Series A, Bd. 12, pp 151-182, Vienna, 1961.

Vowinckel, E., and Taylor, B., Energy Balance of the Arctic: Evaporation and Sensible Heat Flux over the Arctic Ocean, Arch. Meteor. Geophys. Biokl. Serie B.

Walmsley, J.L., Ice Cover and Surface Heat Fluxes in Baffin Bay, Manuscript Report No. 2, Marine Sciences Center, McGill University, Montreal, October, 1966.

INITIAL DISTRIBUTION LIST

		No. Copies
1.	Defense Technical Information Center Cameron Station Alexandria, VA 22314	2
2.	Library, Code 0142 Naval Postgraduate School Monterey, CA 93940	2
3.	Chairman, Code 68 Department of Oceanography Naval Postgraduate School Monterey, CA 93940	1
4.	Chairman, Code 63 Department of Meteorology Naval Postgraduate School Monterey, CA 93940	1
5.	Dr. A. R. Milne 836 Land's End Rd. Sidney, British Columbia V8L 3R9	5
6.	Dr. R. Paquette, Code 68Pa Department of Oceanography Naval Postgraduate School Monterey, CA 93940	2
7.	CAPT. E. L. Tummers Weapons Division CFFS HALIFAX Nova Scotia, CANADA B3K 2X0	1
8.	Director Naval Oceanography Division Navy Observatory 34th and Massachusetts Avenue NW Washington, D.C. 20390	1
9.	Commander Naval Oceanography Command NSTL Station Bay St. Louis, MS 39529	1

10. Commanding Officer — 1
Naval Oceanographic Office
NSTL Station
Bay St. Louis, MS 39529

11. Commanding Officer — 1
Fleet Numerical Oceanography Center
Monterey, CA 93940

12. Commanding Officer — 1
Naval Ocean Research and Development Activity
NSTL Station
Bay St. Louis, MS 39529

13. Office of Naval Research (Code 480) — 1
Naval Ocean Research and Development Activity
NSTL Station
Bay St. Louis, MS 39529

14. Scientific Liaison Office — 1
Office of Naval Research
Scripps Institution of Oceanography
La Jolla, CA 92037

15. Library — 1
Scripps Institution of Oceanography
P. O. Box 2367
La Jolla, CA 92037

16. Library — 1
Department of Oceanography
University of Washington
Seattle, WA 98105

17. Library — 1
CICESE
P. O. Box 4803
San Ysidro, CA 92073

18. Library — 1
School of Oceanography
Oregon State University
Corvallis, OR 97331

19. Commander — 1
Oceanographic Systems Pacific
Box 1390
Pearl Harbor, HI 96860

20. Chief, Ocean Services Division — 1
National Oceanic and Atmospheric
Administration
8060 Thirteenth Street
Silver Springs, MD 20910

21. Commanding Officer — 1
Naval Polar Oceanography Center, Suitland
Washington, DC 20373

22. Department of Oceanography — 1
University of British Columbia
Vancouver, B.C.,
Canada, V6T1N5

23. Dr. E. F. Roots, — 1
Office of the Science Advisor,
D.F.E.
Ottawa, Ontario
Canada K1A0H3

24. Library — 1
Defence Research Establishment Pacific,
Fleet Mail Office,
Esquimalt, B.C.
Canada

25. U.S. Department of Commerce, — 1
NOAA
Environmental Data Service
Boulder, Colorado 80302

26. MARINE SCIENCES CENTRE — 1
McGILL UNIVERSITY,
3620 University St.
P.O. Box 6070
Montreal, Quebec
Canada H3A2T8

27. Dr. R. W. Skinner — 1
Advisor, Department of Environmental Affairs
Department of Energy, Mines and Resources,
580 Booth St.
Ottawa
Canada K1AOE4

28. L.G.L. Ltd. — 1
2453 Beacon Ave.,
Sidney, B.C.,
Canada V8L1X7

29. Polar Continental Shelf Project 1
4th Floor, City Centre Towers,
880 Wellington St.
Ottawa
Canada K1A0E4

30. Library 1
Ocean and Aquatic Sciences,
Department of Fisheries and Oceans,
240 Sparks St.
7th Floor, West,
Ottawa, Canada K1A0E4

31. Library 1
Arctic Biological Station
Ste-Anne De Bellevue,
P.O. Box 400
Quebec
Canada, H9X3L6

32. Dr. Knut Aagaard 1
Department of Oceanography
University of Washington
Seattle, WA 98195

33. Dr. L. K. Coachman 1
Department of Oceanography
University of Washington
Seattle, WA 98195

34. A.P.O.A. Information Service 1
P.O. Box 1281
Postal Station M
Calgary, Alberta
Canada T2P2L2

35. Library 1
Atmospheric Environment Service
4905 Dufferin St.
Downsview, Ontario,
Canada, M3H5T4

36. Library 1
Arctic Weather Centre
Edmonton International Airport
P.O. Box 9860, Edmonton, Alberta
Canada, T5J2T2

37. Arctic Sciences, Ltd. 1
Sidney, B.C.
Canada, V8L3S1

38. Library 1
Institute of Ocean Sciences, Patricia Bay
P.O. Box 6000
9860 West Saanich Rd.
Sidney, B.C.
Canada V8L4B2

39. Frozen Sea Research Group 1
Institute of Ocean Sciences, Patricia Bay,
P.O. Box 6000,
Sidney, B.C.
Canada, V8L4B2

40. Mr. Fred Barber 1
Ocean and Aquatic Sciences
Department of Fisheries and Oceans,
240 Sparks St.
7th Floor, West,
Ottawa, Ontario
Canada K1A0E6

41. Ice Central 1
D.F.O.
Trebla Bldg.
473 Albert St.
Ottawa, Ontario
Canada K1A0H3

42. Library 1
Imperial Oil (Canada) Ltd.
111 St. Clair Ave. W.
Toronto, Ontario
Canada, M4VIN6

43. Library 1
Dome Petroleum Ltd.
P.O. Box 200
Calgary, Alberta
Canada, T2P2H8

44. Dr. J. C. O'Rourke 1
Dome Petroleum Ltd.
P.O. Box 200
Calgary, Alberta
Canada, T2P2H8

45. Cold Regions Research & Engineering Lab 1
P.O. Box 282
Hanover, NH 03755

46. Dr. Reid A. Bryson 1
Institute for Environmental Studies
University of Wisconsin
1225 W. Dayton Street
Madison, WI 53706

47. Librarian 1
Naval Arctic Research Lab
Barrow, AK 99723

48. Director, Institute of Polar Studies 1
Ohio State University
125 South Oval Drive
Columbus, OH 43210

49. Mr. Robert C. Faylor 1
Arctic Institute of North America
1619 New Hampshire Avenue NW
Washington, DC 20009

50. Dr. Kenneth L. Hunkins 1
Lamont-Doherty Geological Observatory
Torrey Cliffe
Palisades, NY 10964

51. Mr. Beaumont Buck 1
Polar Research Laboratory Inc.
123 Santa Barbara Street
Santa Barbara, CA 93101

52. Dr. Kou Kusunoki 1
National Institute of Polar Research
Kaga 1-9-10, Itabashi-Ku
Tokyo, Japan

53. Dr. T. E. Armstrong 1
Scott Polar Research Institute
Cambridge, CB2 1ER
England

54. Dr. Svenn Orvig 1
McGill University
Department of Meteorology
P.O. Box 6070
Montreal 101, Quebec, Canada

55. Dr. K. M. Rae 1
Vice President for Research
University of Alaska
Fairbanks, AK 99701

56. Mr. Walter I. Wittmann 1
Naval Oceanographic Office
Code 7600
Washington, DC 20390

57. Mr. M. M. Kleinerman 1
Project Manager for Arctic ASW
US Naval Ordnance Laboratory
White Oak, MD 20910

58. Polar Information Service — 1
Office of Polar Programs
National Science Foundation
Washington, DC 20550

59. Departmental Library-Serials — 1
Department of the Environment
Ottawa, Canada K1A OH3

60. Woods Hole Oceanographic Institute — 1
Document Library LO-206
Woods Hole, MA 02543

61. Dr. Donald W. Hood — 1
Institute for Marine Science
University of Alaska
Fairbanks, AK 99701

62. Defence Research Board — 1
Department of National Defence
190 O'Connor Street
Ottawa, Ontario K1A OZ3,
Canada

63. Norsk Polarinstitutt — 1
Rolfstangvn 12, Postboks 158
1330 Oslo Lufthavn,
Norway

64. Dr. W. M. Sackinger — 1
Department of Electrical Engineering
University of Alaska
Fairbanks, AK 99701

65. Manager, Inuvik Research Laboratory — 1
Box 1430
Inuvik, Northwest Territories XOE OTO
Canada

66. Library — 1
Bedford Inst. of Oceanography,
Darmouth, N.S.,
Canada, B2Y4A2

67. OCS Arctic Project Office — 1
611 Elvey Geophysical Institute
University of Alaska
Fairbanks, Alaska 99701

68. Library 1
Canadian Centre for Inland Waters,
Dept. of Fisheries and Oceans
867 Lakeshore Rd.
Burlington, Ont.
Canada L7R4A6

69. Ice Research Project 1
McGill University
Rutherford Physics Bldg.
3600 University St.
Montreal, P.Q.
Canada, H3A2T8

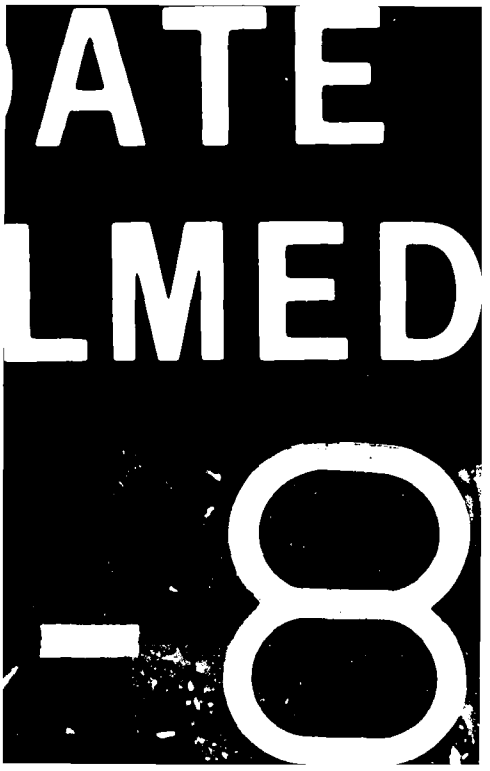
ATE
LMED
-8